Abstract

Diagnostics of the state of conservation of a building, for monitoring and conservation purposes, currently refer to costly and time-consuming technologies and instruments. They often require invasive actions, or they are difficult to apply. The aim of this research is to define, analogously to other fields of Engineering, innovative diagnostic approaches, to support the experts, in the phase of knowledge, before planning an intervention. The evaluation of the general conditions of a building have been proposed through the analysis of colored point clouds or texturized polygonal meshes, acquired by means of photogrammetry, in order to recognize and classify pathologies, as defined by sectorial standard.

Specific mapping and computerized evaluation routines have been created, for the detection of various decay morphologies, through qualitative and quantitative analysis systems. Digital Image Processing and Machine Learning techniques have been adopted and implemented on high resolution three-dimensional models (dense point clouds), related to case studies of significant historical-artistic interest.

Cover image: elaborated 3D model of the north tower, Bashtova Fortress (Albania)

DICATECh

2022

Rosella Alessia Galantucci

Innovative methods and techniques for diagnostics and monitoring of architectural heritage, through digital image processing and machine learning approaches

POLITECNICO DI BARI

06

2022

D.R.R.S

Doctor of Philosophy in Environmental and Building Risk and Development

Coordinator: Prof. Michele Mossa

XXXIV CYCLE
Curriculum: ICAR 10

DICATECh

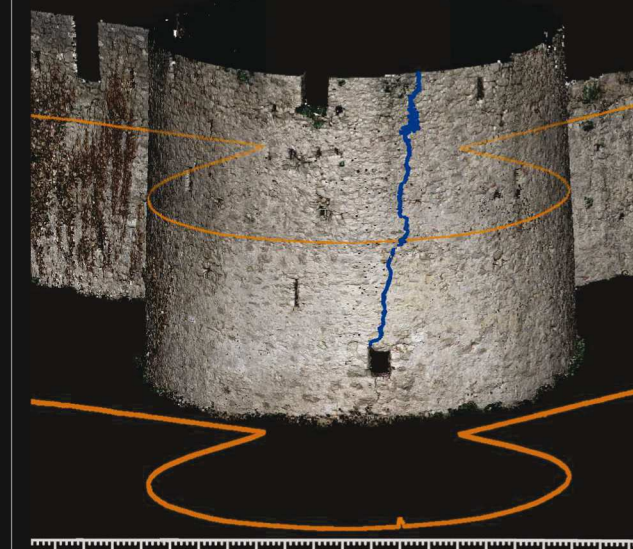Department of Civil, Environmental, Building Engineering and Chemistry

Rosella Alessia Galantucci

Innovative methods and techniques for diagnostics and monitoring of architectural heritage, through digital image processing and machine learning approaches

Prof. Fabio Fatiguso
Department of Civil, Environmental, Building Engineering and Chemistry

LIBERATORIA PER L'ARCHIVIAZIONE DELLA TESI DI DOTTORATO

Al Magnifico Rettore
del Politecnico di Bari

La sottoscritta Rosella Alessia Galantucci nata a Bari il 28/08/1991

residente a Bari in via Piccinni 186 e-mail rosella.galantucci@poliba.it

iscritto al 3° anno di Corso di Dottorato di Ricerca in "Rischio, Sviluppo Ambientale, Territoriale ed Edilizio" ciclo 34°

ed essendo stato ammesso a sostenere l'esame finale con la prevista discussione della tesi dal titolo:

"Metodi e tecniche innovative di diagnostica e monitoraggio di beni architettonici mediante approcci di digital image processing e machine learning"

DICHIARA

1) di essere consapevole che, ai sensi del D.P.R. n. 445 del 28.12.2000, le dichiarazioni mendaci, la falsità negli atti e l'uso di atti falsi sono puniti ai sensi del codice penale e delle Leggi speciali in materia, e che nel caso ricorressero dette ipotesi, decade fin dall'inizio e senza necessità di nessuna formalità dai benefici conseguenti al provvedimento emanato sulla base di tali dichiarazioni;
2) di essere iscritto al Corso di Dottorato di ricerca "Rischio, Sviluppo Ambientale, Territoriale ed Edilizio" ciclo 34°, corso attivato ai sensi del *Regolamento dei Corsi di Dottorato di ricerca del Politecnico di Bari"*, emanato con D.R. n.286 del 01.07.2013;
3) di essere pienamente a conoscenza delle disposizioni contenute nel predetto Regolamento in merito alla procedura di deposito, pubblicazione e autoarchiviazione della tesi di dottorato nell'Archivio Istituzionale ad accesso aperto alla letteratura scientifica;
4) di essere consapevole che attraverso l'autoarchiviazione delle tesi nell'Archivio Istituzionale ad accesso aperto alla letteratura scientifica del Politecnico di Bari (IRIS-POLIBA), l'Ateneo archivierà e renderà consultabile in rete (nel rispetto della Policy di Ateneo di cui al D.R. 642 del 13.11.2015) il testo completo della tesi di dottorato, fatta salva la possibilità di sottoscrizione di apposite licenze per le relative condizioni di utilizzo (di cui al sito http://www.creativecommons.it/Licenze), e fatte salve, altresì, le eventuali esigenze di "embargo", legate a strette considerazioni sulla tutelabilità e sfruttamento industriale/commerciale dei contenuti della tesi, da rappresentarsi mediante compilazione e sottoscrizione del modulo in calce (Richiesta di embargo);
5) che la tesi da depositare in IRIS-POLIBA, in formato digitale (PDF/A) sarà del tutto identica a quelle **consegnate**/inviate/da inviarsi ai componenti della commissione per l'esame finale e a qualsiasi altra copia depositata presso gli Uffici del Politecnico di Bari in forma cartacea o digitale, ovvero a quella da discutere in sede di esame finale, a quella da depositare, a cura dell'Ateneo, presso le Biblioteche Nazionali Centrali di Roma e Firenze e presso tutti gli Uffici competenti per legge al momento del deposito stesso, e che di conseguenza va esclusa qualsiasi responsabilità del Politecnico di Bari per quanto riguarda eventuali errori, imprecisioni o omissioni nei contenuti della tesi;
6) che il contenuto e l'organizzazione della tesi è opera originale realizzata dal sottoscritto e non compromette in alcun modo i diritti di terzi, ivi compresi quelli relativi alla sicurezza dei dati personali; che pertanto il Politecnico di Bari ed i suoi funzionari sono in ogni caso esenti da responsabilità di qualsivoglia natura: civile, amministrativa e penale e saranno dal sottoscritto tenuti indenni da qualsiasi richiesta o rivendicazione da parte di terzi;
7) che il contenuto della tesi non infrange in alcun modo il diritto d'Autore né gli obblighi connessi alla salvaguardia di diritti morali od economici di altri autori o di altri aventi diritto, sia per testi, immagini, foto, tabelle, o altre parti di cui la tesi è composta.

Luogo e data Bari, 01/04/2022   Firma _____

Il/La sottoscritto, con l'autoarchiviazione della propria tesi di dottorato nell'Archivio Istituzionale ad accesso aperto del Politecnico di Bari (POLIBA-IRIS), pur mantenendo su di essa tutti i diritti d'autore, morali ed economici, ai sensi della normativa vigente (Legge 633/1941 e ss.mm.ii.),

CONCEDE

- al Politecnico di Bari il permesso di trasferire l'opera su qualsiasi supporto e di convertirla in qualsiasi formato al fine di una corretta conservazione nel tempo. Il Politecnico di Bari garantisce che non verrà effettuata alcuna modifica al contenuto e alla struttura dell'opera.
- al Politecnico di Bari la possibilità di riprodurre l'opera in più di una copia per fini di sicurezza, back-up e conservazione.

Luogo e data Bari, 01/04/2022   Firma _____

Politecnico
di Bari

Department of Civil, Environmental, Building Engineering
and Chemistry
Environmental and Building Risk and Development
Ph.D. Program
SSD: ICAR/10–TECHNICAL ARCHITECTURE

Final Dissertation

Innovative methods and techniques for diagnostics and monitoring of architectural heritage, through digital image processing and machine learning approaches

by
Galantucci Rosella Alessia

Supervisor:

Prof. Fabio Fatiguso

Coordinator of Ph.D. Program:
Prof. Michele Mossa

Course n°34, 01/11/2018-31/01/2022

Department of Civil, Environmental, Building Engineering and Chemistry

Environmental and Building Risk and Development Ph.D. Program

SSD: ICAR/10–TECHNICAL ARCHITECTURE

Final Dissertation

Innovative methods and techniques for diagnostics and monitoring of architectural heritage, through digital image processing and machine learning approaches

by

Galantucci Rosella Alessia

_____

<u>Referees:</u>

Prof.ssa Manuela Grecchi

Prof. Camilla Mileto

<u>Supervisor:</u>

Prof. Fabio Fatiguso

Coordinator of Ph.D Program:

Prof. Michele Mossa

_____

_____

Course n°34, 01/11/2018-31/01/2022

D.R.R.S

POLITECNICO DI BARI

06
2022

Innovative methods and techniques for diagnostics and monitoring of architectural heritage, through digital image processing and machine learning approaches

Prof. Fabio Fatiguso
Department of Civil, Environmental, Building Engineering and Chemistry

Rosella Alessia Galantucci

D.R.R.S

Dottorato in Rischio e Sviluppo ambientale, territoriale ed edilizio

POLITECNICO DI BARI

06

2022

Coordinatore: Prof. Michele Mossa

XXXIV CICLO
Curriculum: ICAR 10

DICATECh
Dipartimento di Ingegneria Civile, Ambientale, del Territorio, Edile e di Chimica

Metodi e tecniche innovative di diagnostica e monitoraggio di beni architettonici mediante approcci di digital image processing e machine learning

Prof. Fabio Fatiguso
Department of Civil, Environmental, Building Engineering and Chemistry

Rosella Alessia Galantucci

EXTENDED ABSTRACT (eng)

In Civil or Building engineering, the assessment of the state of conservation of a building or an infrastructure is fundamental, for monitoring and conservation purposes. This is of paramount importance also in the context of Cultural Heritage, where artefacts are denoted by historic-artistic interest, and often in widespread damaged conditions. The actual state of practice refers to costly and time-consuming technologies and equipment, often requiring invasive actions, or difficult applications. In Civil Engineering, several research works address these criticalities through the implementation of digital technologies like image processing or artificial intelligence. However, most proposals are applied on 2D data, with substantial losses of 3D information, and often single-defect oriented. On the contrary, in Cultural Heritage domain their diffusion is still scarce, with reality-based 3D data used mainly as reference for geometrical survey. In addition, there is a substantial lack of unified protocols for the acquisition and processing of data, finalized to the quantitative inspection of built heritages.

In light of this, the aim of this research is to define, analogously to other fields of Engineering, innovative diagnostic approaches, to support the experts in the phase of knowledge, before planning an intervention. The evaluation of the general conditions of a building has been proposed through the analysis of reality-based 3D data, acquired by means of photogrammetry. Specific mapping and computerized evaluation routines have been created, for the detection of various decay morphologies, as defined by sectorial standards, through qualitative and quantitative analysis systems. Digital Image Processing and Machine Learning techniques have been adopted and implemented on high resolution three-dimensional models (dense point clouds, texturized polygonal meshes), to define distinct pipelines tailored on the basis of the kind of damage to investigate (geometry-based or colour-based alterations). A scalar strategy was outlined, articulated in different paths and levels of details.

Furthermore, they have been tested on a plurality of case studies of significant historical-artistic interest, belonging to the territorial, regional or international, cultural heritage. Their heterogeneity, in terms of epoch, building type, surface material,

architectural components and decay phenomena, allowed the experimental application of the proposed workflows, demonstrating their suitability and adaptability to the building diagnostic domain. Indeed, exterior walls, portals and pillars of Palmieri residential palace (XVIII century), portions of a tower in the medieval fortress of Bashtovë (XV century), or the interiors of the Romanesque cathedral of San Corrado (XII/XIII century), were considered because they are all characterized by decay phenomena expressed by changes in the geometry and shape, like stone surface decay (lacks, erosions, alveolizations..) or static instabilities (crack patterns). While specific areas of the archaeological site of Egnatia (I century B.C), or internal environments of ex-convents, like San Leonardo and Cappuccini, were selected, in light of chromatic-based modifications consistently affecting them, mainly ascribable to humidity problems. Those conditions have been monitored within intervals of years, in order to control their evolution overtime.

The present research lays out an advancement in the analysis and control of the state of conservation of buildings, especially in cultural heritage domain, providing an articulated methodological workflow, to obtain and collect investigation data for the pre-diagnosis phase. Some principal contributions concern the possibility to achieve both qualitative and quantitative insights on different decay morphologies, starting from reality-based 3D data, with remote, non-invasive, semi-automatic procedures, in support of diagnostic activities. Furthermore, flexibility and scalability are paramount conditions, to address the peculiarity of the diagnostic process, in the perspective of a reduction of time cost requirements, a simplification of the investigation plan and a minimization of dependence from the technician's expertise.

key words

Cultural Heritage, Building Diagnostics, Monitoring, Photogrammetry, Digital Image Processing, Machine Learning

EXTENDED ABSTRACT (ita)

Nell'ambito dell'ingegneria civile e edile la valutazione dello stato di conservazione di un edificio o di un'infrastruttura è di fondamentale importanza, a fini di monitoraggio e di conservazione, tanto più in riferimento al patrimonio architettonico di interesse storico-artistico in condizioni di diffuso degrado. In tale contesto, il rilievo e la diagnostica attualmente fanno riferimento a tecnologie e strumentazioni onerose per costo e tempo, che sovente presuppongono interventi invasivi o di difficile attuazione. Nel campo del monitoraggio di infrastrutture diversi studiosi affrontano queste criticità attraverso l'implementazione di tecnologie digitali come l'image processing o l'intelligenza artificiale. Tuttavia, la maggior parte delle metodologie sono spesso orientate al riconoscimento di un'unica tipologia di difetto, e applicate su dati bidimensionali, comportando quindi la perdita di informazioni tridimensionali. Al contrario, la loro diffusione è ancora piuttosto limitata nel settore dei beni culturali, ambito nel quale i modelli tridimensionali reality-based sono utilizzati principalmente come riferimento geometrico. Inoltre, vi è una mancanza di protocolli unificati per l'acquisizione e l'elaborazione dei dati, finalizzati all'ispezione e al controllo del patrimonio costruito.

In virtù di tali considerazioni, il lavoro di ricerca ha preso avvio dalla necessità di definire, in analogia a prassi esplorate in altri settori dell'ingegneria, approcci di diagnostica innovativa, di supporto agli operatori nella fase di conoscenza di un manufatto, preliminare alla progettazione di un intervento. Il progetto di ricerca mira ad un esame delle condizioni generali di un edificio mediante specifiche metodiche di valutazione computerizzata qualitativa e quantitativa di dati fotogrammetrici, volta all'individuazione e alla mappatura delle morfologie di degrado definite nelle normative di settore. Nel dettaglio, tecniche di digital image processing e machine learning sono state implementate su modelli tridimensionali ad alta risoluzione (nuvole di punti, mesh poligonali testurizzate), configurando opportune strategie scalari, ad un livello di dettaglio crescente, in relazione alla tipologia di degrado da investigare (alterazioni basate sulla geometria o sul colore).

Tali procedure sono state validate su una pluralità di casi studio di rilevante interesse storico-artistico, appartenenti al patrimonio culturale territoriale, a scala regionale o internazionale. La grande eterogeneità, in termini di epoca, tipologia costruttiva, materiali, componenti architettonici e fenomeni di degrado, ha permesso un'ampia applicazione sperimentale dei flussi di lavoro proposti, dimostrandone l'idoneità e adattabilità alla diagnostica degli edifici. Esempi come la facciata esterna, il portale e i pilastri di palazzo Palmieri (XVIII secolo), la torre nord della fortezza medievale di Bashtovë (XV secolo), oppure gli interni della cattedrale romanica di San Corrado (XII/XIII secolo), sono stati presi in considerazione poiché caratterizzati da patologie associate a cambiamenti nella geometria e nella forma degli elementi architettonici, riconducibili al degrado superficiale della pietra (mancanze, erosioni, alveolizzazioni..) o a fenomeni di instabilità statica (quadri fessurativi). Di contro, alcune aree del sito archeologico di Egnazia (I secolo a.c.), o alcuni ambienti interni degli ex conventi di San Leonardo e dei Cappuccini (XVI secolo), sono prevalentemente interessati da alterazioni su base cromatica, attribuibili soprattutto a problemi di umidità. Tali condizioni sono state monitorate in intervalli di anni, al fine di osservarne l'evoluzione nel tempo.

La presente ricerca propone un avanzamento nell'analisi e nel controllo dello stato di conservazione degli edifici, in particolare nel settore dei beni culturali, attraverso un articolato flusso di lavoro metodologico, finalizzato ad ottenere informazioni utili per la fase di pre-diagnosi. I principali contributi riguardano la possibilità di ottenere un approfondimento qualitativo e quantitativo su diverse morfologie di degrado, a partire da dati tridimensionali reality-based, mediante procedure remote, non invasive, e semi-automatiche, a supporto delle attività diagnostiche. Inoltre, la flessibilità e la scalabilità dell'approccio sono condizioni fondamentali, nell'ottica di una limitazione di costi e tempi, di una semplificazione del piano di indagini e di una riduzione della soggettività e dipendenza degli esiti dalle competenze del tecnico.

key words

Patrimonio architettonico, Diagnostica per gli edifici, Monitoraggio, Fotogrammetria, Digital Image Processing, Machine Learning

INDEX

LIST OF FIGURES

11

LIST OF TABLES

INTRODUCTION

General context of the research

In the last decades, the field of restoration and refurbishment of the built heritage gained an increasing interest, because of the considerable number of existing buildings in need of renovation. Most of them are in widespread conditions of degradation, structural instabilities, and in many cases abandonment, due to a variety of factors such as obsolescence, lack of maintenance, atmospheric agents, climatic changes and calamitous events.

These considerations are even more valid in case of architectures with historical-artistic value, according to the UNESCO definition of "cultural heritage"[1] [1].

As a consequence, there is an urgency to carry out interventions, for their protection, conservation and valorisation, in order to recover their integrity, functionality and aesthetics and to give them a new life over time.

A primary aspect in every restoration or maintenance project, concerns the assessment of the residual performance of an artefact, through the development of a well-structured knowledge and diagnostic process, for the identification of the main historic characters, construction techniques, phases and modifications, and the general state of conservation [2].

Owing to the complexity and heterogeneity of the existing architectural heritage, all these elements should be inserted in an organic framework, for a comprehensive understanding of the building, ensuring a harmonization of the single parts and an optimization of time and techniques.

Indeed, the qualification process, better known as *building diagnostic,* is a composite and articulated task, performed through a plurality of data collection methods and techniques, enabling the identification of types, causes and remedies for building faults, anomalies and defects. The research of evidence of malfunction and problems affecting

---

[1] The UNESCO definition of *Cultural Heritage* includes monuments, groups of buildings, sites of "outstanding universal value from the point of view of history, art or science" ([1]).

the building, or its parts is utterly important to identify the main phenomena and their causes, in order to avoid the occurrence of serious failure.

There exist different kind of measuring techniques and instrumentation, mainly categorized according to their level of interaction with the object of investigation: they are destructive, if altering samples of its materials; intrusive, when temporarily affecting its performances, or non-intrusive, if they do not modify the whole system at all [3].

Generally non-invasive investigations are performed as on-site surveys and physical measurements, with the help of hand-held instruments such as flexometers, laser distance meters, Vernier calipers; crack meters deformeters; photography, infrared thermography, ecc; or sensors embedded in the building [3] [4].

All these diagnostics techniques come into a workflow (Fig. 1), organized in three fundamental macro-areas (preliminary knowledge, pre-diagnosis, diagnosis), which starts from the observation of the technical features, the general state of conservation and the visible defects. It goes into detail of the probable causes of the detected anomalies and the formulation of a diagnostic campaign plan (pre-diagnosis), until the definition of a final diagnosis, as a result of the elaboration and interpretation of all the data retrieved from non-destructive and non-destructive tests [2].

the diagnostic process

the diagnostic tools

physical structure failure

performance failure

anomalies survey

Visual check;
Colour photographs with standard chromatic scales;
Infra-red photographs;
Stereo-photographs;
Dimensional survey with metric tools

| 1 anomaly | 2 anomaly | k-1 anomaly | k anomaly |

prediagnostic analysis

Surveyed anomalies observation;
Specific bibliographies;
Study of building materials and components, technology, ect.;
Historical analysis of:
building technologies used at time of building construction;
construction technology used for the building component;
Diagnostic tree

| 1 prediagnosis | 2 prediagnosis | 3 prediagnosis | 4 prediagnosis |

instrumental/analytical survey

Quantitative/qualitative non-destructive methods for on-site tests;
Quantitative/qualitative destructive methods for on-site tests;
Researches with sample extraction for laboratory analysis;
Simulation on scale model

diagnostic analysis

Analysis of the instrumental survey results by physical/mathematical methods;
Fault tree;
Diagnostic tree;
Physical/mathematical methods and models;
Analysis of:
Components design process,
Components construction process,
Components assembling process,
External contextual data,
Use patterns fo inner environment,
Mainteinance interventions performed during building life cycle
Performance studies (performance programme check)

| 1 diagnosis | 2 diagnosis | 3 diagnosis |

cause identification

information dissemination

Anomalies/pathologies classified lists
Diagnostic handbooks/guides for comparison;
Handbook/guides for surveys and diagnostic procedures;
Fault tree;
Diagnostic tree;
Good building guides

requalification process

Analysis

Pre-diagnosis

Diagnosis

Fig. 1 - Diagnostic process [2]

Preliminary knowledge is oriented to the acquisition of information for a historical and technical-constructive qualification, the occurred structural or functional modification and the state of conservation of the artefact (Fig. 2). These objectives can be reached essentially through the historical research, in archives, libraries, heritage conservation institutions, land registries, and direct testimonials. While the direct on-site survey includes geometry, materials and construction techniques documentation, through the help of traditional metric tools (flexometer, distolaser, total station theodolite, laser scanner); photographic documentation; mapping of pathology and surface decay patterns (visual inspection and manual annotation on survey-sheets, and crackmeters or deformometers, in case of anomalies connected to the structure) [2] [5].
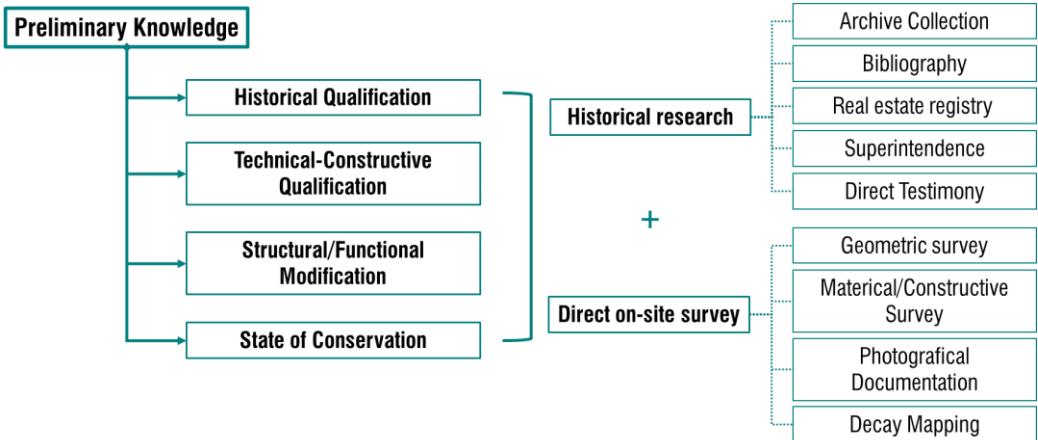
Fig. 2 – Illustration of the preliminary knowledge phase (image elaborated by the author, based on [5])

The pre-diagnostic phase allows the formulation of initial hypothesis on the detected anomalies, thanks to the results of the preliminary Knowledge. This is a fundamental step for the elaboration of an optimized diagnostic plan.

Given the complexity of the problem, there are some instruments which constitute a support or a guide for the professionals, to organize and orient the diagnostic investigations (fault-tree, diagnostic tree or model-based analysis), as illustrated in Fig. 3.
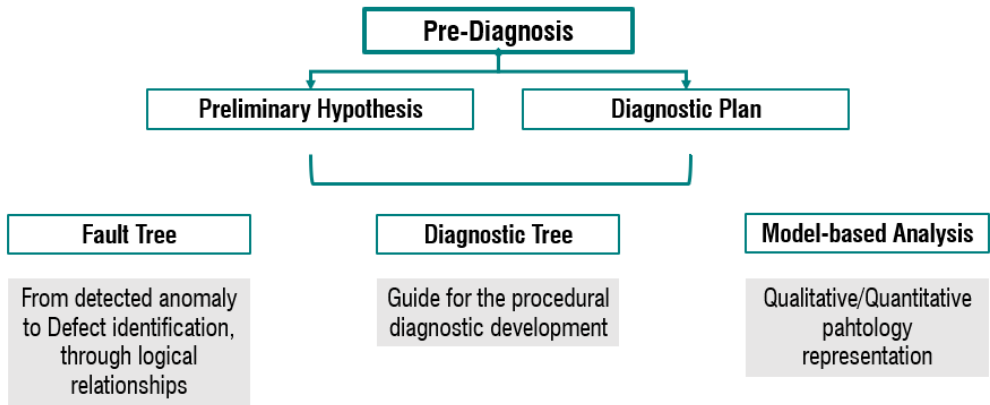
Fig. 3 – Pre-diagnosis: instruments (image elaborated by the author, based on [5])

The third macro-area concern the diagnosis of the detected anomalies, the identification of their causes and the planning of adequate interventions for the requalification process (Fig. 4). In this phase quantitative and qualitative destructive or non-destructive analyses, and experimental investigation (samples and tests) are performed, to obtain a deeper understanding of the detected phenomena and formulate a diagnosis. There are a variety of techniques, depending on the kind of anomalies to analyse. The outcomes are represented by a final formulation of a diagnosis, retrieved form the combination of the outputs of investigation tests, as projected in the pre-diagnosis phase, and the prior knowledge acquired along the previous phases[2].

Nevertheless, the state of art and practice in building diagnostic presents some critical issues: some aspects should be carefully taken into consideration, in order to properly shape the whole diagnostic procedure, particularly in relation to methodologies and techniques for architectural heritages.

First of all, in the preliminary knowledge, the direct on-site survey, as shown in Fig. 5, leading to the decay mapping, is a time consuming and demanding procedure, heavily influenced by the professional experience of the surveyors.
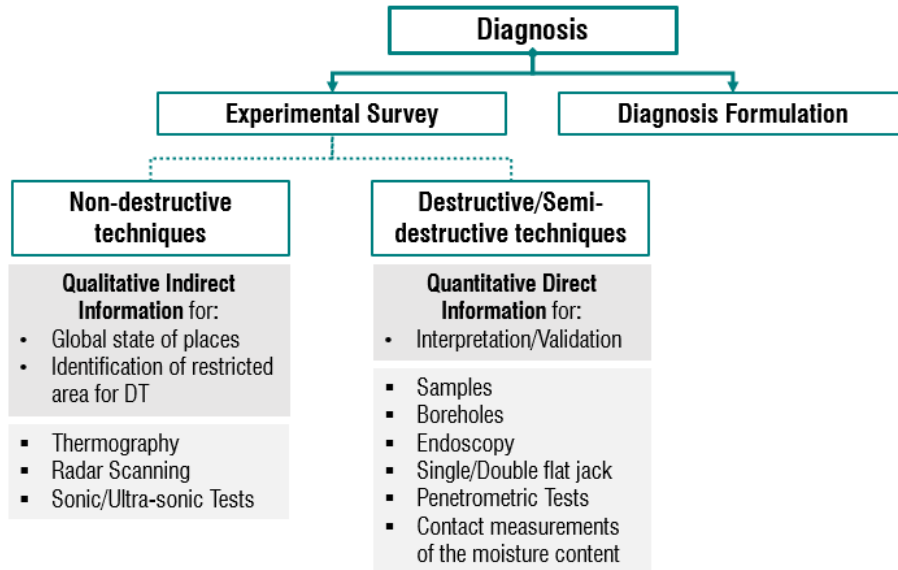
Fig. 4 – Diagnosis (image elaborated by the author, based on [5])

Hence, its results have to be considered as qualitative and subjective. The technician's knowledge and skills play a fundamental role in determining the reliability of the outcomes, the possibility to assess building's capability and to extrapolate a prognosis about the likely behaviour of the building in the future [3].
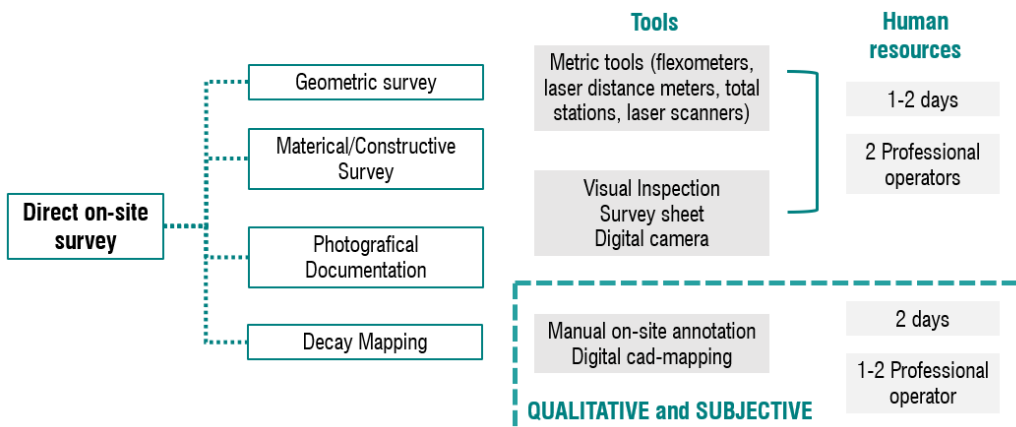
Fig. 5 - Specific focus on direct on-site survey (image elaborated by the author, based on [5])

After the preliminary knowledge (resulting from the on-site survey), and the preliminary hypothesis formulated in the pre-diagnosis phase, it is important to perform experimental tests on areas and components previously identified. As far as the diagnostic phase is concerned, there exist a plurality of alternatives, whose choice should be oriented to the goal of the investigation, in order to calibrate destructive and non-destructive tests. The various techniques and instrumentations require a certain level of expertise of the operators [2].

Furthermore, it is important to make the process as objective as possible, endorsing a wide use of non-invasive techniques, whose advantage lays in the possibility to cover extended areas, obtaining large amounts of information, without compromising the integrity and the identity of the artefact.

Therefore, the whole diagnostic process requires an optimization of time and costs, through a systematization of the current procedures, formulating new protocols and implementing innovative approaches.

To this end, a key role could be accomplished by ICT (Information and Communication Technologies) and digital technologies. Research advancements are increasingly concentrating on the collection and integration of heterogeneous data (documentary sources, on-site survey, analytical processing,…); but most of all for the regulation of innovative on-site diagnostic procedures, minimizing the use of intrusive techniques.

In particular, the development of three-dimensional models from reality-capture and photo-modelling is progressively acquiring interest in the field of documentation, preservation and maintenance of cultural heritage [13] [14] [15].

Literature gaps

Virtual reconstructions are applicable in numerous sectors such as: building production, control of single building components or entire buildings, diagnostics of the state of conservation and monitoring in construction, civil engineering and, especially, in the field of architectural restoration.

The current state of art highlights a great suitability of these techniques to diagnostic investigations, because they are non-invasive and contactless survey methods,

avoiding the risk of accidental damages, which could undermine the durability of the artefact [6–9] [16].

In light of this, some themes have been explored:

1) Integration of 3D technologies for digital documentation in historic buildings
2) Reality-based 3D data in Cultural Heritage
3) Image processing for damage detection
4) Artificial intelligence for image-based damage recognition and classification
5) Point cloud segmentation and classification
6) Change detection for monitoring and control of decay

In literature, the main gaps related to these subjects concern the use of reality capture 3D data mainly as reference for geometrical survey, while decay maps are still produced according to manual and traditional operations, and eventually linked to 3D models or virtual environments. There is a lack of unified protocols for the acquisition and processing of data, finalized to the quantitative inspection of built heritages.

The majority of automatic or semi-automatic image processing or artificial intelligence procedures are developed for civil infrastructure control and monitoring. Furthermore, they are applied mainly on 2D data, with a substantial loss of 3D information, and single-defect oriented.

Besides, at present segmentation and classification of point cloud in the field of built heritage, addresses mostly geometrical survey and architectural components detection.

Research aim

Reverse Engineering techniques make it easy to obtain high-resolution 3D models, even in case of wide and complex objects, which are suitably adoptable in the field of surface analysis and characterization. Indeed, the research started from the crucial consideration that three dimensional models play a fundamental role for sharing, interpreting and elaborating diagnostic data.

In this regard, the present work is focused on the exploration and research of the possibilities offered by the integration of reality capture-based models within the knowledge and diagnostic process, related to an architectural asset and its preservation

over time. Three-dimensional data, in the form of photogrammetric or laser scanning point clouds, could provide a considerable support to the technicians, within the whole diagnostic process, for a series of scopes, at different steps:

- Support in the inspection and clinical auditing
- Preliminary observation of the visible decay, with the possibility of remote assessment and control of decay patterns related to the constructive elements
- Groundwork for non-destructive or destructive tests planning, through an expeditious detection of affected areas
- Simplification of the investigation plan, with less invasive analyses and time and cost reduction
- Contactless, indirect detection and measurement of multiple decay morphologies
- Objective examination of pathologies through quantitative and geometric information
- Quantitative monitoring for the understanding of the decay progression overtime.

These objectives have been accomplished by the definition, testing and validation of non-invasive investigation approaches, with the help of non-destructive analyses and advanced surface metrology instruments on three-dimensional models, for the assessment and post-diagnosis control of the state of conservation of the architectural heritage.

Within innovative diagnostic procedures and workflows, deriving from consolidated lines of research ([15], [17], [18]), which exploit the role of augmented 3D data or environments, the present Ph.D. thesis is oriented to the achievement of a consolidated knowledge of the state of conservation of the artefact, from both direct and indirect interrogation of 3D photorealistic models, with an increasing level of accuracy (Fig. 6). As far as the methodological approach is concerned, in Fig. 7, a schematic representation of the operative workflow followed within the research project is proposed, where three fundamental phases are identified: data acquisition, quantitative analysis and decay monitoring.
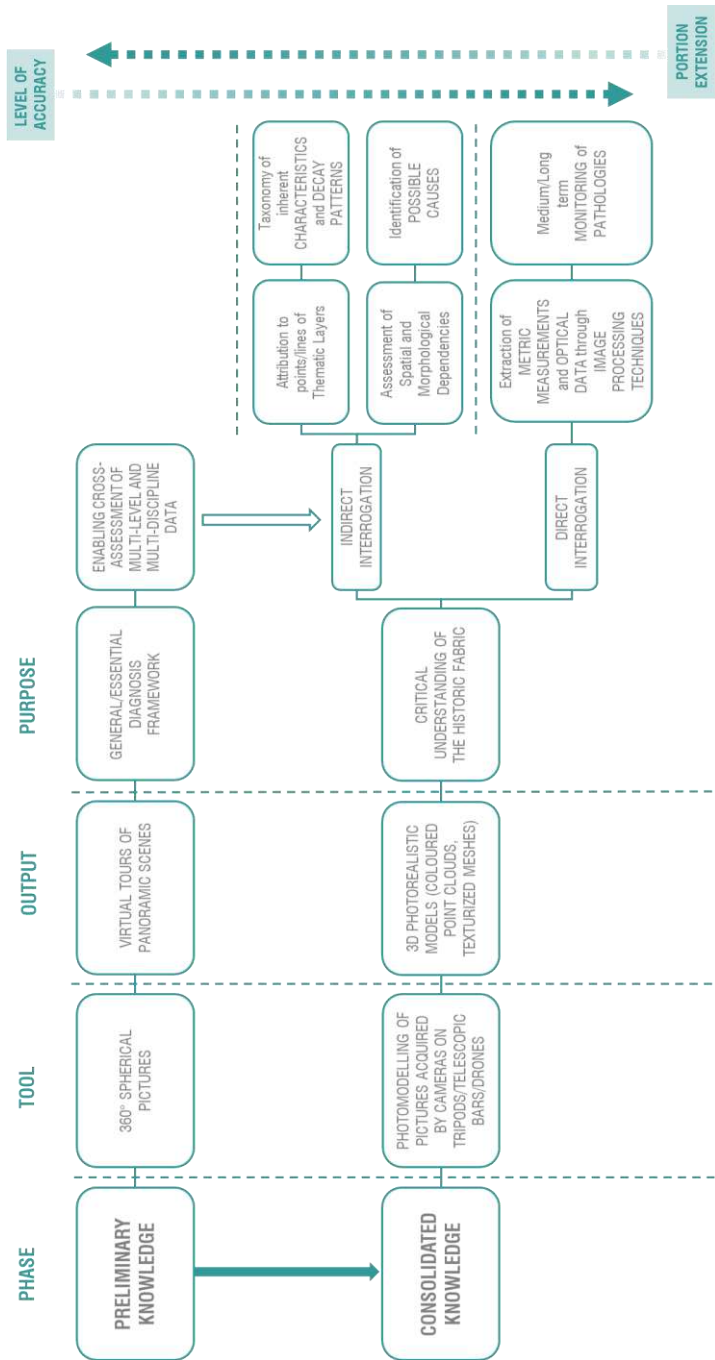
Fig. 6 – Innovative diagnostic procedures in building diagnostic pathology (image based on [17])

Main contributions

The main contribution of this research work is represented by an advancement in the analysis and control of the state of conservation of buildings and cultural heritage, through reverse engineering (photogrammetry, laser scanning, etc.), artificial intelligence and ICT systems, for the development of a thorough digital semi-automatic workflow, for decay analysis purposes. Image processing and machine learning routines have been implemented on point clouds, providing some principal advantages summarized as follows:

- Guidelines about innovative diagnostic procedures
- Operative framework for assessment and control of state of conservation
- Implementation of remote and non-destructive analysis
- Availability of new routines for decay detection
- Reduction of time cost requirements
- Simplification of equipment and its use
- Minimization of dependence from the technician's expertise
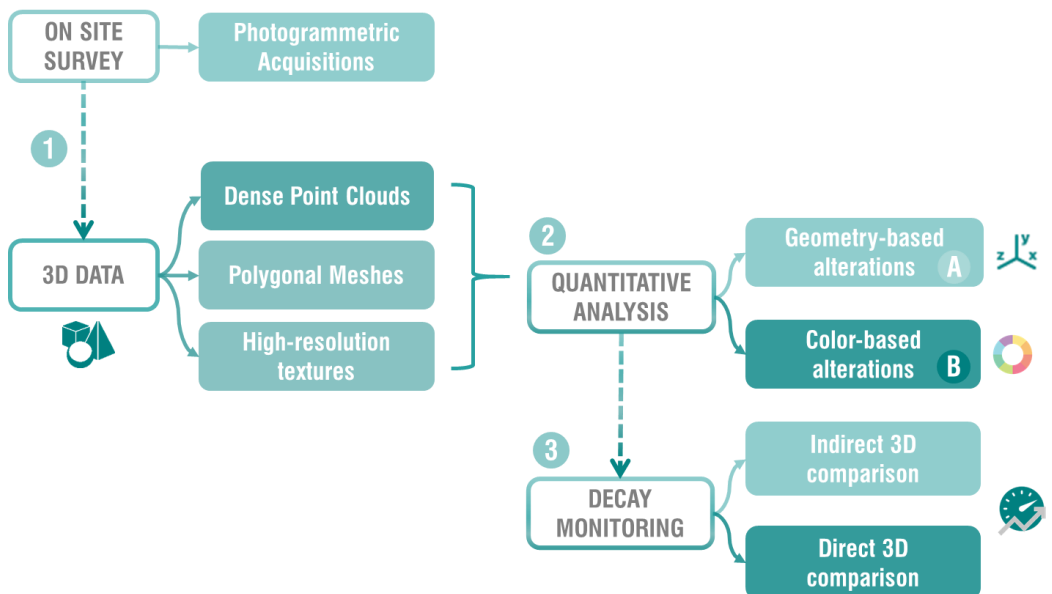
Fig. 7 - Schematic representation of the operative workflow

Structure of the thesis

The structure of the thesis is organized according to the principal topics faced and developed during the Ph.D. work.

After this introduction of the general context, the problem statement and the objectives of the research, the first part of the thesis (Section 1) provides overviews on international and national standards (Section 1.1), a comprehensive state of art in the field of non-destructive diagnostic techniques (Section 1.2), the integration of 3D technologies for digital documentation of the state of conservation in historic buildings (Section 1.3), with a particular focus on the use of reality-based 3D data in Cultural Heritage (Section 1.4). A second section of this chapter is dedicated to innovative damage detection and monitoring techniques, through the employment of digital image processing techniques (Section 2.1), artificial intelligence (Section 2.2), point cloud segmentation and classification (Section 2.3) and change detection (Section 2.4) for diagnostic and monitoring purposes.

The second chapter (PART 2) in first place proposes a theorical and operative workflow, in relation to the adoption of digital photogrammetry, to obtain 3D reconstruction of architectural heritages with diagnostic purposes (Section 4). Afterwards it examines the innovative approaches and protocols formulated along the Ph.D research work, on the one hand, for the quantitative assessment of the state of conservation of the artefact (Section 5), with separate approaches for geometry-based and colour-based alterations (Sections 5.1 and 5.2 respectively), and, on the other hand, for the geometric segmentation of architectural elements, to which decay forms could be associated (Section 5.3). In Section 6, approaches for the monitoring and control of occurring phenomena are presented, in order to prevent failures and serious damages.

The third part is organized in four sections, following the macroscopical organization of the methodological part (PART 2). A first section describes the selection of case studies, with heterogeneous and peculiar characteristics, with reference to heritage type, materials and constructive techniques, morphology, and construction age (Section 7).

In particular, a plurality of case studies was investigated, with specific experimental on-site and laboratory activities:

- Palmieri Palace (Monopoli, Bari, Italy - XVIII century) (Section 7.1)
- Bashtovë Fortress (Bashtovë County, Tirana, Albania - XV century) (Section 7.2)
- San Corrado Cathedral (Molfetta, Bari, Italy – XII/XIII century) (Section 7.3)
- S. Leonardo ex-convent (Monopoli, Bari, Italy – XVI century) (Section 7.4)
- Cappuccini ex-convent (Conversano, Bari, Italy – XVI century) (Section 7.5)
- Egnazia Cryptoporticus (Fasano, Brindisi, Italy – I century BC) (Section 7.6)

Consequently, an overview of the equipment and the technical details of the multiple acquisition campaigns is proposed (Section 8).

A total number of 21 on-site campaigns have been concluded, for the survey and acquisition of 3D data of 10 case studies (among which there are the cases illustrated above), for a total number of about 45 hours exclusively dedicated to the photogrammetric acquisition.

For the data processing and analysis, the 3D photogrammetric data reconstruction (including the whole process) took about 490 days.

Table 1 synthetically illustrate the typologies of works related to each case study.

The third section concerns: the application of the above-mentioned geometry-based (Section 9.1 A) and colour based (Section 9.2 A) alteration pipelines to the selected heritages; and an exemplificative experimentation of the segmentation of the architectural elements (9.3 A). Finally, Section 9 A accounts for monitoring and control analyses on the case studies. Concurrently, the outcomes of the applications are illustrated and discussed.

The final discussions summarize the principal achievements of the research work (Section 10). While, the last chapter addresses the fundamental conclusions, the highlighted criticalities, and possible future developments of the present work.

Afterwards, acknowledgements, references and a brief Curriculum Vitae.

Table 1- Synoptic table correlating case studies with the kind of analysis performed

		Palmieri Palace	Bashtovë Fortress	San Corrado Cathedral	S. Leonardo Ex-Convent	Cappuccini Ex-Convent	Egnazia Cryptoporticus
QUANTITATIVE ANALYSIS	Geometry-based alteration	[Image Processing Routines, Change detection]	[Image Processing Routines, Change detection]				
		[Geometric Feature Extraction, Change detection]	[Geometric Feature Extraction, Change detection]				
				[Change detection]			
	Colour-based alteration				[Range definition for moisture detection]		
					[Point cloud-based unsupervised machine learning]	[Point cloud-based unsupervised machine learning]	[Point cloud-based unsupervised machine learning]
					[Comparison with texture-based supervised learning]	[Comparison with texture-based supervised learning]	[Comparison with texture-based supervised learning]
DECAY CONTROL	Indirect 3D comparison	[Application of same routines]					
		[Measurements on 3D data]					
	Direct 3D comparison	[Change detection]	[Change detection]				
		[Cross-sections' evaluation]	[Cross-sections' evaluation]				

Legend:

- Image Processing Routines
- Geometric Feature Extraction
- Change detection
- Range definition for moisture detection
- Point cloud-based unsupervised machine learning
- Comparison with texture-based supervised learning
- Application of same routines
- Measurements on 3D data
- Change detection
- Cross-sections' evaluation

PART 1

OVERVIEW OF
BUILDING DIAGNOSTIC
AND CONSERVATION
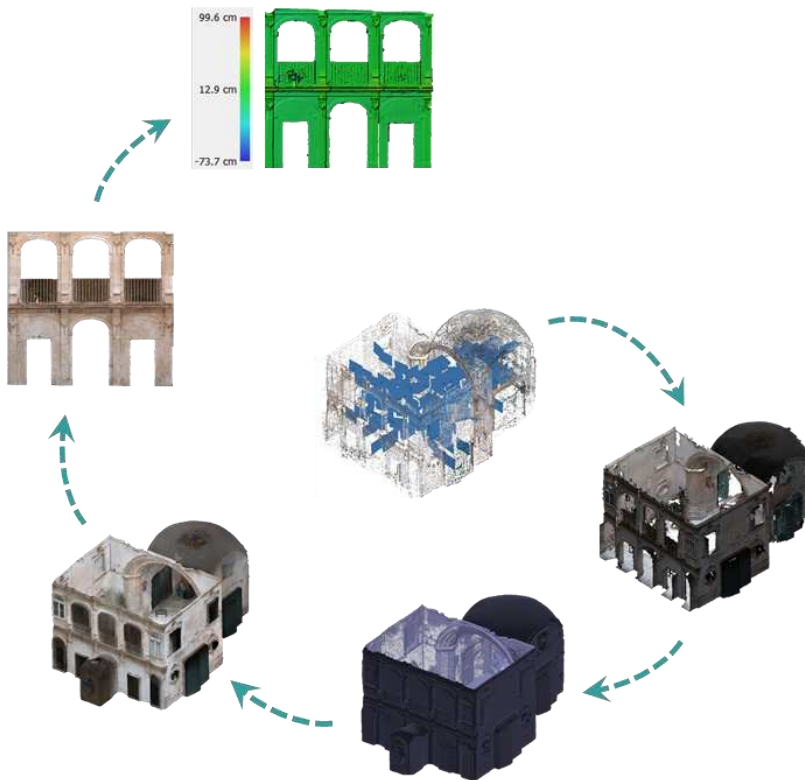
1. GENERAL CONTEXT OF BUILDING DIAGNOSTIC IN CULTURAL HERITAGE

1.1. International and National Standards and Guidelines

From an historical point of view, the reference standard framework in the field of Cultural Heritage refers to national, European and International conventions, charters, and declarations. By way of example, it is worth to mention the Venice Charter (1964), addressing the problem of the architectural restoration and the importance of conservation of historical asset of a building and the urban environment around it, after the Second World War [19]; the Italian Charter for Restoration (1972), elaborated by Cesare Brandi, who established the objects of preservation, protection and restoration [20]; the European Charter of the Architectural Heritage (1975), defining important concepts and principles for heritages [21], or the more recent ICOMOS Charter (2008), which identifies seven fundamental concepts for the comprehension and interpretation of cultural heritage sites [22].

The principles expressed in the above mentioned charters were assimilated in European Standards, which collect definitions, guidelines, good practices, examples to operate in perspective of conservation, maintenance and restoration of built heritages [23–25]. Going into detail, the on-site survey and the decay mapping of visible alterations in historic building is supported by a reference standard framework, which refers, most of all, to few international and national standards.

Indeed, in the national context, further legislations aimed at describing decay and pathologies of Cultural Heritage, specifically. In 1977, the Central Institute for Restoration (ICR) created the NorMaL Commission (Normalization of stone materials), who elaborated the NorMaL code 1/88 (Lexicon for the description of alterations and macroscopic degradations of stone materials). It provided a first classification of alterations on stone materials, with specific attention on the terminology, the definitions of the causes and the corresponding graphical representations [26].

NorMaL 1/88 has been replaced by UNI 11182 (2006), elaborated by the UNI – Cultural Heritages - Normal technical commission, which describes the form of visible alterations, affecting natural and artificial stone materials. It identifies 27 different

typologies of decay, accompanied by a textual and visual description of pathologies insisting on different materials [27].

The international ICOMOS 'Illustrated glossary on stone deterioration patterns' (2008) provides a common language, in order to recognize and compare degradation patterns. It supplies a qualitative differentiation in five categories of decay phenomena (cracks and deformation, detachment, features induced by material loss, discoloration and deposits, biological colonization), which is further articulated in sub-classes containing all the peculiar alterations (Fig. 8) [28].

Fig. 8 – Five macro-areas of surface alteration, identified by ICOMOS ([28])

However, in the field of Cultural Heritage there aren't rules for a quantitative analysis of decay through parameters and thresholds, which could be useful to automatically distinguish different defects typologies and to evaluate the risks connected to the architectural element [16]. In fact, every surface defect could be described by a set of features, related to its main characteristics, for a colour analysis, dimension verification and alteration assessment [29]. The existing standards do not contemplate the possibility to create a classification of damages, based both on qualitative and quantitative information about their geometry and extension, like for example in other fields of building or civil engineering, where in relation to pavement textures defect parameters are provided [30] [31]. Or standards for the geometric classifications of imperfection, like in the field of welding, in which shape descriptors are used to assess and quantify defects like longitudinal, diagonal, radial cracks, cavities and porosity [32] [33,34].

Within Cultural Heritage domain, a series of national standards and guidelines, like D.P.C.M. 23/02/2006, refers to qualitative evaluations of damage level in churches or historic buildings after seismic events, defined on the basis of experts' on-site observations. Specific guidelines provide insights on how to understand the failure phenomena, connected to the damage level [35] [36] [37]. In [38], quantitative thresholds are defined for decay patterns, in terms of percentages of failure extension. While the NTC 2008 provide indications for the evaluation of the state of conservation of masonry buildings, associating a confidence factor to each of the three levels of knowledge [39].

Another interesting hint comes from the national guidelines for the evaluation of the masonry quality, through the Masonry Quality Index (IQM), which enclose factors like the direction of acting loads, the structural behaviour (expressed as masonry quality). This is useful for the definition of quantitative criteria for the evaluation of the state of conservation of a masonry, through the translation of qualitative judgements into numerical indexes, by extrapolating features and descriptors from the reality-based 3D models [40][41] [42].

1.2. Non-destructive diagnostic techniques

As mentioned in the Introduction, the building diagnostic process is accompanied by conspicuous on-site surveys and experimental campaigns. Diagnostic tests are differentiated, according to the extensibility of their application and to their intrusiveness. Non-destructive techniques provide indirect information about the global state of conservation of places, with mainly qualitative outcomes; but, on the other hand, they allow the localisation of restricted critical areas, requiring in-depth analyses, through semi-destructive or destructive techniques. These typologies of inspection provide quantitative and direct information, for an interpretation and validation of the hypotheses. Nevertheless, they involve a direct interaction with the object, and consequently they might alter the state of places or affect the integrity of the artefact, so that a minimization of their use is utterly important. As a consequence, a paramount objective of current research in diagnostic field concerns the implementation or

definition of new non-destructive techniques, in order to retrieve as much information as possible, and particularly quantitative data, useful for diagnosis formulation.

The importance of non-destructive techniques as fundamental tools and preliminary steps for the achievement of an in-depth knowledge of the state of conservation of a building has been extensively demonstrated by a plurality of authors in the international landscape. In recent years, prevailing research lines were directed to the growth of innovative techniques, involving novel methods, instruments and tools, from the massive spreading of digitalization in different fields, or looking for original methods to exploit consolidated techniques.

As illustrated in Fig. 4, the main non-destructive techniques are: thermography, for the detection of water under the surface, the presence of different materials, or the thermic distribution, by means of infrared cameras; radar scanning, which analyses the reflection of electromagnetic waves, whose differences reveal the interfaces between materials with different dielectric constants; sonic/ultrasonic tests, which consider the time of flight of mechanical waves on low or high frequency, to detect the presence of voids or discontinuities.

Conversely, destructive techniques are:

- Samples, restricted area of coating removed to understand the masonry stratigraphy;
- Boreholes, cylindrical samples extracted to verify hypotheses on the stratigraphy or on the state of conservation of the masonry;
- Video-endoscopy, a video sensor introduced in a hole in the masonry, for a visual assessment of the stratigraphy and the conservation conditions;
- Single/double flat jacks, metal plates inserted in specific mortar cuts, in order to quantify the masonry compression strength or the operating stress;
- Penetrometric tests, for the compression strength of the mortar joints, through a vibration induced by a beating mass;
- Contact measurements of the moisture content, through the application of two electrodes, which measure the electrical resistivity of the masonry layers, corresponding to the humidity content [5].

The above-mentioned techniques must be related to the kind of pathologies mainly affecting an architectural heritage, and particularly a masonry building, according to the alterations catalogue inserted in UNI 11182 -2006 ([27]) and in the International Glossary on Stone Deterioration Patterns([28]). In experimental surveys of architectural heritages, the main anomalies to be considered are crack and moisture patterns. For the analysis of a crack pattern both thermography and sonic/ultrasonic tests could be useful: the first identifying interior fracture planes or discontinuity, resulting from a different response of the air to the infrared radiation; the second, respectively for multiple layers or single layers masonry, considering the higher crossing time of mechanical waves in correspondence with a fracture plane. In these areas, samples could be useful for a further validation of the detected phenomena. In the case of moisture patterns, thermography allows the evaluation of the presence of water under surface, as well as radar scanning, because of the low reflectivity/high absorption of the electromagnetic signal in presence of water. Boreholes can be extracted to perform laboratory tests or contact measurements of the moisture content (through the application of two electrodes to measure the electrical resistivity of the masonry layers, corresponding to the humidity content) (Fig. 9) [5].

In [43], the main non-destructive techniques like geo-radar, thermography, infrared photography, magnetometry, are applied to Italian cultural heritages.
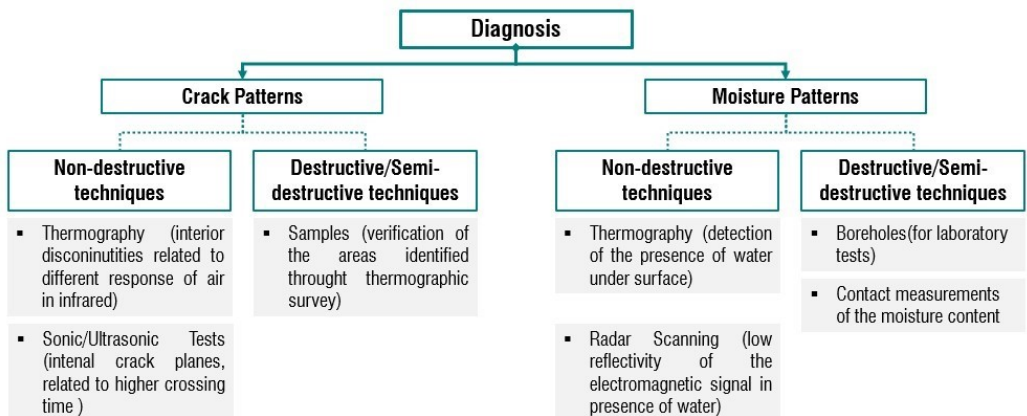
Fig. 9 – Correlation among non-destructive or destructive tests and the main pathologies to be detected in cultural heritages (image elaborated by the author, based on [5]).

In the last decades, beside these well-known diagnostic techniques, other alternatives are progressively spreading, based on ICT and digital technologies, for the documentation and general conservation of cultural heritages. Or, more specifically, innovative techniques finalized both to the knowledge of the artefact and to the investigation of decay phenomena by which it is affected.

As far as ultrasonic tests are concerned, hybrid ultrasonic methods have been used for the evaluation of the state of conservation of historical plasters, and particularly to search detachment in the architectural elements of thin vaults [44], [45]. Alternatively, ultrasonic pulse velocity (UPV) measurements were linked to 3D models, within a digital environment, to add quantitative information on qualitatively determined decay patterns [46].

In the perspective of deepening the knowledge of a heritage building, Agrafiotis et al. (2017) added to a conventional geometric survey of the visible surface, 3D models of the hidden structures, retrieved from ground penetrating radar radargrams (GPR) [47]. Indeed, the issue of 3D data augmentation with heterogeneous annotations related to non-destructive techniques was explored also in relation to thermography. For example, De Vita et al. (2019) applied thermal imaging and thermo-fluxometry to a historical building, to assess transformations or interventions, exterior or under surface degradation, and the masonry thermal capacity, for energy retro-fitting and renovation purposes [48]. In addition, thermography have been used also to obtain three-dimensional thermal models, for a comprehension of the as-is conditions of historic buildings or archaeological settlements [49] [50] [51]. In the same context, several authors addressed the issue of 3D geometric and thermal point clouds registration, for a thermal attribute mapping of building façades, within BIM or GIS environments [52] [53] [54].

In a similar way, other authors merge heterogeneous images (near infrared or multispectral images) with RGB images, to the purpose of acquiring supplementary information for the decay detection and control of the state of conservation [55] [56].

X-ray tomography or fluorescence have been adopted for the non-destructive appraisal of the results of cleaning processes on marble surfaces [57]. While, computed

tomography, combined with grey-level co-occurrence matrices allowed to detect micro-damages on concrete surfaces [58] [59].

Other works were aimed at the fusion of multiple-sources non-destructive tests data, into a unique integrated workflow, enclosing Digital Image Processing (DIP), Infrared Thermography (IRT), Laser Levelling (LL), Ambient Vibration Testing (AVT), and Ground-Penetrating Radar (GPR). They were all considered as boundary conditions for FEM analysis [60].

An exploratory review of the principal technological solutions for rehabilitions of heritage sites has been proposed by Kumar et al. (2020), where ultrasonic testing, 3D surface analysis, Nuclear magnetic resonance, 3D X-ray tomography, Image processing technique, or thermography are mentioned [61]. In parallel, also robotic applications have been developed in the field of cultural heritage inspection and conservation, to monitor inaccessible areas, with the help of robot prototypes [62].

1.3. Integration of 3D technologies for digital documentation in historic buildings

In the context of innovative diagnostic, especially in the field of Cultural Heritage, a significant role is played by integrated digital platforms for documentation of the state of conservation of historic buildings.

Indeed, in the last decade, several academics conducted their research efforts towards the creation of novel platforms, for the knowledge deepening, the integration of multiple sources of data, the annotation or semantic enrichment of 3D models [63], [64] [65] [66].

To mention some of them, a web collaborative platform *Aïoli*, was structured as an operative environment, in which photogrammetric models are enhanced through the Reflectance Transformation Imaging (RTI), to highlight non-visible details at naked eye [67]. *MONDIS* (MONument Damage Information System) is an informative system based on an ontological structure, as a support for documentation and deductive reasonings related to Cultural Heritage assessment [68], [69]. Else, another web platform, *NUBES*, entails the augmentation of 3D models, with links to 2D alteration maps [70]. In other research experiences, workflows were proposed for the link of 3D

heritage clouds and 2D orthophoto, on which deterioration patterns are manually highlighted, with the purpose of HBIM environments creation [71] .

As a further development, integrated digital environments were created, for the remote monitoring of architectural structures, through the elaboration of data deriving from on-site installed sensors. They are aimed especially to perform periodic measurements on detected cracks, which activate a risk alert system when values exceeds from determined thresholds [72], [73], [74]. In other cases, platforms involve also users' experiences and feedbacks, which concur to determine severity indexes, through mobile applications [75].

Other perspectives and possibilities are offered by the implementation of augmented or virtual reality (AR/VR) within digital three-dimensional environments, both for documentation, knowledge and conservation purposes.

For example, Nespeca et. al (2018) propose the integration of 360° panoramas within 3D digital models, for the virtual documentation of museum collections [76]. AR/VR are identified also as a faster and cheaper alternative with respect to reality-capture techniques (photogrammetry and laser scanning), when the lasts are not viable, for multiple documentation purposes enclosing damage analysis [77] [78]. Conversely, research is directed also to the retrieval of immersive virtual environments from laser scanning or photogrammetric 3D reconstruction, in order to operate a discrimination between two levels of detail: low definition for dissemination or fruition, and high definition for conservation [79].

Also, in the *NEPTIS* project integrated survey techniques led to the creation of the focused software *Conceptouring* and a related web-platform, for the understanding and dissemination of building spatial relationships [66]. Accordingly, Bekele et al. (2018) realized a comprehensive overview of digital technologies in Cultural Heritage, with particular attention to augmented and virtual reality, in terms of acquisition techniques, devices, systems or aims [80].

De Fino et al. add non-destructive diagnostic tests results into AR/VR environments or photogrammetric models, within a complete diagnostic workflow, at increasing levels of detail from preliminary to in-depth knowledge [18] [81]. Their results led to the

definition of an immersive digital platform *VERBUM*, for the collection and management of a plurality of information [82]. While, Napolitano et al. (2019) used image-based documentation and augmented reality for structural health monitoring scopes, with the manual annotation of degradation maps on 3D data in virtual environments [83].

In [84], a toolbox is presented, for the manipulation of raw data in the form of 3D point clouds, for documentation purposes. It is an immersive environment, in which it is possible to manipulate 3D data, using 2D planes to extract and visualize information. The architectural point clouds are inserted into the Virtual Reality platform *Immersia*. The manipulation by the user is performed in a virtual reality environment, interacting with the various tools and parameters.

A third macro-area, in relation to digital environments and platforms, concerns the utilization of the Geographic Information System (GIS), in combination with 3D scanning data, and eventually associated to Heritage Building Information Modelling (HBIM) for: documentation and management purposes in support of restoration activities [85], [86]; visualization of spatial and temporal changes in buildings [87]; automatic predictions of buildings degradation, in response of weather conditions observation and other environmental factors [88].

For example, some authors illustrated integrated workflows, enclosing reality-capture data and 3D GIS, for the creation of thematic maps related to decay mapping, risk representation and diagnosis formulation [89] [90] [91] [92].

1.4. Reality-based 3D data in Cultural Heritage

Reality-based three-dimensional data, obtained from photogrammetry or laser scanning, are applicable in numerous sectors such as: building production, control of single building components or entire buildings, diagnostics of the state of conservation and monitoring in construction and civil engineering. In the last decades, reverse engineering acquired a fundamental role in Cultural Heritage domain. In particular, photogrammetry is suitable to diagnostic investigations, because it provides non-invasive remote survey methods collecting a huge quantity of unorganized information, which could be extracted for diagnostic and monitoring purposes [6–8]. The greatest

advantage is represented by the affordability of equipment and procedures (easy-to-use standard level cameras, without specific requirements) [16].

However, in the field of Cultural Heritage, these techniques are still mostly used for documentation, touristic, cultural, historical dissemination, or geometrical survey [11,12] [13], virtual or 3D printed representations [79] [93] [94], for a better comprehension of the artefact itself.

Indeed, a plurality of researchers highlight the spreading of image-based techniques in Cultural Heritage domain, for digital documentation purposes, as a starting point for a more articulated process of enrichment and analysis [95] [96], with a view on the affordability of survey modelling techniques like photogrammetry, both at urban or at building scale [97] [98]. In [99], a state of art of the principal image-based and computer vision techniques, for the reconstruction of reality-based 3D models is proposed. Tucci et al. (2017) underline the importance of 3D documentation in the restoration process, within a multi-scale approach, for the creation of thematic maps and virtual restoration [100]. Nespeca et al. (2016) obtained thematic maps from 3D models of the artefact, to classify stones, to recognize carvings or previous restorations, the presence of detachment, corrosion or loss of material [101].

A specific research domain is focused on the digital documentation of archaeological sites, combining aerial (UAV), terrestrial and spherical photogrammetry or laser scanning, to acquire high-resolution orthoimages or 3D reconstruction, in support of archaeologist excavation and documentation activities [102] [103] [104] [105] [106]. Several examples are illustrated, like the application to Palacio Tschudi (Chan Chan, Peru) [107], to Huaca Arco Iris, (Chan Chan, Peru) [108], or to two archaeological areas of difficult access in the Sultanate of Oman [109]. While Aragón et al. (2018) propose different low-cost photogrammetric methods, for the documentation of underwater cultural heritages exposed to anthropic risk [110].

At the same time, in-depth comparisons have been realized between image-based and range-range based techniques, to highlight advantages and drawbacks of each one, in relation to the specific cultural heritage application [10] [14] [111] [112]. For example, Di Angelo et al. (2018) implemented a Analytic Hierarchy process (AHP) method to

select the best 3D scanning technique, within a plurality of choices like aerial, terrestrial or close-range photogrammetry, structured-light, triangulation-based or time-of-flight laser scanner [113]. Given the heterogeneity of cultural heritages in terms of scale, from archaeological site to single architectural element, it is not possible to determine a unique solution, to achieve 3D reconstruction and digital documentation. Indeed, several authors propose the integration of image and range-based techniques, in order to exploit reciprocal advantages, in hybrid techniques for close-range photogrammetry with laser scanning [114] [115], or multi-scale and multi-resolution 3D models, combining aerial photogrammetry and laser scanning [116].

Again, Moyano et al. (2020) collate close-range photogrammetry and Terrestrial Laser Scanning (TLS) on the basis of the point density of point clouds, verifying the models' accuracy through extracted profiles comparison [117].

While, in [118], four different scanning systems have been applied for the reconstruction of a Neolithic dolmen, to increase the level of detail in accordance with the scanned object, providing an overview of the main advantages and drawbacks.

Also, Valero et al. (2016) compared and merged different reality-capture technologies (TLS and photogrammetry) for the monitoring of historical buildings, on the basis of a series of criteria, such as: data completeness (max/mean point density), efficiency (processing time), data accuracy and precision (Haussdorff distance between point clouds). They demonstrate the value of photogrammetry, as cost-effective and accurate alternative to TLS, previa appropriate acquisition planning [119].

2. INNOVATIVE DAMAGE DETECTION AND MONITORING TECHNIQUES

While the use of 3D virtual reconstruction is already widespread in the areas of documentation, dissemination and fruition, their employment in support of the diagnostic process seem less explored [15].

Indeed scientific literature, about reality-based 3D models, in relation to the evaluation and control of the state of conservation and residual performances of historic buildings, is still under development, introducing elements of novelty both in procedures and tools, like, for example, imaging techniques based on automatic routines for the detection of technical characteristics and surface alterations; or machine learning algorithms for the segmentation and classification of material-construction types. They are already adopted in other research fields, concerning most of all, monitoring and control of infrastructures.

2.1. Image processing for damage detection

Image processing is widely developed for the condition assessment of civil infrastructures. A plurality of research works combines sequences of image processing algorithms, to perform fully automatic or semi-automatic procedures on images of concrete structures or road pavement surfaces.

Indeed, a large quantity of studies focus on the detection of cracks, through the elaboration of images with specific algorithms. In [120], a comprehensive state of art about crack detection on concrete surfaces is provided. They analysed fifty papers in which alternative solutions to the manual inspection are proposed, organized according to data acquisition system or image processing technique.

A common workflow have been identified, articulated in a first pre-processing step for the data preparation (noise reduction, image enhancement, morphological operators,…), an actual image processing stage, enclosing binarization, edge extraction, thresholding, to isolate the desired defect, and a computational phase, in which crack measurements are retrieved through geometric feature extraction.

For example, in [121], thematic maps representing the strain field of a surface are elaborated on the basis of displacements among homologous circular grid targets on time series images. In this work, high-pass filter has been used for image enhancement, morphological operators for noise reduction, Otsu's thresholding for binarization, and geometric descriptors to compute crack parameters like width. The same concept of applying image processing algorithms to rectified images in a time interval, for the retrieval of displacements and deformations, is illustrated by Yang et al., who adopt the digital image correlation method to detect thin cracks on concrete surfaces [122]. A similar workflow is applied to transform images acquired through charge coupled devices, with weighted median filter for noise removal, opening for image enhancement, Otsu's thresholding for binarization. These steps are preliminary to compute geometric features like eccentricity, corresponding to the probability of being a crack [123]. In [124], image processing procedures like edge extraction, binarization and thresholding have been tested to detect cracks on images of glass surfaces.

Others proposed a multi-stage calculation, through Canny edge detector (gaussian filter, intensity gradient, non-maximum suppression, double threshold) to identify edges within the image; machine learning for the classification of detected edges as cracks or non-cracks; curve fitting to describe cracks with feature vectors and compute their geometric characteristics [125] [126].

As far as edge detection is concerned, in [127], Canny edge has been compared with Sobel edge, a faster procedure that isolates areas with higher change rate in the brightness gradient, for crack detection on road pavements. In alternative, statistical filtering like particle filter has been applied to video frames, performing numerical comparisons of image RGB-distribution matrices, following the idea that the colour distribution around a crack is gaussian [128]. While in [129], the gaussian distribution of the 2D cross-section is used to detect cracks through Savitzky-Golay filter, after a pre-processing with Phase Symmetry-Based Crack Enhancement, an algorithm which operates identifying objects with a tree topology as representative of cracks. In another work, crack patterns have been retrieved thanks to the Laplacian of a gaussian algorithm, which detect fast changes in intensities, analogous to cracks [130].

The majority of studies in this area are applied on images, within a 2D environment, thus disregarding the third dimension, related to crack depth. Therefore, a further development of the previous approaches concerns the inclusion of the depth perception within the crack detection workflows. This aspect was faced in different ways. Some authors utilize photogrammetric depth maps (2D images with scalar fields representing depth) [133] [134]. Others apply image processing filters directly on 3D surfaces, for example of road pavements, on the basis of cracks depth or surface normal orientation [135] [136] [137].

As far as general condition assessment is concerned, a minor number of studies proposed the use of image processing for the detection of multiple kinds of alterations, including in the investigation other forms of decay besides cracks.

Koch et al. (2015) proposed a state of art of visual condition assessment for infrastructure inspection, in light of the principal phases of each procedure (pre-processing, segmentation, feature extraction, object recognition, structural analysis), enclosing a plurality of defects (delamination, spall, efflorescence, rust staining, cracking, abrasion) related to the constructive element on which they emerge, with related quantitative condition states. [138]. For example, railroad images have been treated with denoising, morphological operators, thresholding, feature extraction and object detection, for the recognition of obstacles or spalling [139]. For the assessment of concrete spalling or deformations, further advancements have been brought by the association of image processing algorithms to best fitting procedures (total least square method, ransac,…), applied on 3D data deriving for laser scanning or photogrammetry, for the control of construction quality [140], the assessment of severity levels bridge elements, according to the National Bridge Inspection Standard (NIBS) [141], or following probabilistic approaches [142].

In Cultural Heritage domain, the state of art and practice is quite diverse, because the automatic or semi-automatic decay detection is still little explored, although in recent years, some methodologies have been experimented. Former works adopted photogrammetric orthoimages, for the extraction of cracks, through Canny edge detection and binarization [7]. While in the ultimate lustrum, some authors proposed

damage detection approaches on 3D data, acquired from Unmanned Aerial Vehicles (UAV) [8] [143]. Others exploit TLS data for specific aims: to measure the thickness of a vault [144]; as reference to realize a Finite Element Method (FEM) model, for the observation of vibration, rotation and flexion [145]. Three dimensional photogrammetric data have been used also for the displacement analysis at different scales, from macro-elements (naves, façades,..) to constructive elements (walls, columns, pillars,…), until the level of single architectural components (capital, archivolt,…) [146]; for the detection of ageing carvings on plasters, through surface curvature computation, edge detection (Frangi filter), and colour enhancing to increase shadings [147]; or to map weathering effects like scaling on small monuments [148].

2.2. Artificial intelligence for image-based damage recognition and classification

In a complementary way, both in civil and building engineering, and partially in Cultural Heritage, artificial intelligence has been integrated to digital image processing, for damage recognition and classification, but always on 2D images. Mishra et al. (2021) provide a review of the principal state of art artificial intelligence techniques for the structural monitoring of built heritage: from support vector regression (supervised learning based on predictive algorithms), Naïve Bayes (supervised classification based on Bayes theorem), fuzzy logic, adaptive neuro-fuzzy inference system, random forest (randomly choosing variables to build trees as candidate sets of variables), k-nearest neighbourhood (based on the Euclidean distance between data with similar attributes), artificial neural network (reproducing the biological functioning of human brain), and Convolution Neural Networks (used for crack detection on concrete/pavement images) [148].

This multiplicity of methods are adopted for visual inspection and condition assessment. In particular, supervised machine learning has been used to automatically detect and classify plural defects (longitudinal and transversal crack, patches and potholes) on road pavement images [149]. Supported vector machine has been considered in a series of applications, to automatically classify alterations like cracks, mortar missing, brick damage on brick masonry walls, concrete surfaces or bridge

components, after a training with sets of significant texture features or multi-features vectors of images [150] [126] [151]. In alternative, supported vector machine helped urban scale classifications on high-resolution multispectral images, to distinguish roof, façades, shadows, built-up areas, or base soil [152].

On the other hand, deep learning, and particularly, convolutional neural network, has been adopted to identify the main classes of visible pathologies on a masonry bridge, or to rapidly locate unaffected areas, with a three-step procedure: manual annotation of defects in dataset images; segmentation of images in smaller window patches, for the CNN training, defect classification strategies [153], or with a sliding-windows techniques [154] [155].

In alternative, other approaches combine different deep learning strategies, with the double function to firstly locate cracked areas through region-based convolutional neural network, and then to segment cracks, or to extract features for the crack width and length computation, thanks to structured random forest edge detection [156], and to fully convolutional neural network [157], [158], [159].

With respect to stone surfaces of monuments or architectural heritages, there are fewer research works, proposing deep learning or artificial neural network systems for crack detection [160], or weathering defect classification, like flaking, contour scaling, cracking, differential erosion, black crust, efflorescence, higher plants, and graffiti [161]. A further advancement is represented by the work of Gong et al. (2021), who perform an object recognition of the main architectural elements, by applying deep learning procedures (edge-enhanced CNN - Mask R-CNN) on 2D images. Results are projected onto a texturized 3D mesh model, and, for repetitive objects losses, are computed by reciprocally comparing analogous elements and exploiting surface symmetries. The procedure was tested on small portion of the Great Wall in China [162].

2.3. Point cloud segmentation and classification

As already mentioned in the previous sections, image processing and artificial intelligence are gradually emerging in the field of Cultural Heritage. Therefore, certain

approaches focus on their application on reality-capture 3D data (TLS or photogrammetric point clouds), instead of 2D images, but most of all for geometric segmentation scopes. The underlying demand is to extrapolate organized and meaningful information, from noisy, sparse and unorganized datasets, such as point clouds, through segmentation, which allows the gathering of pixels or points with similar features into homogeneous regions [163] [5]. Until now, segmentation approaches utilize spatial and geometrical relations between points to morphologically distinguish objects [164].

Indeed, some authors provide surveys of the principal up-to-date point cloud segmentation and classification methods, categorized on the basis of their clustering criteria. Nguyen et al. (2013) realized a taxonomy of segmentation methods, distinguishing five main types: edge-based (based on normal, gradients, principal curvatures), region-based (seeded/unseeded or bottom-up/top-down), attribute-based, model-based (Hough transform, RANSANC, MLESAC, MSAC, PROSAC), graph-based [165]. Grilli et al. (2017) added a further group, related to the application of machine learning procedures like k-means or hierarchical clustering, pinpointing three classification modes: supervised (a large amount of annotated data is needed for the training), unsupervised (no annotations are requested), interactive (the user can guide the segment extraction by providing feedbacks about the outcomes) [166]. Updates have been supplied also by Hossain et al. (2019), which analyse strength and weaknesses of each segmentation techniques, in relation to software tools [167].

Hybrid techniques, exploiting region-growing or model-fitting segmentation through RANSAC, identify main architectural elements like roof, walls, façades [168] [169] [170], or objects in general [171] [172].

Barsanti et al. (2017) started from region-growing and other state of art methods, for the segmentation of architectural elements of a temple, in order to retrieve a FEM model from the segmented meshes [173].

Other authors adopt region growing approaches on octree-based voxelated representation, for urban environments segmentation and extraction of building parts

[174], or to distinguish multi-planar masonry façades, on the basis of depth values [175].

As far as machine/deep learning is concerned, it is possible to find a plurality of experimentations about the geometric segmentation of point clouds, aimed at the recognition of constructive elements like arches, walls, columns, capitals, cornices, freezes, floors, … A preliminary step to accomplish this objective, is represented by geometric features extraction, useful for the training of classifiers (covariance features, normal-based features, height-based features,…). Multiple methods have been tested and compared, such as: random forest [176] [177] [178] [179], one-versus-one, 1D and 2D CNN, Bidirectional Long Short-Term Memory layer (Bi-LSTM) [180] [181],or a Dynamic Graph Convolutional Neural Network [182] [183] [184].

Going towards smaller elements scale, a proposal for the automatic segmentation of masonry ashlars and mortar joints, has been translated in a specific CloudCompare plugin [185]. The pipeline is based on the application of 2D continuous wavelet transform on the depth maps, estimating a width value for the mortar joints and producing a binarized map, adjusted through the application of morphological operators, and then projected onto a 3D model. The outcomes have been further analysed, in order to identify areas of mortar recess, likely corresponding to vulnerable regions of the masonry [186].

All the illustrated methodologies for point cloud segmentation, even with the inclusion of artificial intelligence, have been valorised for architectural elements recognition, above all. However, interesting opportunities are represented by the exploitation of reality-capture 3D data, for the assessment of the state of conservation of architectural heritages. In fact, more recent works started to investigate this issue, by integrating colour-related features to the geometric ones. For example, Valero et al. (2019) evaluated isolated regions according to geometry-related parameters (ratio outliers/inliers, roughness, mean distance, distribution of normal vectors, area, elongation, rectangleness, circularity, number/area of unconnected defective areas), texture-related parameters (contrast, energy, correlation, homogeneity) and colour-related parameters (dispersion of hue, dispersion of value, range of hue, range of

value), to recognize and classify defects like erosion, delamination, mechanical damage, non-defective areas [187]. This process is performed at a single masonry ashlar level, in continuation with the geometry segmentation mentioned in [186].

Unsupervised texture-based or pixel-based segmentation methods, applied on 2D orthoimages or UV maps and then reprojected in 3D, have been experimented for the automatic recognition of different building techniques or the presence of previous restoration works on ancient walls [188] [181].

Apart from these few examples, colour-based segmentation of point clouds remain related to geometric object recognition [189] [190]. Furthermore, colour-based segmentation is essentially linked to 2D images, where region-growing act on colour similarity and spatial proximity, for the detection of decay patterns recognizable from their predominant colours or their chromatic differences [191] [192], for the perception of aesthetic decay in the limestone, according to the colour distribution of the façades [193]; to document the presence of carvings and grooves on rock art panels, through exaggerated shading [194], or to detect rust stains on painted steel surfaces [195].

2.4. Change detection for monitoring and control of decay

The last investigated aspect, in relation to decay detection on reality-based 3D data, concerns the evolution of pathologies over time, and their control and monitoring, through the comparison of time series of data.

A plurality of solutions have been proposed, like the detection of colour changes on photogrammetric 2D images (orthoimages, DEMs or depth maps), from archaeological bass-reliefs to historical buildings or at a territorial scale [191] [196] [197] [198]. While the application of neural network techniques on sequential crack images, acquired in time intervals, led to the control of crack patterns developments [199]. In alternative, planimetric and vertical comparison of topographic maps and TLS scanning assessed changes occurred in an ancient theatre [200].

With respect to 3D data, deviation maps among point clouds and digital microscope data provided a salt damage control on stone surface [201], or an evaluation of cleaning treatments on wall paintings, through the localization of dirt crusts layers [202].

Hallerman et al. (2015) utilized geo-referenced UAV 3D data of masonry structures, for remote measurements and documentation of changes, to overcome limits of time consuming and labour intensive current practices [8] [203].

Post-disaster monitoring, by comparing before and after laser scanning point clouds, have been used to assess displacements, in case of a fire event, to analyse damages and plan interventions [204]. In addition, accuracy evaluations of reality-based 3D data have been realized, with respect to Total station acquisitions, demonstrating that LIDAR acquisitions are sufficient for general evaluations of post-disaster needs [205]. Going further, the processing of pre- and post-event high-resolution satellite images of earthquake affected heritage buildings, with advanced texture and feature extraction algorithms, allowed a fast damage survey of buildings [206]. Another research provides earthquake damage assessment for reinforced concrete walls, through BIM models enclosing geometric information, materials properties and the recognition of constructive elements, in order to determine a strength analysis model, a damage mode, and a damage severity [207].

The integration of meteorological time series with photogrammetric reconstructions helped to build a predictive graph database and a dynamic digital model, to understand and localize future weathering decay on heritage buildings [208].

While a three-year monitoring project, to evaluate the structural stability of the Olympic theatre in Vicenza, by confronting FEM models derived from photogrammetry and TLS [209]. Also, TLS and photogrammetry data have been exploited to quantify displacements occurred in an archaeological wooden roof structure, within a time interval, from the computation of the strain field [210], or from the deviation between the as-is point cloud and the ideal parametric model [211] [212].

3. GAPS IN KNOWLEDGE

In summary, what emerged from this overview is that the state of practice in building diagnostics is characterized by the need of unified procedures, combining the plurality of possibilities offered by the existing diagnostic techniques. The whole process is laborious and time consuming and needs to be adapted to the great heterogeneity of applications in Cultural Heritage. Furthermore, the knowledge phase strongly relies on technicians' ability and experience, with qualitative and subjective outcomes, which require to be completed with destructive analyses. On the contrary, the minimization of contact and intrusiveness of the diagnostic process is of paramount importance, in order to preserve historic buildings integrity.

In relation to the main themes investigated, the state of art revealed some specific gaps in knowledge. As far as the use of reality-capture for built heritages is concerned, the main shortcomings pertain the employment of reality-based 3D data mainly as reference for geometrical surveys, with a qualitative inspection and traditionally produced decay maps, used only as links to 3D models or virtual environments. Three-dimensional environments are exploited most of all for digital documentation, fruition and dissemination of cultural contents.

The diffusion of image processing methods allowed the creation of semi-automatic or automatic defect detection routines. However, they are mainly applied for the inspection, control and monitoring of civil structures (bridges, roads,..), while fewer approaches are developed in the Cultural Heritage domain. Moreover, the majority of civil structures inspection methods are single-defect oriented (crack patterns) and, above all, applied on 2D images, thus excluding the third dimension, essential for the evaluation of decay phenomena on 3D structures. The same considerations can be transferred to the use of artificial intelligence, chiefly adopted on images and focused on crack detection. In Cultural Heritage, it is still limited, by the difficulty to acquire great numbers of sample data to train machine or deep learning procedures, because of their huge variability of conditions (epoch, materials, constructive techniques, pathologies,..).

As far as point cloud segmentation is concerned, point clouds or texturized polygonal meshes are used primarily, for geometric segmentation purposes, and, particularly, for the recognition of the architectural elements.

Therefore, the present research work starts from the great potentiality of reality-capture and 3D models, aiming to address these gaps, in relation to some specific objectives:

- A remote assessment of constructive elements and visible decay patterns
- A support in inspection and auditing, for diagnostic tests planning
- A simplification of the investigation plan, with less invasive analyses
- The objective examination of pathologies through quantitative and geometric information
- A quantitative monitoring for decay progression understanding.
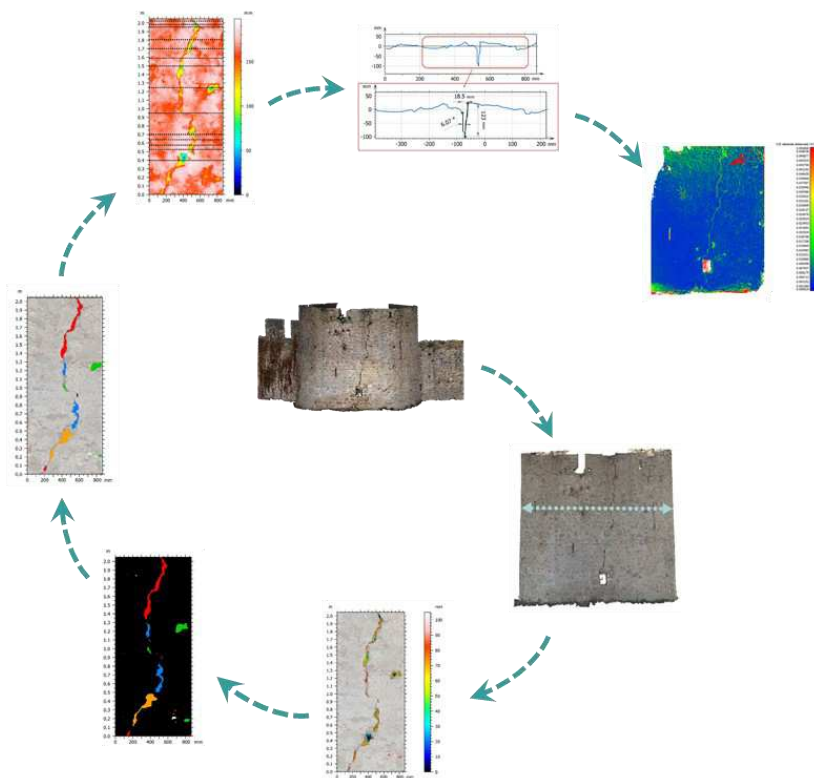
The second part of the thesis is dedicated to the illustration of the novel methodological approaches developed along the Ph. D. course. Nevertheless, a first premise is dedicated to the presentation of a photogrammetric theorical and operative workflow, for the achievement of reality-based three-dimensional reconstruction of architectural heritages, for diagnostic and monitoring analysis purposes (Fig. 10). Thereafter, a plurality of innovative approaches is proposed, in order to accomplish, both the assessment and monitoring of the state of conservation of the artefact. As far as decay detection is concerned, two separate methods address geometry-based and colour-based alterations visible on the surface. In addition, the geometric segmentation of architectural elements enables their association with the assessed damage morphologies. Moreover, multiple approaches are presented for the monitoring and control of occurring phenomena, in order to prevent failures and serious damages.
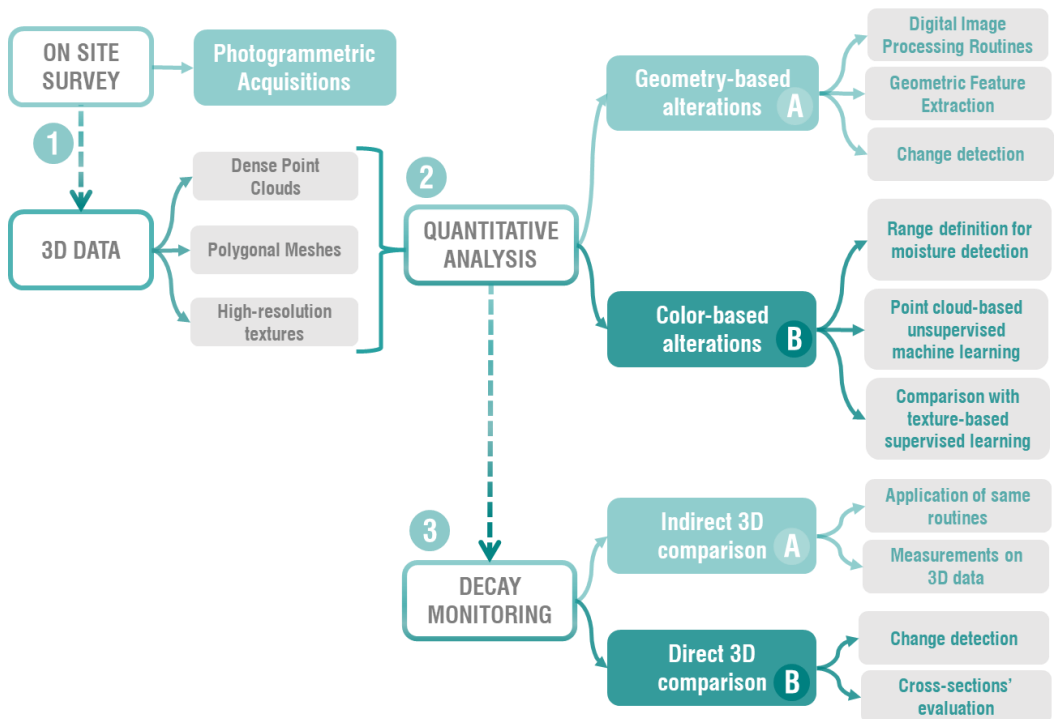
Fig. 10 – Novel methodological workflow

4. REALITY-BASED 2D/3D DATA ACQUISITION THROUGH REVERSE ENGINEERING

The first phase of the proposed methodological workflow concerns the acquisition of reality-capture 2D/3D data through reverse engineering techniques.

Reverse engineering is a process enabling the restitution of information through the deconstruction of a real object, even in case of large-scale and highly complex artefacts. The main outputs are represented by high-resolution virtual 3D data in the form of point clouds or texturized polygonal meshes.

The principal acquisition techniques are photogrammetry and 3D laser scanning, both mass-capture approaches for the digital survey, since they can acquire large amounts of data, appropriately selected during the processing phase.

The difference among the two techniques is the principle on which the geometric reconstruction of 3D coordinates is based: the first uses photographic images as fundamental measurement tools, to retrieve shape and location of an object (image-based), while the second exploits the return time of the emitted electromagnetic signals (range-based).

Photogrammetry is often preferable as scanning technique, due to the availability and affordability of instrumentation (compact cameras, bridge or reflex cameras, tripods or telescopic rods, drones) and the great adaptability of the method to the order of magnitude of the elements to be investigated.

4.1. Photogrammetry

4.1.1. Image alignment – Orientation - Collinearity
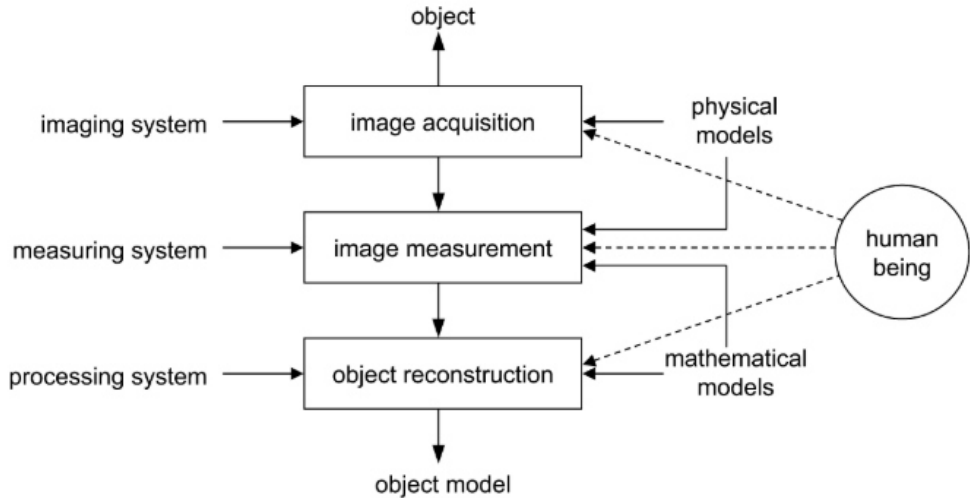
Fig. 11 – Photogrammetric acquisition/restitution process [213]

Photogrammetry can be defined as a process for the acquisition of data about a real object, in order to retrieve measurements and interpretations (Fig. 11). Information obtained from images are the source for the reconstruction of the 3D volume of the object, both from a geometric and radiometric point of view [214].

Indeed, this technique is based on central projection imaging, according to which shape and position of an object are determined, through beams of rays connecting points of the image and the corresponding perspective centres. In order to retrieve the geometry of an object, and to know its coordinates, it is necessary to refer to at least a pair of images (stereoscopy). To this end, images must be calibrated according to four types of orientation:

 i) internal (beam of rays relating to the object in space)

 ii) external (position and orientation of the beam of rays, with respect to the coordinates of the object in space)

 iii) relative (relative position and orientation of the cameras)

iv) absolute (scale, position and orientation of the 3d model, in relation to the coordinate system of the object in space).

Internal orientation parameters describe: the geometric model of the camera and the position of the perspective centre, in relation to a reference system fixed in the camera (image coordinate system); and the distortion (radial and tangential) of the image, represented by deviations from the ideal pinhole central projection camera. These parameters are quite invariants in the photogrammetric survey, since they are linked to the characteristics of the camera model provided by the manufacturer. In internal calibration, the scale factor of a photogrammetric image *(m)* should be taken into account, consisting of the ratio between the distance of the object from the perspective centre *(h)* and the main distance between the image plane and the perspective centre *(c)* (4. 1).

$m = h/c$

(4. 1)

External orientation parameters, on the other hand, specify position and orientation of the camera in the global coordinate system[2]. These parameters are calculated starting from points of known global coordinates.

Images are transformed by collinearity equations, according to which, at the acquisition time, point on object, shooting centre and point on image are on a straight line and the image is formed on a planar sensor.

This condition is expressed by relations between coordinates of the point on the image, of the corresponding point on the object and of the shooting point. These relations define the central perspective of a 3D object, through nine independent parameters: three of internal orientation (main distance c, principal point coordinates ξ_0 and η_0); six

---

[2] Shooting centre coordinates *xyz* and relative rotations between camera and object, expressed through the three asset angles of the camera at the moment of image acquisition

of external orientation (absolute coordinates of the acquisition centre X_0, Y_0, Z_0, attitude rotations r_{ij}[3]) (4. 2).

$$X = X_0 + (Z - Z_0)\frac{r_{11}(\xi - \xi_0) + r_{13}(\eta - \eta_0) - r_{13}c}{r_{31}(\xi - \xi_0) + r_{32}(\eta - \eta_0) - r_{33}c}$$

$$Y = Y_0 + (Z - Z_0)\frac{r_{21}(\xi - \xi_0) + r_{22}(\eta - \eta_0) - r_{23}c}{r_{31}(\xi - \xi_0) + r_{32}(\eta - \eta_0) - r_{33}c}$$

$$(4. 2)$$

The three-dimensional spatial coordinates of each point on the object can be retrieved from the images, based on the mutual position of the cameras that reproduce the same points of the object [213] [215].

---

[3] $r_{11} = cos\ \varphi\ cos\ \kappa$

$r_{12} = cos\ \omega \cdot sen\ \kappa + sen\ \omega \cdot sen\ \varphi \cdot cos\ \kappa$

$r_{13} = sen\ \omega \cdot sen\ \kappa\ -\ cos\ \omega \cdot sen\ \varphi \cdot cos\ \kappa$

$r_{21} = -\ cos\ \varphi\ \cdot sen\ \kappa$

$r_{22} = cos\ \omega \cdot cos\ \kappa\ -\ sen\ \omega \cdot sen\ \varphi \cdot sen\ \kappa$

$r_{23} = sen\ \omega \cdot cos\ \kappa + cos\ \omega \cdot sen\ \varphi \cdot sen\ \kappa$

$r_{31} = sen\ \varphi$

$r_{32} = -\ sen\ \omega \cdot sen\ \varphi$

$r_{33} = cos\ \omega \cdot cos\ \varphi$

4.1.2. 3D data reconstruction
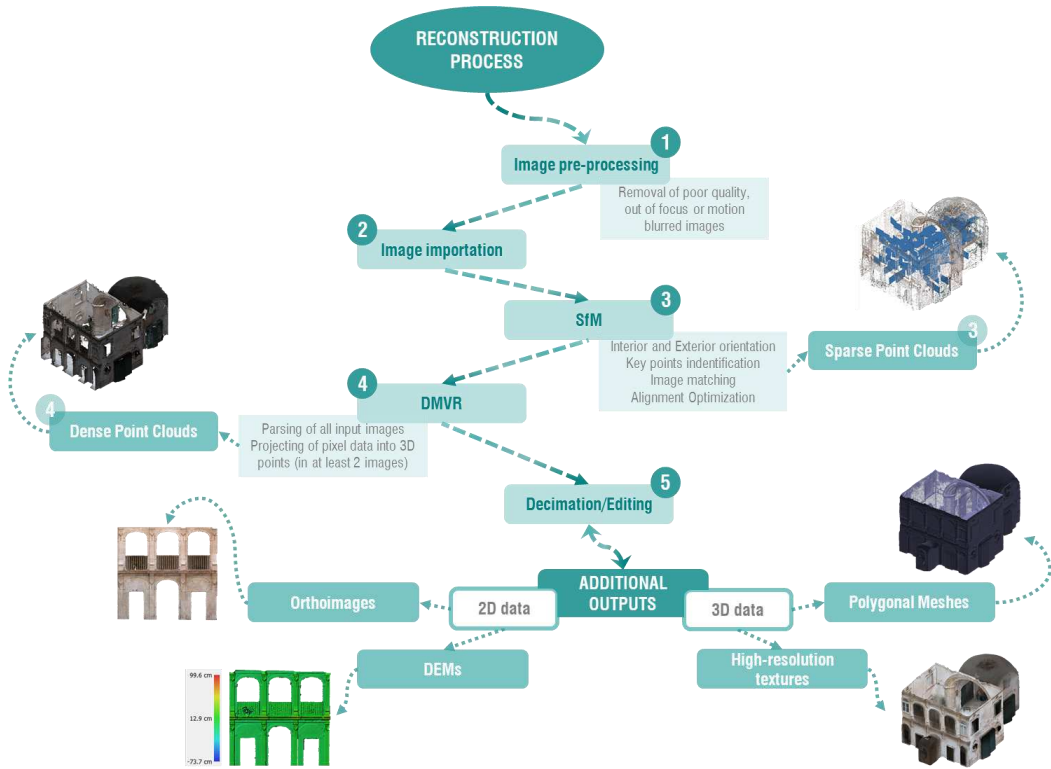
Fig. 12 – Graphical representation of the reconstruction process, followed in digital photogrammetry

Once the on-site acquisition is completed, 3D data reconstruction takes place according to Structure from Motion (SfM) [4] and Dense Multi-View 3D Reconstruction (DMVR) [5] algorithms (Fig. 12).

All the possible correspondences between pairs of images are combined and projected in 3D space. In other words, pixel data are transformed into 3D points, according to the computer vision algorithm Scale-Invariant Feature Transform (SIFT). It relies on the consideration that every object of the input images can be described by a series of significant points (key points), connoted by a good repeatability (independently from

---

[4] Structure from motion: process of estimating 3D structures from sequences of 2D images

[5] Dense Multi-View 3D Reconstruction: 3D models' reconstruction starting from unordered sets of images of the object, acquired from different points of view.

lighting conditions or noise level of the image). They are used to learn the object characteristics and to recognize them in other images. Indeed, photo are aligned by identifying and matching key points, recurring in pairs of adjacent images.

The application of SfM entails the estimation of interior and exterior orientation (as mentioned in section 4.1.1) of each image and all the possible relative orientation between pairs. Triangulation is used to retrieve relative positions of image pairs, and the process is optimized by the application of bundle adjustment, to bundle connecting camera perspective centres and 3D projected points. The output of the image alignment is a sparse point cloud made of tie points (key points matched in at least two images) [216].

The DMVR algorithm is responsible for the reconstruction of dense point clouds, through the estimation of all the possible features/key points, even those with low repeatability. They are representations of 3D structures, useful for understanding the distribution of shapes and the volume of the object in space, because they are made by a set of *xyz* coordinate points and their normal vectors in a shared reference system. Each point is enriched by radiometric values (in grayscale or colour scale).

The photogrammetric process produces several two and three-dimensional outputs beyond point clouds, such as polygonal meshes[6], textures[7], ortho-images[8] (Fig. 12).

The first kind of output of the photogrammetric process is the point cloud. Its quality is greatly influenced by the resolution of the images and the limits imposed to the number of points. A point cloud of a large object, like an architectural artefact, is composed by tens of millions of points. A polygonal mesh is generated on the basis of the point cloud, so its quality is strictly influenced by the resolution of the cloud. The geometry and the number of polygons in which the model must be divided can be choosen, in order to obtain a better approximation of the surfaces, especially if they are mainly curvilinear

---

[6] Sets of polygons, generally triangles, described by their vertices, edges, faces and faces' normal vectors.

[7] 2D images, reproducing the visible quality of the object, projected on polygonal meshes.

[8] Ortho-rectified 2D image, deriving from the stitching of input images.

and complex. A mesh model may be completed by high-resolution textures, which provide a real-colour representation of the scanned object.

High-resolution ortho-mosaics have a superior quality than single images and they are not affected by perspective errors and distortions, because they are reconstructed from a great number of images, which are aligned and joined together [4].

---

[11] X and Y define a plane parallel to the object, while Z represent the depth-coordinate

4.2. Photogrammetric workflow

4.2.1. Guidelines for the acquisitions

Photogrammetric scans consist of a series of photographic acquisitions, carried out according to some specific criteria, for the reconstruction of high or very high-resolution virtual 3D models.

The equipment consists of simple and easy-to-use instrumentation:

1. Compact, bridge or reflex digital cameras, with optical systems varying on the basis of the required resolution;
2. Camera supports (telescopic rods, tripods, UAV), depending on the position/accessibility of the elements to be scanned;
3. Mobile devices for remote shooting (tablet or smartphone);
4. Measuring instruments (laser distance meter, tape measure, bubble level, calibrated bars), for the localization of the shooting position and the collection of reference measurements useful for photogrammetric model scaling.

The expected quality of the output should be determined before the photogrammetric campaign, in order to guarantee the needed level of detail and information on the 3D data. It is important to clarify that the generic term "quality" encloses three different aspects/concepts: camera or scanner resolution, which refers to the smallest measurable element (geometric resolution refers to the physical size of the smallest measurable element); accuracy, indicating how much a measured quantity on 3D data is consistent with its actual value; precision, corresponding to the repeatability of a measure.

In particular, photogrammetric survey resolution is related to the size, in real world, of an element represented by a single pixel (ground sample distance *gsd*), which is a function of focal length (*f*), shooting distance (*H*) and pixel size (*p*) (4. 3).

$$gsd = (H/f) \times p$$

(4. 3)

The acquisition planning should be carried out, systematizing all factors affecting the quality of the outputs:

- camera (sensor size, sensor's number of pixels, focal length of the lens);
- object to be surveyed (extension, planimetric development, volume);
- site configuration (shooting distance, presence of physical obstructions);
- scans execution (percentage of overlap between adjacent images).

In Fig. 13, a pyramidal schematization of the principal aspects and related factors affecting the quality of the output of photogrammetric scans is presented, showing the influence of their variation in increasing or decreasing the quality level.
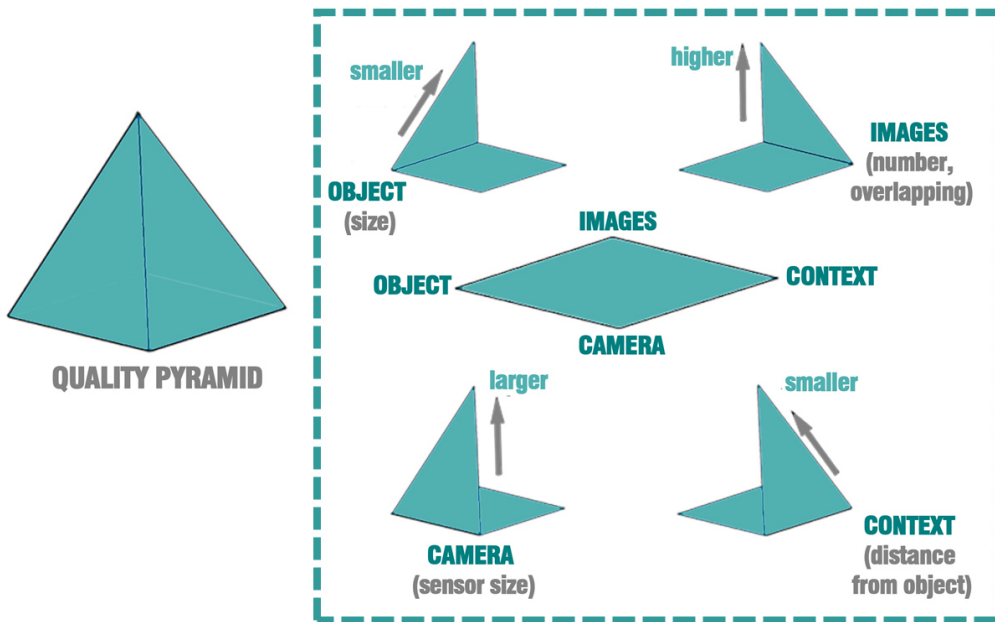
Fig. 13 – Graphical schematization of the principal factors influencing the quality of a photogrammetric scan (figure elaborated by the author, based on [215]).

As far as the optical system is concerned, to ensure constant shooting parameters, fixed focal length lenses are preferred, with focal lengths of 50-60 mm, for highly detailed data, and of 16-20 mm, for general acquisitions. Telephoto lenses (80-300 mm) have too limited field of view, resulting in scarce overlapping between images. Wide angles (8-10 mm), on the other hand, produces considerable distortions, in contrast with high quality output requirements.

Images must be acquired from at least two different points of view, with the camera parallel to the plane of the object. For an optimal result, it is better to choose equidistant shooting positions (with a constant step in x and y), at a pre-fixed distance from the object, depending on the demanded degree of overlap (about 80% between consecutive images, along the shooting direction; around 60% between adjacent lines, orthogonal to the shooting direction). It is important to consider also the lighting conditions of images, which should be preferably analogous, with uniform and diffuse light.

Shooting distance has a significant influence on the final quality, but is also strictly related to the configuration of the building and its context (accessibility, obstacles,…). Three ranges of distances have been identified, on the basis of the on-site experimentation:

- long distance (5-10 m) for general acquisitions of the entire building;
- medium distance (2-5 m) for more detailed acquisitions;
- short distance (0.5-1.5 m) for specialized acquisitions of single architectural components [5].

According to the experience acquired during former campaigns, these distances can be associated to different levels of 3D data resolution (Table 2):

Table 2 – Experimental correlation between shooting distance and 3D data resolution (ground sample distance, *gsd*)

SHOOTING DISTANCE	3D DATA RESOLUTION
m	*cm/pixel*
5-10	0.5-1
2-5	0.1-0.5
0.5-2	0.01-0.1

In the first range, compact mirrorless or bridges cameras are adequate, with wide-angle lenses used in automatic mode.

In the second range, scans can be carried out with mirrorless cameras or SLR (single lens reflex) cameras alternatively, with intermediate-angle lenses, at shooting distances in a range of 2-5 meters.

In the third range, SLR cameras should be preferred, with intermediate or narrow-angle lenses, at a shooting distance ranging from 0.5 meters to 2 meters. In the acquisition

phase it could also be necessary to use integrative ring flashes. In this case, photos should be taken with the help of a tripod, in manual mode, in order to decide and set proper times and aperture.

Given that the point cloud of an architectural artifact has an order of magnitude of several tens of thousands of points. The level of detail and the information content increase with the number of points and the size of the point cloud, together with the processing times and computational requirements. Therefore, the entity of the photogrammetric scanning campaign should be proportioned to the desired degree of information, which is always related to the aim of the survey.

On the basis of the shooting distance-resolution ranges, illustrated in Table 2, it is possible to assert that a *gsd* of 0.5/1 cm/px is sufficient for a first assessment of the visible state of conservation of a surface. 3D data do not contain much information, but they are useful to get a comprehensive idea of the overall state of places of an entire building, in rapid acquisition and processing times (fruition purposes).

A *gsd* of 0.1-0.5 cm/pixel corresponds to a higher number of details, for the retrieval of quantitative data about macroscopic alterations, connected to surface decay phenomena induced by material losses (erosion, lacks, mortar joints ejection, alveolization,…) (diagnostic purposes). In order to detect smaller alterations (cracks, micro-cracks, with amplitudes even below the millimeter) a very low *gsd* is preferred (0.01-0.1 cm/px), corresponding to really high-resolution of 3D data.

In order to properly orient and scale 3D data at the end of the process, in the acquisition phase, targets (ground control points) are put on the object, at known distances, as dimensional reference [17].

4.2.2. Operative workflow

The operative photogrammetric scanning protocol can be summarized in the following steps (Fig. 14):

1) Acquisition of information about the size and the geometry of the artefact (for example, approximate reconstruction of volumes using Google Maps or Bing Map).

2) Definition of the purpose of the survey and the required level of detail, on the basis of an on-site preliminary observation.

3) Choice of camera and lenses and calculation of the main scanning parameters (shooting distance, overlapping between images, number of photos, ...).

4) Verification of the weather conditions, in order to avoid rain, or too definite shadows. A cloudy sky represents the ideal condition for photogrammetric acquisitions.

5) On-site acquisition of more than two measures on the artefact, in order to get a reference measure to scale the model once the three-dimensional reconstruction has been completed. To this purpose, it is also useful to place markers at known distances on the object. The more the markers are distant, the less the result of the 3D model scaling is affected by error.

6) On-site tracing of a reference path, in correspondence of the predetermined shooting positions.

7) Setting of the shooting parameters (time, aperture, focus), in order to choose the optimal combination related to the on-site conditions. A normal exposure is preferred, with a uniform distribution of light inside the frame, without excessively shaded or lighted areas. Therefore, the use of camera flash is not recommended, since, unlike for ring flashes, light is not scattered, and it involves the loss of information.

8) Images acquisition. It is important to consider that images should be acquired, so that each element is captured from at least two different points of view, with a constant pace in x and y[11], at a pre-determined distance based on the required percentage of

---

[11] X and Y define a plane parallel to the object, while Z represent the depth-coordinate

overlapping between images. Two consecutive images should never be acquired with the camera in the same position because they could be difficult (or impossible) to align.

9) Images importation within photogrammetric reconstruction software, after the removal of poor quality, blurred or out of focus images.

10) Eventual pre-processing of the selected images, in order to adjust/uniform their exposure parameters.

11) Images alignment and optimization, for the retrieval of cameras mutual positions, the generation of sparse point clouds (tie points), and the optimization of the camera locations.

12) Scaling and orientation of the sparse cloud, fixing *xyz* coordinates of at least three points, measured on-site in a user-defined coordinate system. A minimum of two perpendicular distances are required. Selected points are characterized by an easy recognition in the images. Usually, they coincide with targets put on the object.

13) Sparse cloud decimation, removing points with high reprojection error[12] or high reconstruction uncertainty.

14) Dense point cloud reconstruction, setting the desired quality (which influence the eventual resolution reduction in the input images, the size of the input data and the processing time) and the depth filtering (for the removal of outliers/noisy points).

15) Processing of other photogrammetric outputs (polygonal meshes, textures, orthoimages, DEMs).

---

[12] It estimates the distance between a 3D point and the true point projection.
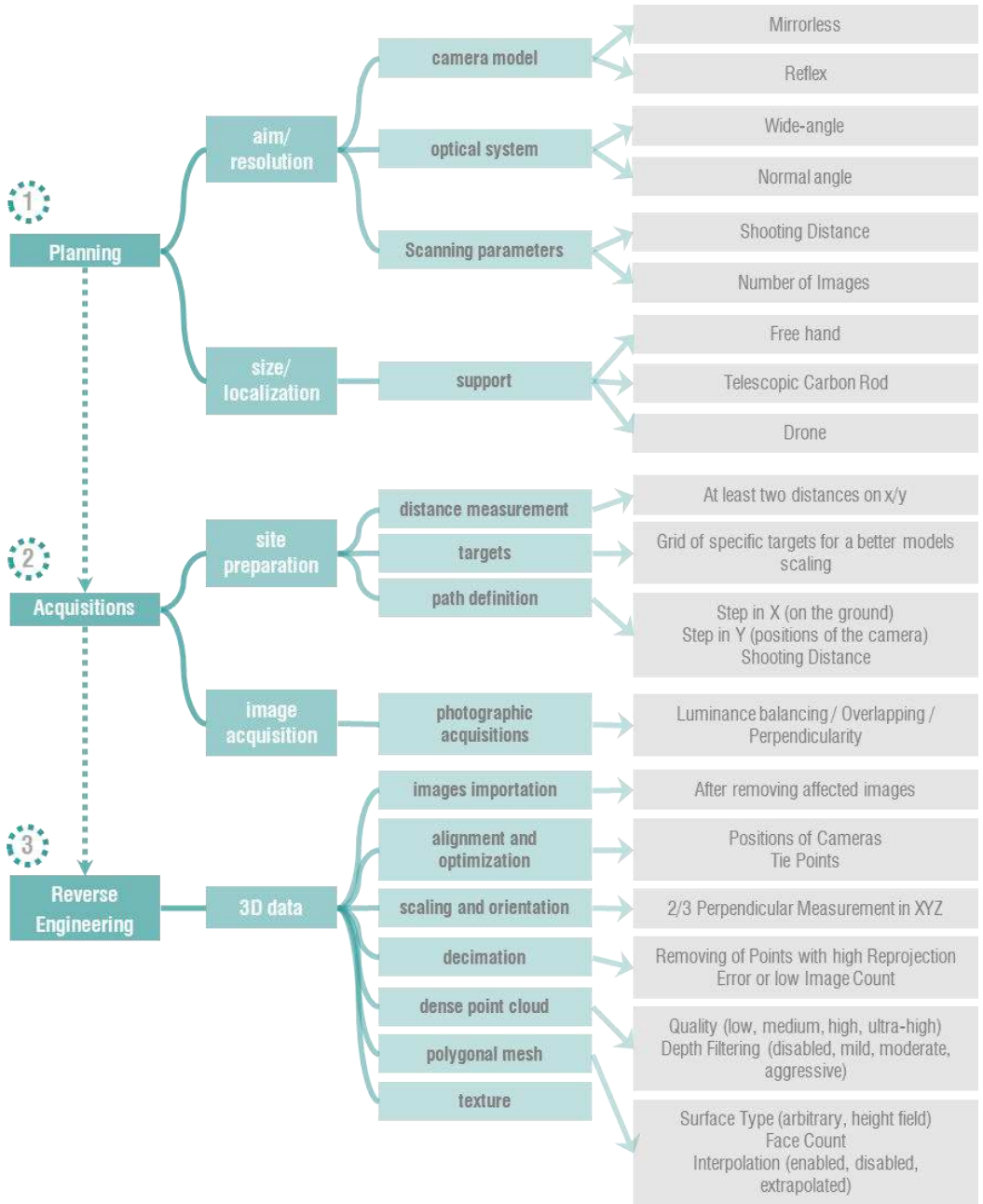
Fig. 14 – Operative workflow, illustrating all the different steps of the photogrammetric survey

5. INNOVATIVE ROUTINES FOR THE QUANTITATIVE ASSESSMENT OF VISIBLE DAMAGES AND SURFACE ALTERATIONS ON ARCHITECTURAL ARTEFACTS

In this section a methodological approach is proposed, focused on the role of photogrammetric 3D data, eventually inserted in virtual immersive environments, in support of the assessment, mapping and interpretation of decay evidence, within the building diagnostic process, in order to reach a consolidated level of knowledge about the artefact.

The procedure is oriented to the creation of innovative protocols for the restitution of onsite conditions, with reference to their spatial and morphological setting, to understand the origin of a phenomenon, like for example a static instability or a humidity problem.

Indeed, the possibility to survey and classify pathologies through quantitative metric and optical data contained in 3D models, entails a critical understanding of damages, and involves a simplification and rationalization of the diagnostic process and of the plan of investigations.

3D data, in form of point clouds, retrieved from the photogrammetric workflow, represent input models for the application of digital image processing and machine learning routines, with knowledge purposes, oriented to analyse the state of conservation of architectural heritages.

As introduced in section 4, one of the first considerations concerns the identification of the aim of the investigation, in order to properly plan and dimension the acquisition phase, and to distinguish the kind of routine to perform on 3D data.

In this regard, two macro-categories of surface decay have been differentiated, depending on their most characteristic set of features. The separation has been applied to masonry building surface pathologies, on the basis of the definitions illustrated in national or international standards in the field of architectural heritage, like UNI 11182 -2006 ([27]) and the International Glossary on Stone Deterioration Patterns([28]). In particular, geometry-based alterations refer to all those defects deriving from a

modification of the original geometry of the artefact or one of its parts. They enclose cracks[13] and deformations[14], or feature induced by material loss[15].

While colour-based alterations are related to colour changes visible on the surface, most of all due to the presence of water or chemical agents. They are grouped in discoloration and deposit, and biological colonization (Fig. 15).

The explored approaches are grouped according to the two macro-categories, because each of them, correspondingly, is described by its representative set of features (geometric or radiometric), and follows peculiar paths, as illustrated in the diagram in Fig. 16 (see A and B).

Indeed, point clouds can be treated with different processing routines, according to the kind of pathology to analyse: in presence of crack patterns, deformations, or generic degradation of stone surfaces (lacks, alveolization, erosions, ...), geometric information (*xyz* coordinates and normal vectors of each point) can lead to a quantitative determination of alterations; on the other hand, in order to detect decay patterns related to humidity (moist area, biological patina, vegetation, ...) it is convenient to act on the colour information.

---

[13] "Crack: individual fissure, clearly visible by the naked eye, resulting from separation of one part from another" [28]

[14] "Deformation: change in shape without loosing integrity, leading to bending, buckling or twisting of a stone block." [28]

[15] This category includes all those defects related to the deterioration of the stone surface, due to the loss of material, caused by weathering, chemical/biological factors or anthropogenic causes [28].
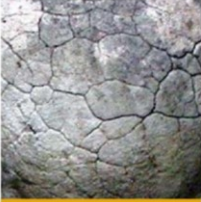
CRACK & DEFORMATION / FISSURE & DÉFORMATION

DETACHMENT / DÉTACHEMENT

FEATURES INDUCED BY MATERIAL LOSS / FIGURES INDUITES PAR UNE PERTE DE MATIÈRE

DISCOLORATION & DEPOSIT / ALTÉRATION CHROMATIQUE ET DÉPÔT

BIOLOGICAL COLONIZATION / COLONISATION BIOLOGIQUE

CRACK . FISSURE
Fracture . Fracture
Star crack . Fissuration en étoile
Hair crack . Microfissure
Craquele . Craquellement
Splitting . Clivage

DEFORMATION . DÉFORMATION

BLISTERING . BOURSOUFLURE
BURSTING . ECLATEMENT
DELAMINATION . DÉLITAGE
Exfoliation . Exfoliation

DISINTEGRATION . DÉSAGRÉGATION
Crumbling . Emiettement
Granular disintegration . Désagrégation granulaire
■ Powdering, Chalking . Pulvérulence, Farinage
■ Sanding . Désagrégation sableuse
■ Sugaring . Désagrégation saccharoïde

FRAGMENTATION . FRAGMENTATION
Splintering . Fragmentation en esquilles
Chipping . Epaufrure

PEELING . PELAGE
SCALING . DESQUAMATION
Flaking . Ecaillage
Contour scaling . Desquamation en plaque

ALVEOLIZATION . ALVÉOLISATION
Coving . Creusement

EROSION . ÉROSION
Differential erosion . Erosion différentielle
Loss . Perte :
■ of components . de constituants
■ of matrix . de matrice
Rounding . Erosion en boule
Roughening . Augmentation de rugosité

MECHANICAL DAMAGE . DÉGÂT MÉCANIQUE
Impact damage . Trace d'impact
Cut . Incision
Scratch . Rayure
Abrasion . Abrasion
Keying . Bûchage

MICROKARST . MICROKARST
MISSING PART . PARTIE MANQUANTE
Gap . Trou

PERFORATION . PERFORATION
PITTING . PITTING

CRUST . CROÛTE
Black crust . Croûte noire
Salt crust . Croûte saline

DEPOSIT . DÉPÔT
DISCOLOURATION . ALTÉRATION CHROMATIQUE
Colouration . Coloration
Bleaching . Décoloration
Moist area . Assombrissement dû à l'humidité
Staining . Tache

EFFLORESCENCE . EFFLORESCENCE
ENCRUSTATION . ENCROÛTEMENT
Concretion . Concrétion

FILM . FILM
GLOSSY ASPECT . ASPECT LUISANT
GRAFFITI . GRAFFITI
PATINA . PATINE
Iron rich patina . Patine ferrugineuse
Oxalate patina . Patine d'oxalates

SOILING . ENCRASSEMENT
SUBFLORESCENCE . SUBFLORESCENCE

BIOLOGICAL COLONIZATION . COLONISATION BIOLOGIQUE
ALGA . ALGUE
LICHEN . LICHEN
MOSS . MOUSSE
MOULD . MOISISSURE
PLANT . PLANTE

Fig. 15 – Five macro-areas of surface alteration, identified by ICOMOS ([28])

3D DATA – Quantitative analysis – point clouds

Geometry-based alterations A
- Digital Image Processing Routines
- Geometric Feature Extraction
- Change detection

→ CRACK-PATTERNS + FEATURE INDUCED BY MATERIAL LOSS

Color-based alterations B
- Point cloud segmentation for moisture detection
- Unsupervised machine learning for chromatic alterations
- Unsupervised/supervised learning for chromatic alterations

→ HUMIDITY PATTERNS + CHROMATIC ALTERATIONS

Fig. 16 – Diagram of the methodological approaches, defined to perform quantitative analyses of decay.

5.1. Geometry-based alteration approaches
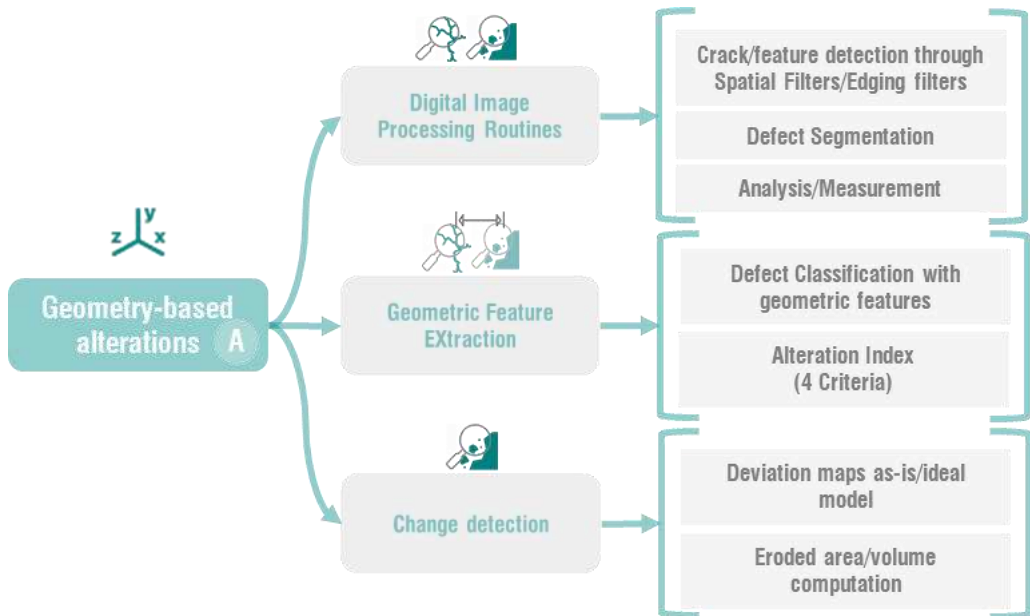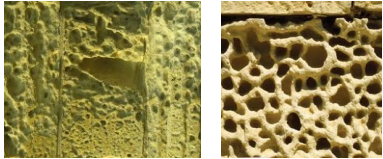
Fig. 17 – Workflow focused on the section of geometry-based alteration

In this section, a series of routines are presented, for the detection and quantification of geometry-based alterations, through the application of image processing techniques (Fig. 17). Three different approaches have been followed: the first, enclosing the processing of point clouds through sequences of algorithms for the segmentation and isolation of the geometry-based defect (cracks and feature induced by material losses); the second for the quantification and feature characterization of detected areas; the third, as an alternative, for the quantitative determination of a particular kind of defect (erosion, related to marine salts). In Table 3, the investigated decay morphologies are illustrated and defined, according to the national and international standards for visible decay on masonry surfaces [27][28].

Table 3 – Geometry-based alterations, according to the nomenclature, definitions and graphical representation included in [27][28]

ALTERATION	STANDARD DEFINITION	GRAPHICAL REPRESENTATION
Crack/ Fratturazione o fessurazione	**DEFINITION:** Individual fissure, clearly visible by the naked eye, resulting from separation of one part from another. **CAUSES:** Cracking may be due to weathering, flaws in the stone, static problems, rusting dowels, vibrations caused by earth tremors. **SUB-TYPES:** fracture, star crack, hair crack, cracquele, splitting	
Erosion/ Erosione	**DEFINITION:** Loss of original surface, leading to smoothed shapes **CAUSES:** Erosion may have natural and/or anthropogenic causes. It can be due to chemical, physical or/and biological processes. **SUB-TYPES:** differential erosion, loss of components, loss of matrix, rounding, roughening	
Missing Part/ Mancanza	**DEFINITION:** Empty space, located in the place of some formerly existing stone part. Protruding and particularly exposed parts of sculptures (nose, fingers, arms) are typical locations for material loss resulting in missing parts. **SUB-TYPES:** gap	
Alveolization/ Alveolizzazione	**DEFINITION:** Formation, on the stone surface, of cavities (alveoles), which may be interconnected and may have variable shapes and sizes (generally centimetric, sometimes metric). **CAUSES:** It is related to differential weathering, due to inhomogeneities in physical or chemical properties of the stone. **SUB-TYPES:** coving	

ALTERATION	STANDARD DEFINITION	GRAPHICAL REPRESENTATION
Pitting	**DEFINITION:** Point-like millimetric or sub-millimetric shallow cavities. The pits generally have a cylindrical or conical shape and are not interconnected. **CAUSES:** It is due to partial or selective deterioration. Pitting can be biogenically or chemically induced, especially on carbonate stones.	
Deformation/ Deformazione	**DEFINITION:** Change in shape without loosing integrity, leading to bending, buckling or twisting of a stone block. **CAUSES:** presence of unbalanced loads on the surface	

5.1.1. Semi-automatic procedures on point clouds, for 3D surface decay analysis, through digital image processing routines

Quantitative analysis of point clouds goes through a pre-processing phase, in analogy with digital image processing, by rectification algorithms and spatial noise reduction filters.

The first steps comprehend the use of levelling algorithms, to eliminate any orientation errors and to make the surface mainly orthogonal to the observation point, and shape removal operators to flatten curvatures. The former consisting in the identification of the geometric shape (generally a plane) which best approximates the measured points (i.e. least square method[16]); the latter, on the other hand, which allows the removal of the predominant shape from a surface, thanks to a geometric transformation (best fitting polynomial of variable degree), so that a chiefly curve surface (like for example a column or a tower) can be quantitatively described as a prevailing planar area.

The shape removal algorithm approximates the investigated surface with a polynomial function of degree n, according to the equation (5. 1), and it subtracts this function from the measured surface (defined as $z=f(x,y)$).

$$z_n(x,y) = \sum_{i=0}^{n} \sum_{j=0}^{n} a_{ij} x^{ij}$$

(5. 1)

where $i,j \leq n$ and a_{ij} are calculated through the least square method.

Noise reduction algorithms are meant to remove anomalous or redundant values, resulting from reconstruction errors, by replacing them with nearest neighbouring values. By way of example, the median noise reduction algorithm put the median value of a pre-fixed neighbourhood of points, only in place of the coordinates belonging to the lower (from 0 to 25%) or upper quartiles (from 75 to 100%) of the values of their neighbours [217].

---

[16] It consists in calculating the equations of a plane, which minimizes the sum of the squares of distances, between each point to be levelled on the surface and the point on the geometric reference form, which best fits the measured points [254].

Afterward, a plurality of specialized investigations can be carried out, aimed at identifying morphological alterations (cracks, features induced by material losses), by means of digital image processing procedures involving the use of: false-colour maps, edge extraction algorithms, thresholding, binarization and segmentation of models, profiles extraction. Different schemes have been followed, for the two above-mentioned pathologies, according to their morphological aspect.

Decay evidence like single cracks (or crack patterns) are characterized by sudden variations of the surface slope, in correspondence with the boundaries of the crack. Hence, edge-extraction algorithms are suitable for their detection and measuring, because they enhance discontinuities (high frequencies), and eliminate small variations (low frequencies) in intensity, thus strengthening contours[17].

The gradient filter, for instance, is based on the retrieval of the gradient vector[18] of an image (or in this case of a model). The underlying geometric property of the gradient is that it leads to the maximum variation direction (greatest change rate), corresponding to the edges of the object. The algorithm works by subtracting points near the central one of the neighbourhoods, according to the major slope searched among four directions at least [217].

This means that the first derivative of the function f (x, y, z), at a point in the generic direction r, with angle ϑ, as expressed by Eq. (5. 2), must be derived in the direction of maximum discontinuity, by assigning to the derivative function a null value, as in Eq. (5. 3):

$$\frac{\partial f}{\partial r} = \frac{\partial f}{\partial x}\frac{\partial x}{\partial r} + \frac{\partial f}{\partial y}\frac{\partial y}{\partial r} + \frac{\partial f}{\partial z}\frac{\partial z}{\partial r}$$

(5. 2)

$$\frac{\partial}{\partial \theta}\left(\frac{\partial f}{\partial r}\right) = 0$$

(5. 3)

---

[17] Sets of points lying on the border between two regions of the image or model

[18] The gradient is defined as a vector, whose components are partial derivatives of the function, with respect to the reference Cartesian axes.

Therefore, the gradient vector *(Gradf)* corresponds to the maximum value of the derivative $\partial f / \partial r$ in the direction of maximum variation (Eq. (5. 4):

$$Gradf = \nabla f = \frac{\partial f}{\partial x}i + \frac{\partial f}{\partial y}j + \frac{\partial f}{\partial z}k$$

(5. 4)

where *i,j,k* are the unit vectors of *x,y,z* axes [218] [5].

The output of the gradient filter application is a binarized surface point cloud, where points located in areas of maximum discontinuity are distinguished from the remaining points (Fig. 18). As a matter of fact, the distribution of gradient values and its magnitude on the surface is useful to determine points where the slopes vary gradually and points where they vary more rapidly (edges).
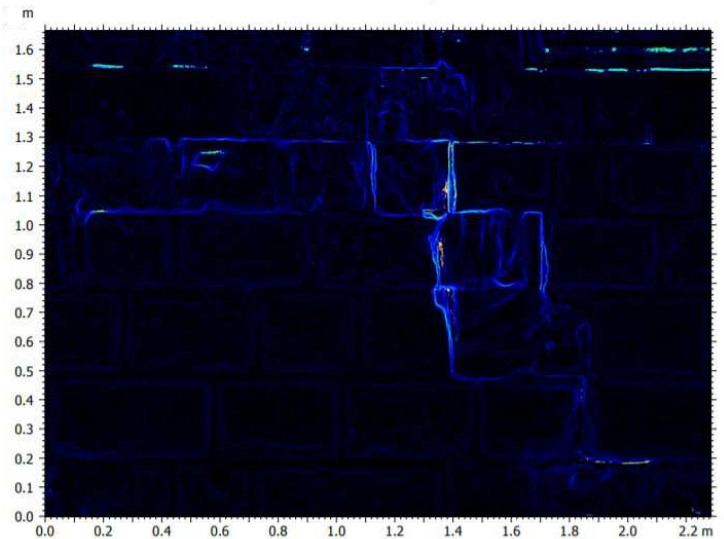
Fig. 18 – Example of application of edge-extraction on a masonry surface

While for the identification of other decay morphologies involving material losses (lacks, cavities, erosion), placed at greater depth with respect to the surface of the object, segmentation algorithms, like thresholding or binarization, are particularly convenient (Fig. 19). Thresholding belongs to segmentation methods, referring to a scalar field computed for an attribute and then compared to a threshold value [219].

In the specific case, the application of height thresholds, which artificially trim the surface in correspondence to selected depth values, consent to isolate and study only those elements within a prefixed range (chosen on the basis of the order of magnitude of the examined objects). In fact, modifying thresholds, it is possible to vary the range of inclusion, and to adapt them to the purpose of the segmentation (isolation of affected areas) [220].

To achieve surface segmentation, another alternative is the binarization of the surface, which, analogously to the thresholding, apply a threshold to a surface, producing a binarized image as output, in which the areas above the threshold (foreground) are distinguished from the areas below the threshold (background).
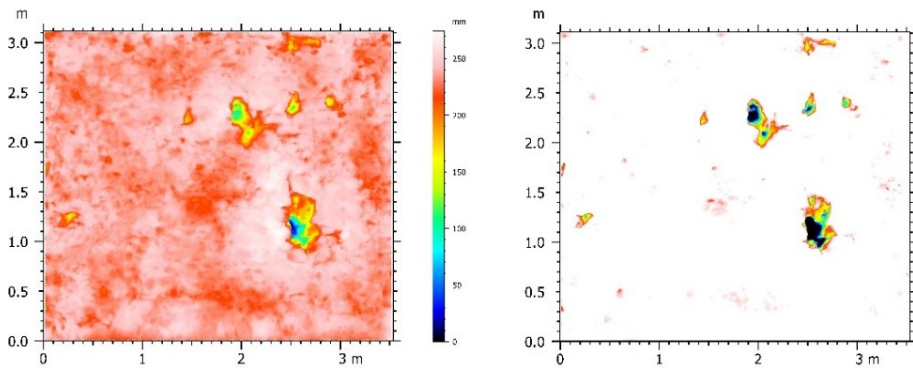
Fig. 19 - 3D representation of a restricted masonry wall area, on which thresholding have been applied [4].

Areas affected by crack patterns or surface decay, detected thanks to the application of the image processing algorithms illustrated in this section, can be determined and described quantitatively, through a further step, the watershed segmentation method[19]. It subdivides the surface into smaller regions[20], of which it is possible to calculate the main geometric characteristics (perimeter, area, volume, average/minimum/maximum diameter), in order to quantify the extension of decay phenomena, and to extract other

---

[19] It is a region-based segmentation method, which consider the surface as a topographic landscape, and divides it in dales and hills, of which it computes the main geometric characteristics [217][255].

[20] The smaller region is determined on the basis of the similarity of their characteristics, and they are also called grain or motifs.

significant feature useful for defect classification purposes, as it will be described in section 5.1.2 (Fig. 20).

In Fig. 21, a graphical representation of the image processing workflow is proposed.
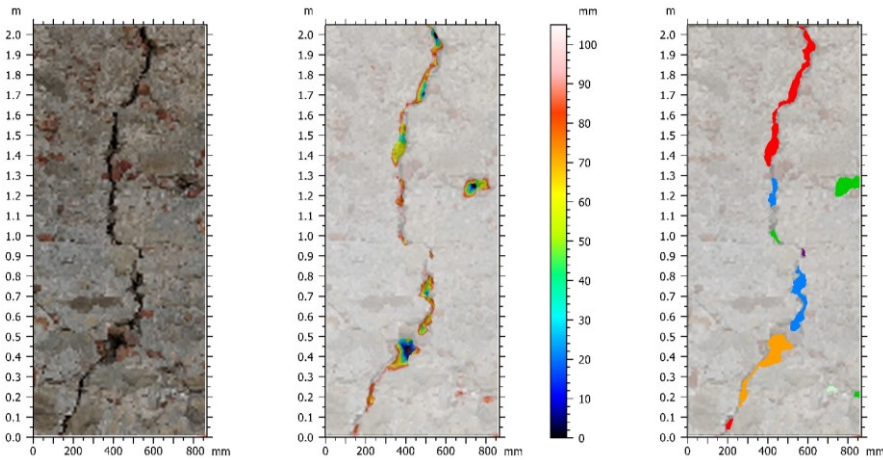
Fig. 20 - From left to right: point cloud of a masonry wall; application of the threshold operator; segmentation of the identified areas into regions (indicated by different colours).
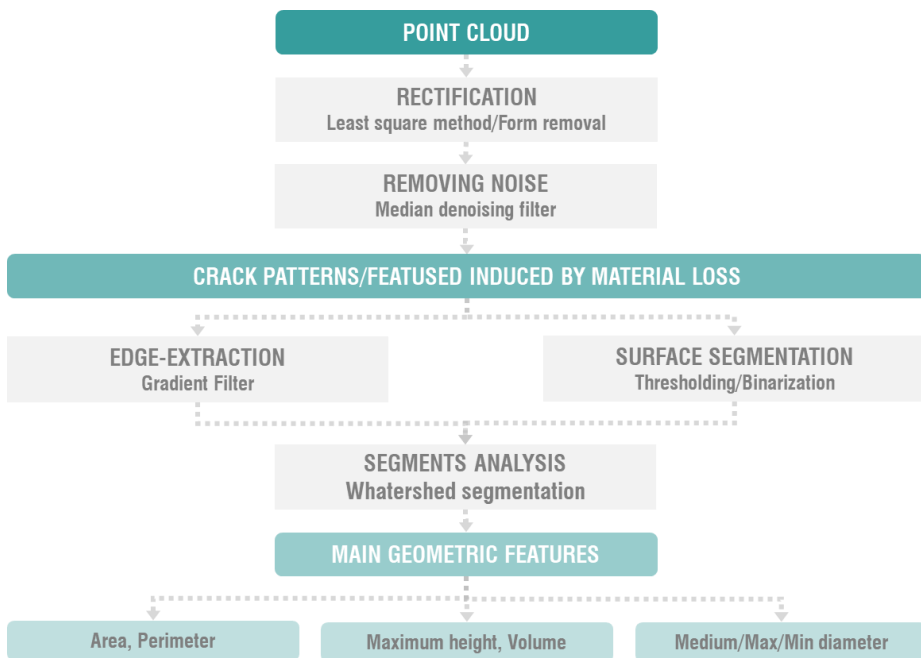
Fig. 21 - Flow chart illustrating a protocol, for detecting and measuring cracks or features induced by material loss, starting from a point cloud (based on [4]).

5.1.2. Feature extraction for the quantification, measurement, and classification of geometry-based damages

As illustrated in section 5.1.1, the application of digital image processing algorithms to reality-capture 3D data leads to the retrieval of quantitative information about geometry, extension (area, volume) and distribution of geometry-based decay morphologies on the affected objects.

Furthermore, the processing of point cloud allows the extraction of meaningful features, for the discrimination among different kinds of geometry-based pathologies: cracks on the one hand, features induced by material losses on the other hand. In fact, segmentation procedures, provide a discretization of the examined surface and a computation of their descriptive characteristics in a three-dimensional environment.

The goal is to quantitively parametrize the two above-mentioned typologies of defects, on the basis of the features retrieved from 3D data of the artefact, leading to an integration of the existing standards in Cultural Heritage field, which describe pathologies only under a qualitative point of view.

As a matter of fact, features can be considered as attributes, in support of a discrimination and subsequent assignment of unique labels to each segmented region, according to the feature-based characterization of a surface. They are differentiated into three categories: 1) attributes related to the single element dimension (e.g. feature size, height, area, volume, etc.), 2) shape descriptors, invariant with respect to scale, rotation and location, and 3) attributes concerning the relationships between neighbour elements (location, orientation, density, number of connected elements, etc.) [217] [219]. These attributes are particularly helpful for the identification and classification of segments into specific pathology classes, because they describe their geometrical characteristics, both in terms of boundaries and of regions. In Table 4 the main parameters taken into consideration for the purpose of the research are summarized [223].

The depth (height) of a segment indicates if a defect is superficial or deep. Area and boundary descriptors like perimeter, maximum and minimum diameter, express the flat dimensions of the defect. Volume helps understanding its three-dimensional size. While

aspect ratio, roundness and compactness are shape descriptors, useful to distinguish among the two main categories of cracks or features induced by material loss.

Table 4 – Features related to the single regions [16]

Parameter	Description
Height (h)	Depth of the motif
Perimeter (p)	Length of the segmented region boundary
Area (A)	Horizontal area of the motif
Volume (V)	Void volume of the motif
Co-flatness (H)	Maximum vertical distance between the central pit and the pits of adjacent motifs
Min diameter (Dmin)	Smallest diameter of the motif measured from its centre of gravity
Max diameter (Dmax)	Biggest diameter of the motif measured from its centre of gravity
Aspect ratio (AR)	Ratio between the maximum diameter and the minimum diameter. If the value is close to 1, the form of the grain is close to the form of a disk. If the value is high, the grain is oblong $$AR = \frac{Dmax}{Dmin}$$
Roundness (R) (Circularity)	Ratio between the area of the grain and the area of the disk having as diameter the maximum diameter of the grain. This value is close to 1 for a circular grain, and smaller than 0.5 for an oblong grain $$R = \frac{4Area}{\pi(Dmax)^2}$$
Compactness (C)	Ratio between the equivalent diameter and the maximum diameter. This ratio is close to 1 for a grain with the form of a disk, or smaller than 0.5 for an oblong grain. $$C = \frac{\sqrt{(\frac{4}{\pi}Area)}}{Dmax}$$
Eccentricity (e)	Ratio of the distance between foci (c) and the major axis/diameter of the grain $$e = \frac{c}{Dmax}$$
Form Factor (FF)	Ratio between the area of the grain and the squared perimeter. $$FF = \frac{4\pi Area}{P2}$$
Orientation (O)	Angle of the axis of the grain
Angularity (An)	Angle between walls of the grain
N° connected components (NC)	Number of connect elements

The elaboration of a quantitative detection and classification approach, goes through the correlation among geometry-based alterations pertaining to the two macro-categories, and the features illustrated in Table 4, which refer to the geometry or to the topology of the element. In Table 5, this interconnection is proposed explicitly. The underlying consideration is that each parameter, and its variation ranges, can be

significant for a peculiar aspect of an imperfection, in order to quantitatively describe and assign a motif to specific a category of defect [16] [29].

Table 5 – Correlation among features and decay morphologies (extracted from [16])

Alteration	Description	Quantitative Parameters
Crack	Loss of continuity in the material that implies reciprocal displacement of sections.	h, A, V, Dmin, Dmax, AR, R, O
Lack	Loss of three-dimensional elements (arm of a statue, an amphora handle, piece of relief decoration, etc.)	h, A, V, Dmin, Dmax, AR, R
Erosion	Removal of material from the surface that in most cases is compact.	h, A, V, H, Dmin, Dmax
Cavities	Presence of cavities of variable shape and size, called "alveoli", often interconnected and with non-uniform distribution	h, A, V, Dmin, Dmax, AR, R
Pitting	Formation of blind holes, numerous and close together. The holes have a hemispherical shape with a maximum diameter of few millimetres	h, A, V, Dmin, Dmax, AR, R
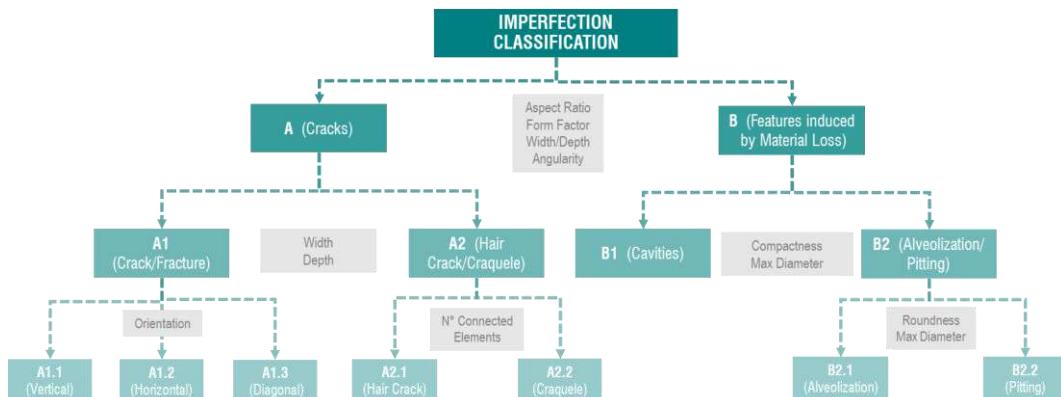
Fig. 22 - Classification of alterations on the basis of characteristic descriptors [29]

In Fig. 22, a likely discrimination among alteration classes, at different levels of detail, is illustrated. The first separation is functional to assign the detected motifs to one of the two macro-categories (A-cracks; B-feature induced by material loss). Both of them can be associated to simple ideal geometries, like rhombus for cracks (A), due to its elongated shape, and disk/circle for features induced by material loss (B), especially cavities or alveolizations. In this regard, among the parameters illustrated in Table 4, the most representative are the shape descriptors like *aspect ratio* and *form factor*, expressing the ratio of major and minor diameter of a grain and the ratio between area

and perimeter of a grain, respectively. In fact, if a grain is circular these numerical values converge to 1, otherwise they assume values diverging from it, which stands for an oblong shape, nearer to the geometry of rhombus. For the identification of discriminant thresholds of the two features, geometrical considerations have been followed. The basic consideration is that, given two grains with the same area, the divergence between the two diameters (comparable to major and minor axis of a rhombus or an ellipse) reaches a specific value, which could represent a lower limit for the category of elongated shapes. This threshold is related to the amplitude of the acute angle of the ideal rhombus (around 30°). The respective threshold value of *aspect ratio* is 4, and, consequently, it is possible to derive the threshold value for the *form factor*, if expressed as a function of the *aspect ratio* (Eq. (5. 5).

$$Form\ factor = \frac{\pi(Aspect\ Ratio)}{2(1+Aspect\ Ratio^2)}$$

(5. 5)

In summary, a grain can be considered as elongated if the acute angle of the ideal rhombus is lower than 30°, which leads, respectively, to an aspect ratio equal to or major than 4, and a form factor equal or inferior to 0.38. These thresholds help separating the two classes A and B, in the first place.

Secondly, it is necessary to include other features in the analysis, to confirm this hypothesis, because, for example, there could exist an alteration pertaining to class B, but with an elongated shape. To this end, it is important to consider dimensional features like *width* and *depth* to check the results of the first separation, given that alterations related to B (features induced by material loss) usually are not deep, with respect to A (cracks), which on their side have a really small width.

In addition, cracks have always nearly vertical walls. Hence, the *angularity* of the walls of the grain leads to a further confirmation that the examined grain belongs to class A or B. These last features can be determined through the extraction and analysis of transversal profiles, crossing the examined grains.

The *width* parameter could be a discriminant factor also to deepen the classification level, within class A, to furtherly distinguish between cracks (A1), hair-

cracks/craqueles (A2). In this case, the *width* threshold is deduced from the standard ICOMOS 2008 [20], which establish that a hair-crack/craquele (A2) have a *width* < 0.1 mm. Going toward the third level of classification, features like *orientation* defines the main direction of the detected crack (A1), among vertical (A1.1), horizontal (A.2) and diagonal (A.3). This step is relevant, together with its localization (constructive element) for the understanding of the typology of static instability. For example, a vertical crack located on a pillar/column, or a wall could correspond to a structural deficiency. While diagonal cracks could indicate a vertical translation or a primary rotation.

Conversely, the number of connected components could suggest a separation within A2, between single hair-cracks (A2.1) and craqueles (A2.2).

For the class B, an analogous reasoning has been followed, considering features like *compactness*, *roundness* and *maximum diameter* [29].

The definition of this workflow is functional to perform a remote classification of the morphologies of decay affecting the analysed surface, from the reconstructed photogrammetric 3D data, through the definition of automatic routines, which operates progressive choices between at least two alternatives (at each step), according to the indicated threshold values.

A further phase concerns the determination of a damage index (*I*) associated to each alteration, in relation to specific geometric aspects, on the basis of suitable criteria, resulting from the combination of the afore-mentioned features [224]:

- *Form f*: a combination of aspect ratio, roundness and compactness, expressing the shape of a grain;
- *Depth (d)*: the medium height of a grain, calculated as the ratio between volume and area;
- *Uniformity (u)*: calculated as the ratio between the maximum height and the medium height;
- *Volume (v)*: the three-dimensional size of the grain.

Three levels have been identified, to which a numerical range is associated (1-3), from the best to the worst level. They are correlated to each of the four criteria, with distinct weights, varying in correspondence of each defect [225].

The four criteria are combined with their weights, to form an overall damage index, related to the alteration:

$$I = W_f * C_f + W_d * C_d + W_u * C_u + W_v * C_v$$

<div align="right">(5. 6)</div>

Where:

- w are the weights
- C are the criteria

The damage index stands in an interval from 1 to 8, as a results of the combination of the chosen weights (w_f, w_d, w_u, w_v). A proper classification can be achieved only through the combination of all the four criteria, in order to avoid misleading results [16].

5.1.3. Damage evaluation of eroded limestone architectural elements

Limestone artworks such as statues, columns of architectural components, are often affected by erosion, due to weathering, wind, chemical factors, ... These phenomena are strongly related to the geographic localization and to the climate to which the artifact is exposed. In fact, especially in coastal areas, erosion is a considerably widespread form of decay.

In this section, a pipeline is proposed for the detection and monitoring of the eroded areas affecting limestone, starting from reality-based 3D data. A quantitative computation of eroded areas and volumes can be performed, through a direct comparison of reality-based clouds and their corresponding ideal 3D model. The aim is to highlight differences eventually occurred between a hypothetical original unaffected surface (initial condition) and actual and successive states of conservation of the element. This process can be regarded to as 3D change detection.

In this case, the photogrammetric model is useful for a double aim: the first is the geometric retrieval of an ideal 3D model from the dense cloud, the second is the determination of the as-is condition at the moment of the acquisition.

At this stage, the ideal model is compared with the as-is dense cloud, through the application of an iterative closest point approach, based on the nearest neighbour distance algorithm. For each point of the ideal model, it searches the nearest point in the as-is point cloud, thanks to the Euclidean distance computation (Eq. (5. 7).

$$D = \sqrt{(p_x - q_x)^2 + (p_y - q_y)^2 + (p_z - q_z)^2}$$

$$(5.7)$$

Another alternative, for distance computation, goes through a preliminary phase of identification of core points and corresponding normal vectors, in order to calculate distances between the two clouds following directions of the normal vectors. With respect to the previous algorithm, an additional step is considered, concerning the identification of the optimal scale for a best fitting with a plane, in order to understand the best scale of neighbourhood, at which normal vectors have to be estimated [217].

The output is a searchable deviation map represented in false colours, in which it is possible to know both the absolute distance and the distances split in the three axes, for each point of the reference (ideal cloud) and its correspondent in the compared (as-is) cloud.

This product is linked to the as-is dense cloud, which is enriched with the additional information of the absolute distance. A distance threshold, consistent with the size of holes of the eroded areas, is then established to segment the as-is cloud, in order to exclude from the computation those differences due to geometric irregularities of the architectural element.

The segmentation is functional to isolate the damaged areas, and to quantify their extension in terms of area, volumes and other geometrical features.

The workflow can be applied also for the comparison of two or more as-is models, acquired in consistent time intervals, in relation to the specific situation, to control and monitor the spreading of the phenomenon and its rapidity.

The operative workflow is sum up in some fundamental steps, as delineated in Fig. 23:

1. Photogrammetric acquisition
2. 3D data reconstruction, to generate the as-is point cloud
3. 3D modelling, to retrieve the corresponding original mesh model
4. 3D decimation/resampling, to transform the mesh into a point cloud
5. Change detection, to compute cloud-to-cloud deviation between ideal and as-is clouds
6. Point cloud segmentation, to isolate affected areas
7. Quantitative analysis, to compute their extension

ERODED AREAS EVALUATION

1 **Photogrammetric acquisition**

2 **3D data reconstruction**
As-is dense point cloud

3 **3D modelling**
Ideal reality-based 3D mesh model

4 **3D resampling of ideal model**
Ideal dense point cloud

5 **Change detection**
Cloud-to-cloud deviation

6 **Point cloud segmentation**
Isolation of eroded areas

7 **Quantitative analysis**
Geometric features computation
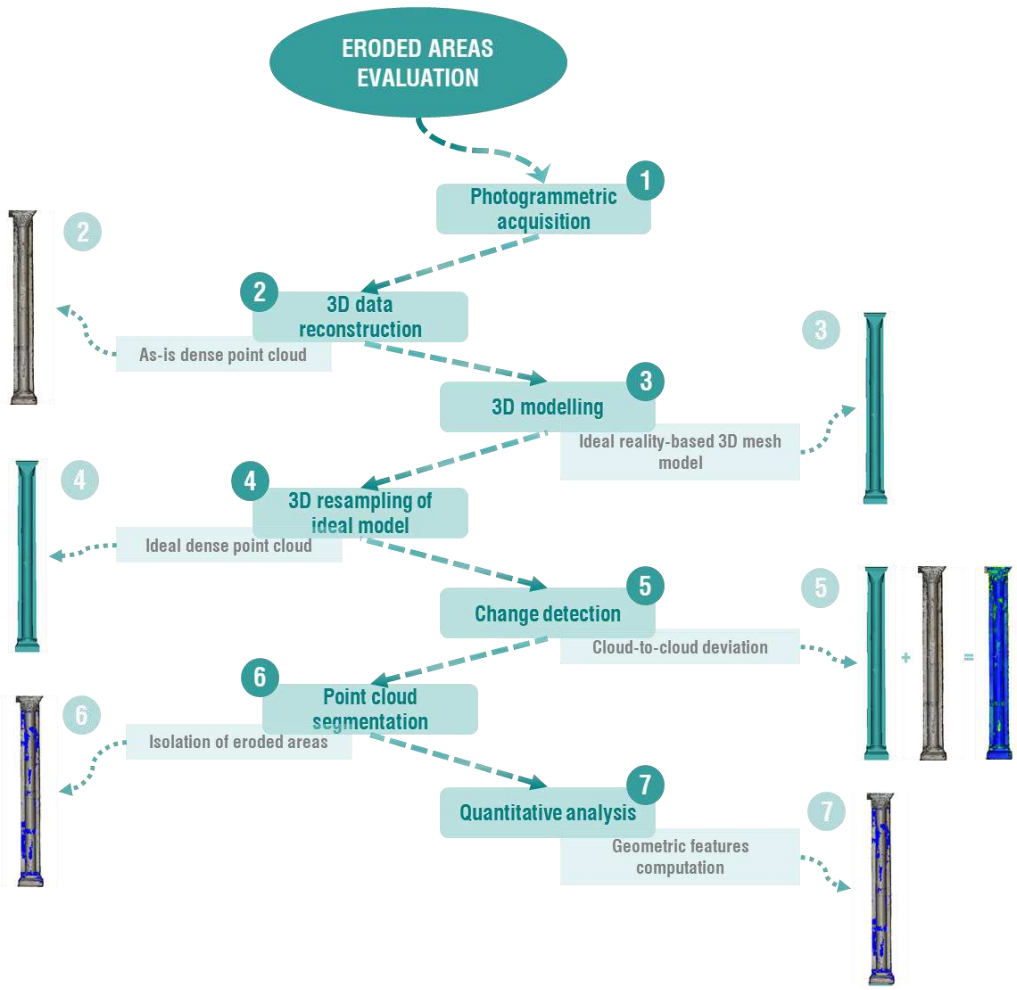
Fig. 23 – Operative workflow, for the evaluation of eroded areas, from point clouds

5.2. Colour-based alteration approaches

As already introduced in the current section, colour-based alterations are characterized by chromatic variations of the surface, often related to humidity, weathering, salts or chemical agents. This category encloses a series of decay morphologies, such as chromatic alteration, moist areas, biological patina or colonization, deposit,…

In Table 6, the colour-based alterations considered in this section are reported, with their description and representation, according to the national and international standards [27] [28].

As a consequence, in order to detect chromatic modifications of the examined surfaces, it is necessary to extract and analyse the colour information enclosed in photogrammetric 3D data, which could be in form of radiometric values, in correspondence of each point of the cloud, or in form of high-resolution texture (a bidimensional image, projected onto the 3D mesh model).

In sections 5.2.1 and 5.2.2, two different machine learning approaches are illustrated, which segment point clouds, to detect and measure chromatic based alterations, within a progressive process of development. While in section 5.2.3, the cloud-based approach is compared to a texture-based segmentation and classification method.

To this end, a premise must be done about the concept of segmentation, which represent the basis of a large number of algorithms adopted in image processing.

Segmentation of 2D or 3D data allows a partitioning of the original data into smaller segments or clusters, on account of similar characteristics or features, [226], [227].

As mentioned in section 5.1, in case of 3D data like point clouds, every point in the dataset is enriched both by geometrical (3D coordinates, normal vectors) and radiometric (RGB triplets) information. Therefore, segmentation could act on the two kinds of attributes, according to the scope of the analysis.

Table 6 – Colour-based alterations, according to the nomenclature, definitions and graphical representation included in [27][28]

ALTERATION	STANDARD DEFINITION	GRAPHICAL REPRESENTATION
Discolouration/ Alterazione cromatica	**DEFINITION:** Natural change of the stone colour in one to three of the colour components: hue, value and chroma. **CAUSES:** It can be produced by salts, by the corrosion of metals, by micro-organisms, or by exposure to fire. Otherwise, it is related to the presence of pipe leakage, rising damp, hygroscopic behaviour due to the presence of salts, condensation. **SUB-TYPES: colouration**, bleaching, **moist area**, **staining**	
Soiling/ Colatura	**DEFINITION:** Deposit of a very thin layer of exogenous particles giving a dirty appearance to the stone surface, often with parallel trend. **CAUSES:** It can be produced from atmospheric pollutants or from particles transported by running water or heating convection.	
Biological colonization or patina/ Colonizzazione biologica	**DEFINITION:** Macroscopically verifiable presence of vegetation layer on the surface. Or thin and homogeneous layer, consisting mainly of microorganisms, variable in consistency, colour and adhesion to the substrate. **CAUSES:** Colonization of the stone by macro and micro-organisms such as bacteria, cyanobacteria, algae, fungi and lichen. **SUB-TYPES:** biofilm, alga, moss, lichen	
Deposit/ Deposito superficiale	**DEFINITION:** Accumulation of exogenic material of variable thickness. **CAUSES:** Splashes of paint or mortar, sea salt aerosols, atmospheric particles such as soot or dust, remains of conservation materials such as cellulose poultices, blast materials etc...	
Efflorescence/ Efflorescenza	**DEFINITION:** Generally whitish, powdery or whisker-like crystals on the surface. Efflorescences are generally poorly cohesive and commonly made of soluble salt crystals. **CAUSES:** It is commonly due to the result of evaporation of saline water present in the porous structure of the stone.	

There exist a variety of methods for the point cloud segmentation, distinguished according the aggregation criterion, which acts on specific properties or features of data (like geometry, colour, size, shape, scale patterns,...).. The most widespread are: edge-based methods, which look for the discontinuities among contiguous elements (pixels in images, points in point clouds); and region-based methods, which, on the contrary, concentrate on similar properties.

In this second part of the methodology the attention is put on the colour information, in relation to the detection of colour-based changes, which can occur on a masonry surface (see Table 6). Since water, weathering or chemical agents act on the radiometric properties of a material, clusters have to be gathered on the basis of the chromatic proximity of their elements. In light of this, the proposed approaches can be associated to region-based methods, which on their side, are furtherly separated into two main categories, depending on the starting point of the segmentation pipeline. If they start from a unique region, they can be considered unseeded, and the region is progressively sub-divided according to certain features (region splitting). Otherwise, if they start from multiple regions or seed points (as many as the points/pixels of the original dataset), they are seeded and they aggregate neighbour points in the same regions (region growing/merging) [220]. Other segmentation methods can be recalled as: attribute-based, acting on the point attributes, previously derived from the point cloud; model-based, like RANSAC (RANdom SAmple Consensus) and Hough Transform, which find mathematical models or geometrical primitives to fit the original data; or graph-based, which consider the point cloud as a graph (each point is a vertex) [226]. Besides, point cloud segmentation can be achieved also through machine learning, artificial intelligence algorithms, in which machines understand how to take decisions on the basis of relations highlighted in the dataset. As far as artificial intelligence is concerned, there are two fundamental approaches: supervised segmentation, in which sematic categories and relations among data are learnt from user-defined annotations; unsupervised segmentation, where no annotations are produced and data are segmented according to a previous parametrization of the algorithms [227].

On account of the provided framework, the choice of the proper segmentation strategy is strongly influenced by the objective of the analysis, that, in this case, is the kind of decay morphologies investigated (Fig. 24).
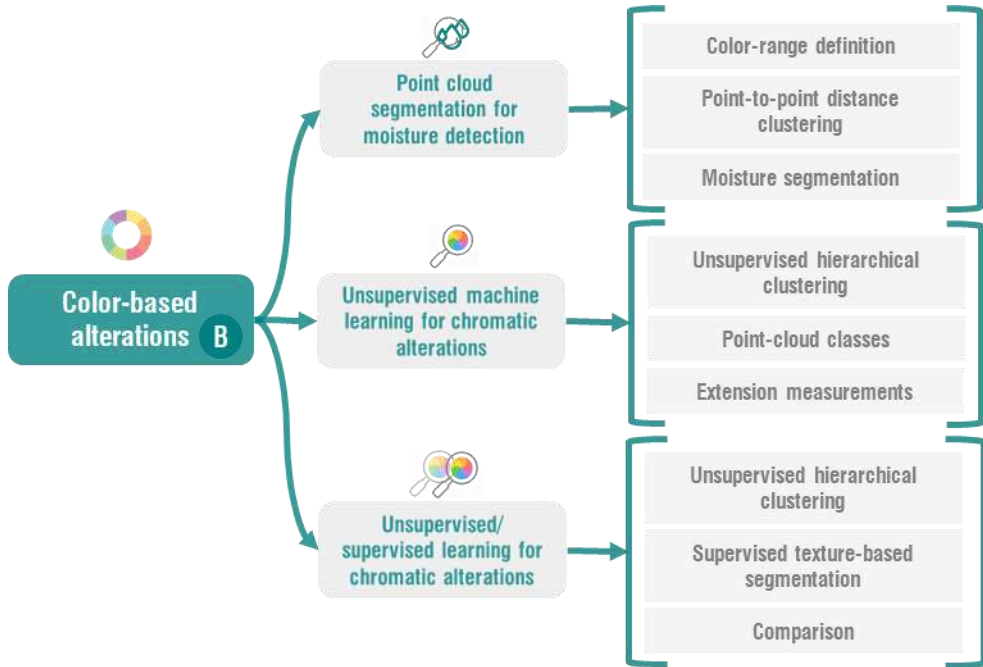
Fig. 24 – Workflow concerning pipelines related to chromatic-based alterations
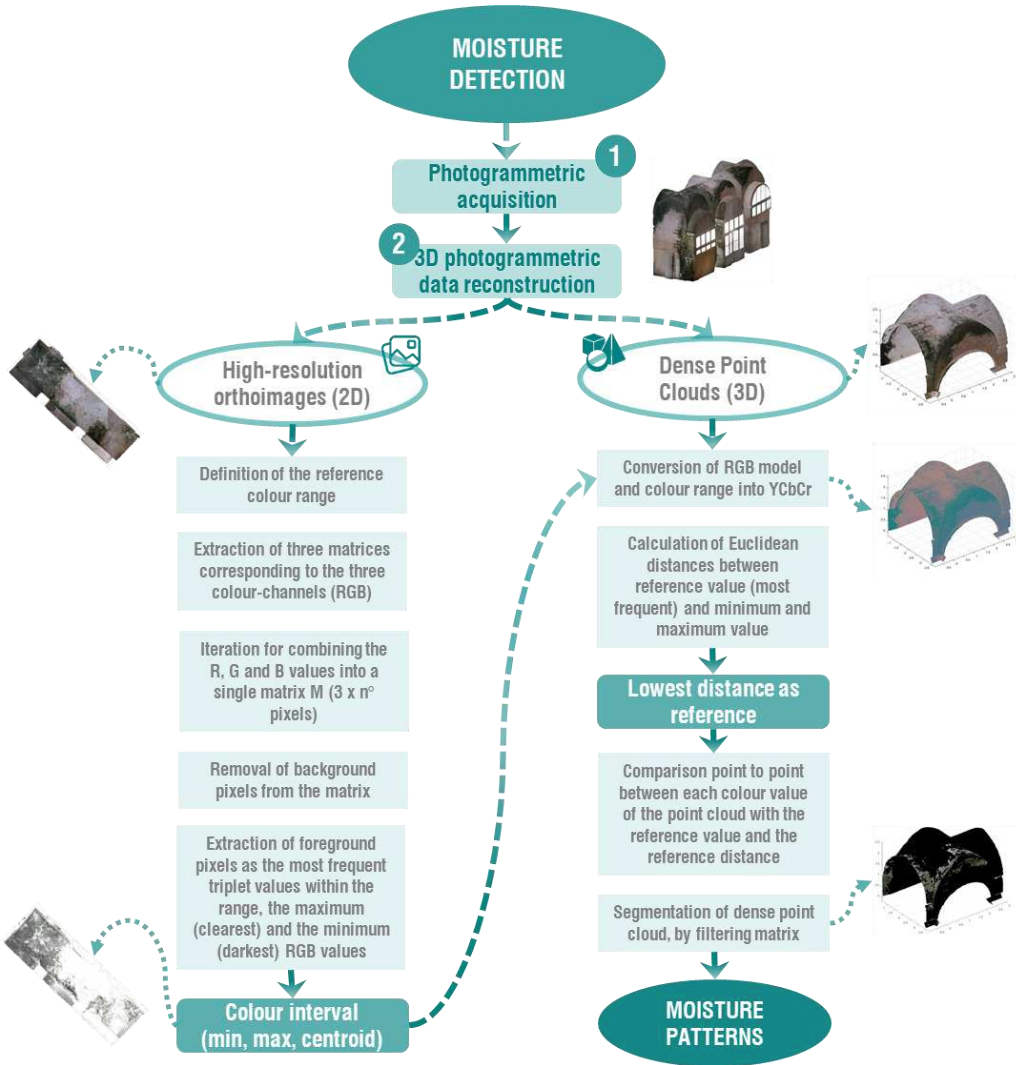
Fig. 25 – Workflow of point cloud segmentation for moisture detection purposes (based on [164])

In this paragraph, a first segmentation approach is proposed, for the identification of two kinds of defect, biological patina or colonization (Fig. 25). The paramount assumption is that the evidence of these alterations is represented by a vegetation layer adherent to the surface, recognizable most of all through its chromatic aspect,

expressed in a quite limited colour range, varying from green to grey and black, despite the surface nature and micro-climate conditions.

Starting from this consideration, a pipeline combining region-based and attribute-based procedures has been developed. It works clustering points according to the chromatic proximity of their colour attribute, which is expressed in terms of geometric proximity of colour triplets, as attributes related to each point of the point cloud. The colour information of a point is compared with its neighbourhood's information, in order to isolate points with similar properties from the background (the rest of the model).

In the first place, a reference colour interval, related to the defect investigated, has to be defined, identifying the central or seed point and expanding the interval to the boundaries (minimum and maximum) [228].

Going into detail, the segmentation process has been split into two main parts: the first, performed on high-resolution orthoimages, for the retrieval of the reference colour range; the second, for the effective point cloud segmentation, including or excluding points according to the reference interval.

The first routine identifies the colour interval from orthoimages, representing areas affected by biological patina or colonization, on which, thanks to image processing manual filtering operation the colours of interest are isolated and extracted (Fig. 26). Then a series of iterative cycles have been implemented on the orthophoto, with the purpose of identifying the seed point (most frequent value within the interval) and the extreme values of the range of interest (minimum and maximum).

In particular, given that in a 2D images the colour information is represented by three matrices[21], with the same size of the image ($m \times n$)[22], these matrices are extracted and combined into a single matrix (n° pixels x 3). At this point the most frequent triplet is searched, as a combination of the most recurrent value of each channel (reference value/seed point - $RGB_{xef,}$). The minimum (darkest - RGB_{min}) and the maximum (clearest - RGB_{max}) are the boundaries of this interval.

---

[21] One for every component of the colour model

[22] m = pixel length and n = pixel width
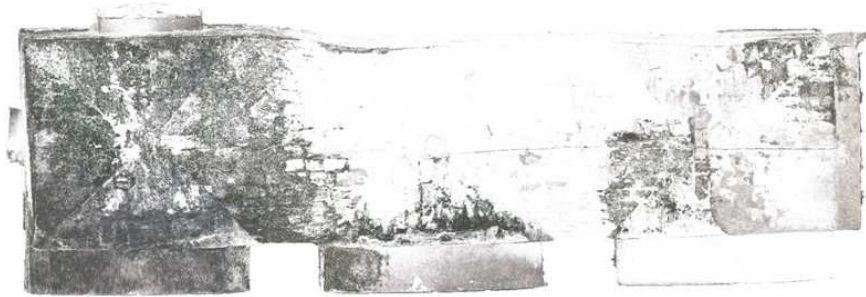
Fig. 26 – Example of extraction of range of interest from the high resolution orthophoto

Once the interval is defined, in order to segment the point cloud, it is necessary to execute some pre-processing operations, regarding, first of all, the conversion of the colour attribute of the original 3D data, from the RGB (red, green and blue) to another more proper colour space.

This is because RGB is an additive colour model, in which colours are expressed by many combinations of the primary spectral components of red, green, and blue, distributed in a Cartesian coordinates system. All the three components are related only to the chrominance and not to the luminance, which is manifested through the fusion of the three components. As a consequence, this colour model is not consistent with human eyes perception, affected by the presence of lights and shadows. In addition, metric distance does not correspond to the colorimetric distance between colours [189] [229].

To this end, in a pre-processing stage, it is necessary to convert the point cloud chromatic data (RGB triplets) into another colour space, enclosing lighting and shadowing factors, and, therefore, more suitable to the purpose of a colour-based point cloud segmentation.

For the aim of detecting biological colonization/patina, YCbCr has been adopted, where Y stands for the luma component (i.e image brightness), while Cb and Cr are the chrominance components, computed as the difference between a reference value and red and blue components, respectively. The conversion is performed as a mathematical transformation (Eq. (5. 8), applied to the matrix collecting chromatic coordinates of each point of the cloud (colormap), and, concurrently, on the colour values defining the range (RGB_{min}, RGB_{max}, RGB_{ref}).

$$\begin{bmatrix} Y' \\ Cb \\ Cr \end{bmatrix} = \begin{bmatrix} 0.2126 & 0.7152 & 0.0722 \\ -0.1146 & -0.3854 & 0.5 \\ 0.5 & -0.4542 & -0.0458 \end{bmatrix} \begin{bmatrix} R' \\ G' \\ B' \end{bmatrix}$$

(5. 8)

Hereafter, a second routine has been developed, for the automatic 3D segmentation of the point cloud, with the objective of isolating and quantifying areas affected by biological colonization/patina, according to the values determined through the first routine and converted in the YCbCr colour model ($YCbCr_{min}$, $YCbCr_{max}$, $YCbCr_{xef}$). To determine the amplitude of the interval, Euclidean distances between the *reference value* ($YCbCr_{xef}$) and the *minimum* ($YCbCr_{min}$) and *maximum value* ($YCbCr_{max}$) respectively are computed (Eq. (5. 9), (5. 10). The lowest between D_1 and D_2 is chosen as threshold value or reference distance (D_{ref}) for the segmentation.

$$D_1 \,(YCbCr_{ref}, YCbCr_{max}) = \sqrt{((Y_{ref} - Y_{max})^2 + (Cb_{ref} - Cb_{max})^2 + (Cr_{ref} - Cr_{max})^2)}$$

(5. 9)

$$D_2 \,(YCbCr_{ref}, YCbCr_{min}) = \sqrt{(Y_{ref} - Y_{min})^2 + (Cb_{ref} - Cb_{min})^2 + (Cr_{ref} - Cr_{min})^2}$$

(5. 10)

A point-to-point evaluation compares the reference distance D_{ref} with the distance D_p (Eq. (5. 11) of each point from the reference value ($YCbCr_{xef}$). Indeed, only those points at lower distance (D_p), with respect to the threshold value D_{ref} are included in the segmentation.

$$D_p \,(YCbCr_{ref}, YCbCr_p) = \sqrt{(Y_{ref} - Y_p)^2 + (Cb_{ref} - Cb_p)^2 + (Cr_{ref} - Cr_p)^2}$$

(5. 11)

The output of this procedure is a binarized point cloud, on the basis of the proximity of chromatic components of points, where the foreground represents biological patina/colonization, isolated from the remaining part of the cloud (background). The extracted areas can be quantified, both in terms of percentage over the total, and in terms of size and volume (Fig. 27) [164].
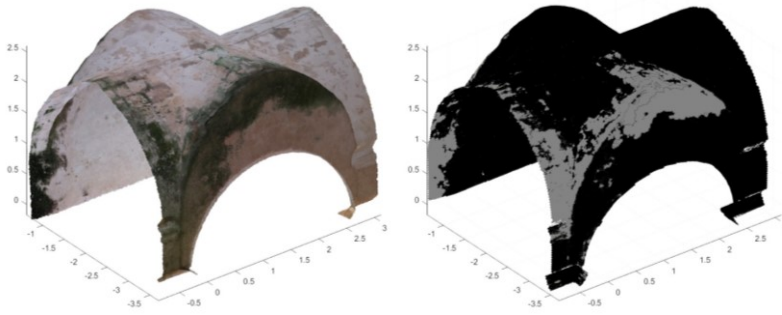
Fig. 27 – 3D model of a cross-vault, consistently affected by biological colonization/patina. Left: original point cloud. Right: binarization and isolation of affected area

5.2.2. Unsupervised and clustering-based machine learning for automatic point cloud segmentation, for chromatic-based detection

In light of an augmentation of the pipeline described in section 5.2.1, which is aimed at the detection of a unique kind of alteration (biological colonization/patina), a procedure is presented, based on the automatic segmentation of point clouds of architectural environments (cloisters, rooms, façades), with the scope of distinguishing a plurality of colour-based decay morphologies, like chromatic alteration, moist area, spots/deposits,…They can be related to a variety of causes, beyond humidity, as chemical factors, weathering, marine salts, dust soot… Also, their manifestation reveals a diversity in their chromatic aspect. As a result, an approach based on the identification of reference colour ranges for each defect, like the one illustrated in section 5.2.1, is not convenient.

Starting from this premise, artificial intelligence has been preferred as segmentation technique, and, particularly, machine learning methodologies applied to 3D data, as point clouds or mesh models.

After a careful examination of different methods existing in the field of machine learning, looking both at supervised and unsupervised procedures, an unsupervised pipeline based on clustering algorithms has proved to be particularly suitable for the chromatic segmentation of the cloud.

Indeed, the leverage of these solutions is that they do not need pre-fixed annotations, as previously declared (section 5.2), because it is the algorithm itself that introduces labels, after a preliminary parametrization by the user. This aspect makes them particularly suitable to the application of detecting masonry surface pathologies, characterized by a great complexity and heterogeneity.

At this stage, three clustering algorithms have been compared, in order to find the more consistent: minimum Euclidean distance, k-means and hierarchical clustering.

The first two are based on the preliminary determination of a parameter, as partitioning criterion for the clusters' creation. In the first case, a minimum Euclidean distance between points of different clusters has to be fixed. While the second is an iterative algorithm, where a number of k clusters are identified. It starts randomly choosing the

corresponding *k* centroids, and varying their positions at every iteration, until the total inner cluster variance[23] reaches its minimum value [220]. As highlighted in [230], k-means clustering works only if the number of clusters (k) is known in advance.

While the third algorithm, does not require a former selection of parameters, because it organizes data autonomously in hierarchical representation (binary cluster trees or dendrograms[24]) (Fig. 28) [230].

Hierarchical clustering is structured in two kinds of approaches:

1) Agglomerative (or bottom-up), starting at the bottom of the dendrogram, and recursively merging pairs of clusters with the smallest intergroup dissimilarity

2) Divisive (or top-down), proceeding from a single cluster at the top, and iteratively dividing each cluster into two, characterized by the highest dissimilarities between groups [231].
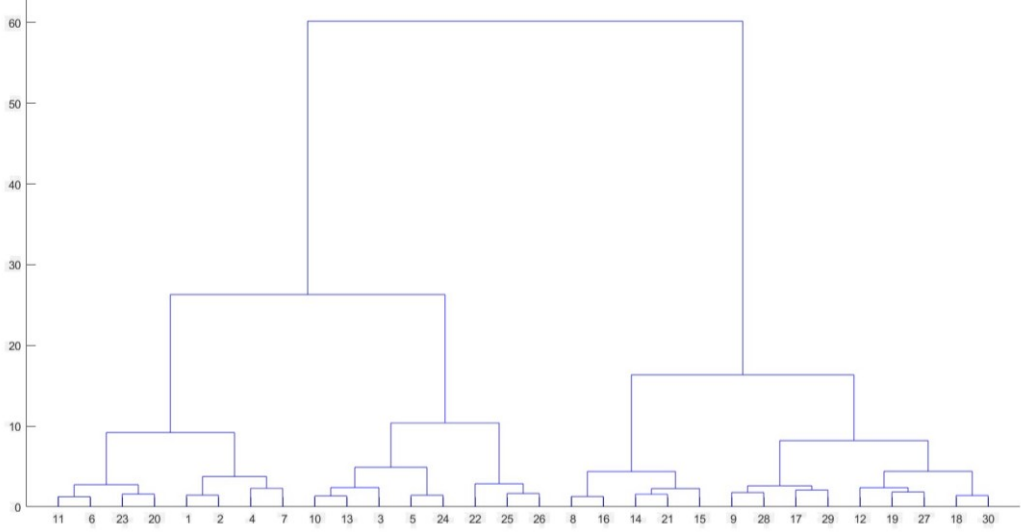
Fig. 28 – Example of dendrogram

---

[23] The total inner cluster variance is represented by the average distance of all the observation into a single cluster, from the cluster mean [231].

[24] They are hierarchical representations, where at each level separate clusters at a lower level are merged. At the top of the dendrogram, there is a single cluster containing all the data, progressively separated, according to similarities/dissimilarities in the observations, until the base of the graph, where each cluster corresponds to a single observation [231].
The main characteristic of a dendrogram is that subsects of data can include one another, but they cannot intersect [230].

In this case, the procedure is agglomerative and it adopts the Ward's minimum variance method as merging criterion [230]. Given that hierarchical clustering is iterative, it begins computing the squared Euclidean distance between singleton clusters[25], with the aim of minimizing, at each level of the hierarchy, the total inner cluster variance[26], computed according to Eq. (5. 12):

$$d(r,s) = \sqrt{\frac{2n_r\, n_s}{(n_r + n_s)}} \sqrt{(x_r - x_s)^2 + (y_r - y_s)^2 + (z_r - z_s)}$$

(5. 12)

Where:

- x_r, y_r, z_r are the coordinates of the centroid of cluster r
- x_s, y_s, z_s are the coordinates of the centroid of cluster s
- n_r and n_s are the number of elements in clusters r and s [232].

Once the unsupervised approach has been established, also in this circumstance, the issue related to the colour-space has to be addressed (section 5.2.1). Here, various models have been tested, beyond RGB and YCbCr, always considering the importance of the lighting and shading factors to achieve a proximity with the human perception [189]. Specifically, hierarchical clustering has been applied to four different colour-spaces, to compare the results and to determine which one is the most performing in the segmentation of chromatic changes in a masonry surface. They are:

- HSV (Hue, Saturation, Value), where Hue is measured as the angle expressing the rotation around the vertical axis (from 0° red, to 120° green and 240° blue); Saturation, ranging from the vertical axis 0 (unsaturated), to the value 1 (fully saturated) on the external surface of a cylindrical model; and Value corresponding to brightness
- YCbCr (Luminance, blue and red difference chroma components), already illustrated in section 5.2.1

---

[25] Singleton clusters are clusters containing a single observation

[26] It is the sum of squares of the distances of the instances from the centroid before and after fusing two clusters

- YIQ (Luminance, In-phase, Quadrature), where Y is the luminance value, and I and Q are the two chrominance values, corresponding approximately to the amounts of blue and red in the colour

- YUV (Luminance, blue projection, red projection), where Y is the luminance, and U and V stand for the deviations of red and blue from the luminance respectively (Fig. 29).

In HSV, in contrast with RGB, chromaticity is separated from intensity or brightness, and, therefore, lighting/shadowing factor does not influence the component related to the chrominance (Hue), but only the component related to the brightness [233].

The last three colour-spaces are qualified by the relevance of the luminance as opposed to the chrominance (to which reduced bandwidth are associated), where the luminance corresponds to the perceived energy of a light source by the human visual system [120].
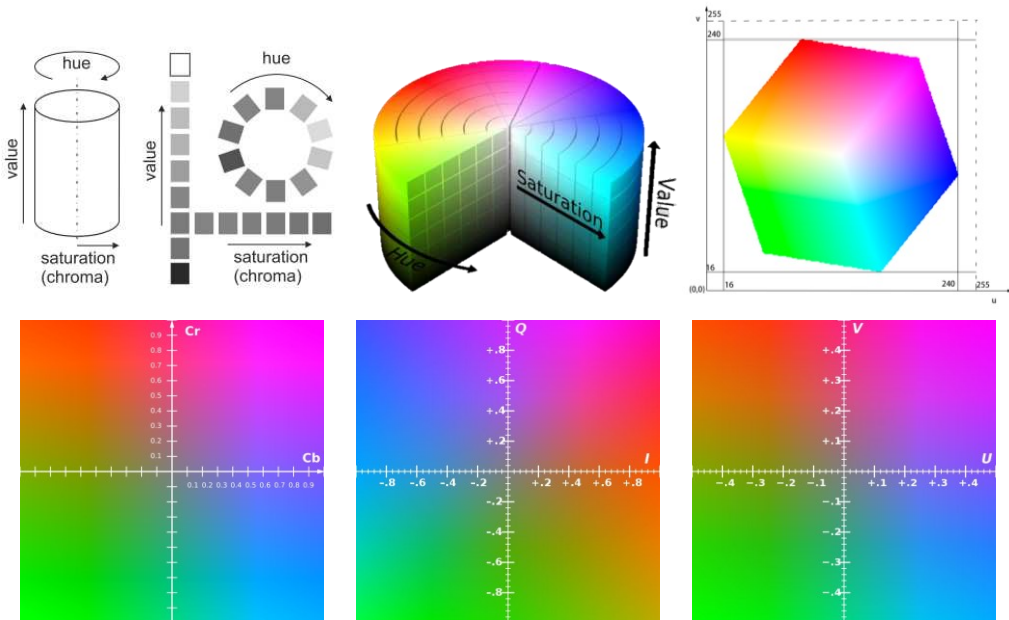
Fig. 29 – Graphical representations of the four investigated colour spaces: HSV, YCbCr, YIQ, YUV ([220], [234], [235]).

The chromatic conversion from RGB to the four colour spaces is obtained, thanks to mathematical transformations applied to RGB triplets contained in a point cloud.

The transition from RGB to YCbCr has been already described in section 5.2.1 [217] [220].

For example, the conversion from RGB to HSV follows Eq. (5. 13) [217]:

$$H = \begin{cases} \theta & \text{if } B \leq G \\ 360 - \theta & \text{if } B > G \end{cases}$$

$$\theta = \cos^{-1}\left\{ \frac{\frac{1}{2}[(R-G)+(R-B)]}{\left[[(R-G)^2 + (R-B)(G-B)]^{1/2}\right]} \right\}$$

$$S = 1 - \frac{3}{(R+G+B)}[\min(R,G,B)]$$

$$I = \frac{1}{3}(R+G+B)$$

(5. 13)

While the modifications RGB-YIQ and RGB-YUV happen according to Eq. (5. 14)(5. 15), respectively [236]:

$$\begin{bmatrix} Y \\ I \\ Q \end{bmatrix} \approx \begin{bmatrix} 0.299 & 0.587 & 0.114 \\ 0.5959 & -0.2746 & -0.3213 \\ 0.2115 & -0.5227 & 0.3112 \end{bmatrix} \begin{bmatrix} R \\ G \\ B \end{bmatrix}$$

(5. 14)

$$\begin{bmatrix} Y' \\ U \\ V \end{bmatrix} = \begin{bmatrix} 0.299 & 0.587 & 0.114 \\ -0.14713 & -0.28886 & 0.436 \\ 0.615 & -0.51499 & -0.10001 \end{bmatrix} \begin{bmatrix} R' \\ G' \\ B' \end{bmatrix}$$

(5. 15)

The output of this pipeline is a segmented point cloud with clusters organized in a tree-like structure, which is cut according to the number of defects to detect (chromatic alteration, moist area, biological patina/colonization, spots, deposit,…). Every decay pattern is associated to its colour range. Then clusters, associated to their defect class can be quantitatively described, with the extraction of geometric parameters (area, volume, percentage extension).

This kind of information, derived from clusters segmented in the four colour spaces; have been compared in order to establish the most consistent results, with respect to manually annotated ground truth samples.

A synthesis of the methodological workflow elaborated in this section is proposed in Fig. 30.
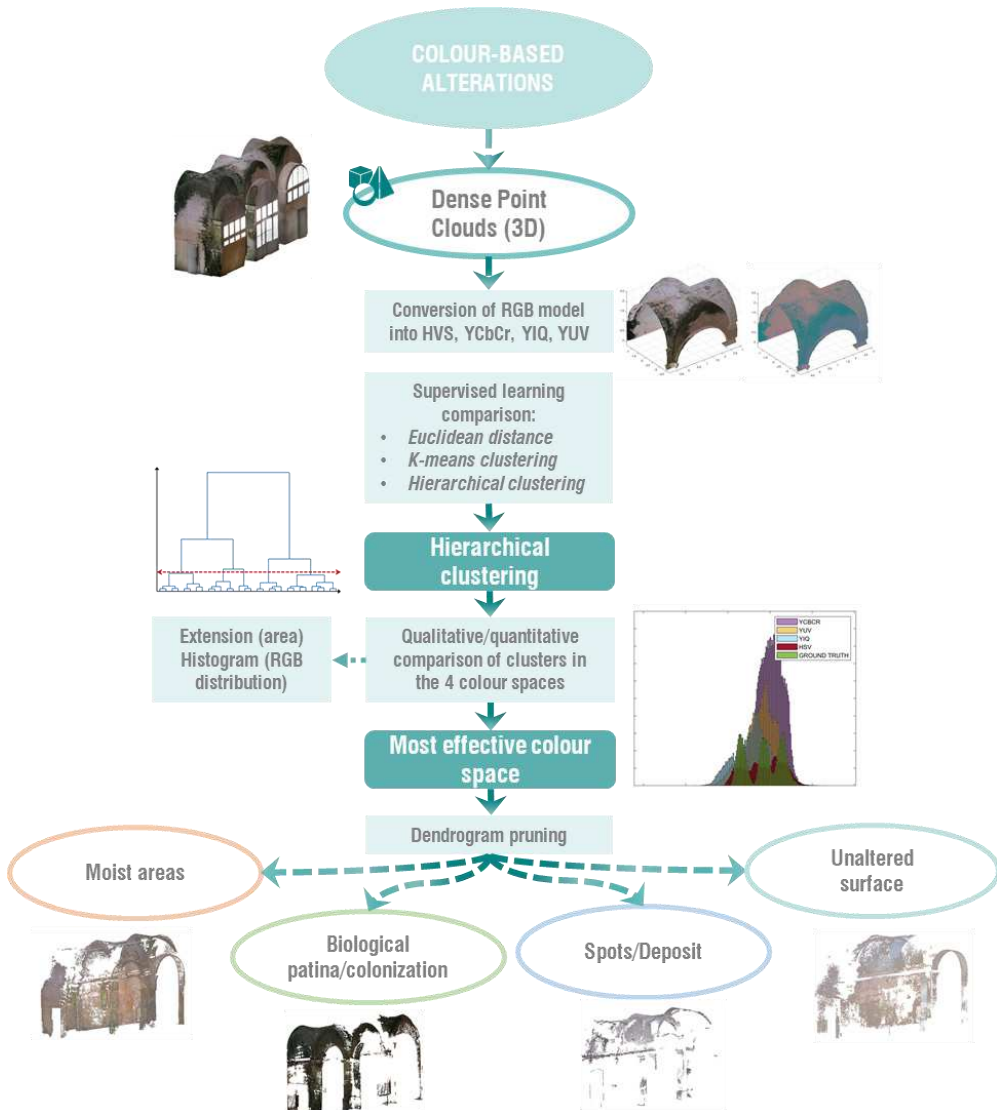
Fig. 30 - Methodological workflow (based on [232])

5.2.3. Comparison between cloud-based unsupervised and texture-based supervised machine learning approaches

In this section, the unsupervised point cloud segmentation pipeline, proposed in section 5.2.2, is compared to a state-of-art supervised texture-based machine learning procedure, always aimed at detecting alterations on a chromatic basis.

In this case, a supervised approach is applied to high-resolution textures (2D image), retrieved from photogrammetric models of architectural elements or building environments [188] [181]. Up to now the recalled methods have been applied to photogrammetric-based orthoimages, UV maps or textures, for the purpose of assessing the general state of conservation of a surface (like a wall), or the constructive elements and materials, or the masonry pattern. In [5] texture-based machine learning segmentation is applied to masonry walls of an historical artefact, to distinguish and classify some forms of chromatic alterations.

On account of this, a pixel-based segmentation is obtained as the product of the application of a random forest learning algorithm, in relation to a set of features and annotated data preliminarily provided by the user. Random forest builds randomized decision tree in each iteration, on the basis of the input data, in order to determine reliable predictors for the classification [230]. Indeed, random forests coincide to a compound of tree predictors, depending on the values of random vectors, all characterized by the same distribution [238].

The application of supervised learning to a texture/orthoimage/UV map goes through a few fundamental steps. After the extraction of 2D data on which the segmentation procedure has to be performed, some relevant features have been selected, on the basis of which the splitting of pixels would be done. These features represents a series of operations to be performed on data, like denoising, edge extraction, blur removing, … Then, a number of annotated samples, representative of each class of the classifier are provided, to process the training phase. Once the learning procedure on the labelled areas is completed, the segmentation is extended to the whole 2D data. The outputs are segmented pixels, divided according to the classes determined at the beginning (chromatic alteration, moist area, biological patina/colonization, spots, deposit,…).

The execution of this pipeline, as alternative to the one proposed in section 5.2.2, is functional to a comparative evaluation of the results obtained from both of them, in order to highlight their outcomes and drawbacks, which will be illustrated in section 9.

5.3. Geometric segmentation of point clouds to identify architectural elements

In parallel with procedures for the survey of geometric and colorimetric alterations, model fitting has been explored for the geometric segmentation of a point cloud representing an architectural environment. This aspect is convenient to the purpose of automatically associating decay patterns to specific architectural elements, at a macroscopic level of detail, like walls, columns, pillars,…

Shape detection or best fitting algorithms are suitable because they find primitive shapes to approximate 3D data. For example, the efficient RANSAC (RANdom SAmple Consensus) algorithm, proposed by Schnabel et al. (2007), which construct candidate shape primitives (planes, cylinders, spheres,…) in correspondence of randomly selected minimal sets from the source data [172]. The algorithm considers the smallest number of points to define a geometric primitive, which is, in turn, verified for all the points in the dataset, to comprehend the number of points a single primitive could cover. This is a recursive process, focused on the identification and extraction of the shape approximating the major number of points. A limit of acceptance is established in advance, representing the probability of existence of a better candidate, for a determined set of points. Once a primitive is extracted, the corresponding points are excluded and the algorithm follows the same scheme for a new primitive, tested on the other points. To perform the pipeline on the analysed data, a series of parameters are defined:

• kind of primitive (plane, sphere, cylinder, cone, torus);
• minimum number of points to uniquely define a primitive;
• maximum distance between the set of points and the primitives;
• sampling resolution (distance between neighbouring points in the data);
• maximum angular deviation between point normal and primitive;
• probability that no better candidate exists [172] [232].

6. MONITORING BUILDING DECAY PATTERNS BY PHOTOMODELLING BASED 3D MODELS FOR THE REMOTE DIAGNOSIS AND CONTROL OF THE HERITAGE ARCHITECTURE

In cultural heritage, and, more generally, in the built heritage, there is another utterly important aspect, beyond the assessment of the state conservation at a definite moment, concerning the necessity to monitor the decay progression over time. Also in this regard, three-dimensional data (point clouds, polygonal meshes, texturized models) could represent a valuable alternative, for the remote control of previously recognized decay patterns or particularly critical conditions. Point clouds of the same artefact or part of it, acquired at different periods, within a properly extended time interval, are useful to establish whether some changes occurred in the examined structure, in relation, for example, to static instabilities (crack patterns, displacements, deformations,...), stone surface alterations (erosion, alveolization, lacks) or humidity patterns (moist areas, biological patina/colonization). The analysis of 3D data represents a support in understanding the advancements of decay morphologies, quantifying them and their changes in a three-dimensional environment, allowing professionals to determine the presence of critical conditions, and their level of urgency, to carry out corrective interventions, or simply providing a confirmation that no changes occurred.

This leads to the definition of semi-automatic image processing or machine learning routines to extract and compare relevant quantitative information from point clouds acquired in pre-determined time intervals, toward the control and monitoring of physical changes in heritage buildings.

To this end, two different procedures have been outlined, in order to provide a theorical and operative guidance for the implementation of remote control of artefacts: they entail direct (B) or indirect (A) comparison of 3D data (Fig. 31).

It is worth to underline that to accomplish a quantitative comparison, it is necessary to establish in advance the goal of the control activities and therefore the kind of decay to evaluate, in order to properly dimension the acquisition campaign (focal length, shooting distance, overlapping between images, number of images,...), in relation to

the desired level of detail (see section 4.2.2). In fact, the size of the minimum characteristic determines the needed resolution. By way of example, for the assessment of macroscopically visible alterations, such as displacement, deformations or surface decay (in the order magnitude of centimetres), there are not rigid requirements about the 3D data resolution. On account of this, for an expeditious evaluation of changes, also 3D data acquired, with different purposes or equipment, could be collated to retrieve useful information. While smaller alterations require a greater resolution of 3D data.
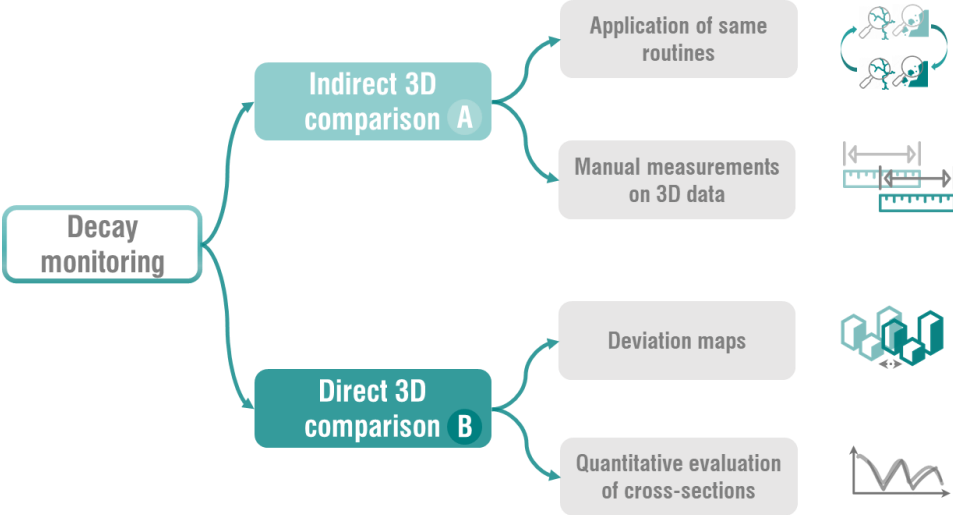
Fig. 31 – General workflow for remote monitoring and control on 3D data

6.1. Indirect monitoring and control of decay patterns on built heritage

In this section, the indirect comparison among 3D data is illustrated. In particular, the procedure starts from the pipelines presented in sections 5.1and 5.2, for the detection and quantification of geometry-based and colour-based alterations respectively. In first place, they are applied to 3D data (point clouds, meshes) acquired at different time intervals, to assess and quantify eventual modifications due to decay progression.

The comparison is accomplished by opposing the outcomes of the application of the image processing/machine learning routines on the same point clouds, in terms of geometrical characteristics or descriptors (area, volume, length, depth,…), obtained after the point cloud segmentation.

Indeed, the most significant correlation concerns distance measurements between corresponding relevant points in two distinct models, the height of selected points, with particular attention to those at a greater depth, visible and measurable from cross sections, but also the computation of geometric attributes like area, volume, perimeter of grains.

In addition, it is possible to manually perform a series of punctual measurements, concerning horizontal, vertical or oblique distance between two points, angle between segments, distance between parallel lines.

They could be interesting, for example, to compute and monitor overtime the amplitude of a specific crack, the distance between two neighbouring cracks, the size of a missing part, or the diameter of a cavity [4] [15] [17].

6.2. Direct monitoring of the state of conservation of the architectural heritage

A direct comparison of point clouds, as well, is useful for monitoring the advancement of crack or moisture patterns or generic surface alterations (erosion, lacks, alveolization, …), as well. In this case, a change detection is performed, to rapidly observe discrepancies between 3D data of the same architectural element, acquired in a time interval.

In order to achieve this kind of analysis, it is preferable to take into consideration point clouds characterized by comparable resolutions (i.e. analogous ground and height resolutions[27]), and a congruous number of points, to prevent the results from being affected by the divergence of resolution.

The first step of the procedure concerns the alignment and registration of the two clouds, choosing one of them as the reference. An expeditious method to align two entities is picking at least three equivalent point-pairs on the object. This coarse alignment can be improved, reducing also the error, through the ICP algorithm (Iterative Closest Point), which consists in an iterative process for the identification of the best match between the two clouds. Indeed, the algorithm minimize registration errors (Root Mean Square Error or RMSE) until a pre-determined value (6. 1).

$$RMSE = \sqrt{\frac{\sum_1^n (y_{ir} - y_{ic})^2}{n}}$$

(6. 1)

In Eq. 6. 1, y_{ir} is the value of a point in the reference model, y_{ic} is the value of the corresponding point in the compared model and n is the number of points of the cloud. In order to apply the algorithm to the clouds, some main parameters must be set in advance, such as the RMSE minimum threshold, number of iterations of the process and final overlap of the two models.

The aligned 3D data are useful to compute cloud-to-cloud (or cloud-to-mesh) distances, i.e. to calculate the deviation between two point-clouds (or between a point cloud and a mesh), through the 'nearest neighbour distance'. It consists of the Euclidean distance between each point of the compared cloud and their nearest point in the reference cloud (Eq. (6. 2).

---

[27] Ground resolution: minimum distance on the ground between two closely located objects distinguishable as separate objects (parallel to the plane of the façade)
Height resolution: difference in height of the intersection of two homologous beams from adjacent photographs, when one of the two rays moves a pixel along the line connecting the two projection centres (perpendicular to the plane of the façade)

$$D = \sqrt{(p_x - q_x)^2 + (p_y - q_y)^2 + (p_z - q_z)^2}$$

<div align="right">(6. 2)</div>

In this equation *P(x,y,z)* is the point in the reference cloud, while *Q(x,y,z)* is the corresponding point in the compared cloud.

If the *Reference* point cloud is not dense enough the computation of distances is not properly precise. Therefore, the distance (D) should be replaced by the distance between the point in the compared cloud and the distance of a mathematical model fitted on the 'nearest' point and several of its neighbours.

The mathematical model better represents the surface, because it is independent of the cloud sampling, and it can be chosen by the user, among the least square best fitting plane, Delaunay triangulation, or quadratic height functions. It is important to underline that in all these computations the same roles (*Reference* and *Compared* model) of the clouds are preserved.

It is also possible to act on the way the neighbours are extracted around each 'nearest' point in the reference cloud, by setting a fixed number of neighbours, or by providing the radius of a spherical neighbourhood. The results of the computation can be observed as absolute distances or as distances split in the three dimensions (x, y, z) [17].

6.3. Semi-automatic procedure to control displacements and crack deepening from transversal section quantitative comparison

Further valuable information can be retrieved from the quantitative pairwise comparison of transversal profiles, extracted in critical sections. To this end a semi-automatic procedure has been created. It starts with a pre-processing phase, focused on the profiles cleaning.

First of all, for each transversal section duplicate points, under a user-defined threshold distance, are removed. This means that all the neighbours standing at a lower distance, with respect to the threshold, are considered as duplicates of the examined points, and consequently removed. In the case of architectural heritages, a proper threshold could be considered in the order of magnitude of a tenth of a millimetre, in order to avoid the loss of information about geometry or decay.

In addition, the presence of noisy data in the cloud could produce some extraneous values, which affects the result of the profiles quantitative comparison. For this reason, before the overlapping, the two interpolated profiles have to be further cleaned, removing or substituting outliers.

Among the various methods, the median is particularly efficient. It works identifying as outliers elements at more than three scaled median absolute deviations (MAD) from the median (Eq. (6. 3)).

$$\mathrm{MAD} = \mathrm{median}(|A_i - \mathrm{median}(A)|)$$

(6. 3)

The detected outliers are replaced with the value of the previous non-outlier point.

Each extracted profile is compared with its correspondent, acquired in a different time, in order to evaluate eventual changes. Before performing a quantitative analysis focused on computing the difference between two corresponding profiles, the scattered or non uniform sequence of points of the single profile is transformed into regularly spaced 2D or 3D data. This means that sections are interpolated in a regular xy grid (with a constant pace and fixed axes limits), so that a comparable number of points is extracted from the original profiles, and the difference between the two can be computed as a point-to-point distance, correlating corresponding points of the grid.

For the profile interpolation, a triangulation-based nearest neighbour interpolation has been preferred, among other tested methods (like cubic, natural neighbour, cubic or biharmonic spline), which supports both 2-D and 3-D interpolation, because it better approximates the curvature of the input profiles.

It is a widespread image processing interpolation method, which computes the neighbour values of a point and substitutes them to its original value in the input data. The adopted interpolation methods employ Delauny triangulation, for the identification of neighbours.

The choice of the grid pace is made on the basis of the size of surface defects or element units under investigation. For example, for the observation of displacements, a proper order of magnitude is of 0.5/1 cm, while for the identification of eventual crack development, it is necessary to adopt a narrower interval, in the order of 1 millimetre and above. The reduction of the grid cell size produces a notable increasing of computational costs, that is why it is necessary to scale the approach according to the scale of the object and the aim of the investigation.

After data preparation, the two sections are overlapped, and the eventual differences are quantitatively determined, with a point-to point difference of corresponding points of the interpolated profiles (before and after). The output is a 2D curve, where the y-axis represents the difference value and the x-axis its position in the interpolated grid. In order to compute the divergence numerically, trapezoidal numerical integration is used, which subdivide the area under the curve into finite trapezoidal elements, according to the following equation (Eq. (6. 4):

$$\int_a^b f(x)dx \approx \frac{b-a}{2N}\sum_{n=1}^{N}(f(x_n)+f(x_{n+1})) = \frac{b-a}{2N}[f(x_1)+2f(x_2)+...+2f(x_N)+f(x_{N+1})]$$

(6. 4)

This area can be considered representative of eventual displacements or changes in general, observed in the section plane. In addition, in order to highlight regions affected by the advancement of decay phenomena like cracks, or features induced by material loss (erosion, cavities, stone/mortar joint losses,...), expressed by surface excavation, a focus is put only on positive differences between pre and post.

PART 3

EXPERIMENTAL
APPLICATION

The proposed procedures were applied and tested on a variety of case studies, belonging to the territorial (regional or international) cultural heritage, chosen according to some criteria:

- Age of construction (from the I century BC, to the XVIII century AC);
- Building type (residential palace, ex-convent, medieval fortress, church, archaeological area);
- Surface materials (smooth or ashlar limestone, tuff, brick, plaster);
- Architectural environments and related shapes (façade, pillar, column, vault, wall, cloister, cryptoporticus);
- Decay phenomena (static instabilities: crack patterns, displacements, deformation; surface deterioration: erosion, alveolization, lacks; colour-based alterations: moisture patterns, chromatic alterations, spots, deposits).

In particular, the experimentation concerned the following architectures, grouped according to the applied procedures:

A. Detection of geometry-based alterations and monitoring

1) *Palmieri Palace* (Monopoli, Bari, Italy – XVIII century AC), a vast noble residential palace, with great historical artistic value. The investigation was focused on specific parts: portal and small portions of the main façade (ashlar limestone or tuff), affected by surface decay like erosion, alveolization, lacks; or pillars of the atrium, damaged by static instabilities (crack patterns). For these situations image processing and feature extraction routines were applied, and they were also monitored overtime (Part 2: sections 5.1.1,5.1.2, 6.1, 6.2; Part 3: sections 9.1.1, 9.1.2, 9.1, 9.2);

2) **Fortress of Bashtovë** (Bashtovë County, Kavajë, Albania - XV century AC), a medieval fortress, made by brick walls and towers. The north-tower is affected by a static instability, for which it was investigated with image processing and feature extraction pipelines, but also monitored overtime, after a seismic event (Part 2: sections 5.1.1,5.1.2, 6.2, 0; Part 3: sections 9.1.1, 9.1.2, 9.2, 9.3);

3) **San Corrado's Cathedral** (Molfetta, Bari, Italy – XII/XIII century AC), a Romanesque cathedral, erected near the seaside, and therefore affected by evident and evolving erosion phenomena, due to the severe effect of marine aerosol. Some significant architectural elements were treated (half-column, barrel vault), according to the damage evaluation routine for the quantitative detection of eroded limestone (Part 2: section 5.1.3; Part 3: section 9.1.3);

B. Detection of colour-based alterations

4) **Ex Convent of San Leonardo** (Monopoli, Bari, Italy – XVI century AC), an ex-convent, actually abandoned, and therefore heavily subjected to humidity (biological patina/colonization, moist area), and other colour-based alterations (chromatic alterations, spots, deposit). The plastered surface of the cross-vaulted cloister was considered for the application of unsupervised cloud-based hierarchical clustering routine and compared with texture-based supervised learning (Part 2: sections 5.2.1, 5.2.2, 5.2.3, 5.3; Part 3: sections 9.2.1, 0, 9.2.2);

5) **Cappuccini Ex-Convent** (Conversano, Bari, Italy – XVI century AC), an abandoned ex-convent, whose interiors are consistently affected by humidity and other colour-based alterations. Two architectural volumes were used to test and validate the unsupervised cloud-based hierarchical clustering routine (Part 2: sections 5.2.2, 5.3; Part 3: sections 0, 9.3);

6) **Cryptoporticus of Egnazia** *(Fasano, Brindisi, Italy – I century BC)*, a four-arms, barrel-vaulted cryptoporticus, within the Roman archaeological area of Egnazia, characterized by extended moisture patterns. One of the four arms, the south-west, was analysed by the unsupervised cloud-based hierarchical clustering routine and compared with texture-based supervised learning (Part 2: sections 5.2.2, 5.2.3; Part 3: sections 0, 9.2.2).

7. CASE STUDIES

7.1. Palmieri Palace *(Monopoli, Bari, Italy – XVIII century AC)*

The Palmieri Palace is a noble residential building, located in Monopoli (Puglia, Italy), in the homonymous square largo Palmieri (Fig. 32). The construction dates to the 18th century, by Marquis Palmieri's family, native of France. The building is an example of late-Baroque architecture, with a coexistence of influences from Lecce and Naples.

Fig. 32 – Geographical localization of Palmieri Palace, within the historical centre of Monopoli, in proximity of the seaside

The main façade is marked by rusticated ashlars at the base and a smoothed stone cornice at the top. A pair of Ionic columns and semi-columns in limestone, supporting the entablature and the upper floor balcony, adorns the entrance. The upper floor loggia is decorated by the family emblem. Also, the cornices of the windows of the three floors are in limestone, while the majority of the façade is covered by tuff (Fig. 33).

Through the portal, it is possible to reach an atrium or internal courtyard (Fig. 34), where there is the access to the stone staircases, leading to the upper floors (three apartments) and to the solar roof. On the ground floor, near to the main door, there were stalls for horses, the coach depots and the stocks [240].

Fig. 33 - High-resolution texturized polygonal mesh of the main façade, with a zoom on the portal [4],[16].

The fabrication includes in its foundations some of the oldest structures, characterized by large, buried compartments, now occluded by more recent walls. In 1767, Giuseppe Palmieri, the designer architect of the building, refers to a new plan that he would have designed "in place of the demolished one".

Fig. 34 – High-resolution texturized polygonal mesh of the internal courtyard, with a focus on the lower part of the staircase façade [4],[16].

The ground floor was partially occupied by servants and by the wood and food storage. At the main floor, there was the apartment of Palmieri family, which consisted of a series of rooms, developed around the atrium, covered by frescoed false vaults. The most important room is the "gallery", intended to host art collections of ancient artifacts such as amphorae, coins and paintings. Near the gallery there was the private chapel, typical element of the eighteenth-century buildings, with a decorated altar. The top floor, instead, was dedicated to guests, friends or relatives.

The identification of the architect is uncertain, but some researchers thought at the Apulian architect Vincenzo Ruffo (1749-1794), Vanvitelli's pupil and designer of other local buildings, such as Palazzo Alberotanza in Mola and Castle Marchionne in Conversano. This hypothesis was contested by the researcher Michele Pirelli, who stated that Vincenzo Ruffo was too young at the time of the construction. Instead, Mimma Pasculli Ferrara attributes the project to Giuseppe Palmieri (1725-1792), who participated to the construction of the Cathedral, the Episcopal Palace and the "Muraglione" in Monopoli. Besides, he designed also another palace in Ostuni, for the same family [240,241].

The actual general conditions and organization of the artefact are the result of several changes during the late centuries. After the death of the first owner, Francesco Paolo Palmieri, in 1797, the property ran into long periods of abandonment, until the early years of the 1900. In 1907, the top floor of the building became a male orphanage; instead, in 1921 the whole building turned in a School of Arts and Crafts. The years of neglect put the artefact in critical conditions: the roof and the façade required interventions. Consequently, in 1930, the first structural works, by Eng. Sant' Erchia, consisted in the application of the "sew-unsew" to replace damaged stones of the pillars, in the facade of the internal atrium, collapsed because of compression stresses (Fig. 34). In 1950, further works were carried out, including a series of changes on the third floor, including the construction of an elevator. After an earthquake, in 60's, the existing school was evacuated and then completely abandoned. The last restoration works date back to the 80s [240]. At present the building is abandoned, and both the internal and the external components are deteriorated, and they required interventions [4],[16].

To synthetize, the major problems affecting the palace, and, therefore, the objects of investigation, are:

- Widespread surface deterioration of the external façade, showing up in form of erosion, alveolization, lacks, observed both in critical areas of the rusticated basis, and in the entrance portal.
- Static instability of the pillars of the internal atrium, visible through crack patterns.

7.2. Fortress of Bashtovë *(Bashtovë County, Kavajë, Albania - XV century AC)*

The medieval Fortress of Bashtovë, located near the Shkumbin River and the Adriatic shoreline in Central Albania, is a national monument candidate to be included in the UNESCO World Heritage Site list (Fig. 35). It was erected during the domination of the region by the Venetian Empire (XV century), over an existing Byzantine structure (6th century), attested by decorative architectural details [242].

Fig. 35 – North-east façade

It is an architecture made of local sandstone, with a quadrangular development, perimetral walls, three entrances and four towers at the corners, of which only two still exist. The overall dimensions are 60 x 90 m in plan, with a walls' thickness around one metre, and a towers height of about 12 metres. The western wall was reconstructed during the XVIII century. Except for the western tower, the perimetral walls and the towers still preserve a global integrity, guaranteed also by interventions in respect of the original materials and assets, also in the castle proximity [143].

As far as the state of conservation is concerned, a particular attention has been dedicated to the north tower (Fig. 36), which is affected, on one hand, by phenomena of structural deficiency, visible from a huge vertical crack covering almost the whole height of the tower, and, on the other hand, by widespread alterations (cavities, holes, alveolization) ascribable to stone deterioration [29].
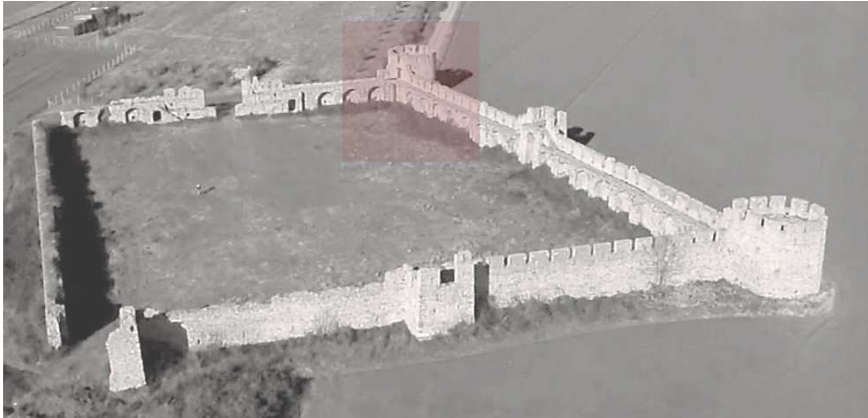
Fig. 36 – Localization of the north tower (red area) of the Fortress of Basthovë.

In light of its conservation, an important event should be considered: in 2019, two considerable seismic events took place in Albania, in a range of two months (21/09/2019 and 26/11/2019). The first one had its epicentre in Durres, at a 10 km depth (Fig. 37). It had a magnitude of 5.6 (Richter scale) in its epicentre and 5 (Modified Mercalli Intensity – MMI) in Bashtovë. The major damages were reported in Durres and Tirana (110 houses and 7 buildings).

SHAKING	Not felt	Weak	Light	Moderate	Strong	Very strong	Severe	Violent	Extreme
DAMAGE	None	None	None	Very light	Light	Moderate	Moderate/heavy	Heavy	Very heavy
PGA(%g)	<0.0464	0.297	2.76	6.2	11.5	21.5	40.1	74.7	>139
PGV(cm/s)	<0.0215	0.135	1.41	4.65	9.64	20	41.4	85.8	>178
INTENSITY	I	II-III	IV	V	VI	VII	VIII	IX	X+

Scale based on Worden et al. (2012)   Version 1: Processed 2020-06-06T00:10:43Z
△ Seismic Instrument ○ Reported Intensity   ★ Epicenter

Fig. 37 – Seismic event of 21/09/2019, with epicentre in Durres [244]

While a second stronger event had its epicentre 22 km far from Durres at a 38 km depth (50 km far from Bashtovë) (Fig. 38). The magnitude was of 6.3 (Richter scale) in the epicentre and 6 MMI in Bashtovë. In this case, several damages were registered in multiple municipalities (Shijak, Durres, Kruja, Tirana, Kamza, Kavaja, Kurbin and Lezha) [245].

On the basis of the historic seismicity of the area around Bashtovë (6.2-6.3 MMI), and the intensity of the two events, both in line with this information, it is possible to establish an expected qualitative level of damage. Indeed, the Modified Mercalli Scale correlates the shaking magnitude of the event with damages occurring on people, objects or buildings. For masonry buildings, like the actual case study, 6 MMI means that some walls and parapets of poorly constructed buildings could crack [246] [247]. The Fortress, together with other cultural heritages, have been included in the list of monuments to be inspected and monitored, within the "Albania Post-Disaster Needs Assessment" realized in February 2020, because of its critical conditions (fragile state of walls, static instability phenomena) [245].
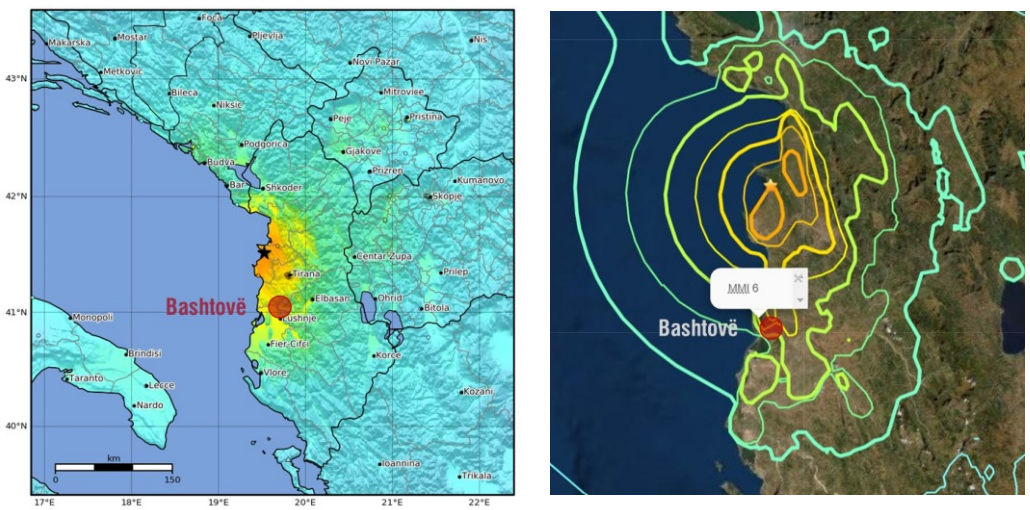
Fig. 38 - Seismic event of 26/11/2019, with epicentre in Durres [244]

7.3. San Corrado's Cathedral *(Molfetta, Bari, Italy – XII/XIII century AC)*

San Corrado's Cathedral, erected between the XII and XIII centuries, is located in Molfetta (Bari, Italy), in the old town, facing the sea, both on the north and the west-side (Fig. 39). The church represents a unique architecture, because it merges characters of two Apulian Romanesque schemes: the dome in axis with the central nave, embedded in a pyramidal structure (outside), connected to lateral half-barrel vaults (inside); and the widespread basilica's layout with crypt, apses and towers.

Fig. 39 - Geographical localization of San Corrado's Cathedral, within the historical centre of Molfetta, in proximity of the sea, both on the north and the west side

There is not any documentation about the original structure of the building, especially concerning the location of the main access and the project for the crypt. Moreover, the presence of chapels on the side that should have constituted the main façade indicates successive modifications to the original project, probably due to the sea advancement and the quay corrosion. Indeed, in the first half of the XX century, a bastion protecting the church from the sea, on the west-side, was demolished, presumably because of the construction of the quay (Fig. 40).

On the north-side, the actual main façade lacks a pinnacle: it is completed only by the octagonal tambour and the pyramidal structure, covering the western dome. The façade is decorated by a simple central rose window, aligned with the portal, and three single-lancet windows. Two low structures, placed near the central entrance, correspond to two chapels realized in the XIV century.

The north façade is articulated in two small lateral buildings, leaned against the main body, corresponding to S. Catherine and S. Giuliano chapels. The last is covered by a pitched roof made of a local stone named "chiancarelle".
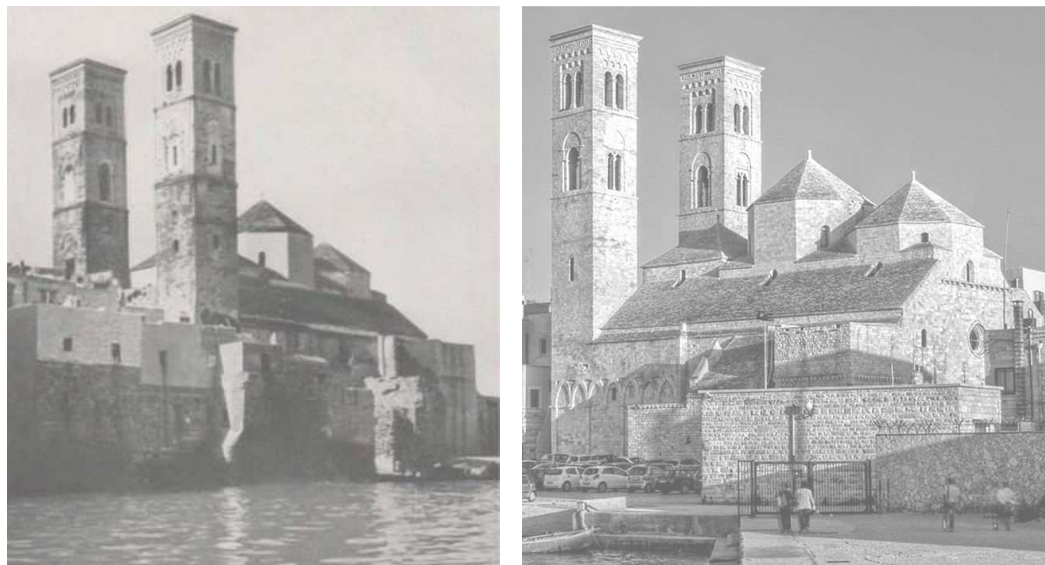
Fig. 40 - West façade of San Corrado's cathedral, from the seaside (XIX century on the left, XXI century, on the right) [248]

The east façade, in correspondence of the apse (non-visible from the outside), is enclosed between two towers. It is decorated by a crossed-arches motif and it accessible only from a narrow street. The towers are characterized by three orders of windows, one lancet and mullioned alternatively, and a flat roof instead of a pyramidal one. They have a square plan and the interior made of six levels covered by barrel-vaults.

The plan presents noticeable irregularities in the asymmetrical axes of the naves, but also in the decorative apparatus. The transept is characterized by blind arches,

interrupted by a vertical line connecting two different phases of the project development. The interiors are organized into three naves and a transept of two lateral spans. The naves are divided by four pillars with decorated capitals, to form three quadrilaterals covered by hemispherical domes, and six half-barrel-vaulted aisles, two in correspondence of each quadrilateral (Fig. 41).

The pillars have three band-capitals towards the main nave and a lowered capital toward the aisles. Their decoration varies from a Byzantine style to a more naturalistic one. The three domes are distinguished for their shape and height: the western and the eastern have a circular base and hemispherical section. The eastern is the lowest, covered by a square pyramidal roof. The central dome is the highest (23.5 m high), with its ovoid section, and an octagonal base pyramidal roof (like the western).

The actual decorative aspect results from a restoration intervention of the XX century, aimed at removing the Baroque coatings covering the internal walls [249].
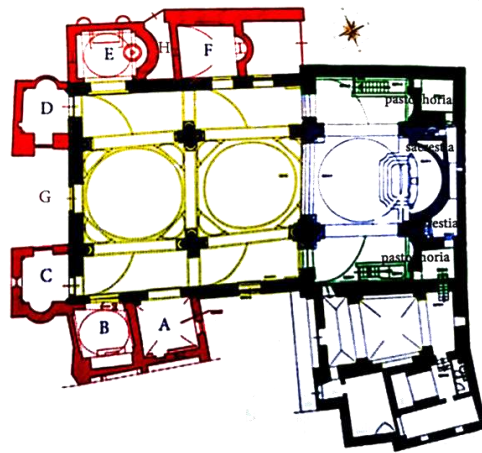
Fig. 41 – Church plan, with historic phases, since the Armenian-Byzantine until the Romanesque [249].

As represented in Fig. 39, San Corrado is located near the seaside, and therefore exposed on the north and west sides. As a consequence, exterior and interior surfaces are strongly affected by the presence of marine aerosol, which contributes to the disgregation of stones and to a rapid progression of the erosion. These decay morphologies are particularly spread in the interiors, in critical areas in direct contact with marine air. In fact, the half-barrel vaults, the perimetral arches of the three spans, and some pillars show diffuse eroded areas.

7.4. Ex Convent of San Leonardo *(Monopoli, Bari, Italy – XVI century AC)*

The ex-convent of San Leonardo is a XVI century building located in the old town of Monopoli (Bari, Italy) (Fig. 42). The fabric is characterized by an irregular plan developed in two levels in elevation, around the main cloister. Each space is covered by barrel, cross or mirror vaults. The external walls are made of tuff ashlars and limestone decorative elements, in correspondence of the portals. Close to the convent fabric there is the church, a representative architecture of the XXXVIII century, combining Ionian and Corinthian classical orders with Baroque decorative elements.

Fig. 42 - Geographical localization of San Leonardo Ex-convent, within the historical centre of Monopoli

The original core of the monastery was built in 1555, and, in the following centuries, further parts were added to the nucleus, until the late 18th century. Indeed, the history of S. Leonardo follows the history of the female Benedectine community, resident in Monopoli since 1000, and particularly in a "new convent" built around 1500. A more recent phase concerns the construction of the bell tower, the renovation, the expansion of the monastery and the construction of the new church (1721-1745).

At the end of the XVI century, it was built and decorated with chapels and paintings. Over the years, several maintenance interventions were necessary on the entire

building: a new chapel, stone staircases, a small new roof for the nurse, a belvedere (soon collapsed) and the bell tower in the early XVIII century; a new church, in place of the demolished one and a new fabric. In 1762, an old, frescoed crypt was discovered, concurrently to the demolition of the previous church Fig. 44. In the XIX century, monastic orders and convents were abolished, and all the built heritages were dedicated to functions of public utilities, like schools, hospitals,... As a consequence, in 1910, S. Leonardo was transformed in a secondary school, with little interventions, like new stairs and bathrooms, by the Eng. Sant' Erchia (Fig. 43). It kept this function until 1994, when the building was abandoned [250]. The actual state of conservation of the convent is compromised by extended humidity patterns, vegetation, deposit of organic materials,.... Therefore, some environments have been chosen, to test and validate the pipelines for colour-based alterations.
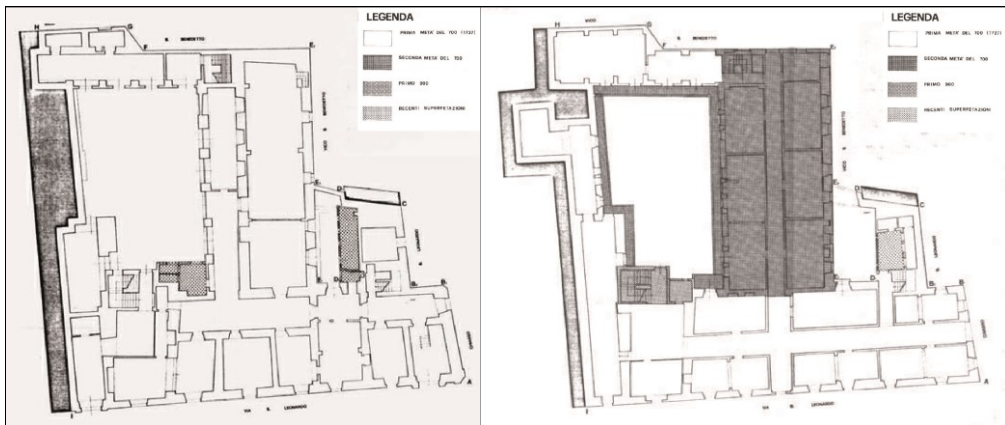
Fig. 43 - Plan of ground and first floors, with successive modifications (in grey)

Fig. 44 – Interior façade toward the cloister; wall-fresco of the Crypta.

7.5. **Cappuccini Ex-Convent** *(Conversano, Bari, Italy – XVI century AC)*

The Cappuccini ex-convent is located in Conversano (Bari, Italy), in the northern part of the town, outside the urban consolidated areas near the cemetery (Fig. 45).

Fig. 45 - Geographical localization of the Cappuccini ex-convent, on the northern part of Conversano, out of the city centre

Its construction dates back to the XVI century, when a hospice for monks was commissioned and declared a formal convent, together with the construction of the adjacent church. Indeed, as for the ex-convent of San Leonardo, the building is composed by two fabrics, hospice and church. In 1629, the convent was expanded, in order to reach 32 cells, a handcraft laboratory and a woollen mill. The interventions of 1629 involved the creation of a vertical connection between ground and first floor of the east wing, closing two arcades of the cloister, and creating side chapels in the church. In 1861 the convent was definitively suppressed and passed to the public property, starting a period of abandonment. After being acquired by the municipality of Conversano, the convent held different functions until the '70, when it was definitely abandoned.

As far as the morphology is concerned, the church is oriented to north, while refectory and daily use spaces, like kitchen and cells, are exposed to light.

The building is characterized by a complex architectural stratification (Fig. 46). Indeed, the layout of the functional static scheme is rigorous, on the west and south wings. On the contrary, the east side shows a lack of correspondence between ground and first floor. The expansion of the convent led to the addition of the sacristy and other rooms, on the north-east, both on ground and first floor. The cloister is the centre of the plan development, as fulcrum of the friar's community. In the initial project it was squared, but it was transformed in rectangular, with barrel-vaulted arcades on two sides (south and east). On the west side, the portico was demolished.
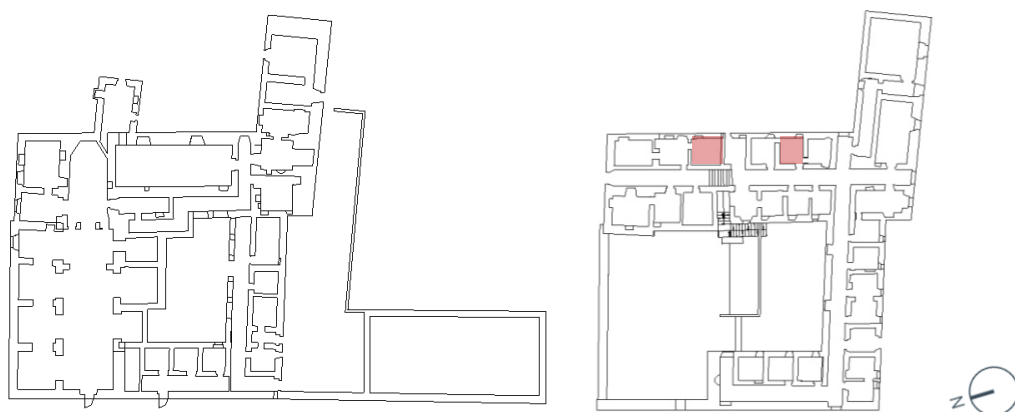
Fig. 46 – Planimetry: ground floor (on the left), first floor (on the right)

The entire building is in total abandonment, which caused diffuse degradation and severe static problems. Along the years, partial restoration interventions were realized, essentially aimed at preventing the structure collapse, like the installation of stone buttresses on the south side.

A widespread decay characterizes the whole structure, and particularly some barrel-vaulted architectural units, on the first floor, where humidity patterns are related to a clear discontinuity between vertical walls and vaults.

7.6. Cryptoporticus of Egnazia *(Fasano, Brindisi, Italy – I century BC)*

The Cryptoporticus of Egnazia is situated inside the archaeological site of Egnazia, an ancient Messapian, Roman and later Paleo-Christian city, located near the seaside, in Fasano (Brindisi, Italy) (Fig. 47). Defensive walls, forum, amphitheatre, houses, basilicas, along the remains of Via Traiana, are part of the ancient urban settlement which, survived until the 10th century A.D. The wall (7 m high and 2 km long) surrounded the Messapian town. Outside the wall, there are the two necropolises: the west (with pit, chamber and half-tombs), and the east.

Fig. 47 - Geographical localization of the Archaeological site of Egnazia (red circle), and the Cryptoporticus (red rectangle)

The acropolis, on the norther side of the city, was realized between the XV century BC. and the IX A.D, on an artificial hill, dominating the whole landscape. It was the first nucleus of the settlement. On the plateau there are the foundations of a periptery temple from the Hellenistic period, while on the land side there is a fortification, with angular bastions.

Some important public buildings and spaces arose on the Trajan Way. The amphitheatre, whose name is only conventional, because there aren't some fundamentals elements typical of this kind of building (tiers, basement,…). Probably, it had functions like subsidiary square to the forum and market.

Several religious buildings took place in the urban fabric, like the Civil Basilica, a public meeting building, dedicated to the administration of justice and business. It had a rectangular plan, with an internal portico of 4 x 8 columns and a layout typical of the Augustan age. On the side of the acropolis, it is connected to the Three Graces' Hall, a large mosaic-paved room. The basilica went through some transformations, between the end of the III and IV centuries AD, which led to a Christian church, with a double central colonnade and three naves. In addition, there are: the Paleo-Christian Episcopal Basilica, with three naves, a single apse, and three entrances preceded by a portico (narthex); and the Southern paleo-Christian Basilica.

The forum, a trapezoidal square, is paved with tuff slabs and surrounded by a channel for the rainwater outflow and a Doric portico. It is datable to the I century. BC, and it did not constitute the real Roman forum [251].

The Cryptoporticus is an underground structure, dating back to the I century B.C, with four arms of different lengths, partially excavated in the rock and partially realized with opus incertum (cement, stone and mortar), covered with plastered barrel vaults (Fig. 48). On the inner sides of the arms, openings are located at regular distances; two pairs of entrances are placed on the longer side. The structure can be interpreted as covered ambulatory or as deposit for cereals (horreum) [81].

The whole structure of the Cryptoporticus is considerably affected by the presence of water and the lack of air and light, which led to extended humidity patterns. For this reason, the south-west arm of the structure was analysed in detail, with machine learning techniques.

Fig. 48 – Cryptoporticus: top view, interior view.

8. EXPERIMENTAL SET-UP FOR REALITY-BASED 2D/3D DATA ACQUISITION

The six case studies were scanned and virtually reconstructed, through digital photogrammetry, according to the theorical and operative procedure explained in Section 4. The equipment adopted for the acquisition phase includes the following elements:

1) Compact digital camera, mirrorless or reflex (for Close-Range Photogrammetry):
   - Samsung NX 2000 mirrorless compact digital camera, with CMOS APS-C 20.3 Megapixel sensor (sensor resolution of 5472 x 3648 and sensor size of 23.5 x 15.7 mm^2) and interchangeable lenses (16 mm or 20-50 mm)
   - Sony QX1 mirrorless compact digital camera, with APS-C sensor (sensor resolution of 5436 x 3632 and sensor size of 23.2 x 15.4 mm^2)
   - Canon EOS 760D DSLR reflex camera with CMOS sensor with TTL-CT-SIR (sensor resolution of 24.2 Megapixel and sensor size of 22.3 x 14.9 mm^2) with focal length lenses of 60 mm
   - Nikon D850 DSLR reflex camera with CMOS sensor (sensor resolution of 45 Megapixel and sensor size of 35.9 x 23.9 mm^2) with focal length lenses of 50 mm

2) UAS (for Aerial Photogrammetry):
   - Professional quadcopter drone (~ 4 kg), with CMOS sensor camera (min area 9 MPx), integrated wi-fi connection, remote control and 4K video capture (e.g. DJI Inspire 1 Pro)

3) Camera supports:
   - Carbon fibre telescopic rod, On Air Neutech C105, with six sections, which allows an elongation up to 10.5 m
   - Manfrotto Befree Advanced tripod (h min 10 cm-h max 150 cm)

4) Mobile devices:
   - Smartphone or tablet (Android/IOS)

5) Software support (specific app for camera remote control):
   - Samsung Smart Camera

- Sony SmartCam Remote
- Camera Connect (Canon)

6) Measuring instruments:

- Distance laser meter Leica DISTO D510
- tape measure, flexometer
- bubble level

7) Additional lights:

- Macro Ring Light Flash Yongnuo YN-14EX
- Led lights

For every selected case study, the acquisitions were always been planned previously, by using a specific Excel spreadsheet, which relates fundamental parameters concerning optical system, site configuration,…(Fig. 49).

Scanning number	Object area	Shooting distance	Overlapping between consecutive images	Overlapping between adjacent lines	Total number of images	Step in X	Step in Y	Ground resolution	Height resolution	Smallest characteristic on the sensor	Focal lenght
	m2	m	%	%		m	m	cm	cm	mm	mm
1	249.2	5.7	89%	59%	114	0.74	2.97	0.12	0.25	1.2	20.00
2	364.9	13.9	87%	55%	44	1.86	4.45	0.27	0.54	2.7	22.00
3	764.75	10.0	87%	70%	138	1.90	2.92	0.27	0.54	2.7	16.00
4	9.45	1.1	89%	58%	120	0.18	0.45	0.03	0.06	0.3	16.00

Fig. 49 – Example of spreadsheet for the acquisition planning [5].

Given the extension, the complexity and the difficulty of access to the heritages, for each of them, a selection was made, in order to reduce time requirements both in acquisition and reconstruction phases. Indeed, predominantly critical areas, representative of various kind of decay morphologies, were scanned.

The majority of the photogrammetric campaign were personally executed by the Ph.D candidate, within the present research work or in participation of other research projects. Here below the indication of the type and number of scans for each case is reported.

As far as Palmieri Palace is concerned, the photogrammetric campaign, at the beginning, was part of the MIUR Start-up project: PAC02L2_00101 "Contactless diagnosis system of artefacts of significant cultural interest and difficult accessibility with augmented reality" [10]. Then, the acquisitions continued for monitoring purposes, within the Ph.D. research work. They were focused on:

- o Main façade (south-west): 06/11/2015 - 19/02/2016 - 09/06/2017 - 29/07/2019
- Portal: 06/11/2015 - 29/07/2019 - 05/03/2021
- Limestone ashlar masonry (base): 09/06/2017 - 29/07/2019 - 19/06/2020 - 05/03/2021
- Tuff masonry: 09/06/2017 - 29/07/2019
- o Internal courtyard (north-east façade): 06/11/2015 - 23/11/2018
- Right pillar (ground floor): 23/11/2018 - 20/12/2018 - 19/06/2020
- Left pillar (ground floor): 23/11/2018 - 19/06/2020

Table 7 – Palmieri Palace: general acquisitions of main façade and portal, detailed acquisition of small portions of the main façade, courtyard and pillars

		Main façade				Portal		
		General				General		
Data		06/11/2015	19/02/2016	09/06/2017	29/07/2019	06/11/2015	29/07/2019	05/03/2021
Object area	m²	250	802	170	438	56	50	35
Camera model	-	Samsung NX2000	Samsung NX2000	Samsung NX2000	Samsung NX2000	Samsung NX2000	Samsung NX2000	Sony QX1
Focal length	mm	20	22	20	16	20	16	20
Sensor area	Mpx	20	20	20	20	20	20	20
Sensor area	mm²	368.95	368.95	368.95	368.95	368.95	368.95	357.28
Shooting distance	m	6	14	5	11	5	10	4
N° images	-	114	45	170	86	77	17	262
Acquisition time	min	65	44	60	80	63	20	120

		Ashlar masonry				Tuff	
		Detail				Detail	
Data		09/06/2017	29/07/2019	19/06/2020	05/03/2021	09/06/2017	29/07/2019
Object area	m²	6.5	7	10	7	11	7.5
Camera model	-	Samsung NX2000	Samsung NX2000	Samsung NX2000	Sony QX1	Samsung NX2000	Samsung NX2000
Focal length	mm	16	16	16	20	16	16
Sensor area	Mpx	20	20	20	20	20	20
Sensor area	mm²	368.95	368.95	368.95	357.28	368.95	368.95
Shooting distance	m	1.1	1.2	1.5	2.1	1.2	1.1
N° images	-	49	42	58	13	64	39
Acquisition time	min	38	12	14	2	38	11

		Courtyard		Right Pillar			Left pillar	
		General		Detail			Detail	
Data		06/11/2015	23/11/2018	23/11/2018	20/12/18	19/06/2020	23/11/2018	19/06/2020
Object area	m²	170	57		1.3	5	18	5
Camera model	-	Samsung NX2000	Samsung NX2000	Samsung NX2000	Canon EOS 760D	Samsung NX2000	Samsung NX2000	Samsung NX2000
Focal length	mm	20	20	20	60	16	20	16
Sensor area	Mpx	20	20	20	24	20	20	20
Sensor area	mm²	368.95	368.95	368.95	332.27	368.95	368.95	368.95
Shooting distance	m	5	5.5		0.5	1.4	1.6	1.3
N° images	-	170	38	68	107	146	250	114
Acquisition time	min	60	30			55	73	58

The Fortress of Bashtovë was one of the pilot cases of "3D-IMP-ACT Virtual reality and 3D experiences to IMProve territorial Attractiveness, Cultural heritage smart management and Touristic development", Interreg Program IPA CBC Italy Albania Montenegro (2018-2020). Therefore, its acquisitions started in 2018, for digital documentation and cultural dissemination purposes. Given that two considerable seismic events occurred in 2019, after-earthquake acquisitions, were realized in 2020, thanks to the support and the collaboration with Prof. Erald Piperi of the Polytechnic University of Tirana (Albania). In particular the campaign concern:

- General site (outside and inside the walls): 07/11/2018
- North tower: 07/11/2018 - 09/04/2020 - 24/12/2020
- North tower (crack pattern): 07/11/2018 - 09/04/2020 (Table 8)

Table 8 - Fortress of Bashtovë, general and detailed acquisitions

		Exterior	Interior	North tower (NT) - Exterior			NT Exterior	NT Crack
		General	General	General			General	Detail
Data		07/11/2018	07/11/2018	07/11/2018	09/04/2020	24/12/20	07/11/2018	07/11/2018
Object area	m²	400	418	96	37	93	100	11
Camera model	-	Sony QX1	Sony QX1	Samsung NX2000	NIKON D850	NIKON D850	Samsung NX2000	Samsung NX2000
Focal length	mm	20	20	16	50	16	16	16
Sensor area	Mpx	20	20	20	24	24	20	20
Sensor area	mm²	357.28	357.28	368.95	366.91	366.91	368.95	368.95
Shooting distance	m	7.2	8	5	5	9	4	1.2
N° total images	-	329	288	168	170	150	198	34
Acquisition time	min	40	60	30	54	80	24	6

For San Corrado's cathedral, the photogrammetric campaign was part of an international workshop, organized by the Eng. Ph.D. Silvana Bruno, and conducted by Prof. Fabio Fatiguso and Prof. Moyano (University of Siviglia). In particular, the acquisitions were focused on:

▪ Interior:

• Half-barrel vault: 24/7/21

• Arch (entrance to south-western chapel): 24/7/21

• Half-column (north of main entrance): 24/7/21

As far as the photogrammetric acquisition is concerned, the three components (column, half-vault, arch) were acquired with a bridge camera, mounted on a tripod or on a telescopic carbon road, to reach the highest parts (10 m for the half column, 16 m for the half barrel-vault). The acquisition parameters are reported in Table 9.

Table 9 – Photogrammetric campaign for three architectural elements, inside S. Corrado's Cathedral

		Half-barrel vault	Half-column	Arch
		General	General	General
Data		24/07/2021	24/07/2021	24/07/2021
Object area	m²	698	23.4	8.46
Camera model	-	SONY DSC-RX100M2	SONY DSC-RX100M2	SONY DSC-RX100M2
Focal length	mm	10.4	10.4	10.4
Sensor area	Mpx	20	20	20
Sensor area	mm²	118.8	118.8	118.8
Shooting distance	m	27	3.1	2.4
N° total images	-	87	87	135
Acquisition time	min	75	135	7

The ex-convent of San Leonardo (Monopoli, Bari) was photogrammetrically acquired within the Ph.D work, in occasion of the development of a laboratory workshop of the university course of "Recupero e Riqualificazione degli edifici". The scans concerns:

▪ Cross-vaulted volume (adjacent to the main cloister): 12/04/2019 (Table 10)

While, the Cappuccini Ex-Convent (Coversano, Bari), has been included in the selection of case studies, thanks to the Master Thesis of Annamaria Gravina and Valeria Giannuzzi (Polytechnic University of Bari), focusing on:

- Two barrel-vaulted volumes (first floor): 03/2020 (Table 10)

Finally, also the Cryptoporticus of Egnazia, was part of the project 3D-IMP-ACT. The scans interested:

- South wing: 09/11/2018 (Table 10)

Table 10 – Acquisition parameters for the campaigns of San Leonardo, Cappuccini ex-convent, and Egnazia Cryptoporticus

		San Leonardo's Cloister	Cappuccini's room 6	Cappuccini's room 9	Egnazia Cryptoporticus	
		General	General	General	General	General
Data		12/4/19	30/07/2020	01/03/2020	9/11/18	9/11/18
Object area	m^2	68.7	46	56	393	81.9
Camera model	-	Samsung NX2000	Fujifilm X-A10	NIKON D3100	Samsung NX2000	Sony QX1
Focal length	mm	16	23.2	18	16	20
Sensor area	Mpx	20	16	15	20	20
Sensor area	mm^2	368.95	368,95	355,74	368.95	357.28
Shooting distance	m	3.5			3	2.7
N° total images	-	232			736	270
Acquisition time	min	120			60	180

It is important to underline that this list includes only the most representative case studies, for testing and validating the different pipelines explained in sections 5 and 6. However, along the whole research course, many architectural heritages were considered, photogrammetrically acquired, and virtually reconstructed.

After each acquisition campaign, three-dimensional photogrammetric models were e laborated, following the operative procedure illustrated in section 4.2.2, in order to retrieve outputs as dense point clouds, polygonal meshes with high-resolution textures, and, eventually, high resolution orthoimages.

The 2D and 3D reconstruction was carried out by means of different hardware devices, like dual Intel Xeon processor Intel(R) Xeon(R) CPU E5-2630 (128 GB RAM, 64-bit), Intel(R) Core (TM) i7-5820K (32 GB RAM, 64-bit) and Intel(R)Core (TM)i7-8750H (16GB RAM, 64-bit), with at least 4 GB memory for the GPU.

As far as the software support is concerned, Agisoft PhotoScan and Metashape have been used, based on Structure from Motion (SFM) algorithms and Dense Multi-View 3D Reconstruction (DMVR) (Photoscan versions: 1.0.4, 1.4.4; Metashape versions: 1.5.2, 1.6.5, 1.7.0).

9. RESULTS

9. (A) INNOVATIVE ROUTINES FOR THE QUANTITATIVE ASSESSMENT OF VISIBLE DAMAGES AND SURFACE ALTERATIONS ON ARCHITECTURAL ARTEFACTS

9.1. (A) Geometry-based alteration approaches

The methodological approaches concerning geometry-based alterations, proposed in section 5.1, were experimented and validated on point clouds of significant stone architectural elements (walls, pillars, columns, towers, vaults,..), belonging to the case studies described above, and particularly Palmieri Palace, Fortress of Bashtovë and San Corrado's Cathedral. Specimens were chosen, starting from these three cases, in function of their representativeness, related to the kind of element, morphology and type of alterations to which they are subjected. The aim was to achieve heterogeneous reference samples from a historical, constructive, and typological point of view.

In first place, the selection was dictated by the need to study certain morphologies of alteration, such as: a) crack patterns (cracks); b) features induced by material loss (lacks, erosions, alveolizations, cavities).

Some recurrent types of exposed masonry were included in the field of investigation, for example, in squared ashlars of limestone or in stone and brick blocks.

The level of detail of the 3D data has been calibrated on the basis of the defect size. In general, for the study of crack patterns, linked to phenomena of structural instability, detailed acquisitions were performed, to obtain high-resolution point clouds (around 0.1 mm/pixel).

In case of areas characterized by widespread surface degradation, due to the presence of water, weathering phenomena, marine salts or chemical agents, which deteriorate the stone surface (lacks, gaps and expulsion of material at the mortar joints), since the order of magnitude of the defects is higher (it varies from a few millimetres to a few centimetres), resolutions around 1 mm/pixel are high enough to detect the presence of these types of alteration [5].

9.1.1. (A) Semi-automatic procedures on point clouds, for 3D surface analysis of decay, through digital image processing routines - Palazzo Palmieri (Monopoli - XVIII century), Fortress of Bashtovë (Albania - XV century)

The approach illustrated in Section 5.1.1 was applied to samples of the main façade of Palmieri palace (Fig. 51) and of the north tower of the Fortress of Bashtovë (Fig. 52). They are made of ashlar and smooth limestone masonry, in the first case, and of stone and brick walls, in the second one.

In particular, as previously introduced, the regions of the palace façade are connoted by several kinds of geometry-based alterations, related to humidity (rising dampness), weathering and marine salts, which appears in forms like erosions, cavities, lacks (features induced by material loss). While the areas identified in the north tower of the fortress are denoted by the presence of a huge vertical crack covering almost the whole height of the tower (8 metres long), related to a phenomenon of static instability, and diffuse stone decay. These artefacts, even in small portions of the overall surface, enclose many kinds of surface defects, which are relevant for the purpose of the present work.
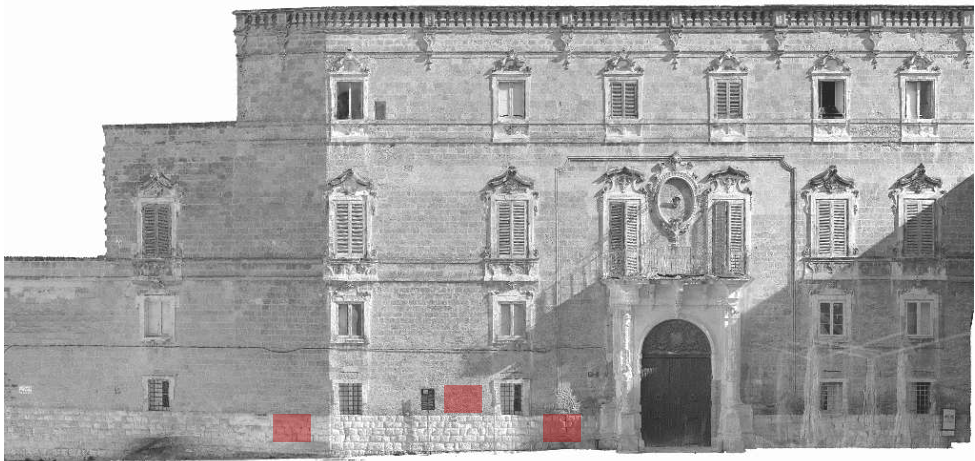
Fig. 51 – Main façade of Palmieri Palace, with the localization of some samples considered for the application of semi-automatic digital image processing routines.

Fig. 52 - North tower of the Fortress of Basthovë. with the indication of samples used for the application of the methodology.

In Table 11 a synthesis of the principal information about the photogrammetric reconstructions is reported, from which it is possible to compare the main parameters for each survey.

Table 11 - Comparison of information about 3D photogrammetric data models

Data		Palmieri Palace						Bashtovë	
		Ashlar masonry				Tuff		NT Exterior	NT Crack
Data		9/6/17	29/7/19	19/6/20	5/3/21	9/6/17	29/7/19	7/11/18	7/11/18
Object area	m²	6.5	7	10	7	11	7.5	100	11
Tie points	N°	756,061	224,528	285,883	257,758	688,251	526,996	1,400,054	1,794,984
Alignment time	min	8	9	8	4		8	50	95
Dense points	N°	30,758,837	6,639,316	27,621,943	54,939,908	44,575,978	29,991,924	130,672,808	33,585,330
Dense time	min	66	5	23	28	72	19	430	6
Faces	N°	6,143,882		199,999		8,915,076			
Vertices	N°	3,074,201		102,388		4,463,425			
Mesh time	min	1		23		45			
Ground Resolution	mm/px	0.267	0.283	0.353	0.416	0.287	0.269	1.05	0.315
Height Resolution	mm/px	0.534		0.706		0.574			
Reprojection Error	pixel	0.308	0.405	0.426	0.389	0.301	0.43	0.693	0.136
Point density	pt/mm²	3.5		2.01		3.04			
Texture time	min	3				6			
Total. time	min	78	14	54	32	123	27	480	101

For the point clouds reconstruction, with the software Agisoft Photoscan, high or ultra-high quality reconstruction parameters and mild depth filtering have been preferred, in order to preserve the original size of photographs and to prevent the loss of information. Samples of the areas were used for the experimentation.

The retrieved point clouds are made of millions of points (from tenths to hundreds of millions), with ground resolutions in a range of from tenth of millimetre to millimetre.

In particular, image processing routines proposed in Section 5.1.1 were implemented on the two small regions of the main façade of Palazzo Palmieri indicated in Fig. 51, together with the two areas (1,2) of the north tower in Fig. 52.
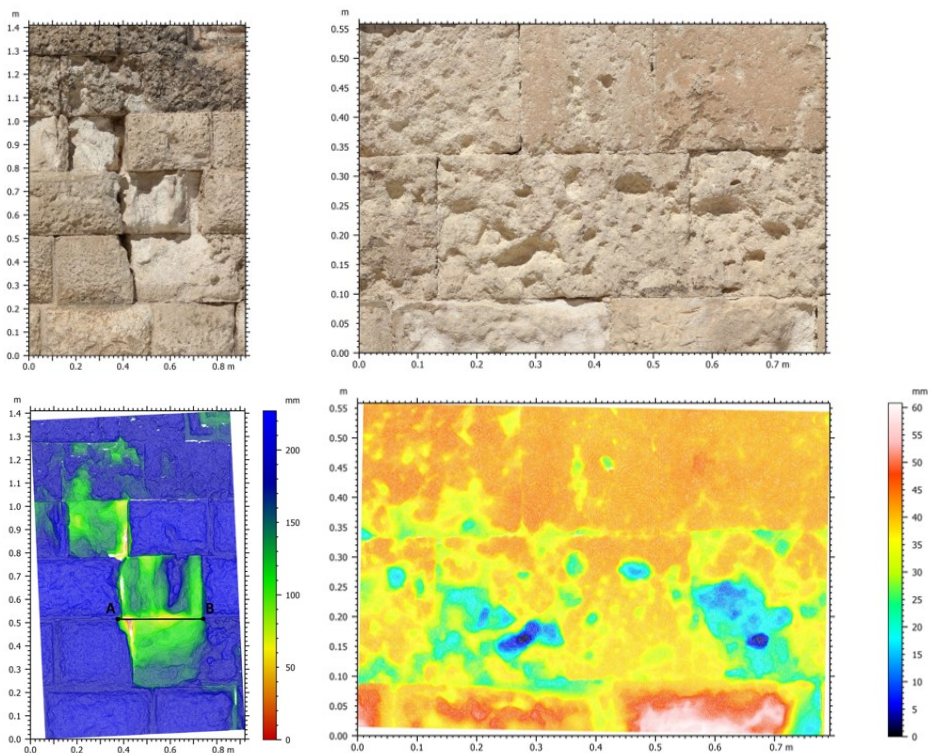
Fig. 53 - Two portions of the main façade of Palmieri Palace. Left: ashlar basement, original point cloud, false colour maps [15] [17].

Multiple analyses were carried out, consisting of a series of spatial and morphological filters, in order to extrapolate quantitative information for the detection of the above-mentioned kinds of alteration. For the application of digital image processing routines,

TalyMap 3D™ (MountainsMap®), a metrology software generally used for laboratory and industrial research, was chosen [252].

The first step concerned the conversion of the point clouds in false-colour maps, which, analogously to Digital Elevation Models (DEMs), represents the 3D coordinates (x, y, z) of each point in a colour scale corresponding to depths. Then the pre-processing stage of levelling and noise reduction took place, by means of least square method and Gaussian filter

For example, in Fig. 53, these steps are applied to the regions of Palmieri Palace, characterized by diffuse stone decay evidence and a crack. While in Fig. 54, there are the two areas of the north tower (Bashtovë fortress), with the corresponding false colour maps.

As far as the tower is concerned, in order to reduce processing requirements, polygonal meshes have been considered, in place of point clouds. In this case, given the curvature of the tower, a further pre-processing step is needed, to remove the main curvature from the examined surfaces, through the help of the form removal operator. A polynomial function of degree 8 have been removed from the analysed polygon meshes (Fig. 54).

At this step, for the detection of cracks, gradient filter extracted edges, and especially the sharpest ones, like the sides of a crack. For a proper segmentation, various sizes of the kernel matrix have been tested, which are suitable to highlight different information. Indeed, the quantity of isolated data increases, from smaller sizes (3x3, 5x5, 9x9), which allow to detect clear contours corresponding to maximum slope variations, to larger matrices (13x13, 19x19, 27x27), for a more detailed comprehension of slight slope variations. The output is a binarized map, where edges are separated from background, and associated to a numerical scalar field representing the gradient (Fig. 55).
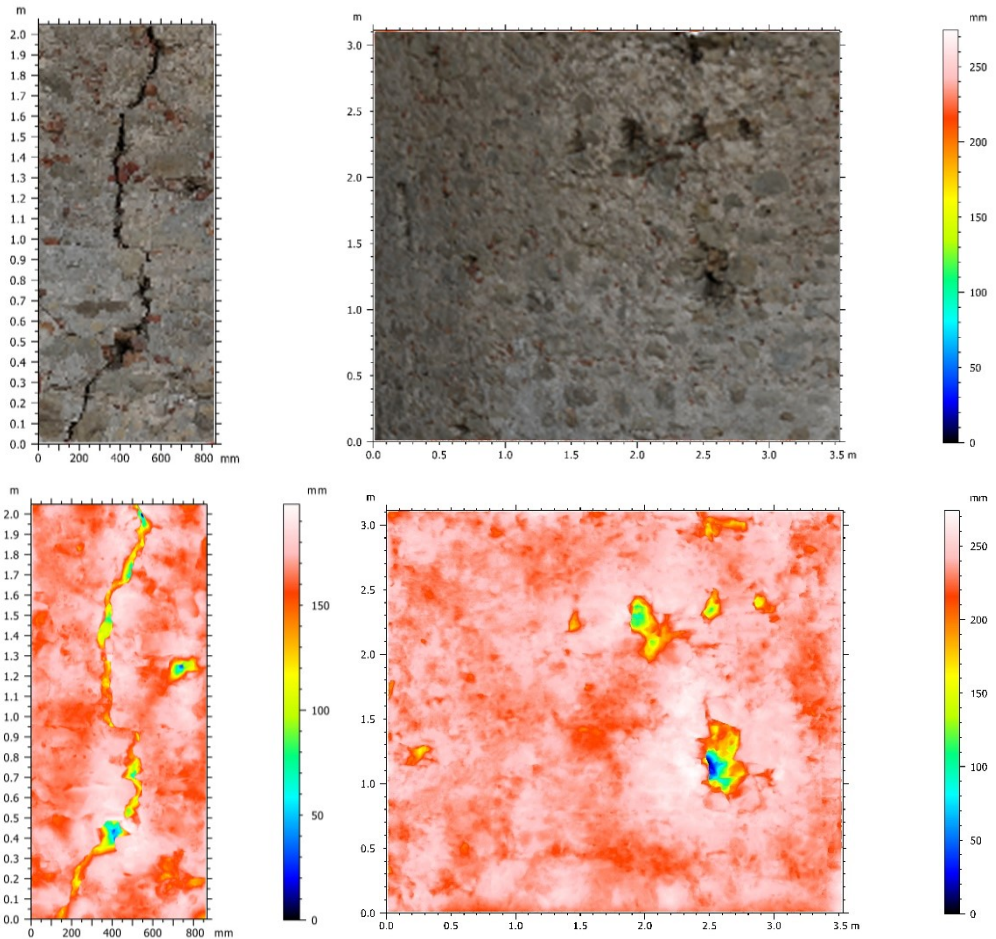
Fig. 54 – Bashtovë fortress. Two portions of the north tower: point cloud, false colour maps of the same regions [4].

Whereas, surface decay, in the form of alveolizations, differential erosions, mechanical damage, perforation, missing parts, was identified through selected depth thresholds, which operate a segmentation and separate elements within a determined interval. The choice of depth thresholds was made in accordance with preliminary on-site measurements, and on the basis of the order of magnitude of the detected defects, like the smallest detectable characteristics of area and depth (Fig. 56).
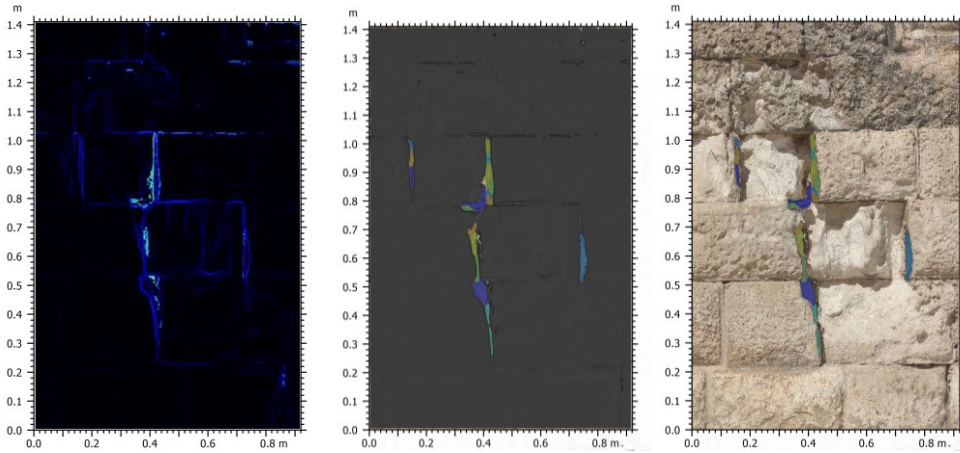
Fig. 55 – Edge extraction (gradient 9X9) and watershed segmentation, with overlapping to the original point cloud

Once the two typologies of defect have been properly isolated, watershed segmentation divided the isolated areas into smaller computable grains, from which quantitative information were retrieved (Fig. 55-Fig. 56).

The area in Fig. 53 (on the left) was separated in 19 elements, which together constitute the whole area of the crack. While the area in Fig. 53 (on the right), was segmented, in 168 motifs (Fig. 56). An additional passage entailed the elimination of too small grains, to be significant as part of an alteration. In this case motifs lying under one of these three dimensional limits have been excluded:

- maximum height (h) < 1 mm
- maximum diameter (Dmax) < 1 mm
- minimum diameter (Dmin) $= 0$ mm
- area (A) < 4 mm^2
- volume (V) < 200 mm^3

Consequently, it was possible to quantify the geometric characteristics of these motifs: area, perimeter, volume, minimum, maximum, average diameter, height, number of adjacent elements, form factor, coplanarity, orientation (Table 12). [4].
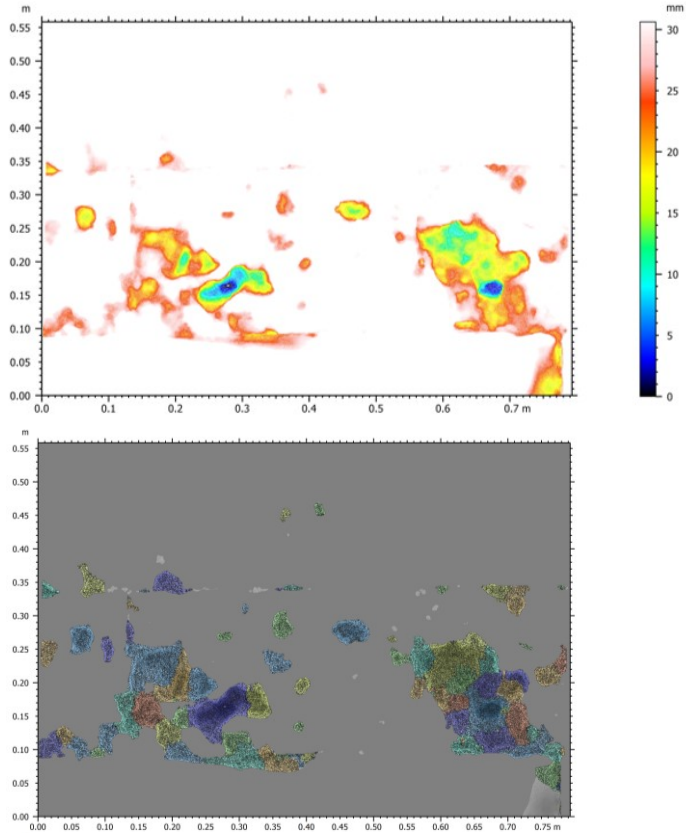
Fig. 56 – a) surface thresholding, to isolate points under threshold, most likely corresponding to defects; b) binarized surface, with the identification of grains [17]

Table 12 – Extract of the parameters computed for each of the detected grains [17]

Number of motifs	168							
Parameters	**Unit**	Grain #1	Grain #2	Grain #3	Grain #4	Grain #5	Grain #6	Grain...
Type of motif		Interior motif	Interior motif	Interior motif	Interior motif	Interior motif	Interior motif	Interio...
Height	mm²	13.3674	7.43910	2.06410	4.02881	3.76548	11.3693	1.84529
Area	mm²	0.00368909	0.00248616	2.74656e-06	0.00103388	0.00337539	0.00180573	1.6348...
Volume	mm³	7489.23	1719.10	0.490651	220.756	1183.93	3415.54	0.1592...
Nb of neighbors		4	12	2	5	15	5	1
Coflatness	m	0.0222013	0.0180667	0.00531044	0.00784362	0.010510	0.0111318	0.0087...
Perimeter	m	10.2334	7.92675	0.00759985	3.51393	11.1917	5.47598	0.0064...
Mean diameter	m	0.070963	0.062249	0.00159581	0.0402076	0.0698284	0.0495371	*****
Min diameter	m	0.0403141	0.0444331	0.000989658	0.0252235	0.0347713	0.0244382	*****
Max diameter	m	0.0973171	0.0811207	0.00255727	0.0518803	0.110474	0.0811335	*****
Form factor		0.00035415	0.000370457	0.398380	0.000759365	0.000248665	0.000582969	0.2566...
Aspect ratio		2.41397	1.82568	2.58399	2.05682	3.17716	3.31995	*****
Roundness		0.396781	0.358397	0.356497	0.352965	0.258575	0.269072	*****
Compactness		0.629906	0.598662	0.597074	0.594109	0.508503	0.518721	*****
Orientation	°	33.3363	108.792	63.8967	42.4267	33.0600	60.1823	83.0626

151

(A) Feature extraction for the quantification, measurement and classification of geometry-based damages - Palazzo Palmieri (Monopoli - XVIII century), Fortress of Bashtovë (Albania - XV century)

The application of digital image processing routines to the above-mentioned samples was functional to the retrieval of geometric features, as illustrated in Table 4 (Section 5.1.2). They were exported in excel spreadsheet and further elaborated. Indeed, after the segmentation of the original cloud or mesh (through edge extraction, thresholding, binarization), the isolation and subdivision of defective areas and subsequent features' computation, a classification of defects have been extrapolated, on the basis of the criteria illustrated in Section 5.1.2, and a corresponding Damage Index, as the linear combination of the four criteria (form, depth, uniformity, volume).

In Fig. 57, the fundamental steps of the pipeline are applied. The extracted features were used to associate the detected grains to different classes of alteration, like for example the macro-categories of cracks (A) and features induced by material loss (B) (see Fig. 22 in Section 5.1.2).
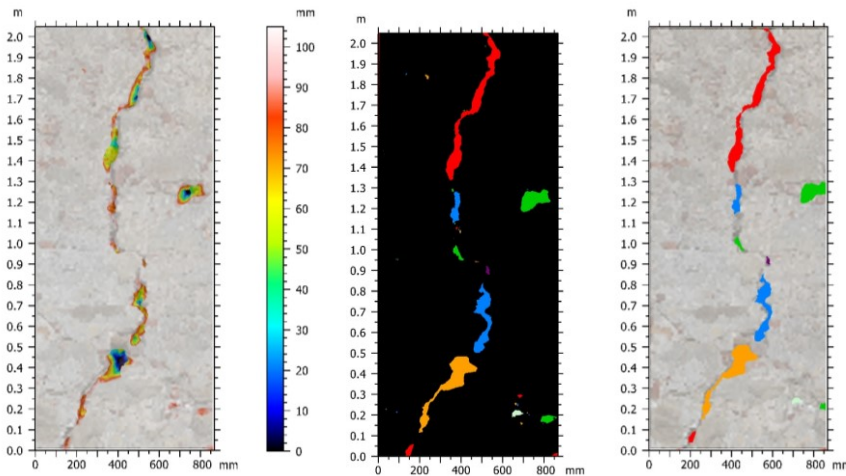
Fig. 57 – North tower, (area 1): binarized surface after the application of a depth-threshold, where the segmented regions correspond to the surface imperfections [5] [29].

Additional parameters were retrieved from the analysis of transversal profiles. Fifteen sections were extracted. The profile contour analysis allowed a quantitative

measurement of width, maximum depth and angularity, in correspondence of the vertical sides of a crack (Fig. 58).
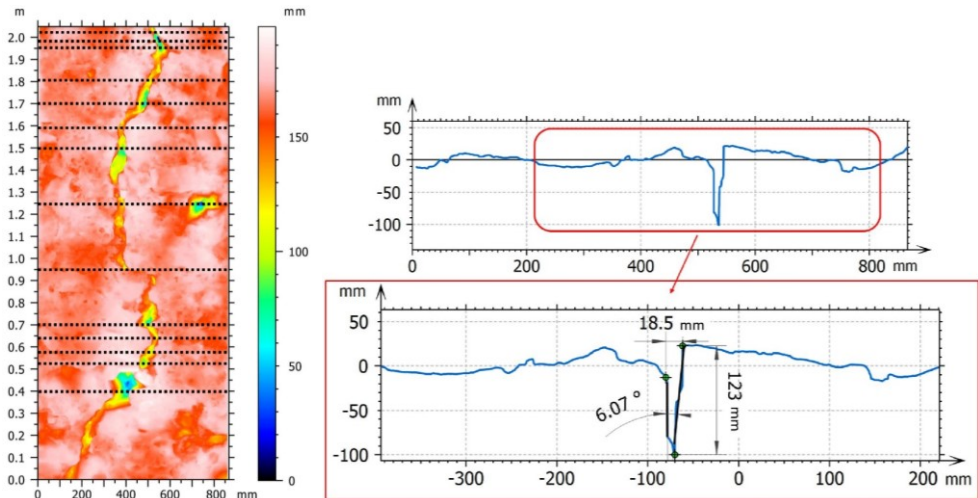
Fig. 58 - Transversal profile extracted from the surface [29].

At this step, threshold values were determined for each of the four criteria (form, depth uniformity, volume), in relation to the mathematical meaning of the parameters composing them (Section 5.1.2).

For classification purposes, peculiar conditions were attributed to the three intervals of each criterion. The form-criterion (F) is strictly related to the mathematical meaning of the parameters, because it is a combination of three different shape descriptors, namely aspect ratio (AR), roundness (R), and compactness (C). It assumes a different value (from 1 to 3), according to the number of conditions it satisfies to be considered as a circular grain (F=1). The grain is pseudo-circular (F=2) if at least one of the conditions is verified (AR < 4 or R > 0,4 or C > 0,5); otherwise, the grain is oblong (F=3) (Table 13).

Indeed, the three parameters effectively describe the shape of a grain (oblong or circular), because they are expressed as functions of the main geometric characteristics of the grain (such as minimum and maximum diameter, area, perimeter…) (Fig. 60).
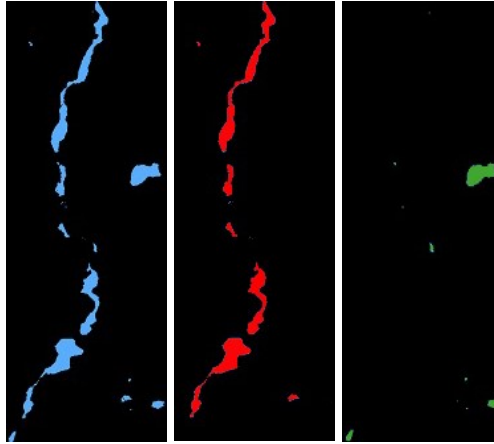
Fig. 60 - Application of a threshold value for the Form criterion, to the binarized image of Fig. 57. From left to right, original image (light blue), oblong grains (red), circular grains (green).

As a consequence, they are consistent with the objective of classification among the two classes A and B (Fig. 22, Section 5.1.2). In fact, if a grain is oblong, it most likely belongs to a crack, but if it is surface or sub-surface it could actually represent a lack or an erosion. In the other criteria, the choice was made, considering the distribution of the quantitative values obtained through the motifs' analysis (Table 13).

Table 13 - Classification of motifs according to four selected criteria, with definition of thresholds [16]

Form (f)		Depth (d)		Uniformity (u)		Volume (v)	
Circular (1)	$AR^{28}<4$ and $R>0,38$ and $C>0,5$	*Surface* (1)	$H_m{}^{29}<2mm$	*Regular* (1)	$\frac{Hmax}{Hmed}<5$	*Minimum* (1)	$V^{30}<200mm^3$
Pseudo-Circular (2)	$AR<4$ or $R>0,38$ or $C>0,5$	*Sub-Surface* (2)	$H_m>2mm$ $H_m<4mm$	*Medium* (2)	$\frac{Hmax}{Hmed}>5$ $\frac{Hmax}{Hmed}<20$	*Medium* (2)	$V>200mm^3$ $V<1000mm^3$
Oblong (3)	$AR>4$ and $R<0,38$ and $C<0,5$	*Deep* (3)	$H_m>4mm$	*Irregular* (3)	$\frac{Hmax}{Hmed}>20$	*Maximum* (3)	$V>1000mm^3$

In Table 14, this approach is applied to three kinds of alteration: cracks, lacks and cavities.

---

[28] Aspect Ratio (AR), Roundness (R), Compactness (C)

[29] Medium height of the grain (H_m), calculated as ration between area and volume

[30] Volume (V)

154

Different weights were hypothesized for each criterion, associated to the specific alterations, on the basis of the experience and technical knowledge about surface decay morphologies. Also, the numerical range of variation for every criterion (from 1 to 3) were sum up.

Table 14 – Definition of weights for each criterion forming the severity index [16]

Alteration	Criterion	Classification	Weight
Crack (A)	Form (f)	Circular (C) = 1 Pseudo-Circular (PC) = 2 Oblong (O) = 3	Wf = 70 %
	Depth (d)	Surface (S) = 1 Sub-Surface (SS) = 2 Deep (D) = 3	Wd = 100 %
	Uniformity (u)	Regular (R) = 1 Medium (M) = 2 Irregular (I) = 3	Wu = 50 %
	Volume (v)	Minimum (MIN) = 1 Medium (MED) = 2 Maximum (MAX) = 3	Wv = 50 %
Cavities (B)	Form (f)	Circular (C) = 1 Pseudo-Circular (PC) = 2 Oblong (O) = 3	Wf = 50 %
	Depth (d)	Surface (S) = 1 Sub-Surface (SS) = 2 Deep (D) = 3	Wd = 30 %
	Uniformity (u)	Regular (R) = 1 Medium (M) = 2 Irregular (I) = 3	Wu = 50 %
	Volume (v)	Minimum (MIN) = 1 Medium (MED) = 2 Maximum (MAX) = 3	Wv = 60 %
Lack (B)	Form (f)	Circular (C) = 1 Pseudo-Circular (PC) = 2 Oblong (O) = 3	Wf = 50 %
	Depth (d)	Surface (S) = 1 Sub-Surface (SS) = 2 Deep (D) = 3	Wd = 20 %
	Uniformity (u)	Regular (R) = 1 Medium (M) = 2 Irregular (I) = 3	Wu = 10 %
	Volume (v)	Minimum (MIN) = 1 Medium (MED) = 2 Maximum (MAX) = 3	Wv = 100 %

These results were combined to define a unique Damage Index, calculated for each motif, as the linear combination of the selected criteria. It has a range of variation from 1 to 8, depending on the weights attributed case by case. The results of this application are shown in Table 15, on the basis of the weights determined in Table 14.

Anyway, it is important to explicit that the use of artificial intelligence could improve the definition of weights for each criterion, in correspondence of each kind of alterations, on the basis of a training on a wide range of case studies.

Table 15 - Spreadsheet with the calculation of the Damage Index of each motif, in case of cavities or lacks (in the first line under the names of the criteria, there are the associated weights) [16]

CAVITIES

N° of motif	DEFINITION OF THE THRESHOLDS				NUMERICAL VALUE ASSOCIATED TO THE THRESHOLDS				CAVITIES				
	Form (f)	Depth (d)	Uniformity (u)	Volume (v)	Form (f)	Depth (d)	Uniformity (u)	Volume (v)	Form (f)	Depth (d)	Uniformity (u)	Volume (v)	Index
									0,5	0,3	0,5	0,6	
1	PC	SS	M	MAX	2	2	2	3	1,0	0,6	1,0	1,8	4,4
2	PC	S	M	MAX	2	1	2	3	1,0	0,3	1,0	1,8	4,1
4	PC	S	M	MED	2	1	2	2	1,0	0,3	1,0	1,2	3,5
5	PC	S	M	MAX	2	1	2	3	1,0	0,3	1,0	1,8	4,1
6	PC	S	M	MAX	2	1	2	3	1,0	0,3	1,0	1,8	4,1
9	PC	S	M	MIN	2	1	2	1	1,0	0,3	1,0	0,6	2,9
10	PC	S	R	MIN	2	1	1	1	1,0	0,3	0,5	0,6	2,4
11	PC	S	M	MED	2	1	2	2	1,0	0,3	1,0	1,2	3,5
12	PC	D	R	MAX	2	3	1	3	1,0	0,9	0,5	1,8	4,2
15	PC	S	-	MIN	2	1	3	1	1,0	0,3	1,5	0,6	3,4
16	PC	S	-	MIN	2	1	3	1	1,0	0,3	1,5	0,6	3,4
17	C	S	M	MAX	1	1	2	3	0,5	0,3	1,0	1,8	3,6
23	PC	D	R	MAX	2	3	1	3	1,0	0,9	0,5	1,8	4,2
24	PC	S	-	MIN	2	1	3	1	1,0	0,3	1,5	0,6	3,4
25	PC	S	M	MED	2	1	2	2	1,0	0,3	1,0	1,2	3,5

LACKS

N° of motif	DEFINITION OF THE THRESHOLDS				NUMERICAL VALUE ASSOCIATED TO THE THRESHOLDS				LACKS				
	Form (f)	Depth (d)	Uniformity (u)	Volume (v)	Form (f)	Depth (d)	Uniformity (u)	Volume (v)	Form (f)	Depth (d)	Uniformity (u)	Volume (v)	Index
									0,5	0,2	0,1	1	
1	PC	SS	M	MAX	2	2	2	3	1,0	0,4	0,2	3,0	4,6
2	PC	S	M	MAX	2	1	2	3	1,0	0,2	0,2	3,0	4,4
4	PC	S	M	MED	2	1	2	2	1,0	0,2	0,2	2,0	3,4
5	PC	S	M	MAX	2	1	2	3	1,0	0,2	0,2	3,0	4,4
6	PC	S	M	MAX	2	1	2	3	1,0	0,2	0,2	3,0	4,4
9	PC	S	M	MIN	2	1	2	1	1,0	0,2	0,2	1,0	2,4
10	PC	S	R	MIN	2	1	1	1	1,0	0,2	0,1	1,0	2,3
11	PC	S	M	MED	2	1	2	2	1,0	0,2	0,2	2,0	3,4
12	PC	D	R	MAX	2	3	1	3	1,0	0,6	0,1	3,0	4,7
15	PC	S	-	MIN	2	1	3	1	1,0	0,2	0,3	1,0	2,5
16	PC	S	-	MIN	2	1	3	1	1,0	0,2	0,3	1,0	2,5
17	C	S	M	MAX	1	1	2	3	0,5	0,2	0,2	3,0	3,9
23	PC	D	R	MAX	2	3	1	3	1,0	0,6	0,1	3,0	4,7
24	PC	S	-	MIN	2	1	3	1	1,0	0,2	0,3	1,0	2,5
25	PC	S	M	MED	2	1	2	2	1,0	0,2	0,2	2,0	3,4

9.1.3. (A) Damage evaluation of eroded limestone architectural elements - quantitative detection through geometric analysis of point clouds - San Corrado Cathedral (Molfetta – XVII century)

The methodology illustrated in section 5.1.3 was applied on some architectural elements of San Corrado's Cathedral, strongly affected by the phenomenon of marine aerosol.

Particularly, for the application of the approach two morphologically heterogeneous architectural components have been chosen:

* right half-column of the interior side of the main façade (the left half column has been recently renovated with a "scuci-cuci" intervention)
* half barrel-vault of one of the lateral naves (Fig. 61).

Fig. 61 - Left: half-column; right: half barrel-vault

As far as 3D data reconstruction is concerned, in Table 16 the main parameters for the different elements are reported.

Table 16 – Photogrammetric 3D data, for the two architectural elements

		Half-barrel vault	Half-column
		General	General
Data		24/07/2021	24/07/2021
Object area	m²	698	23.4
Tie points	N°	698,415	432,055
Alignment time	min	36	24
Dense points	N°	13,872,011	18,449,829
Dense time	min	102	49
Faces	N°		1,000,000
Vertices	N°		771,346
Mesh time	min		20
Ground Resolution	mm/pixel	5.88	0.728
Height Resolution	mm/pixel		1.46
Reprojection Error	pixel	0.494	0.695
Point density	pt/cm²		47.1
Texture time	min		2

The geometrical and morphological difference among the two components allows the application of the approach to distinct cases, in order to verify its versatility.

For both the architectural elements, starting from the photogrammetric as-is point cloud, two corresponding ideal 3D models were created. These models reproduce a hypothetical reality-based original form of the objects, with the ideal shapes modelled using the as-is data as reference, for the sake of comprising all the constructive and dimension irregularities. The 3D model represents an "as-designed" condition, before any modification occurred, due to aging, weathering or marine salts.

The ideal model was transformed into polygonal meshes and successively sampled into a point cloud with comparable number of points, in order to uniform the entities to be collated.

As described in section 5.1.3, the as-is and as-designed models of the two architectural elements were compared, through the nearest neighbour distance algorithm. The deviation maps are shown in Fig. 62, in which the colour scale represents the scale of

absolute distances between corresponding points. At the beginning of the iterative algorithm, a maximum distance was established, on the basis of the order of magnitude of the element and of the defects. For the half-column, the limit was fixed on 20 cm, while for the half-barrel vault the limit is 50 cm, because of the major size of the object (Fig. 62).
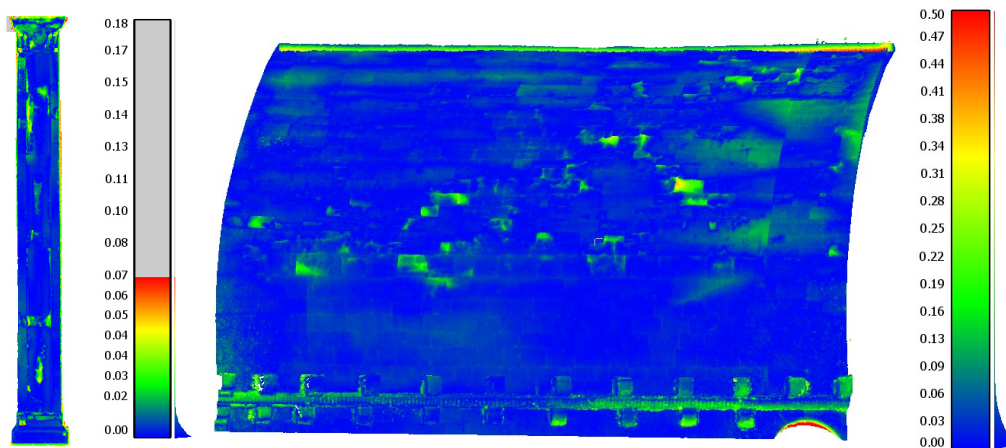
Fig. 62 – Deviation maps representing the cloud-to-cloud distance among ideal models and as-is 3D data

At this step, a further process concerned the filtering of deviation maps, to isolate only differences above and below certain thresholds, discriminating among constructive/reconstruction irregularities and effective alterations. For the half-column, the upper limit is 7 cm, and the lower limit is 7 mm, while for the half-barrel vault the limit was established as 9 cm.

Once the defective areas, corresponding to eroded limestone were isolated, their areas and volume were computed, after a new conversion in polygonal mesh, through the mesh computation algorithm embedded in Agisoft Metashape.

For the construction of the ideal 3D model, software like Autodesk Recap and Autodesk Revit were used, while change detection was performed, with the help of specific tools of CloudCompare and Matlab.

For the half-column, the eroded area is of 5 m^2 (the capital has been excluded from the computation), while for the half-barrel vault the eroded area is of 52 m^2 (Fig. 63 Fig. 64).
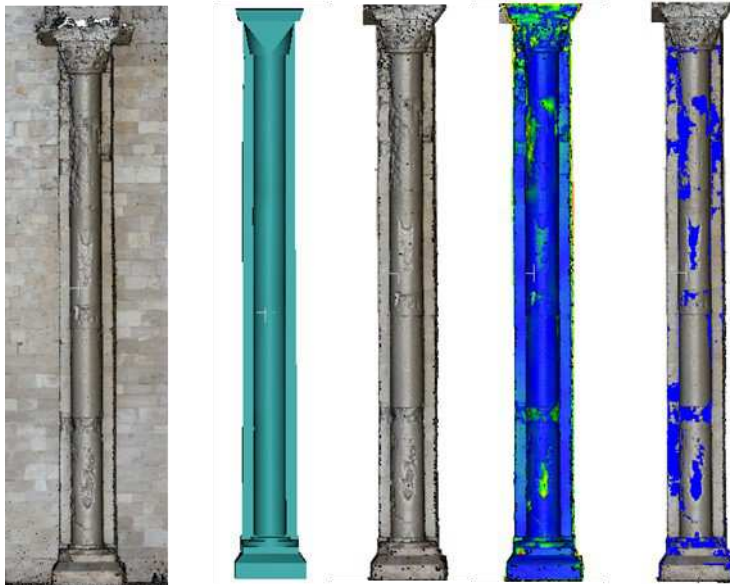
Fig. 63 – Half-column. From left to right: original point cloud, hypothetical ideal model retrieved from it; deviation map, overlapping of results
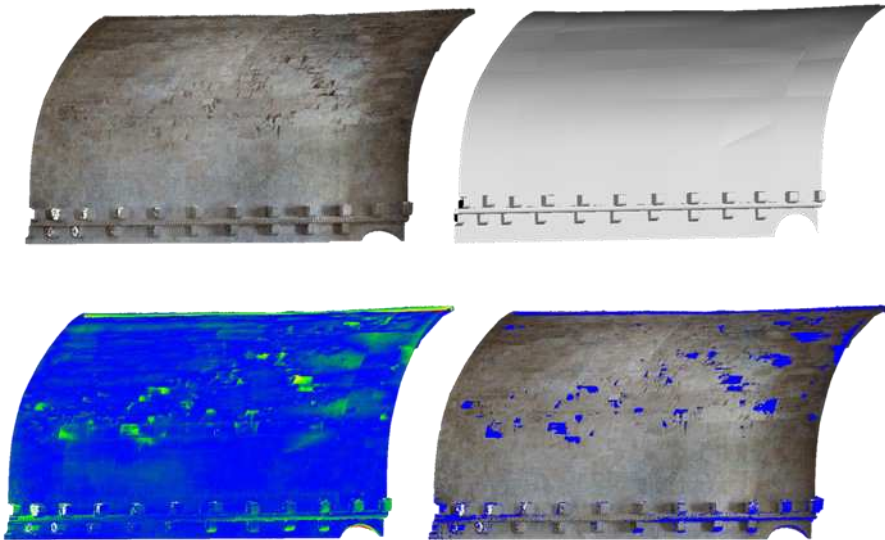
Fig. 64 – Half barrel-vault. Top left: original as is point cloud; top right: corresponding ideal model; bottom left: deviation map; bottom right: overlapping of results

161

9.2. (A) Colour-based alteration approaches

With respect to colour-based decay morphologies, like chromatic alterations, humidity patterns (moist area, biological patina or colonization), spots or deposit, the approaches illustrated in section 5.2 were applied to multiple case studies, of which only three are shown below. They are the two ex-convents, San Leonardo (Monopoli, Bari) and Cappuccini (Conversano, Bari), and the cryptoporticus of Egnazia (Fasano, Brindisi), which are consistently affected by these kinds of pathologies.

9.2.1. (A) Point cloud segmentation for moisture detection on architectural elements - Ex-convent of S. Leonardo (Monopoli – XVI century)

The first approach (section 5.2.1) was applied on a selected region of the main cloister of the convent of San Leonardo (Fig. 65). It is a small architectural unit, corresponding to one of the three cross-vaults of the volume adjacent to the cloister, which is covered by plaster in compromised conditions, visible from the widespread biological colonization and patina. The humidity pattern is denoted by a considerable progression over time, as it is possible to observe in Fig. 65, from the discrepancies between two photos of the cloister, taken in 2010 and 2019, respectively.

Fig. 65 - From left to right: localization of the architectural volume adjacent to the main cloister (ground floor plan), photo of the environment in 2010 and in 2019 [164]

The whole environment was reconstructed. In Table 17 the main photogrammetric parameters are reported.

162

Table 17 – Photogrammetric reconstruction parameters

		San Leonardo's Cloister
		General
Data		12/4/19
Object area	m^2	68.7
Tie points	N°	121,022
Alignment time	min	98
Dense points	N°	22,589,827
Dense time	min	
Faces	N°	4,545,134
Vertices	N°	2,273,983
Mesh time	min	13
Ground Resolution	mm/pixel	0.85
Height Resolution	mm/pixel	3.41
Reprojection Error	pixel	1.05
Point density	pt/mm^2	
Texture time	min	3
Total Rec. time	min	114

In this phase, the three cross-vaults were considered separately, in order to reduce computational costs. Indeed, each point cloud of the cross-vaults have a number of points around 3,000,000 millions. In particular, the application to the central one is proposed, made of 2.850.090 points.

Point cloud segmentation routines were executed, through the software support of MATLAB.

As previously explained, this process was essentially aimed at the detection of biological forms of decay, expressed within a specific colour interval, ranging from green to grey. Therefore, a preliminary routine on 2D images allowed to automatically find the proper colour range. Starting from the high-resolution orthophoto of the vault intrados, retrieved from the photogrammetric reconstruction, three values have been extrapolated, defining the limits of the interval (Fig. 66).

In this case the *reference value (RGB$_{ref}$)* is 91, 91, 86, the *minimum (RGB$_{min}$)* or darkest 68, 70, 65, and the *maximum (RGB$_{max}$)* or clearest 190, 199, 194. These colour triplets

represent a new input variable for the second routine, which is applied to the dense cloud, so in this case on the central vault.

In light of the considerations about colour spaces, the colour interval was firstly converted from RGB into YCbCr ($YCbCr_{min}$, $YCbCr_{max}$,$YCbCr_{xef}$), as well as the point cloud (Fig. 67).

Fig. 66 – High-resolution orthophoto of the vault intrados

The previous passages were functional to define the *reference distance* (D_{ref}), computed as the lowest between maximum and minimum value and the reference one (Eq. (5. 9,(5. 10). For the cross vault the threshold of 0.0229 was used to calculate point-to point distances, according to Eq. (5. 11).
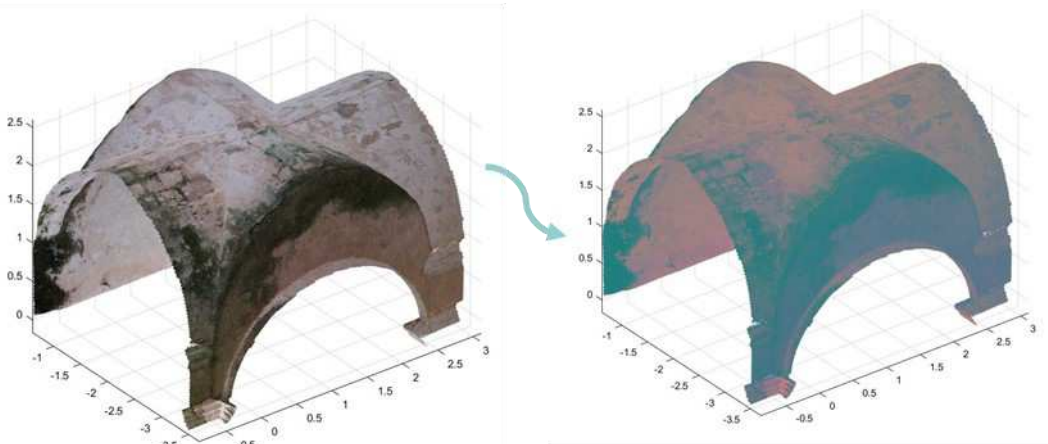
Fig. 67 – Original point cloud (RGB) on the left; conversion in YCbCr on the right [164].

All the points laying below the threshold distance and belonging to the foreground were kept with their original colour, while the others were considered as background, producing a binarized point cloud (Fig. 68).
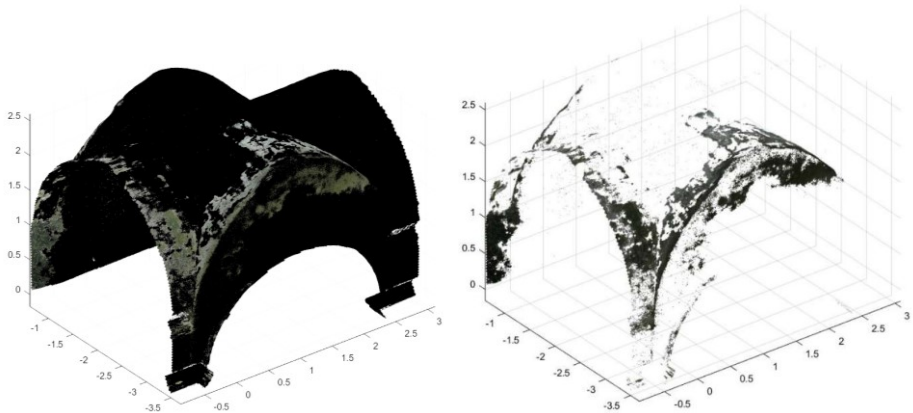
Fig. 68 - Point cloud segmentation and isolation of the dampness phenomena [164]

The isolated regions were quantified, to understand the extension of biological colonization and patina on the examined surfaces. The number of isolated points is 222'052, with an incidence over the total of about 8% [164].

(A) Unsupervised and clustering-based machine learning for automatic point cloud segmentation, for chromatic alterations detection - Ex-convent of S. Leonardo (Monopoli – XVI century), Criptoportico di Egnazia (Monopoli - XVI century B.C.)

The unsupervised clustering-based pipeline (sections 5.2.2 and 5.2.3), aimed at extending the field of investigation to multiple decay evidence, beyond biological patina and colonization, was applied to a plurality of case studies, in order to verify its effectiveness. Here, only three of them are proposed: the architectural volume of the main cloister of San Leonardo (with its three cross-vaults), two barrel-vaulted volumes, on the first floor of the Cappuccini ex-convent, and the south-west wing of the Cryptoporticus of Egnazia. In Table 18, information about 3D reconstruction is provided.

Fig. 69 – From left to right: San Leonardo, Cappuccini ex-convent, Egnazia Cryptoporticus

As it is possible to observe from the photogrammetric reconstructions in Fig. 69, the three of them are characterized by an articulated three-dimensional development, plastered wall surfaces, different lighting conditions, and, most of all, extended humidity patterns, together with a variety of colour-based decay morphologies. In particular, some main classes have been considered, on the basis of the observation of the three case studies: biological patina, biological colonization, spots, deposits and moist areas, and unaltered surfaces.

Table 18 – 3D data parameters for the three case studies

		San Leonardo's Cloister	Cappuccini's room 6	Cappuccini's room 9	Egnazia Cryptoporticus	
		General	General	General	General	General
Data		12/4/19	30/07/2020	01/03/2020	9/11/18	9/11/18
Object area	m²	68.7	46	56	393	81.9
Tie points	N°	121,022			1,973,501	817,139
Alignment time	min	98				687
Dense points	N°	22,589,827	44.810.067	28,979,012	722,325,719	223,578,993
Dense time	min					418
Faces	N°	4,545,134			26,455,568	2,650,943
Vertices	N°	2,273,983			13,297,535	1,328,759
Mesh time	min	13				226
Ground Resolution	mm/pixel	0.85	0.3	0.35	0.69	0.526
Height Resolution	mm/pixel	3.41			1.86	1.86
Reprojection Error	pixel	1.05			0.62	0.547
Point density	pt/mm²					
Texture time	min	3				
Total Rec. time	min	114	0	0	0	1,331
Total time	min	234	0	0	60	1,511

In first place the original point clouds were converted into the four colour spaces (HSV, YCbCr, YIQ, YUV), according to Eq. (5. 13, (5. 14, (5. 15). The hierarchical clustering was applied separately to the four converted point clouds of each of the three architectural element, following the routines explained in section 5.2.2. From the output dendrograms, it was possible to choose a cutting level and extract the correpondent point cloud segments, according to the classification requirements (i.e. number and typology of alterations to detect) (Fig. 70).

Once the segments were extracted, a transversal comparison among equivalent clusters in the four colour spaces was accomplished, in order to understand the most effective colour model for the discrimination among different classes of alterations. Contextually, starting from the on-site survey of the state of conservation, ground truth data were produced, manually segmenting original point clouds and separating the various decay morphologies.
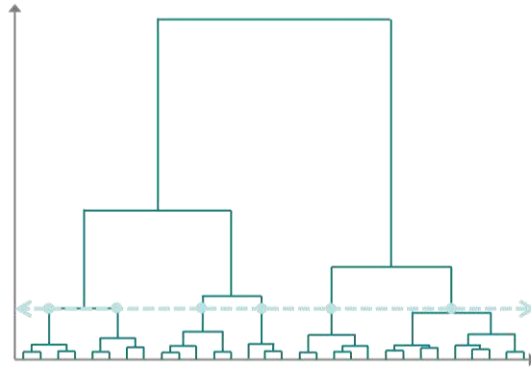
Fig. 70 - Dendrogram for San Leonardo ([232])

For the sake of the experimentation, five or six clusters were generated for each colour space, and then reconverted in RGB to help a visual matching. A qualitative pairwise comparison of the clusters, of each colour space, for each of the four architectural elements, led to the identification of a chromatic correspondence of clusters (Table 19).

Table 19 - Point cloud segmentation: ground-truth (manually labelled portions); HSV clusters; corresponding clusters in the other colour-space (based on [232])

For comparable clusters, in each alteration class, colour-distribution histograms were overlapped, both merged and split in the three RGB channels. Indeed, only clusters with a high percentage of histograms overlapping were considered as analogous, thus excluding those with a little percentage (Fig. 71 Top). Furthermore, histograms of the four analogous clusters of every alteration class were overlapped with their ground truth samples, to find the colour space best approximating them (Fig. 71 Bottom). The results showed that HSV is the most effective, because its clusters have both similar extension (in terms of number of points and percentage) and the most coherent histogram trend with respect to the ground truth.
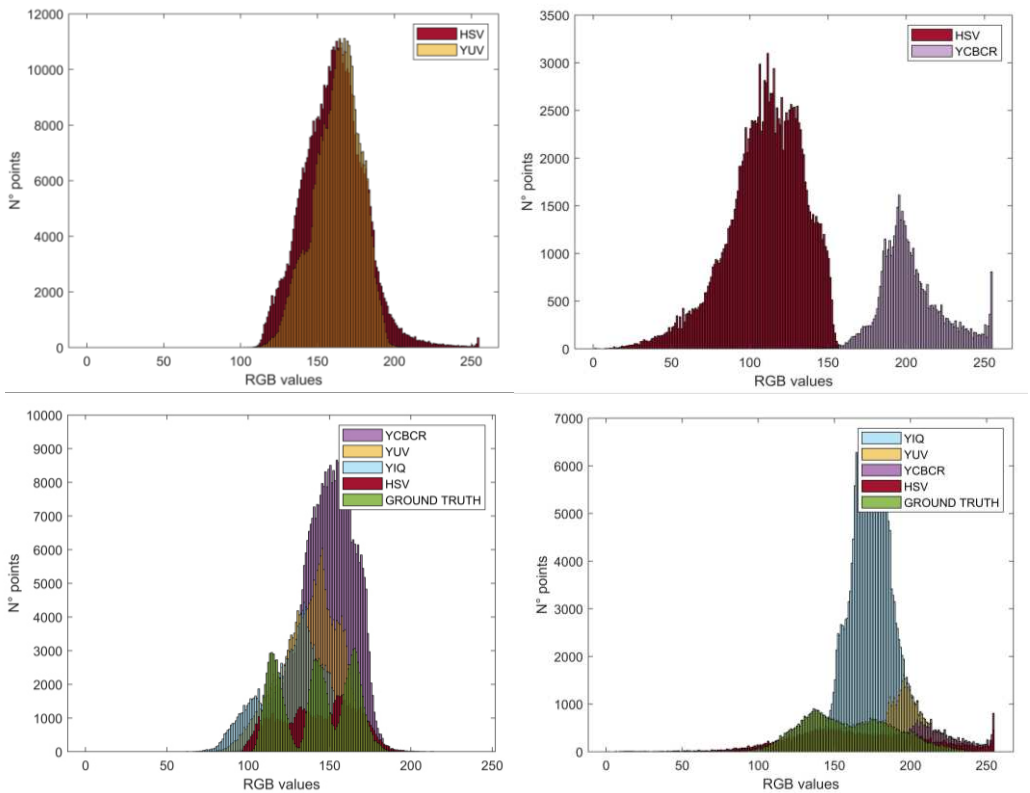
Fig. 71 – Top: pairwise clusters' histogram overlapping (left: 75% overlapping; right: 0.12 % overlapping); Bottom: overlapping between analogous clusters histograms (unified RGB) of the four colour spaces and the ground truth ([232])

Indeed, for the illustrated case studies, the percentage variation among analogous clusters and the ground truth classes (moist area, biological colonization/patina, spots/deposit, unaltered surface, staining) ranges from 1% to 5%, between HSV and ground truth. While in the other colour spaces percentage differences reach even a 30 % of variation. In Fig. 72, the resulting six HSV clusters, for S. Leonardo's cloister, are shown, corresponding to the six classes of moist area, biological patina, biological colonization, spots/deposit, unaltered surface, and pipes.

Fig. 72 – Hierarchical segmentation of San Leonardo' s cloister in HSV: a) moist area (30%); b) biological patina (27%); c) biological colonization (20%); d) spots/deposit (8%); e) unaltered (11%); f) pipes (1%)

Consequently, for each of the three cases the decay morphologies extension is presented in terms of percentage of points over the total (Table 20).

As far as the unsupervised point cloud segmentation is concerned, specific routines were created in MATLAB [232].

Table 20 – Extension of decay morphologies for each case study

		San Leonardo's Cloister	Cappuccini ex-convent (room 6)	Cappuccini ex-convent (room 9)	Egnazia cryptoporticus
Moist area	%	30	10	26	64
Biological patina	%	27	18	18	25
Biological colonization	%	20		20	7
Spots/deposit	%	8	10	19	4
Staining	%	-	6	13	-
Unaltered surface	%	11	57	-	-
Pipes	%	1	-	-	-

9.2.2. (A) Comparison between cloud-based unsupervised and texture-based supervised machine learning approaches - Ex-convent of S. Leonardo (Monopoli – XVI century), Criptoportico di Egnazia (Monopoli - XVI century B.C.)

The results obtained in the previous paragraph (section 0) were confronted with the outcomes of the application of a texture-based machine learning method, as explained in section 5.2.3. It is important to recall that, for validation purposes, both the unsupervised and supervised machine learning methods, were applied to four case studies, including exposed masonry façades of San Luigi church (Polignano – XVII century) and the rural church of SS. Salvatore (Loseto – XV century), in collaboration with the Ph.D. student Antonella Musicco. However, in this section, the two cases of San Leonardo's cloister and the south-west wing of the cryptoporticus of Egnazia are presented.

Given that the execution of the unsupervised segmentation was explained in the previous section, as far as the supervised texture-based segmentation is concerned, first of all, polygonal mesh models and high-resolution textures were retrieved from the photogrammetric data.

Starting from scaled textures of the two models, a preliminary step entailed a manual annotation of samples, representative of the decay classes of biological patina and colonization, spots/deposit, moist area, unaltered surfaces (Fig. 73).

In order to reduce processing requirements, in some cases, like in the south-west wing of the cryptoporticus, original cloud and deriving texturized mesh were divided in separate parts before the elaboration. Also, the features for the training have been selected: in this case Gaussian blur, Sobel filter, Hessian, difference of gaussians and membrane projections were adopted.

After the features setting, the random forest classifier was trained on the annotated samples. The learning phase was functional to perform the classification on the whole non-annotated data.
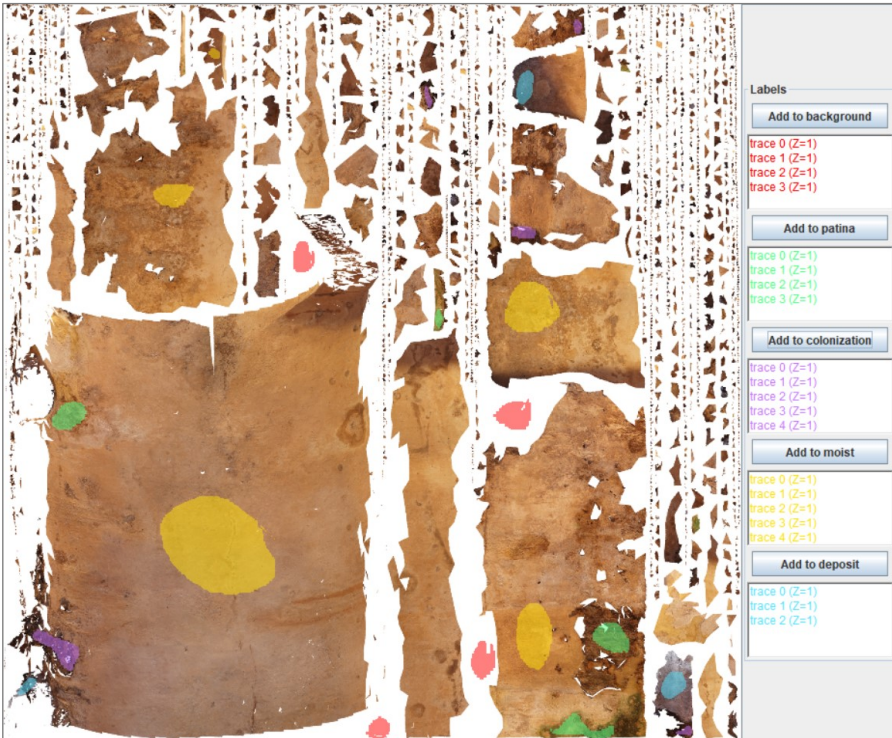
Fig. 73 – Manual annotation for one of the five portions of the south-west wing of the cryptoporticus
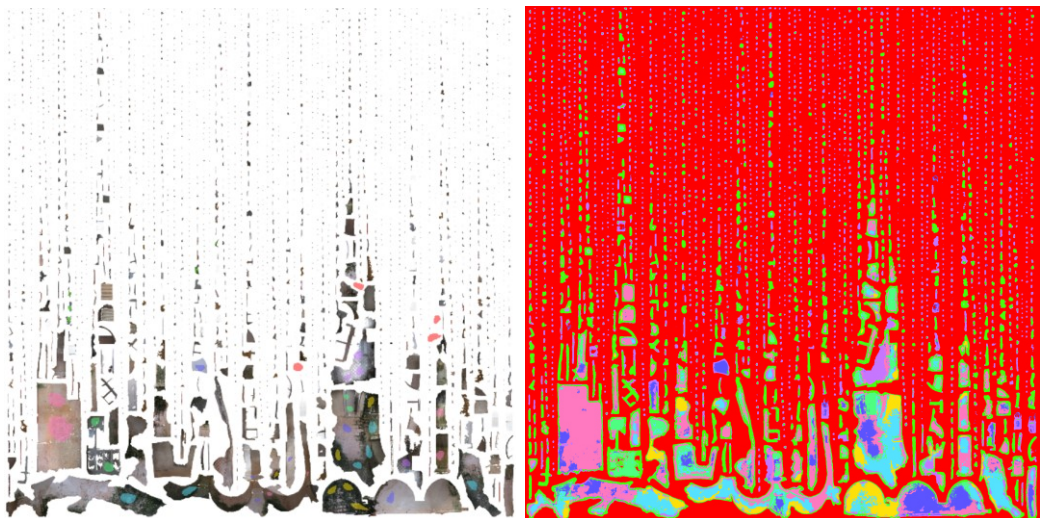
Fig. 74 – San Leonardo' cloister. Left: manually annotated samples; right: classification of the entire texture

These outcomes were then re-projected in a three-dimensional environment, in separate classes corresponding to the categories of alterations chosen at the beginning of the procedure.

In Fig. 75, the classified model of San Leonardo's cloister is proposed, with the same alteration classes shown in Fig. 72.

Fig. 75 – Supervised texture-based segmentation of San Leonardo' s cloister: a) total classified data; b) moist area (41%); c) biological patina (9%); d) biological colonization (37%); e) spots/deposit (4%); f) unaltered (11%)

For validation purposes the outcomes of the two segmentation strategies were quantitatively compared, in terms of number of points and area. These computations were made for all the case studies, both for ground truth, cloud-based segmentation and texture-based classification. Here, only two examples are shown (Table 21, Table 22).

Table 21 - Comparative tables of the outcomes of ground truth (manually segmented), cloud-based and texture-based segmentation for San Leonardo
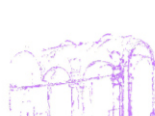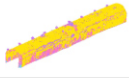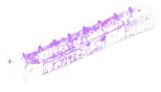
		GROUND TRUTH (GT)		CLOUD-BASED (CB)		TEXTURE-BASED (TB)	
original model							
N° points	pt		1,225,553		1,225,553		1,229,550
Area	m^2		275.16		277.52		250.66
moist area							
N° points	pt		438,609		381,871		498,585
N° points over total points	%		36%		31%		41%
Area	m^2		87.05		82.90		98.39
Area over total area	%		32%		30%		39%
biological patina							
N° points	pt		273,843		266,199		107,226
N° points over total points	%		22%		22%		9%
Area	m^2		74.28		68.62		23.79
Area over total area	%		27%		25%		9%
biological colonization							
N° points	pt		302,541		287,506		451,000
N° points over total points	%		25%		23%		37%
Area	m^2		57.76		56.24		86.70
Area over total area	%		21%		20%		35%
spots/deposit							
N° points	pt		21,596		81,663		43,154
N° points over total points	%		2%		7%		4%
Area	m^2		21.89		22.18		15.36
Area over total area	%		8%		8%		6%
unaltered							
N° points	pt		150,112		181,700		129,719
N° points over total points	%		12%		15%		11%
Area	m^2		30.62		44.56		26.42
Area over total area	%		11%		16%		11%
pipes							
N° points	pt		13,999		11,509		-
N° points over total points	%		1%		1%		0%
Area	m^2		3.56		3.02		-
Area over total area	%		1%		1%		0%

Table 22 – Comparative tables of the outcomes of ground truth (manually segmented), cloud-based and texture-based segmentation for Egnazia cryptoporticus

		GROUND TRUTH (GT)		CLOUD-BASED (CB)		TEXTURE-BASED (TB)	
original model							
N° points	pt		1,500,451		1,502,377		1,503,526
Area	m^2		349.52		312.96		237.06
moist area							
N° points	pt		958,504		955,950		985,353
N° points over total points	%		64%		64%		66%
Area	m^2		168.10		163.75		142.40
Area over total area	%		48%		52%		60%
biological patina							
N° points	pt		352,347		380,798		280,049
N° points over total points	%		23%		25%		19%
Area	m^2		111.21		99.67		50.44
Area over total area	%		32%		32%		21%
biological colonization							
N° points	pt		131,711		104,642		29,938
N° points over total points	%		9%		7%		2%
Area	m^2		40.40		35.00		5.54
Area over total area	%		12%		11%		2%
spots/deposit							
N° points	pt		57,989		60,987		208,186
N° points over total points	%		4%		4%		14%
Area	m^2		29.81		14.54		38.69
Area over total area	%		9%		5%		16%

Finally, to evaluate the segmentation performances, all the ratings to realize a confusion matrix were calculated:

- *True Positive (TP)* = intersection between *Cloud_Based (CB)* or *Texture_Based (TB)* area and *Ground Truth (GT)* area

$$TP = (CB \lor TB) \cap GT$$

(9. 1)

- *False Positive (FP)* = difference between *Cloud_Based (CB)* or *Texture_Based (TB)* area and *True Positive (TP)*

$$FP = (CB \lor TB) - TP$$

(9. 2)

- *False Negative (FN)* = difference between *Ground Truth (GT)* area - *True Positive (TP)*

$$FN = GT - TP$$

(9. 3)

- *True Negative (TN)* = difference between *Total Area (TA)* and the sum of *True Positive (TP)*, *False Positive (FP)* and *False Negative (FN)*

$$TN = TA - (TP + FP + FN)$$

(9. 4)

All the four indicators are necessary to retrieve the performance evaluators:

- *Precision or Positive Predictive Value (PPV)* = ratio between *True Positive* observations and total predicted positive observations (*True Positive + False Positive*);

$$PPV = \frac{TP}{TP + FP}$$

(9. 5)

- *Sensitivity or True Positive Rate (TPR)* = ratio between *True Positive* and number of actual positives (*True Positive + False Negative*);

$$TPR = \frac{TP}{TP + FN}$$

(9. 6)

- *Overall Accuracy (ACC)* = ratio of correctly predicted observation (*True Positive + True Negative*) and total observations (*True Positive + False Positive + False Negative + True Negative*)

$$ACC = \frac{TP + TN}{TP + FP + FN + TN}$$

- *f1-score* = harmonic mean of Precision and Sensitivity

$$f1 = \frac{2TP}{2TP + FP + FN}$$

Overall accuracy works better with symmetric datasets, where values of false positive and false negatives are almost equal. While *f1-score* takes both false positives and false negatives into account, because if their costs are consistently different it is better to look at both *precision* and *sensitivity* [253].

In Table 23, these ratings are reported, for the two cases of San Leonardo (SL) and Egnazia (EG), in correspondence of each alteration class. They vary from very high *overall accuracy* and *f1-score* (around 0,98-0,99) for damp patterns (moist area, biological patina, biological colonization), to low values of the *f1-score* (0,36) in correspondence of the class of spots and deposits in the cryptoporticus. From Table 23, it is possible to collate ratings of both the unsupervised cloud-based (CB) and the supervised texture-based segmentation (TB). For most of the classes, the cloud-based approach consent to accomplish better performances, with higher *overall accuracy* and *f1-score* values.

In the end, a global evaluation of the efficiency of the two methods, enclosing also the outcomes of the other two case studies, San Luigi in Polignano (SLU) and Santissimo Salvatore in Loseto (SS), is readable in five bar charts, one for each detected decay morphology (Fig. 76).

Table 23 – Ratings for the two case studies (San Leonardo, Egnazia), in correspondence of the alterations' classes

		SAN LEONARDO (SL)			EGNAZIA (EG)		
		GT	CB	TB	GT	CB	TB
N° total points	pt	1,225,553	1,225,553	1,229,550	1,500,451	1,502,377	1,503,526
Total area	m^2	275.16	277.52	250.66	349.52	312.96	237.06
moist area							
N° points	pt	438,609	381,871	498,585	958,504	955,950	985,353
Area	m^2	87.05	82.90	98.39	168.10	163.75	142.40
TP	-		347,272	352,988		936,481	953,793
FP	-		34,599	145,597		19,469	31,560
FN	-		91,337	85,621		22,023	4,711
TN	-		752,345	645,344		247,580	239,486
PPV	%		0.91	0.71		0.98	0.97
TPR	%		0.79	0.80		0.98	1.00
f1-score	%		0.85	0.75		0.98	0.98
ACC	%		0.90	0.81		0.97	0.97
biological patina							
N° points	pt	273,843	266,199	107,226	352,347	380,798	280,049
Area	m^2	74.28	68.62	23.79	111.21	99.67	50.44
TP	-		218,666	58,174		341,278	243,092
FP	-		47,533	49,052		39,520	36,957
FN	-		55,177	215,669		11,069	109,255
TN	-		904,177	906,655		833,686	840,246
PPV	%		0.82	0.54		0.90	0.87
TPR	%		0.80	0.21		0.97	0.69
f1-score	%		0.81	0.31		0.93	0.77
ACC	%		0.92	0.78		0.96	0.88
biological colonization							
N° points	pt	302,541	287,506	451,000	131,711	104,642	29,938
Area	m^2	57.76	56.24	86.70	40.40	35.00	5.54
TP	-		261,788	248,737		92,317	28,942
FP	-		25,718	202,263		12,325	996
FN	-		40,753	53,804		39,394	102,769
TN	-		897,294	724,746		1,081,517	1,096,843
PPV	%		0.91	0.55		0.88	0.97
TPR	%		0.87	0.82		0.70	0.22
f1-score	%		0.89	0.66		0.78	0.36
ACC	%		0.95	0.79		0.96	0.92
spots/deposit							
N° points	pt	21,596	81,663	43,154	57,989	60,987	208,186
Area	m^2	21.89	22.18	15.36	29.81	14.54	38.69
TP	-		16,709	259		54,124	46,777
FP	-		64,954	42,895		6,863	161,409
FN	-		4,887	21,337		3,865	11,212
TN	-		1,139,003	1,165,059		1,160,701	1,010,152
PPV	%		0.20	0.01		0.89	0.22
TPR	%		0.77	0.01		0.93	0.81
f1-score	%		0.32	0.01		0.91	0.35
ACC	%		0.94	0.95		0.99	0.86
unaltered							
N° points	pt	150,112	181,700	129,719			
Area	m^2	30.62	44.56	26.42			
TP	-		114,908	81,238			
FP	-		66,792	48,481			
FN	-		35,204	68,874			
TN	-		1,008,649	1,030,957			
PPV	%		0.63	0.63			
TPR	%		0.77	0.54			
f1-score	%		0.69	0.58			
ACC	%		0.92	0.90			
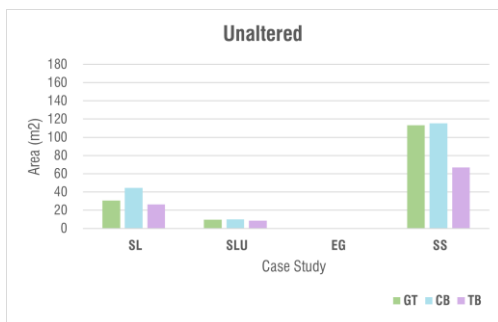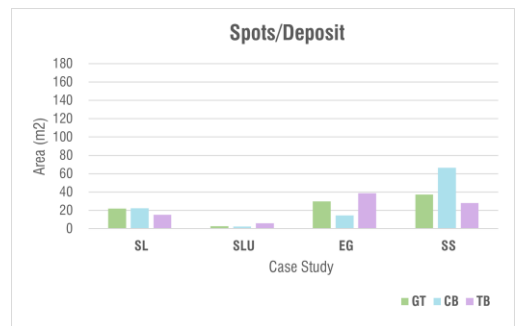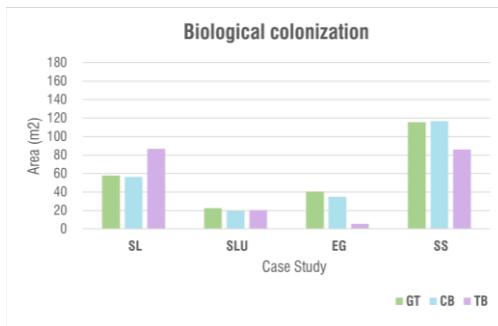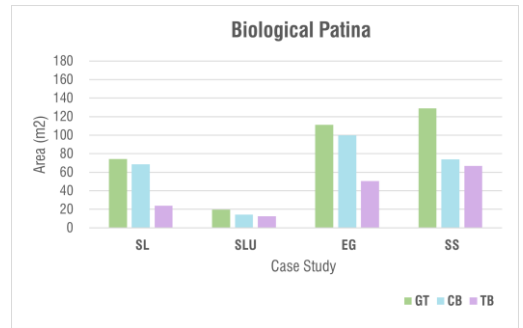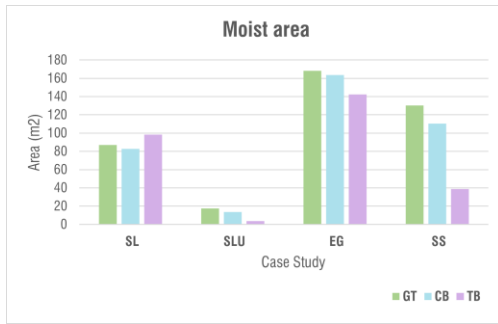
Fig. 76 – Bar charts collating the outcomes of the four case studies, class by class

9.3. (A) Geometric segmentation of point clouds to identify architectural elements

Geometric segmentation of point clouds for the recognition of architectural elements, as described in section 5.3, was tested on two case studies, one cross vault of San Leonardo's cloister, and the two barrel-vaulted volumes of the Cappuccini ex-convent. Here only the cross vault is reported, by way of example. RANSAC, as best fitting algorithm, was applied to the point clouds of these volumes, to detect the main architectural elements composing them (walls, vaults, pillars,…), by their association to geometric primitives: plane-wall, cylinder-barrel vault, cylinder-vault panel, cylinder-column,…

According to the morphology of the architectural volumes, the main parameters were set. For example, for the cross-vault of San Leonardo: the searched primitives were plane and cylinder, the minimum number of points per primitive 2000, the maximum distance between the set of points and the primitives 0.02 m, the sampling resolution (distance between neighbouring points in the data) 0.0034 m, the maximum angular deviation 25°, and the overlooking probability 0.01.

The outcomes are segments of primitives, which correspond to the main architectural elements. In this case six cylinders were isolated, representing the panels of the cross vault, and two planes, which stands for the perimetral vertical walls (Fig. 77).

At this stage, point cloud segmentation was performed on the identified architectural elements. In Fig. 78, an exemplification for the two vertical walls is shown. Some forms of alteration were detected: biological patina/colonization and unaltered surface, for the left-side wall; biological colonization/patina and moist area, for the right-side wall. These results are consistent with the ones obtained from the application of point cloud segmentation on the whole cross vault [232].
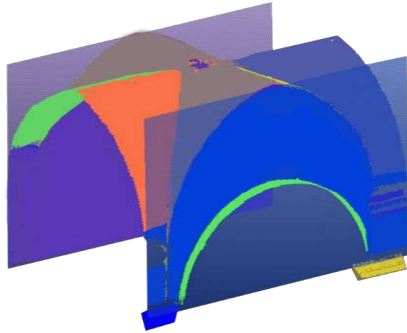
Fig. 77 - Application of the RANSAC to the point cloud of the cross vault of San Leonardo's cloister [232].
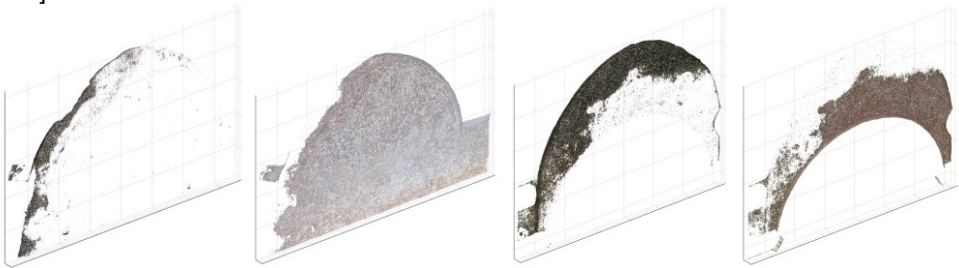
Fig. 78 - From left to right: biological colonization and unaltered surface of the wall on the left; biological colonization and moist area of the wall visible on the right [232].

The recognition and labelling of architectural elements, from unorganized data of point clouds, represents a great advantage in terms of diagnostic knowledge, because it provides the possibility to associate the single architectural element to the damage by which it is affected, thus giving important information about causes and gravity of the assessed decay.

In this light, the research is ongoing, in order to find more accurate best fitting algorithms, or to implement other machine learning systems, like random forest, as illustrated in some recent research projects [176] [178].

9. (B) MONITORING BUILDING DECAY PATTERNS BY PHOTOMODELLING BASED 3D MODELS FOR THE REMOTE DIAGNOSIS AND CONTROL OF THE HERITAGE ARCHITECTURE

Another aspect of the research work is related to the possibility to monitor and control the state of conservation of architectural heritages, through the application of the methodological approaches illustrated in section 9, to selected case studies, and, in particular, to critical areas characterized by the presence of extensive decay. Indeed, image processing routines were applied to photogrammetric 3D data of the same architectural elements, acquired in different points in time, in order to detect and evaluate possible changes occurred in adequate time intervals. These modifications were analysed, in order to verify if they are attributable to decay progression over time. To this end, as already mentioned in section 8, a plurality of acquisition campaigns was realized, for case studies like Palmieri Palace (main portal, ashlar region, internal courtyard pillars) or Bashtovë Fortress (north tower).

9.1. (B) Indirect monitoring and control of decay patterns on built heritage

9.1.1. (B) Palmieri Palace – Surface degradation of an ashlar masonry region

Semi-automatic Image processing routines, illustrated in section 5.1.1, were applied, for example to an ashlar region of the lower part of the main façade of Palmieri palace. In Table 7, the details of the acquisition campaigns show that four different photogrammetric scans were executed, focused on the same area. They started from an existing model of 2015 (retrieved from the general acquisition of the main façade), and they were repeated in 2017, 2019, 2020 and 2021. Comparing all the parameters related to equipment (camera model, lenses focal length, support) and shooting distance, it is possible to observe that they are alike, in order to obtain comparable 3D data in the reconstruction phase. Indeed, in Table 11 3D data specifications are reported, highlighting an analogous ground resolution and reprojection error, for the point clouds corresponding to the four acquisitions. As far as the number of points is concerned, given that a huge number of points (in the order of magnitude of several

millions) requires excessive computational resources, the point clouds were re-sampled, to get a comparable number of points. In the first case, the time interval is of 18 months, from 06/11/2015 to 09/06/2017. The two clouds, with an area of about 7 m^2, an equivalent number of points of around 960.000, and a comparable resolution of about 2,3 mm/pixel, were subjected to the semi-automatic procedure in Mountains Map.

The outcomes reveal that quantitative variations in the order of few centimetres can be detected, in correspondence of defective areas. In fact, from distance measures in Fig. 79, with the relative tables (on the right), it is possible to read these changes.

a)

Name	Unit	A	B	F	G
Distance	mm	265	209	741	401
X1	mm	1487	1466	342	1797
Y1	mm	792	954	1138	216
X2	mm	1752	1675	1083	2197
Y2	mm	793	955	1139	217

b)

Name	Unit	A	B	F	G
Distance	mm	273	206	754	416
X1	mm	1525	1508	352	2
Y1	mm	827	1000	1178	0
X2	mm	1798	1714	1106	2
Y2	mm	833	1000	1178	0
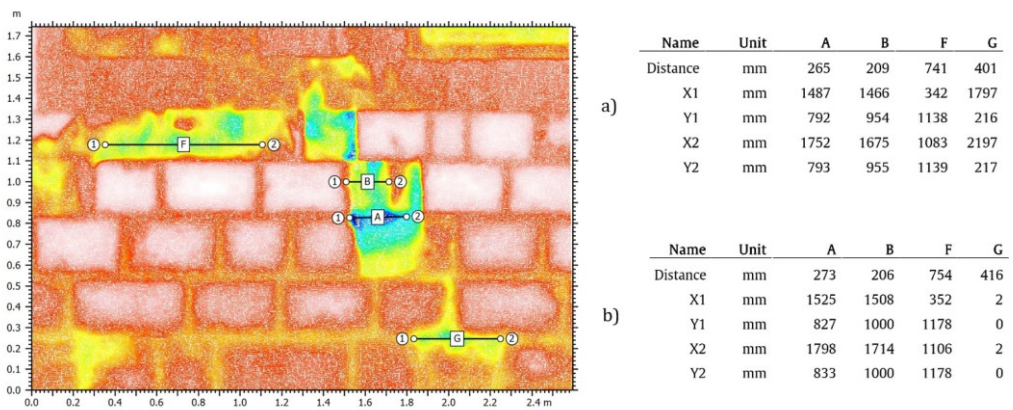
Fig. 79 Comparison between corresponding distances (A, B, F, G) in the two models: a) years 2015, b) year 2017 [4].

The information can be integrated, with the juxtaposition of horizontal profiles, passing through the deepest point. Also, in this case, it is possible to highlight a change, occurred in a time interval of 5 years, which results in a lowering of the point to greater depth (Fig. 80).

Some peaks are no more visible, probably because of a surface smoothing, caused by rising dampness or marine aerosol [4]. The indirect comparison involved also 3D data of the successive campaigns, in order to monitor the progression of the situation.
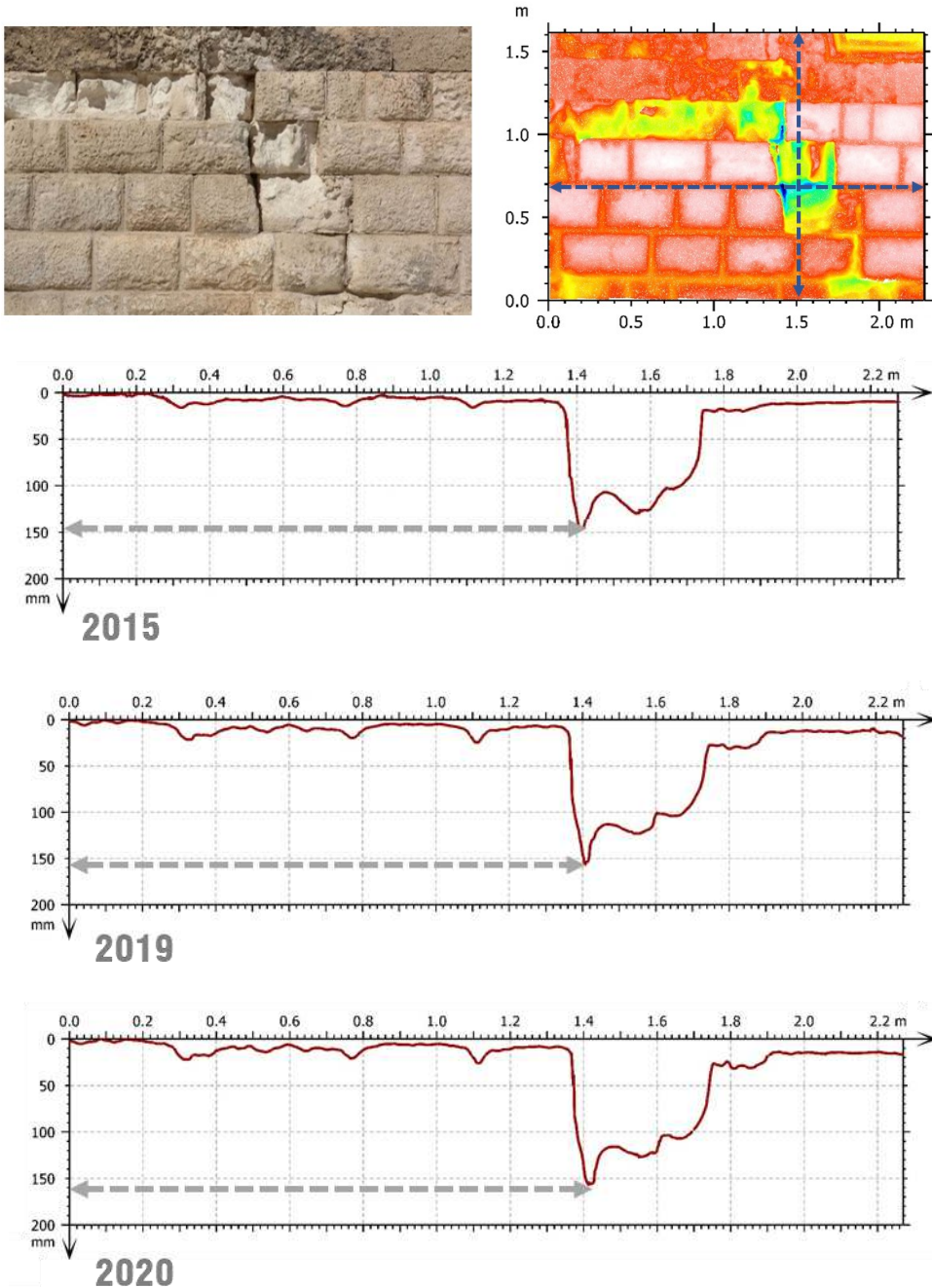
Fig. 80- Extraction of horizontal profiles passing through the deepest point, from year 2015 to year 2020.

9.2. (B) Direct monitoring of the state of conservation of the architectural heritage

As an alternative to a monitoring performed with an indirect matching of data, a more expeditious procedure entailed the direct confrontation of point clouds, to obtain a change detection, representative of the modifications occurred on an architectural element in a precise time interval.

9.2.1. (B) Palmieri Palace – Surface degradation of an ashlar masonry region

The widespread surface degradation of the ashlar masonry region described in section 9.1.1, whose morphologies of cavities, erosions or lacks are mainly related to weathering and rising dampness, emerged also through a direct comparison of point cloudsof the same areas considered in the previous sections. In first place, a eighteen months interval (from 06/11/2015 and 09/06/2017) was evaluated, using comparable point clouds (similar number of points and ground resolution).

To quantify eventual modifications, the first model (2015) was fixed as reference model, while the second (2017) was aligned and registered, thanks to the two methods of pair point picking and Iterative Closest Point, mentioned in Section 6.2 (Eq. (6. 1).

The aligned entities were used to compute the 3D models' deviation. This step was achieved through the nearest neighbour distance, which is a cloud-to-cloud distance calculated according to Eq. (6. 2).

The resulting deviation maps are crucial to understand the advancement of the alterations and how they arise. As a matter of fact, as previously emerged (9.1.1), a progression of the detected alterations, compatible with rising dampness evidence, is visible from the observation of the greatest distances between the two datasets, and where they are located. Indeed, they vary from 3,4 to 4,5 cm, located in correspondence of cavities, lacks or eroded areas (Fig. 81).
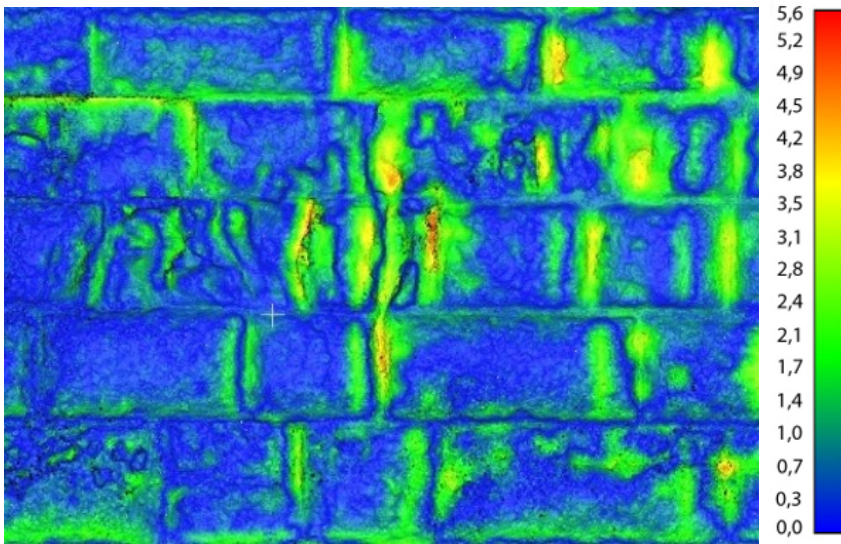
Fig. 81 – Deviation map of the restricted area of ashlar masonry, in the basement of the external façade, with absolute distances (cm) between the two point clouds (06/11/2015 - 09/06/2017)

The illustrated situation is confirmed, by the collation of these results with the outcomes of a well-known non-destructive diagnostic test, the thermography. This is a particularly suitable technique, for the identification of humidy patterns, even when non visible on surface. The thermographic survey, with a FLIR T430s thermo-camera, revealed a qualitative compatibility with the previous findings (Fig. 82).

Defective areas characterized by lacks, cavities and erosions coincide with low appearent temperature regions, both in shape and extent. Therefore, the surface decay morphologies represent the evidence of the rising dampness phenomenon, as a consequence of "cycles of evaporation and absorption, with subsequent deposit of salts on the surface and increase of local mechanical stresses on the stone" [17].

These diagnositc tests, together with the ones proposed in the following section (9.2.2), are part of a research work, realized with the guidance of Prof. Mariella De Fino, and the technical support of the laboratory technician Rocco Rubino.
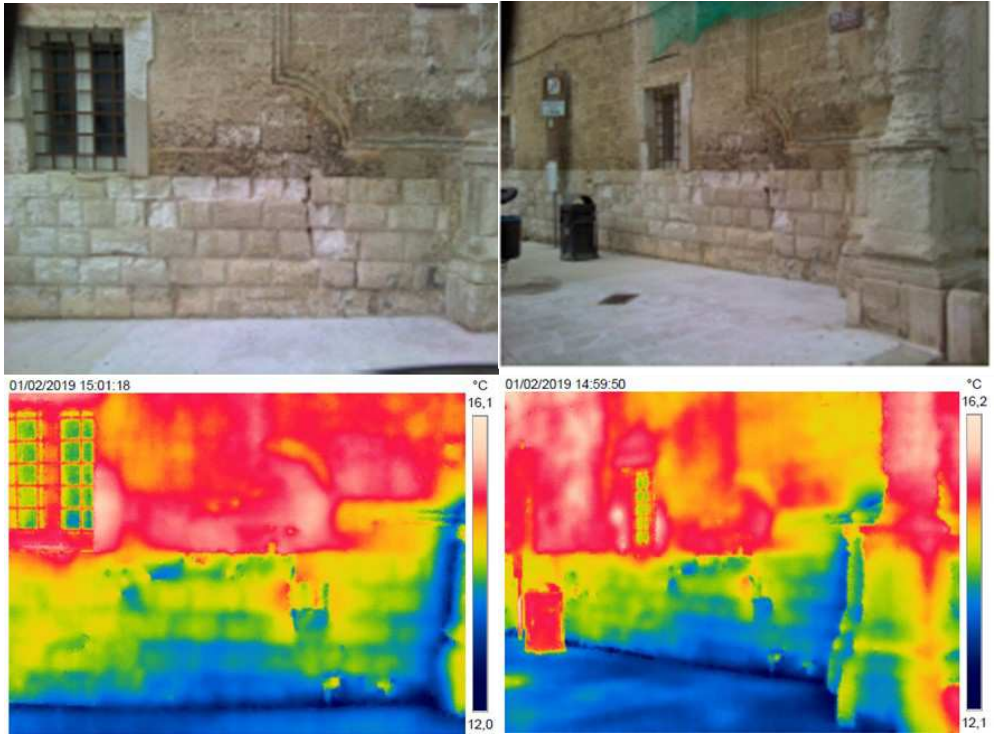
Fig. 82 – Thermographic survey, with visible and infrared representation of the same area (front and lateral view) [17]

9.2.2. (B) Palmieri Palace – Static instability of the right pillar of the internal courtyard

The right pillar of the internal courtyard (Fig. 83), characterized by a crack pattern related to phenomena of static instabilities, was acquired in three different campaigns (06/11/2015, 23/11/2018 and 19/06/2020), as it is possible to observe in Table 7. In this connection it is worth restating that a structural deficiency was highlighted by the presence of vertical and hyperboloid cracks, poor mortar joints and missing parts at the corner of the stone blocks, affecting both the central pillars, at various elevation levels.
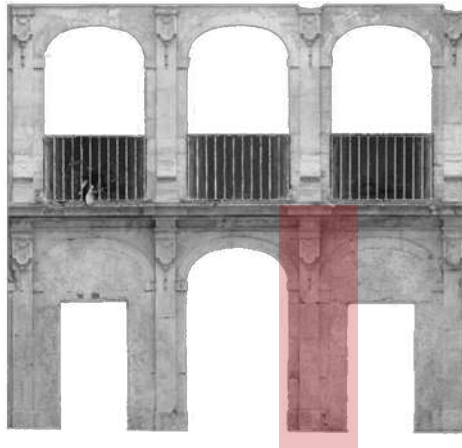
Fig. 83 – Localization of the right pillar, on the façade parallel to the main entrance, in the courtyard.

Table 24 – Main photogrammetric reconstruction parameters for the right pillar [17]

Data		Courtyard		Right Pillar		
		General		Detail		
		06/11/2015	23/11/2018	23/11/2018	20/12/18	19/06/2020
Object area	m²	170	57	18	1.3	5
Tie points	N°	157,972	185,726	97,760	22,518	236,390
Alignment time	min	11	15	20	50	67
Dense points	N°	107,507,214	33,268,081	63,334,317	269,475,206	5,519,473
Dense time	min	41	41	1208	968	50
N° faces	-	21,206,948	6,607,760	4,222,275		
N° vertices		10,628,096	3,316,657	2,127,509		
Mesh time	min	95	471	94		
Ground Resolution	mm/pixel	0.95	1.13	0.421	0.02	0.36
Height Resolution	mm/pixel	1.9	2.26	0.842		
Reprojection Error	pixel	0.81	0.581	1.23	1.04	0.568
Texture time	min		3			
Total Rec. time	min	147	530	1,322	1,018	117

However, only the right pillar at the ground floor level was explicated in detail, because here significant cracks and lacks are located. To allow a proper confrontation, 3D data with analogous resolution were searched, in a time interval of three years (Table 24).

In this case the acquisitions were made at three different levels of detail: the first, more general, to have an idea of the localization of the crack patterns, and to observe macroscopical changes; the second, at an intermediate level of detail, to investigate quantitatively the crack pattern; and the third, at very short distance, with the help of an additional ring flash, to obtain a very high-resolution point cloud and to reconstruct also the lateral sides of a small and thin crack, like the one visible on the right pillar (Fig. 84).
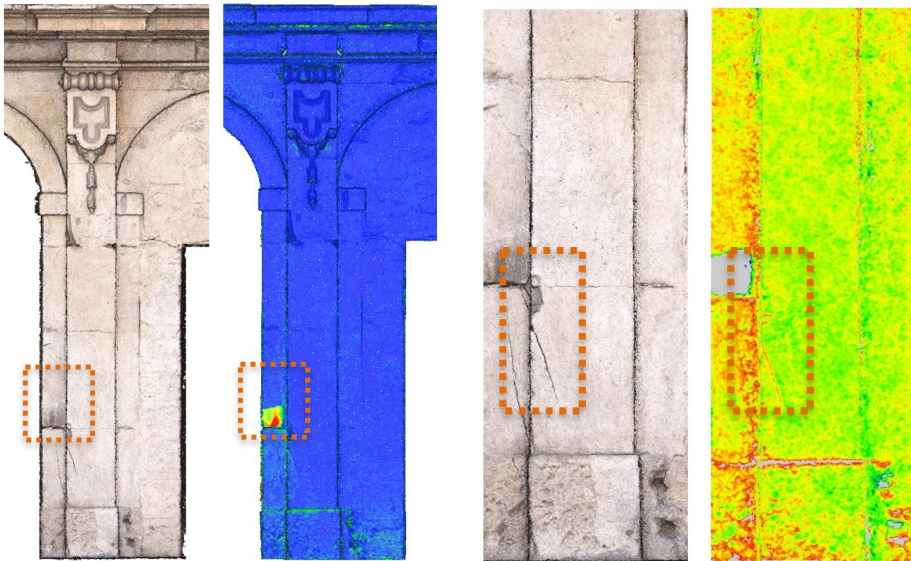
Fig. 84 - Dense point cloud of the right pillar at the ground floor level; correspondent deviation map (distances expressed in cm); zoom to observe the crack pattern [17]

Indeed, from a general acquisition, at a 10 meters distance, nothing relevant about the evolution of decay emerged, whereas, at 5 meters, macroscopic alterations like a great lack on the right pillar in correspondence of a mortar joint, are visible and controllable. Here, deviations of 1-2 cm were detected, portraying an advancement of the alteration, most likely resulting from the ejection of materials, due to static instability (Fig. 85). For

the crack, even though a higher resolution was needed, the only comparable models were the intermediate. Anyway, they were sufficient to register changes in the points located near the edges. In this case, the variations are in the order of 2-3 mm (Fig. 86).
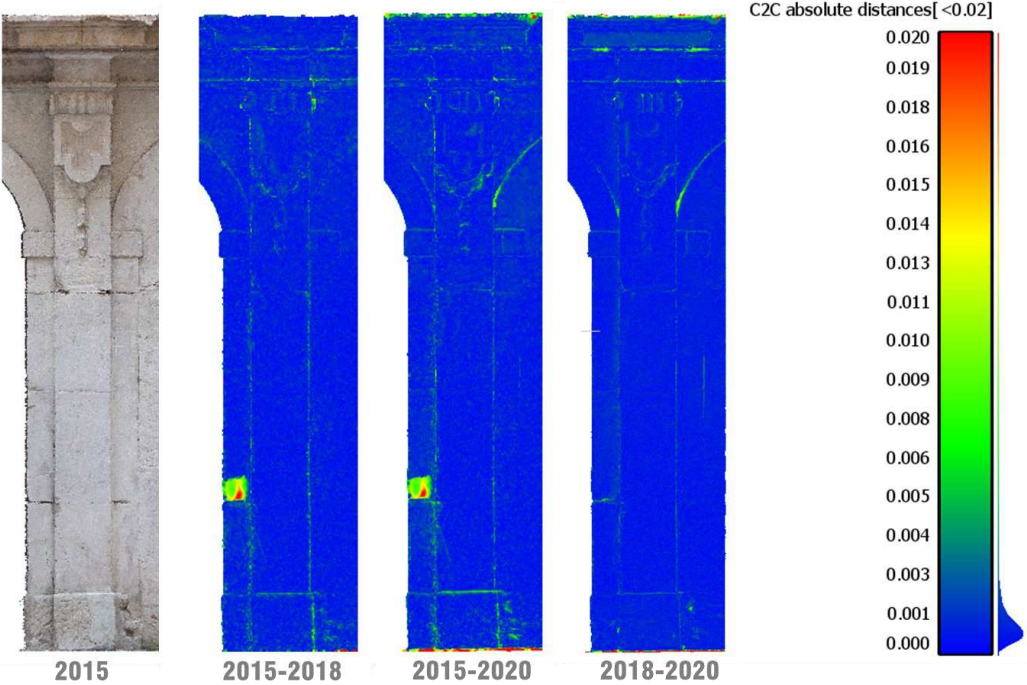
Fig. 85 – Monitoring of macroscopic alterations (lacks, cavities), resulting from the ejection of material, in consequence of the static instability (the scale of absolute distances is expressed in meters)
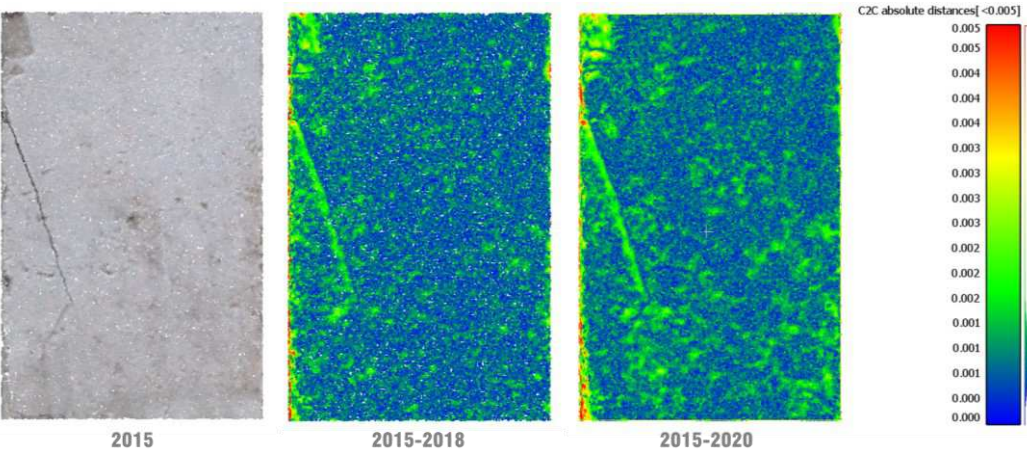
Fig. 86 – Monitoring of the crack in the right pillar (distances are expressed in metres)

190

As in the previous case of rising dampness, also here, the results were matched with data acquired from another non-destructive diagnostic technique. A plurality of ultrasonic tests was realized, with a Boviar CMS-V3H with 55 kHz high frequency emitter. Five tests for each pillar, with twelve selected paths at different heights (Fig. 87). The outcomes are consistent with the results of the 3D models comparison because their analysis highlighted a fluctuation of the ultrasound travel velocity. Given the homogeneous material of the pillars (calcarenites stone), the speed reduction indicates the presence of discontinuities, most likely corresponding to fracture planes and probably covering the whole thickness of the architectural element. Indeed, the structural deficiency, already diagnosed at the beginning of the XX century, still produces forms of surface decay, including the hyperboloid crack progression or missing parts at the corners.

It is worth to restate that these further diagnostic tests were not personally executed by the Ph. D. candidate, but they belong to a research work integrated within the present thesis, and whose main results are published in [17].
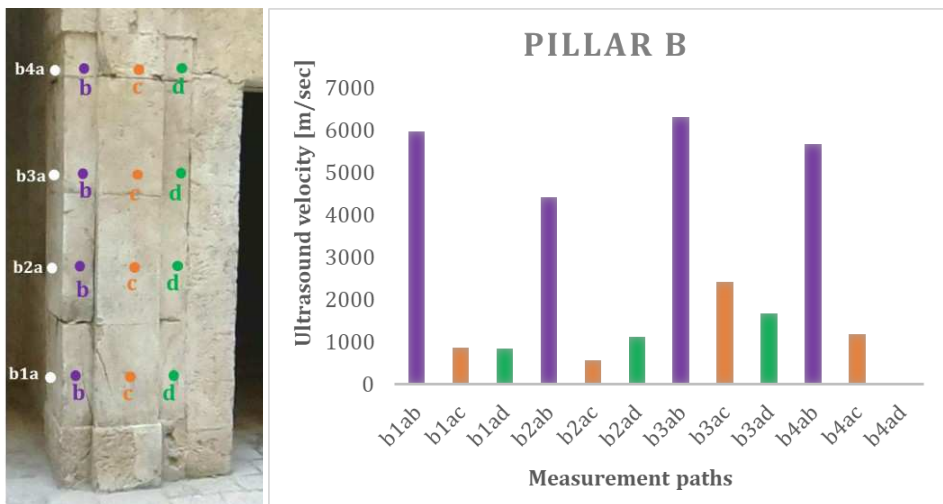
Fig. 87 - Left: ultrasonic tests scheme of the measurement paths connecting n. 4 positions of the emitter (white points) and n.12 positions of the receiver (purple, orange, green); Right: average travel velocities for each measurement path for the right pillar [17]

9.2.3. (B) Palmieri Palace – Surface degradation of the portal (main façade)

The portal of the main façade of Palazzo Palmieri is consistently subjected to erosion phenomena, due to the high presence of marine salts, as a consequence of the proximity to the seaside. With this in mind, two photogrammetric acquisition campaigns were realized, as mentioned in Section 8 (Table 7).

A time interval of six years, from 2015 to 2021, was considered, in order to evaluate the progression of erosion, especially in the columns and relative basements of the portal. However, it is necessary to clarify that, in the last acquisition campaign, the reconstruction was affected by the presence of protection nets, covering the upper parts of the two columns, making it impossible to confront the two capitals (Fig. 88). Partial evaluations were made on the inferior part of the portal.

Fig. 88 – Portal of the main façade. Left: point cloud of 06/11/2015; right: point cloud of 05/03/2021

After removing the disturbing elements, a direct comparison of the two point clouds was accomplished, with 3-points and ICP registration, and, then the computation of the models' deviation. The registration of the two models was affected by the presence of

external elements, like the protection nets, which made it difficult to properly align the two entities. Therefore, the clouds needed to be cut, concentrating the analysis on the lower part of the portal. To better evaluate the eventual changes, a punctual verification was made on the transversal sections, from which differences in the order of magnitude of centimetres were found (Fig. 89).
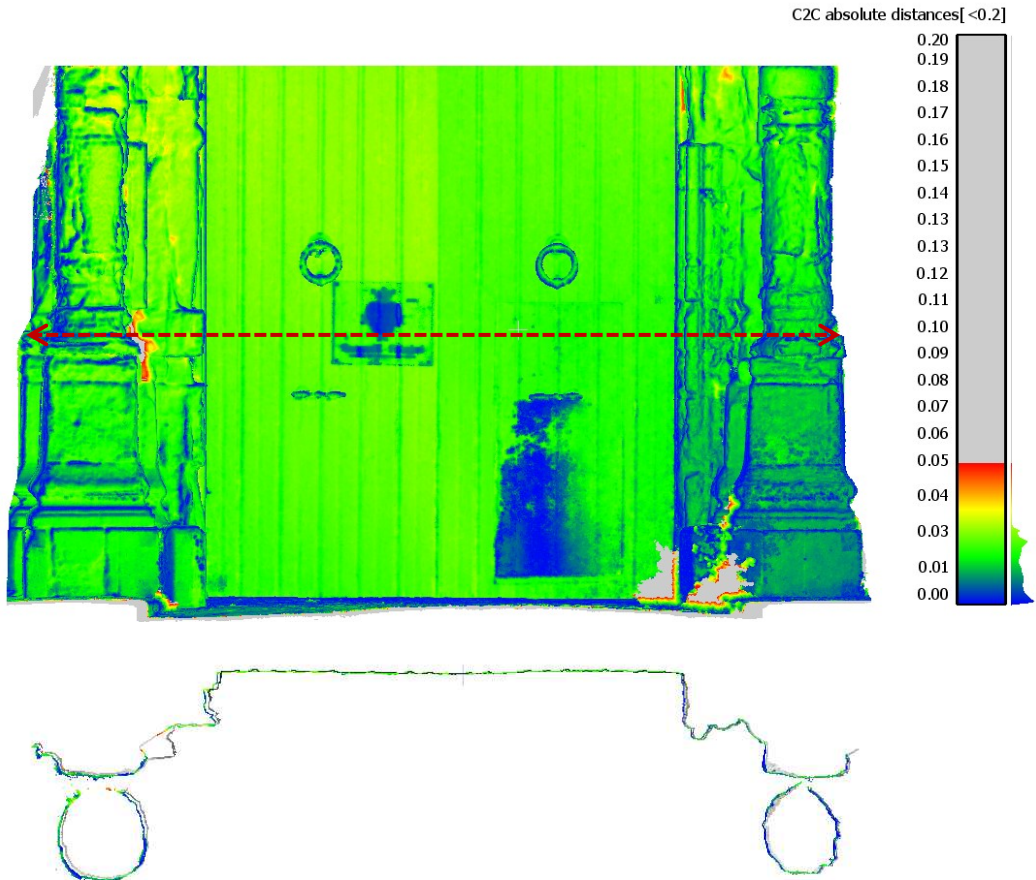
Fig. 89 - Deviation map of the bottom part of the portal, with corresponding transversal sections (scalar field expressed in metres)

Going into detail, both the column bases were confronted separately, thus excluding the wooden front door. The results are visible in Fig. 90 and Fig. 91, representing respectively the right and the left bases.

In the first case, differences are in the order of 1-2 cm (or below), in correspondence of the corners or edges, where a slight loss of material was registered. While in the left

column base, a major lack emerged, in correspondence of which, differences lay between 3 and 7 cm, clearly visible from the cross-sections (Fig. 92).
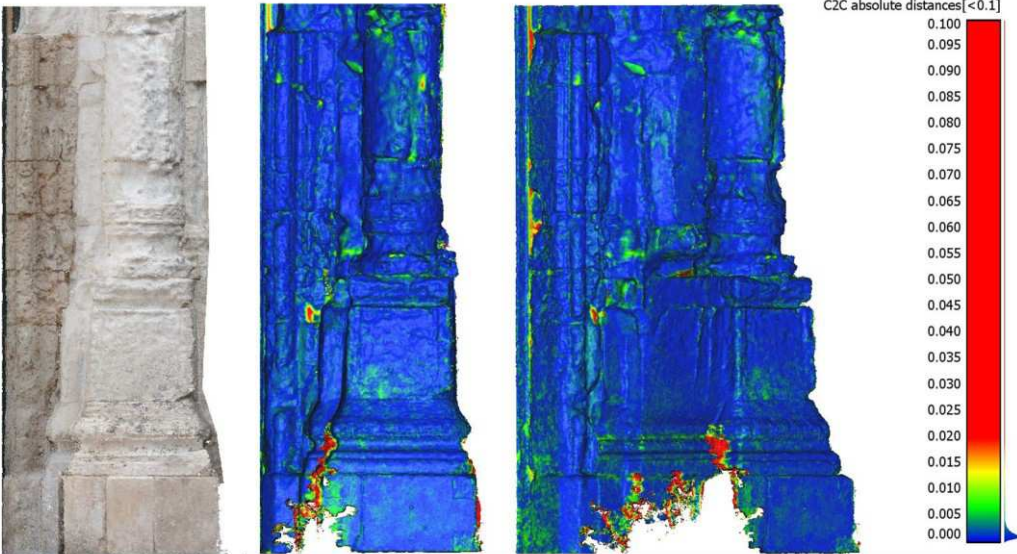
Fig. 90 – Direct comparison of the column base (right side). The absolute distances are expressed in metres.
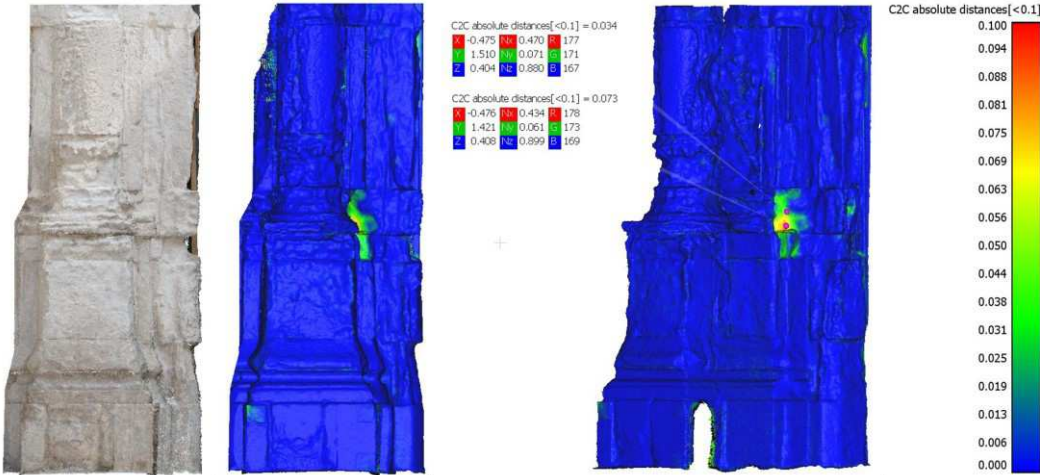
Fig. 91 – Direct comparison of the column base (left side).
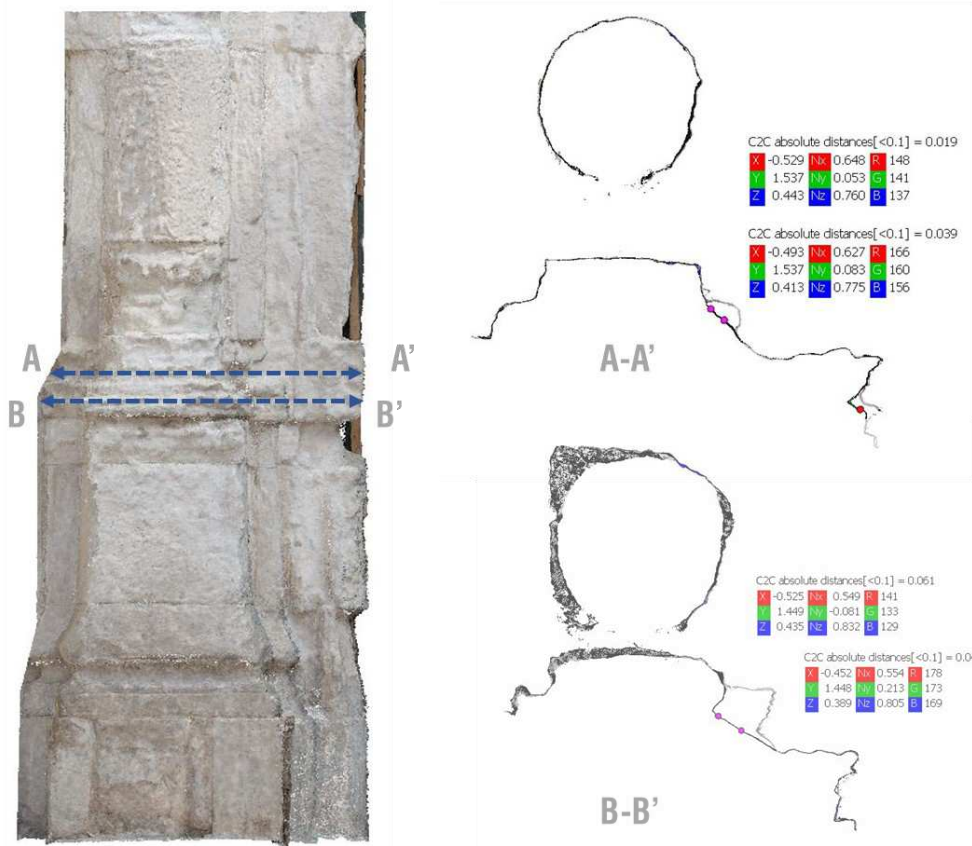
Fig. 92 – Cross-sections extracted from the left column base

9.2.4. (B) Bashtovë Fortress – Static instability in the north tower

As far as the fortress of Bashtovë is concerned, a particular attention was put on the north tower, because it is affected by static instabilities, visible from a huge vertical crack, as already mentioned in section 9.1.1 (Fig. 52). In first place, the tower was acquired, as part of the project "3D Impact", for cultural and touristic dissemination purposes. But reconstructed 3D data have a sufficient resolution to accomplish also diagnostic purposes. In this light, a first phase of diagnostic analysis, based on the acquisitions of 2018, was realized (sections 9.1.1 and 9.1.2).

Fig. 93 – Point cloud of the north-tower, with the indication of the points of the four heights of acquisition

Afterwards, following the two seismic events occurred in 2019 (described in section 7.2), further acquisitions were made, thanks to the help Prof. Erald Piperi (Polytechnic University of Tirana, Albania), for post-disaster assessment purposes (Fig. 93).

In the second campaign, the same acquisition and reconstruction parameters were adopted, in order to make the point clouds equivalent. At this stage, they were directly compared, according to the pipeline explained in section 6.2.

A specific attention was dedicated to the whole reconstruction process, and 3D parameters, in order to impose the same quality for the alignment and dense cloud reconstruction. This aspect was fundamental to obtain comparable ground resolution and reprojection error. Also here, two distinct levels of detail were considered: a first more general level, to evaluate eventual displacements, buckling or macroscopic

alterations; a second more detailed level, to quantify possible crack opening progressions (Table 25).

Table 25 – North tower, processing data

		Bashtovë – North Tower			
		General	Detail	General	General
Data		07/11/2018	07/11/2018	9/4/20	24/12/20
Object area	m²	95	11	37	93
Tie points	N°	8,009,034	1,794,984	4,781,882	8,257,163
Alignment time	min	169,231	95	259,271	259,628
Quality (Alignment)	-	Highest	Highest	Highest	Highest
Dense points	N°	46,451,851	33,585,330	64,369,652	79,982,738
Quality (dense)	-	High	High	High	High
Depth filtering	-	Mild	Mild	Mild	Mild
Dense time	min	83	6	257	170
Faces	N°			2,000,000	
Vertices	N°			1,008,475	
Mesh time	min			57	
Ground Resolution	mm/pixel	1.34	0.32	0.44	0.95
Height Resolution	mm/pixel			0.88	
Reprojection Error	pixel	0.28	0.136	0.30	0.31
Point density	pt/mm ^ 2			1.29	
Texture time	min			4	
Total Rec. time	min	169,314	101	259,589	259,798

The outcomes, represented by the deviation maps in Fig. 94, highlight differences around few centimetres, located in the indicated regions. They are representative of slight displacements and slight variations near the crack, compatible with the damages expected in the area on the basis of the seismic data, referring to the values of the Modified Mercalli Intensity scale (MMI). In fact, as previously declared, for masonry buildings, 6 MMI could produce cracks on poorly constructed walls and parapets [246] [247]. Going into detail, a direct comparison of the cracked area was performed and associated to the indirect collation of transversal sections, from which changes in the order of magnitude of a centimetre are readable (Fig. 95).
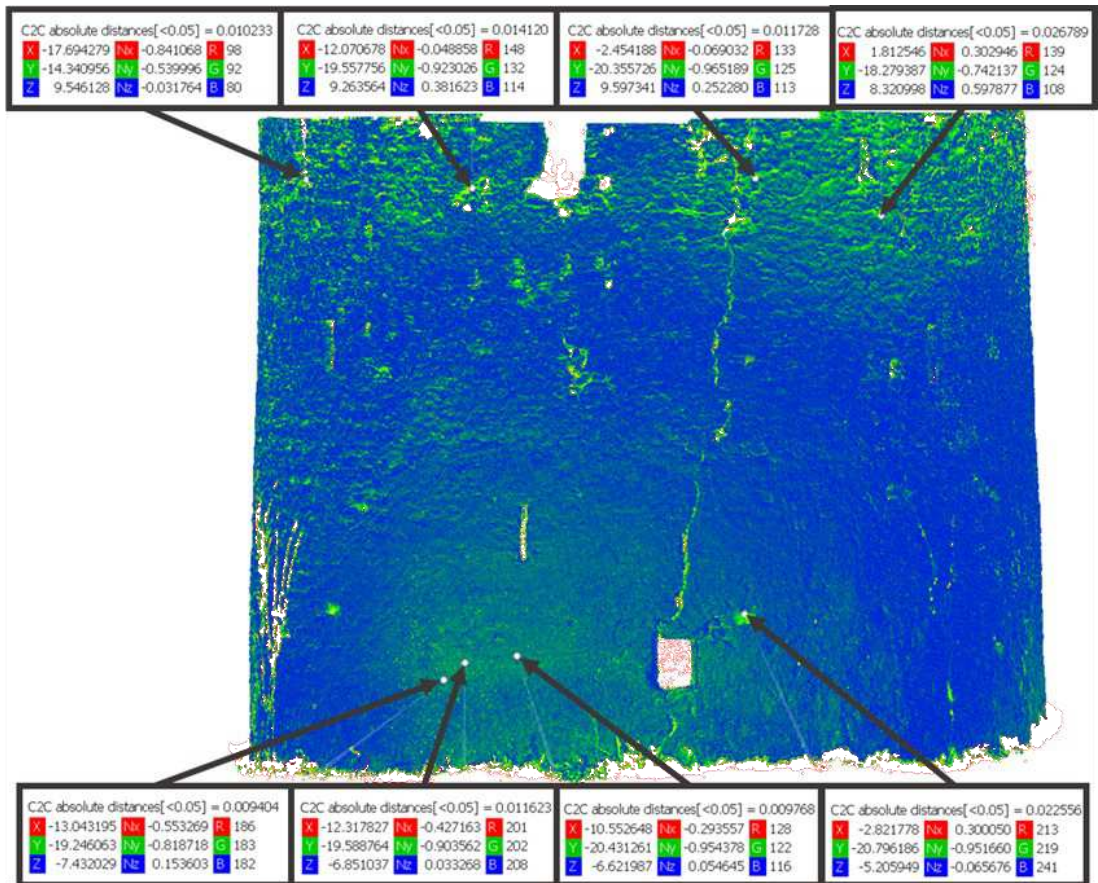
Fig. 94 - Deviation map of the north tower, after the direct comparison of point clouds of 2018 and 2020 point
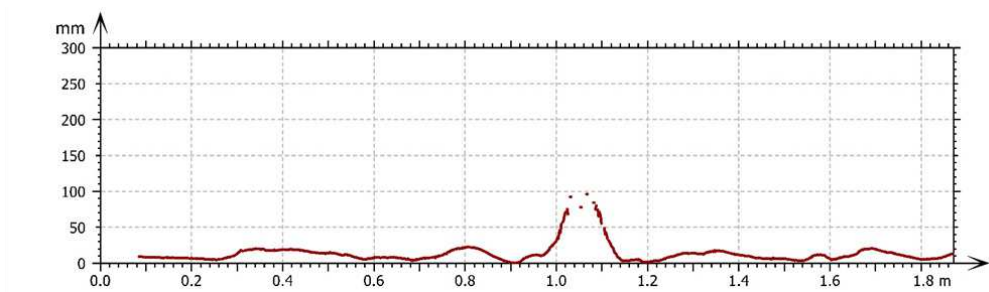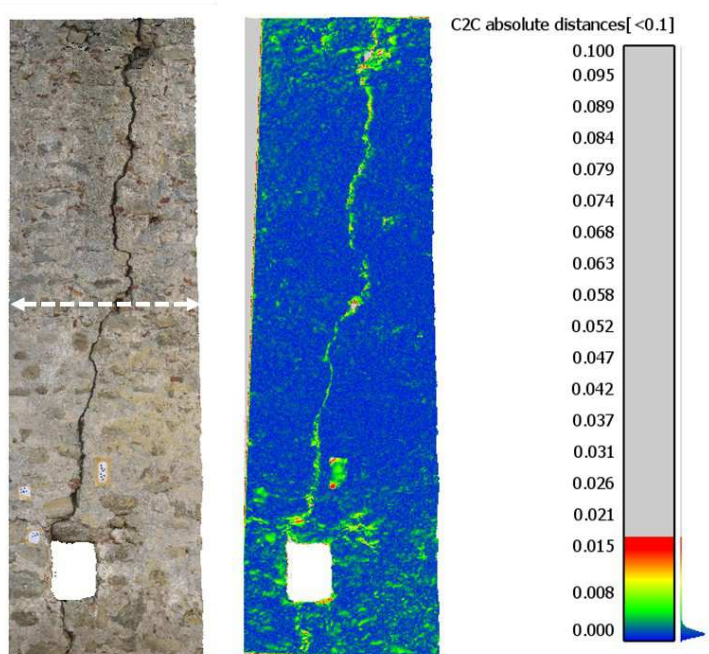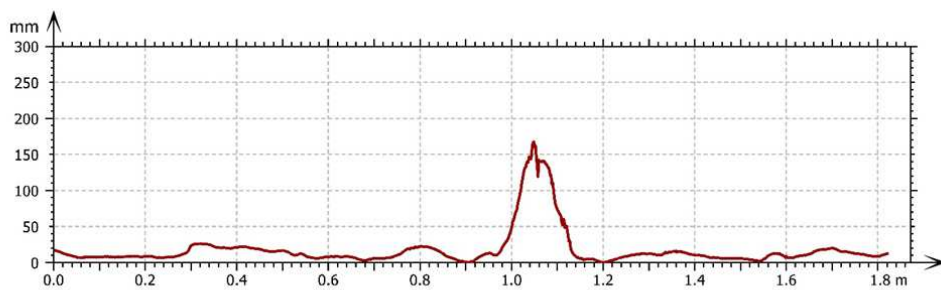
Fig. 95 – Direct comparison and indirect cross sections collation, for the crack area of the north tower. The absolute distances are expressed in metres

9.3. (B) Semi-automatic procedure to control displacements and crack deepening from transversal section quantitative comparison

The last part is dedicated to the validation of the semi-automatic procedure of transversal sections quantitative comparison, for the monitoring of displacements and crack deepening. The procedure illustrated in Section 0, was experimented on the north tower of Bashtovë Fortress, in continuity with the analyses of the previous paragraph.

9.3.1. (B) Bashtovë Fortress – Static instability in the north tower

The north tower was analysed, through the quantitative confrontation of transversal profiles, extracted and overlapped, taken at various heights along the whole object, in order to understand and quantify changes among profiles, corresponding to likely progression of the static instabilities or to displacements occurred, in consequence of the seismic events.

In this case, seven profiles were extracted, at about 1 meter interval, with a profile thickness of 1 cm, and an approximate number of points of 40'000.

They were retrieved from the original cloud, with the help of specific tools in CloudCompare. Also, the pre-processing cleaning step was applied, to remove duplicate points, that, in this case, are points lying under a threshold distance of a tenth of millimetre.

For the sake of simplification, sections have been separated into left and right parts and elaborated independently. Each of the seven profiles (before and after) were interpolated, into a regular grid, with user defined size and pace. The grid pace varied from $n=0.5$-1 cm, for displacement evaluations, and $n=0.01$ cm for crack monitoring. the grid limits for the interpolation are $ymin=-7$, $xmin=2$, respectively, chosen on the basis of the section dimensions. The interpolation followed the Delauny triangulation, for the identification of neighbours. The outcoming analogous profiles were overlapped and their differences quantitatively determined (Fig. 96).

Otherwise, the profiles overlapping is still in the process of development. It requires a wider application and validation of resulting data.
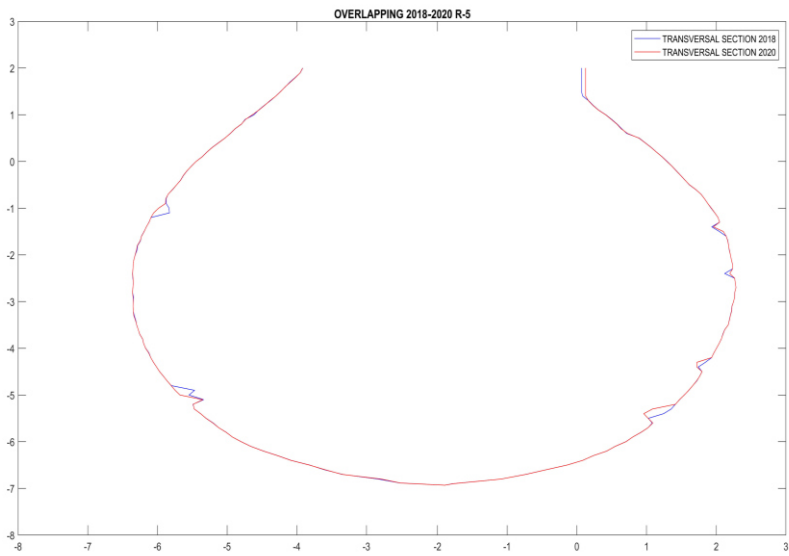
Fig. 96 – Example of transversal profile extraction and comparison

PART 4

DISCUSSIONS

10. RESULTS' DISCUSSION

The research work introduces a methodological approach, to obtain quantitative information about the state of conservation of architectural heritage, with particular attention to the aspects of damage detection, mapping and monitoring. A national and international standard framework was considered for the definition of decay morphologies, including UNI 11182:2006 ([27]) and the International Glossary on Stone Deterioration Patterns([28]). A scalar strategy was outlined, articulated in different paths and levels of details, tailored on 3D point clouds or texturized polygonal meshes, which embodies large amounts of information. They constitute the input data to develop a multiplicity of studies, with the support of image processing or machine learning.

Indeed, low-resolution 3D data (0,5-1 cm/pixel), denoted by rapid acquisition and reconstruction time (eventually exploiting 3D data acquired for diverse purposes) could refer to extensive areas of the buildings, to provide a general idea about the state of conservation, leading to the localization of more detailed investigations. They could provide useful information also in relation to the assessment and monitoring of macroscopically visible alterations, like humidity patterns, features induced by material loss (in the order of magnitude of few centimetres). Medium-resolution models (0.1-0.5 cm/pixel) are useful to analyse crack patterns or mortar joint degradation, with amplitude around few millimetres On the contrary, high or very high-resolution point clouds (0.01-0.1 cm/pixel), characterized by huge time and computational requirements, could be provided for limited areas, with specific criticalities, like small cracks or micro-cracks (Section 4.1.2).

A general criterion emerged from the experimentation, concerning the scale and size of the architectural elements and of the alterations, which have a great influence on the resolution of 3D data, because it should always lie below the smallest defect dimension to detect.

Several forms of alteration can be remotely observed, with non-invasive protocols on 3D data. In light of the heterogeneity of their nature (visual aspect, cause, progression)

they were separated into two macro-areas: geometry-based (Section 5.1) and colour-based alterations (Section 5.2). Likewise, distinct pipelines were delineated.

For geometry-based alterations, image processing algorithms were used, such as noise or form removal algorithm for the dataset preparation; segmentation or binarization, like edge extraction or thresholding, for the detection of crack patters or features induced by material loss (Section 5.1.1).

This procedure, implemented with the help of microscopy analysis software (Mountains Map), has the advantage to be semi-automatic, but it still requires a user interaction in the parameters' settings or in the definition of thresholds.

Watershed segmentation allowed an analysis of segmented grains and successive extraction of geometric descriptors (areas, perimeters, depth, maximum/minimum/medium diameter of a grain, co-planarity, aspect ratio, roundness, compactness, orientation). They were associated to geometry-based alterations, as illustrated in the standard framework, identifying discriminant parameters for each defect. This step, in turn, led to the definition of significant criteria, for decay classification: in this case four criteria were considered (form, depth, uniformity, volume), grouping geometric descriptors. The criteria converged in a unique Damage Index, as a linear combination of the proposed criteria, accomplished by the attribution of different weights of the criteria, for each alteration. In the present work, a proposal for the classification of three alterations (cracks, lacks, cavities) was designed, where weights were formulated on the basis of the experience, the observation of the case studies and the geometrical meaning of parameters.

In light of this, a noticeable contribution of the research is represented by the design of a classification procedure, starting from the selection of meaningful features and potentially discriminant threshold values, among the wide range of information provided by unorganized 3D data, like point clouds. As a consequence, it could represent a starting point for a machine/deep learning system, in order to obtain an automatic classification of defects and a quantification of their entity. Indeed, the research path would take advantage of the implementation of decisional approaches or machine learning systems (like random forest), both to improve the association among

parameters and defects, to expand the number of alterations to classify, and to get more reliable weights (Section 5.1.2).

A third pipeline, within the geometry-based macro-area, is focused on the assessment and quantification of eroded areas on limestone architectural elements. A change detection approach entailed the comparative evaluation of the as-is point cloud and an ideal original model, retrieved from the photogrammetric data. This was applied to architectural elements extensively affected by erosion due to marine aerosol, like columns or vaults. Deviation maps highlighted the differences among correspondent models, allowing to identify and isolate eroded areas. As a result, it was possible to localize and quantify the extension of the phenomenon, in support of the experts, for the comprehension and diagnosis of pathologies, with a simple, non-invasive and reversive technique. A further development could concern an in depth-analysis, to pinpoint and integrate a proper technique for the automatic ideal 3D model retrieval from the photogrammetric point cloud data (Section 5.2.3).

In colour-based alterations domain, two main alternatives were proposed, for an automatic point cloud segmentation, with decay detection and mapping purposes. In the first case, only two main kinds of alterations were searched: biological patina and colonization, appearing in restricted colour ranges. The routines firstly addressed the identification of reference colour ranges, on the basis of which, a filtering procedure consented to accurately isolate these two kinds of defect and to compute their extension with an automatic pipeline (Section 9.2.1). Also in this case, the introduction of machine or deep learning, could enhance the identification of significative colour-ranges and thus the results of automatic segmentation, with a wider dataset for the training.

On account of this, a progress was represented by the application of an unsupervised machine learning method, the hierarchical clustering, to achieve the automatic segmentation of point clouds, segmenting and detecting adjunctive decay morphologies, like moist areas, spots or deposit,... After a comparative evaluation of multiple colour spaces, HSV proved to be the most effective, with respected to manually segmented clusters (ground truth) corresponding to the above-mentioned pathologies.

In fact, other tested colour spaces produced inaccurate segmentation results, both in terms of extension and colour interval. On the one hand, they include multiple non consistent parts in a single cluster and on the other hand, they exclude significative colours from a single range. This outcome is related to the balance between luminance and chrominance components, typical of HSV, in contrast with YCbCr, YIQ or YUV. The great advantage of this second workflow lies in the possibility to simultaneously detect several chromatic damage evidence, providing their quantification and their three-dimensional distribution on complex or irregular surfaces, like barrel or cross-vaults of the ex-convents, without the need to flatten the analysed surface. The validation was accomplished by the application to four heterogeneous case studies, of which only two are presented in this research work.

A further confirmation is offered by the juxtaposition of the unsupervised point cloud segmentation to a supervised texture-based segmentation. Both the procedures were tested against a ground truth dataset, and performance ratings demonstrated that the unsupervised cloud-based approach provides more accurate results, in terms of decay assessment and quantification (Section 9.2.2).

A little drawback in the colour segmentation could be represented by the laborious distinction of colour alterations on decorated surfaces (frescoes, temperas or wall papers). Further studies involve an extensive application of these routines on complex decorative apparatuses. The ongoing research, foremost, aims at applying these procedures to control colour-based alterations over time, after a congruous period, in order to observe eventual modifications.

Supplementary information about the architectural meaning of the analysed surfaces, were achieved through a geometric segmentation, in order to complete the decay assessment, associating the detected damage patterns to the architectural elements on which they are located.

In the contest of decay control and monitoring, the experimentation provides a vision of the great potentialities of reality-based 3D data, to understand the damage progression overtime. This is accomplished not only by the comparison of geometric characteristics (amplitude, depth, area), but, above all, through a direct comparison of

3D data and profiles overlapping, for a change detection and computation of divergences.

For example, the deviation among point clouds acquired within a time interval of eighteen or twenty-four months showed a progression of decay phenomena connected to static instabilities (cracks), in the right pillar of the internal courtyard (Palmieri Palace) and rising dampness (lacks, cavities, erosion), in the external ashlar masonry. Or the structural deficiency of the north tower (Bashtove Fortress), for which a comparison was made, before and after a seismic event (Section 9.2).

In the end, the convenience of the whole process is represented by the possibility to achieve both qualitative and quantitative insights on different decay morphologies, starting from reality-based 3D data, with remote, non-invasive, semi-automatic procedures, in support of diagnostic activities.

Indeed, the present contribution propose an articulated methodological workflow, to obtain and collect investigation data for the pre-diagnosis phase, within the process of assessment and control of the state of conservation. Furthermore, flexibility and scalability are paramount conditions, to address the peculiarity of the diagnostic process, in relation to the complexity of architectural heritages.

CONCLUSIONS AND FUTURE REMARKS

The research work expounded in the current thesis was focused on the exploration and experimentation of innovative apparatuses, to control the state of conservation of an architectural heritage, in the field of restoration and refurbishment of built heritages with historic and cultural values.

The idea started from the consideration of the great possibilities offered by the acquisition of three-dimensional reality-based data, within the cognitive and diagnostic process, outlining a plurality of workflows for the detection, mapping and monitoring of damages, to augment the level of knowledge of the artefact.

The research method entailed the realization of a gradually increasing level of investigation, translated in an incremental methodological approach, which starts from the aspects related to the collection of data, with reverse engineering, and leads to the exploitation of digital image processing and artificial intelligence algorithms, for diagnosis monitoring and conservation purposes.

In first place, an insight on the utilization of digital photogrammetry in the field of architectural heritage, with diagnostic and monitoring purposes, is provided. It is a widespread technique connoted by a great variability of procedures, whose results are influenced by a plurality of parameters (size and kind of object, accessibility, environmental conditions,…). In this light, the decision of the investigation purposes is a paramount preliminary step. In fact, diagnostic procedures, like the ones illustrated in this Ph. D. thesis, requires a high level of detail and high resolution of data (Section 4). Indeed, the proposed strategy is developed around three diagnostic macro-areas, coinciding with as many analytical patterns. An initial discrimination was made on the nature of decay morphologies and their descriptive features, thanks to national and international standards: geometry-based alterations (crack patterns, features induced by material loss,…) on the one hand; colour-based alterations (humidity patterns, chromatic alterations in a broad sense,…) on the other hand. This distinction is related to the screening and detection of surface decay. The third domain concerns monitoring and control, associated to the time advancement.

Starting from a common ground of high-resolution 3D data, in form of coloured point clouds and texturized polygonal meshes, digital image processing pipelines were defined, to assess, isolate and quantify geometry-based alterations (cracks, erosion, cavities,…), exploiting geometric attributes enclosed in the input data (surface descriptors). Algorithms, like edge extraction, thresholding, binarization, were used to segment surfaces, whose main parameters were operated to recognize the different kinds of alterations, and to quantitatively describe them, in relation to the investigated architectural elements (Section 5.1).

Machine learning approaches acquiesced to extract and exploit colour-information enclosed in point clouds, to automatically segment input data into clusters representing colour-based alterations (biological colonization, patina, spots, deposit, chromatic alterations, moist areas,…) (Section 5.2).

Monitoring was achieved thanks to change detection approaches, aimed to find out all the eventual modifications occurred in the artifact, by comparing 3D data acquired in definite points in time. In first place indirect confrontations were considered, as a collation of outcomes of the same procedures applied to corresponding 3D data of the same element. Secondly and more effectively, direct matching of 3D data was made, with the help of 3D models deviation and profiles' analysis (Section 6).

A brief parenthesis was dedicated to the aspect of geometry-based segmentation, for the recognition of architectural elements, relying on best fitting segmentation algorithms (RANSAC). However, this last issue has not been exhaustively investigated, because it is already at the centre of numerous international research projects.

The methodological apparatus was applied to 3D data of architectural elements belonging to a selection of cultural heritages as archaeological sites, ex-convents or noble residential buildings (section 7). They are characterized by a great heterogeneity and thus they were suitable to test and validate the proposed pipelines. Samples of ashlar masonry or local tuff, retrieved from the main façade of Palmieri Palace, subjected to rising dampness phenomena visible as erosion or lacks; or calcarenitic pillars subjected to static instabilities, were treated with image processing routines. Some of them were monitored over time, in order to evaluate the evolution of the

assessed pathologies. The north tower of Bashtove fortress, with its structural deficiency was also monitored, after two considerable seismic events. For the colour-based alterations, different kinds of surfaces were analysed, varying from interiors like underground barrel-vaulted volumes of Egnazia Cryptoporticus, to plastered environments of the ex-convents of Cappuccini and San Leonardo. They presented a wide selection of decay morphologies related essentially to humidity.

In the last analysis, the pipelines defined in this research work proved to be suitable for a plurality of diagnostic purposes, providing a scalable approach. According to the macro-category or specific kind of defect, a level of detail and an operative procedure can be followed.

In summary, some main advantages are represented by:

- Possibility to perform remote, contactless diagnostic investigations
- Complete non-invasiveness, with respect to cultural heritages
- Availability of cost-effective equipment for a simplification of the diagnostic plan
- Plurality of strategies to adopt, case by case, starting from the same input data
- Objective examination and quantification of alterations, in support of technicians for inspection and clinical auditing
- Semi-automatic pipelines for a better and faster damage detection as an alternative to manual and time-consuming traditional decay mapping procedures

These benefits are increased by the consideration that, by virtue of the scalability of the approach, even 3D data acquired for other purposes (geometrical survey, cultural dissemination,..) can be exploited for diagnostic/monitoring purposes. Moreover, the analysis developed are applicable, regardless of the 3D scanning method.

As future remarks, important developments could entail the strengthening of experimental aspects, by widening the case studies selection, for type, morphology, epoque. A further consideration could concern the extension and adaptation of the proposed methodologies to the built heritage, without historic artistic values, but certainly more widespread.

In addition, an augmentation of the level of automation and the simplification of strategies could lead to inclusive digital platforms, where different sources of diagnostic

data could flow into, allowing direct collation and confrontation of data. Further studies could be focused to minimize the user interaction in diagnostic procedure.

Another issue could entail the implementation of artificial intelligence also in geometry-based pipelines, such as random forest for the automatic classification of decay on point clouds, starting from geometric features. These could be integrated by the use of deep learning systems for the automatic recognition of both colour-based and texture-based damages, on high-resolution texturized 3D data.

ACKNOWLEDGEMENTS

In first place, I would like to thank my supervisor Prof. Eng. Fabio Fatiguso, for the great opportunity and confidence in me, and the precious advice, for carrying out such a challenging project, in a stimulating and comfortable environment, allowing me to learn and to grow very much.

The present Ph. D. thesis, especially for the aspect of the campaign acquisition of case studies, was realized thanks to a plurality of projects coordinated by Prof. Eng. Fabio Fatiguso, to which the Ph. D. candidate took part. They are:

- MIUR Start-up project: PAC02L2_00101 "Contactless diagnosis system of artefacts of significant cultural interest and difficult accessibility with augmented reality"
- "3D-IMP-ACT Virtual reality and 3D experiences to IMProve territorial Attractiveness, Cultural heritage smart management and Touristic development", Programma Interreg IPA CBC Italy Albania Montenegro No. 314/1st call for standard projects.

With respect to 3D-IMP-ACT project, a particular acknowledgement is directed to Prof. Erald Piperi of the Polytechnic University of Tirana (Albania), who contributed to the post disaster acquisitions of the Fortress of Bashtovë, in the middle of the pandemic period (2020).

In relation to the experimental campaigns, it is important to mention two spin-offs of the Polytechnic University of Bari, BReD srl (Building Refurbishment and Diagnostic), and Polishape 3D srl (L'innovazione nei sistemi di scansione), which provided the technical equipment to realize on-site acquisitions.

Special gratitude is directed also to the people, who contributed actively to develop part of the experimentation.

First of all, Prof. Eng. Mariella De Fino, who involved the me in several interesting research project and scientific publications; Ph. D. Silvana Bruno and Ph. D candidate Antonella Musicco, with whom I collaborated in plural shared research activities, resulting in valuable common papers; Ph. D. Maria Grazia Guerra and Ph. D candidate Stefano Marino, who contributed in the developments of specific parts of the research, carrying their different background; Prof. Eng. Fulvio Lavecchia, Rocco Rubino, who

helped me in the realization of part of the acquisition campaigns, within MIUR Start-up and 3D-IMP-ACT projects.

REFERENCES

[1]   UNITED NATIONS EDUCATIONAL - SCIENTIFIC AND CULTURAL ORGANISATION, CONVENTION CONCERNING THE PROTECTION OF THE WORLD CULTURAL AND NATURAL HERITAGE, (1972).

[2]   CIB W086, CIB Publication 393. Building Pathology. A State-of-the-Art Report, 2013.

[3]   National Research Council, Building Diagnostics: A Conceptual Framework, in: The National Academies Press, Washington. DC, 1985: pp. 1–46. doi:10.17226/19294.

[4]   R.A. Galantucci, F. Fatiguso, Advanced damage detection techniques in historical buildings using digital photogrammetry and 3D surface analysis, Journal of Cultural Heritage. (2018). doi:10.1016/j.culher.2018.09.014.

[5]   M. De Fino, F. Fatiguso, IL PATRIMONIO COSTRUITO STORICO - METODI NON DISTRUTTIVI E TECNOLOGIE INNOVATIVE PER LA VALUTAZIONE E IL CONTROLLO, architettu, EdicomEdizioni, 2020.

[6]   J. Armesto, P. Arias, J. Roca, H. Lorenzo, Monitoring and assessing structural damamge in historical buildings, The Photogrammetric Record. 23 (2008) 36–50.

[7]   Y. Alshawabkeh, M. El-Khalili, Detection and quantification of material displacements at historical structures using photogrammetry and laser scanning techniques, Mediterranean Archaeology and Archaeometry. 13 (2013) 57–67.

[8]   N. Hallermann, G. Morgenthal, V. Rodehorst, Vision-based monitoring of heritage monuments – Unmanned Aerial Systems (UAS) for detailed inspection and high-accurate survey of structures, WIT Transactions on The Built Environment. 153 (2015) 621–632. doi:10.2495/STR150521.

[9]   S. Nishiyama, N. Minakata, T. Kikuchi, T. Yano, Improved digital photogrammetry technique for crack monitoring, Advanced Engineering Informatics. 29 (2015). doi:10.1016/j.aei.2015.05.005.

[10]   T. Segreto, A. Bottillo, R. Teti, L.M. Galantucci, F. Lavecchia, M.B. Galantucci, Non-contact Reverse Engineering Modeling for Additive Manufacturing of Down Scaled Cultural Artefacts, Procedia CIRP. 62 (2017) 481–486. doi:10.1016/j.procir.2017.03.042.

[11]   R. Scopigno, M. Callieri, P. Cignoni, M. Corsini, M. Dellepiane, F. Ponchio, G. Ranzuglia, 3D models for cultural heritage: Beyond plain visualization, Computer. 44 (2011) 48–55. doi:10.1109/MC.2011.196.

[12]   F. Remondino, Heritage recording and 3D modeling with photogrammetry and 3D scanning, Remote Sensing. 3 (2011) 1104–1138. doi:10.3390/rs3061104.

[13] F. Remondino, S. El-Hakim, Image-Based 3D Modelling : a Review, The Photogrammetric Record. 21 (2006) 269–291. http://www.cs.columbia.edu/~allen/PHOTOPAPERS/remondino_elhakim_phor ec06.pdf.

[14] P. Grussenmeyer, E. Alby, T. Landes, M. Koehl, S. Guillemin, J.F. Hullo, P. Assali, E. Smigiel, Recording approach of heritage sites based on merging point clouds from high resolution photogrammetry and Terrestrial Laser Scanning, International Archives of the Photogrammetry, Remote Sensing and Spatial Information Sciences - ISPRS Archives. 39 (2012) 553–558. doi:10.5194/isprsarchives-XXXIX-B5-553-2012.

[15] M. De Fino, R.A. Galantucci, F. Fatiguso, Mapping and monitoring building decay patterns by photomodelling based 3D models, TEMA Technologies Engineering Materials Architecture. 5 (2019) 27–35. doi:10.17410/tema.v5i1.212.

[16] R.A. Galantucci, F. Fatiguso, L.M. Galantucci, A proposal for a new standard quantification of damages of cultural heritages, based on 3D scanning, SCIRES-IT - SCIentific RESearch and Information Technology. 8 (2018) 121–138. doi:10.2423/I22394303V8N1P121.

[17] M. De Fino, R.A. Galantucci, F. Fatiguso, REMOTE DIAGNOSIS AND CONTROL OF HERITAGE ARCHITECTURE BY PHOTOREALISTIC DIGITAL ENVIRONMENTS AND MODELS, SCIRES-IT - SCIentific RESearch and Information Technology. 9 (2019) 1–16. doi:10.2423/i22394303v9n2p1.

[18] M. De Fino, A. Scioti, R. Rubino, A. Pierucci, F. Fatiguso, 'Augmented Diagnostics' for the Architectural Heritage, International Journal of Heritage Architecture. 2 (2018) 248–260. doi:10.2495/HA-V2-N2-248-260.

[19] Ministero della Pubblica Istruzione, Carta di Venezia, 1964, (1964) 1–3.

[20] Ministero della Pubblica Istruzione, Carta Italiana del Restauro, 1972 - Circolare n° 117 del 06/04/1972, (1972) 1–14.

[21] Council of Europe, European Charter of the Architectural Heritage, (1975) 1–4.

[22] ICOMOS, Carta ICOMOS per l' interpretazione e la presentazione dei siti patrimonio culturale detta Carta di Ename, (2008) 1–6.

[23] EN15898, Conservation of cultural properties. Main general terms and definitions, (2012).

[24] EN16096, Conservation of cultural properties - Condition survey and report of built cultural heritage, (2012).

[25] EN16853, Conservation of cultural heritage - Conservation process - Decision making, planning and implementation, (2017).

[26] ICR Instituto Centrale per il Restauro CNR, Raccomandazioni Normal - 1/88 - Alterazioni macroscopiche del materiali lapidei: lessico, 1988.

[27]   UNI, UNI 11182 Beni culturali - Materiali lapidei naturali e artificiali - Descrizione della forma di alterazione - Termini e definizioni, (2006).

[28]   I.X. International Scientific Committee for Stones, International ICOMOS glossary - Illustrated glossary on stone deterioration patterns, ICOMOS ISC, 2010. www.icomos.org/publications/monuments_and_sites/15/index.htm.

[29]   M.G. Guerra, R.A. Galantucci, Standard quantification and measurement of damages through features characterization of surface imperfections on 3D models: An application on architectural heritages, Procedia CIRP. 88 (2020) 515–520. doi:10.1016/j.procir.2020.05.089.

[30]   UNI 1347301:2002, Caratterizzazione della tessitura delle pavimentazioni mediante analisi dei profili, (2002).

[31]   UNI1347305:2010, Caratterizzazione della tessitura delle pavimentazioni mediante analisi dei profili, (2010).

[32]   UNI, UNI EN ISO 8785 Imperfezioni delle superfici - Termini, definizioni, parametri, (2001) 1–16.

[33]   UNI1391902:2005, Saldatura - Giunti saldati a fascio elettronico e laser - Guida dei livelli di qualità delle imperfezioni, (2005).

[34]   UNI652002:2013, Saldatura e procedimenti connessi - Classificazione delle imperfezioni geometriche nei materiali metallici, (2013).

[35]   Ministero per i Beni e le Attività Culturali, D.P.C.M. 23 febbraio 2006 (G.U. 7.3.2006, n. 55), (2006). doi:10.7390/9324.

[36]   Ministero per i Beni e le Attività Culturali - Gruppo di lavoro per la salvaguardia e la prevenzione dei Beni Culturali dai rischi naturali, SCHEDA PER IL RILIEVO DEL DANNO AI BENI CULTURALI – CHIESE A1, (2006) 1–10.

[37]   S. Papa, G. Di Pasquale, Manuale per la compilazione della scheda per il rilievo del danno ai beni culturali, Chiese, (2011) 1–149.

[38]   Ministero per i Beni e le Attività Culturali, G.U. 22.6.2017 n° 143 - Allegato 1, (2017) 1–14.

[39]   Ministero delle Infrastrutture e deiTrasporti, CIRCOLARE 2 febbraio 2009 , n. 617, (2009) 1–447.

[40]   A. Borri, A. De Maria, Indice di Qualità Muraria (IQM): correlazione con le caratteristiche meccaniche e livelli di conoscenza, 2015. doi:10.7414/PS.6.3.45-63.

[41]   A. Borri, A. De Maria, Allegato 1 - LINEE GUIDA PER LA COMPILAZIONE DELLA SCHEDA IQM, 2015.

[42]   A. Borri, A. De Maria, ESEMPI DI SCHEDE PER LA VALUTAZIONE DELL ' IQM, 2015.

[43]   J.A. Fidler, M. Tallini, G. Croci, C. Borelli, S.-K. Kim, Other tools for investigation

and monitoring, (2011) 105–131.

[44] E. Quagliarini, G.M. Revel, S. Lenci, E. Seri, A. Cavuto, G. Pandarese, Historical plasters on light thin vaults: State of conservation assessment by a Hybrid ultrasonic method, Journal of Cultural Heritage. 15 (2014) 104–111. doi:10.1016/j.culher.2013.04.008.

[45] M. Martarelli, P. Castellini, E. Quagliarini, E. Seri, S. Lenci, E.P. Tomasini, Nondestructive evaluation of plasters on historical thin vaults by scanning laser doppler vibrometers, Research in Nondestructive Evaluation. 25 (2014) 218–234. doi:10.1080/09349847.2014.896964.

[46] K.G. Akoglu, E. Kotoula, S. Simon, Combined use of ultrasonic pulse velocity (UPV) testing and digital technologies: A model for long-term condition monitoring memorials in historic Grove Street Cemetery, New Haven, Journal of Cultural Heritage. (2019). doi:10.1016/j.culher.2019.07.015.

[47] P. Agrafiotis, K. Lampropoulos, A. Georgopoulos, A. Moropoulou, 3D modelling the invisible using ground penetrating radar, in: International Archives of the Photogrammetry, Remote Sensing and Spatial Information Sciences - ISPRS Archives, 2017: pp. 33–37. doi:10.5194/isprs-archives-XLII-2-W3-33-2017.

[48] M. De Vita, G. Massari, P. De Berardinis, L.P. Iglesias, MORE COMPREHENSION , MORE PROTECTION: NON - DESTRUCTIVE TECHNIQUES IN THE SURVEY OF THE FORMER S.SALVATORE HOSPITAL IN L'AQUILA, ITALY, SCIRES-IT - SCIentific RESearch and Information Technology. 9 (2019) 85–94. doi:10.2423/i22394303v9n2p85.

[49] Y.K. Cho, Y. Ham, M. Golpavar-Fard, 3D as-is building energy modeling and diagnostics: A review of the state-of-the-art, Advanced Engineering Informatics. 29 (2015) 184–195. doi:10.1016/j.aei.2015.03.004.

[50] D. Lin, M. Jarzabek-rychard, X. Tong, H. Maas, Fusion of thermal imagery with point clouds for building façade thermal attribute mapping, ISPRS Journal of Photogrammetry and Remote Sensing. 151 (2019) 162–175. doi:10.1016/j.isprsjprs.2019.03.010.

[51] A. Monterroso-Checa, M. Gasparini, Aerial Archaeology and Photogrammetric Surveys Along the Roman Way From Corduba To Emerita. Digitalizing the Ager Cordubensis and the Ager Mellariensis, SCIRES-IT - SCIentific RESearch and Information Technology. 6 (2016) 175–188. doi:10.2423/i22394303v6n2p175.

[52] D. Borrmann, J. Elseberg, A. Nüchter, Thermal 3D mapping of building façades, Advances in Intelligent Systems and Computing. 193 AISC (2013) 173–182. doi:10.1007/978-3-642-33926-4_16.

[53] D. Lin, M. Jarzabek-Rychard, D. Schneider, H.G. Maas, Thermal texture

selection and correction for building facade inspection based on thermal radiant characteristics, International Archives of the Photogrammetry, Remote Sensing and Spatial Information Sciences - ISPRS Archives. 42 (2018) 585–591. doi:10.5194/isprs-archives-XLII-2-585-2018.

[54]   D. Antón, J.L. Amaro-Mellado, Engineering graphics for thermal assessment: 3D thermal data visualisation based on infrared thermography, GIS and 3D point cloud processing software, Symmetry. 13 (2021) 1–20. doi:10.3390/sym13020335.

[55]   J. Sánchez, E. Quirós, Semiautomatic detection and classification of materials in historic buildings with low-cost photogrammetric equipment, Journal of Cultural Heritage. 25 (2017) 21–30. doi:10.1016/j.culher.2016.11.017.

[56]   C.S. Chane, A. Mansouri, F.S. Marzani, F. Boochs, Integration of 3D and multispectral data for cultural heritage applications: Survey and perspectives, Image and Vision Computing. 31 (2013) 91–102. doi:10.1016/j.imavis.2012.10.006.

[57]   F.L. Melquiades, C.R. Appoloni, A.C. Andrello, E. Spagnuolo, Non-destructive analytical techniques for the evaluation of cleaning and protection processes on white marble surfaces, Journal of Cultural Heritage. (2018). doi:10.1016/j.culher.2018.10.013.

[58]   P. Wang, H. Qiao, Y. Li, Q. Feng, K. Chen, Analysis of steel corrosion-induced surface damage evolution of magnesium oxychloride cement concrete through gray-level co-occurrence matrices, Structural Concrete. 21 (2020) 1905–1918. doi:10.1002/suco.202000182.

[59]   L. Zhu, F. Dang, Y. Xue, W. Ding, L. Zhang, Analysis of micro-structural damage evolution of concrete through coupled X-ray computed tomography and gray-level co-occurrence matrices method, Construction and Building Materials. 224 (2019) 534–550. doi:10.1016/j.conbuildmat.2019.07.007.

[60]   E. Diz-Mellado, E.J. Mascort-Albea, R. Romero-Hernández, C. Galán-Marín, C. Rivera-Gómez, J. Ruiz-Jaramillo, A. Jaramillo-Morilla, Non-destructive testing and Finite Element Method integrated procedure for heritage diagnosis: The Seville Cathedral case study, Journal of Building Engineering. 37 (2021). doi:10.1016/j.jobe.2020.102134.

[61]   V. Kumar, R. Singh, I.P.S. Ahuja, M.S.J. Hashmi, On technological solutions for repair and rehabilitation of heritage sites: a review, Advances in Materials and Processing Technologies. 6 (2020) 146–166. doi:10.1080/2374068X.2019.1709310.

[62]   A. Gallozzi, L.J. Senatore, R.M. Strollo, AN OVERVIEW ON ROBOTIC APPLICATIONS FOR CULTURAL HERITAGE AND BUILT CULTURAL HERITAGE,

SCIRES-IT - SCIentific RESearch and Information Technology. 9 (2019) 47–56. doi:10.2423/i22394303v9n2p47.

[63]   L. De Luca, C. Busayarat, C. Stefani, P. Veron, M. Florenzano, NUBES: describing, analysing, documenting and sharing digital representations of heritage buildings, in: Conference on Se- Mantic 3D Media and Content, Feb 2010, Sophia Antipolis, France. INRIA, Semantic 3D Media and Content Conference Proceedings, 2017: pp. 1–4.

[64]   T. Messaoudi, P. Véron, G. Halin, L. De Luca, An ontological model for the reality-based 3D annotation of heritage building conservation state, Journal of Cultural Heritage. 29 (2018). doi:10.1016/j.culher.2017.05.017.

[65]   A. Mandelli, C. Achille, C. Tommasi, F. Fassi, Integration of 3D models and diagnostic analyses through a conservation-oriented information system, in: International Archives of the Photogrammetry, Remote Sensing and Spatial Information Sciences - ISPRS Archives, 2017: pp. 497–504. doi:10.5194/isprs-archives-XLII-2-W5-497-2017.

[66]   L. Trigilia, R. Valenti, S. Gatto, E. Paternò, N. Mariniello, A project for the exploration of cultural heritage in a European area of excellence: The Baroque Circuit of Val di Noto., SCIRES-IT - SCIentific RESearch and Information Technology. 7 (2018) 85–102. doi:10.2423/I22394303V7N2P85.

[67]   A. Pamart, F. Ponchio, V. Abergel, A. Alaoui M'Darhri, M. Corsini, M. Dellepiane, F. Morlet, R. Scopigno, L. De Luca, A COMPLETE FRAMEWORK OPERATING SPATIALLY-ORIENTED RTI in A 3D/2D CULTURAL HERITAGE DOCUMENTATION and ANALYSIS TOOL, ISPRS Annals of the Photogrammetry, Remote Sensing and Spatial Information Sciences. 42 (2019) 573–580. doi:10.5194/isprs-archives-XLII-2-W9-573-2019.

[68]   R. Cacciotti, J. Valach, P. Kuneš, M. Čerňanský, M. Blaško, P. Křemen, Monument damage information system (mondis): An ontological approach to cultural heritage documentation, in: ISPRS Annals of the Photogrammetry, Remote Sensing and Spatial Information Sciences, 2013: pp. 61–66. doi:10.5194/isprsannals-II-5-W1-55-2013.

[69]   P. Kremen, M. Blasko, M. Smıd, Z. Kouba, M. Ledvinka, B. Kostov, MONDIS: Using Ontologies for Monument Damage Descriptions, Art Nouveau Training Materials. (2014) 1–4.

[70]   C. Stefani, X. Brunetaud, S. Janvier-Badosa, K. Beck, L. De Luca, M. Al-Mukhtar, Developing a toolkit for mapping and displaying stone alteration on a web-based documentation platform, Journal of Cultural Heritage. 15 (2014) 1–9. doi:10.1016/j.culher.2013.01.011.

[71]   V. Croce, G. Caroti, A. Piemonte, Propagation of semantic information between

orthophoto and 3D replica: a H-BIM system for the north transept of Pisa Cathedral, Geomatics, Natural Hazards and Risk. 12 (2021) 2225–2252. doi:10.1080/19475705.2021.1960432.

[72]   J. Pereda, R. Vela, A. Lorenzana, I. Lombillo, H. Blanco, L. Villegas, Design and application of an integrated platform of electronic instrumentation, data acquisition and client/server software for remote structural health monitoring of heritage buildings, in: 2014: pp. 577–588.

[73]   I. Lombillo, H. Blanco, J. Pereda, L. Villegas, C. Carrasco, J. Balbás, Structural health monitoring of a damaged church: design of an integrated platform of electronic instrumentation, data acquisition and client/server software, Structural Control and Health Monitoring. 23 (2016) 69–81. doi:DOI: 10.1002/stc.1759.

[74]   A.A. Salah, C. Wiskunde, E. Pauwels, P. De Zeeuw, Multimodal monitoring of cultural heritage sites and the FIRESENSE project, (2011).

[75]   V. Sangiorgio, S. Martiradonna, G. Uva, F. Fatiguso, An Information System for Masonry Building Monitoring, in: 2017 IEEE International Conference on Service Operations and Logistics, and Informatics, 2017: pp. 230–235.

[76]   R. Nespeca, Towards a 3D digital model for management and fruition of Ducal Palace at Urbino. An integrated survey with mobile mapping, SCIRES-IT - SCIentific RESearch and Information Technology. 8 (2018) 1–14. doi:10.2423/i22394303v8n2p1.

[77]   R. Napolitano, Virtual tours and informational modeling for conservation of cultural heritage sites Dear author , Please note that changes made in the online proofing system will be added to the article before publication but are not reflected in this PDF . We also ask , (2018). doi:10.1016/j.culher.2017.08.007.

[78]   I. Trizio, F. Savini, A. Ruggieri, G. Fabbrocino, Digital Environment for Remote Visual Inspection and Condition Assessment of Architectural Heritage, in: Civil Structural Health Monitoring, 2021: pp. 869–886. doi:10.1007/978-3-030-74258-4_55.

[79]   V. Valzano, F. Negro, R. Foschi, The Gallery of the Castromediano's Castle. Three-dimensional reconstruction and virtual representation, SCIRES-IT - SCIentific RESearch and Information Technology. 7 (2018) 13–26. doi:10.2423/I22394303V7N2P13.

[80]   M.K. Bekele, C. Town, R. Pierdicca, E. Frontoni, E.V.A.S. Malinverni, A Survey of Augmented, Virtual, and Mixed Reality, ACM Journal on Computing and Cultural Heritage. 11 (2018) 1–36.

[81]   E. Cantatore, M. Lasorella, F. Fatiguso, Virtual reality to support technical knowledge in cultural heritage. The case study of cryptoporticus in the

archaeological site of egnatia (Italy), International Archives of the Photogrammetry, Remote Sensing and Spatial Information Sciences - ISPRS Archives. 54 (2020) 465–472. doi:10.5194/isprs-archives-XLIV-M-1-2020-465-2020.

[82] F. Fatiguso, E. Cantatore, T. Di Noia, A. Scioti, S. Bruno, A. Pierucci, AMBIENTI DIGITALI PER LA GESTIONE DEL PROCESSO DI RECUPERO DEL PATRIMONIO CULTURALE . IL PROGETTO VERBUM (VIRTUAL ENHANCED REALITY FOR BUILDING MODELLING), in: I Convegno BENI CULTURALI IN PUGLIA DIALOGHI MULTIDISCIPLINARI PER LA RICERCA, LA TUTELA E LA VALORIZZAZIONE, 2021.

[83] R. Napolitano, Z. Liu, C. Sun, B. Glisic, Combination of image-based documentation and augmented reality for structural health monitoring and building pathology, Frontiers in Built Environment. 5 (2019). doi:10.3389/fbuil.2019.00050.

[84] J. Barreau, R. Gaugne, V. Gouranton, Immersive Point Cloud Manipulation for Cultural Heritage Documentation, ERCIM News. ERCIM 2017 (2017) 1–3.

[85] C. Dore, M. Murphy, Integration of HBIM and 3D GIS for Digital Heritage Modelling Integration of HBIM and 3D GIS for Digital Heritage Modelling, in: School of Surveying and Construction Management, Edinburgh, Scotland, 2012.

[86] E.S. Malinverni, A. Giuliano, F. Mariano, 3D information management system for the conservation of an old deserted military site, in: 2018: pp. 183–187.

[87] T. Templin, G. Brzezinski, M. Rawa, Visualization of Spatio-Temporal Building Changes Using 3D Web GIS, IOP Conference Series: Earth and Environmental Science. 221 (2019). doi:10.1088/1755-1315/221/1/012084.

[88] F. Soler, F.J. Melero, M.V. Luzón, A complete 3D information system for cultural heritage documentation, Journal of Cultural Heritage. 23 (2017) 49–57. doi:10.1016/j.culher.2016.09.008.

[89] D.M. Campanaro, G. Landeschi, N. Dell'Unto, A.M. Leander Touati, 3D GIS for cultural heritage restoration: A "white box" workflow, Journal of Cultural Heritage. 18 (2016) 321–332. doi:10.1016/j.culher.2015.09.006.

[90] E.S. Malinverni, R. Pierdicca, A. Giuliano, F. Mariano, A geographycal information system to support restoration activities: a methodological approach experienced upon the case study of Ascoli Satriano Fortress, Applied Geomatics. 10 (2018) 427–439. doi:10.1007/s12518-018-0216-4.

[91] G. Accardo, E. Giani, A. Giovagnoli, The Risk Map of Italian Cultural Heritage The Risk Map of Italian, (2014) 37–41. doi:10.1080/13556207.2003.10785342.

[92] E. Discamps, X. Muth, B. Gravina, F. Lacrampe-Cuyaubère, J.P. Chadelle, J.P. Faivre, B. Maureille, Photogrammetry as a tool for integrating archival data in

archaeological fieldwork: Examples from the Middle Palaeolithic sites of Combe-Grenal, Le Moustier, and Regourdou, Journal of Archaeological Science: Reports. 8 (2016) 268–276. doi:10.1016/j.jasrep.2016.06.004.

[93]   P. Clini, M. El Mehtedi, R. Nespeca, L. Ruggeri, E. Raffaelli, A digital reconstruction procedure from laser scanner survey to 3d printing: the theoretical model of the Arch of Trajan (Ancona), SCIRES-IT - SCIentific RESearch and Information Technology. 7 (2018) 1–12. doi:10.2423/I22394303V7N2P1.

[94]   Polishape 3D srl; Politecnico di Bari; Building Refurbishment and Diagnostics srl; Università degli studi di Napoli Federico II, Progetto PAC02L2_00101 "Sistema senza contatto per la diagnostica con realtà aumentata di manufatti di rilevante interesse culturale e di difficile accessibilità" (documento di lavoro), Bari - Napoli, 2013.

[95]   M. Attenni, C. Bartolomei, M. Hess, A. Ippolito, Survey and modeling: from the process to a methodology, SCIRES-IT - SCIentific RESearch and Information Technology. 7 (2017) 57–72. doi:10.2423/I22394303V7N1P57.

[96]   P. Sestras, S. Roşca, Ştefan Bilaşco, S. Naş, S.M. Buru, L. Kovacs, V. Spalević, A.F. Sestras, Feasibility assessments using unmanned aerial vehicle technology in heritage buildings: Rehabilitation-restoration, spatial analysis and tourism potential analysis, Sensors (Switzerland). 20 (2020). doi:10.3390/s20072054.

[97]   M. Attenni, C. Bartolomei, C. Inglese, A. Ippolito, C. Morganti, G. Predari, Low cost survey and heritage value, SCIRES-IT - SCIentific RESearch and Information Technology. 7 (2018) 115–132. doi:10.2423//I22394303V7N2P115.

[98]   J. Balsa-Barreiro, D. Fritsch, Generation of visually aesthetic and detailed 3D models of historical cities by using laser scanning and digital photogrammetry, Digital Applications in Archaeology and Cultural Heritage. 8 (2018) 57–64. doi:10.1016/j.daach.2017.12.001.

[99]   I. Aicardi, F. Chiabrando, A. Maria Lingua, F. Noardo, Recent trends in cultural heritage 3D survey: The photogrammetric computer vision approach, Journal of Cultural Heritage. 32 (2018) 257–266. doi:10.1016/j.culher.2017.11.006.

[100] G. Tucci, V. Bonora, A. Conti, L. Fiorini, High-quality 3D models and their use in a cultural heritage conservation project, International Archives of the Photogrammetry, Remote Sensing and Spatial Information Sciences - ISPRS Archives. 42 (2017) 687–693. doi:10.5194/isprs-archives-XLII-2-W5-687-2017.

[101] R. Nespeca, L. De Luca, Analysis, thematic maps and data mining from point cloud to ontology for software development, International Archives of the

Photogrammetry, Remote Sensing and Spatial Information Sciences - ISPRS Archives. 41 (2016) 347–354. doi:10.5194/isprsarchives-XLI-B5-347-2016.

[102] G. Guidi, F. Remondino, M. Russo, F. Menna, A. Rizzi, S. Ercoli, A multi-resolution methodology for the 3D modeling of large and complex archaeological areas, International Journal of Architectural Computing. 7 (2009) 39–56. doi:10.1260/147807709788549439.

[103] F. Remondino, S. El-Hakim, S. Girardi, A. Rizzi, S. Benedetti, L. Gonzo, 3D virtual reconstruction and visualization of complex architectures - The "3D-arch project," International Archives of Photogrammetry, Remote Sensing and Spatial Information Sciences. XXXVI (2007).

[104] G. Guidi, M. Russo, D. Angheleddu, 3D survey and virtual reconstruction of archaeological sites, Digital Applications in Archaeology and Cultural Heritage. 1 (2014) 55–69. http://www.sciencedirect.com/science/article/pii/S2212054814000022.

[105] A. Koutsoudis, B. Vidmar, G. Ioannakis, F. Arnaoutoglou, G. Pavlidis, C. Chamzas, Multi-image 3D reconstruction data evaluation, Journal of Cultural Heritage. 15 (2014). doi:10.1016/j.culher.2012.12.003.

[106] J. Katz, A. Tokovinine, The past, now showing in 3D: An introduction, Digital Applications in Archaeology and Cultural Heritage. 6 (2017) 1–3. doi:10.1016/j.daach.2017.09.001.

[107] R. Pierdicca, Mapping Chimu's settlements for conservation purposes using UAV and close range photogrammetry. The virtual reconstruction of Palacio Tschudi, Chan Chan, Peru, Digital Applications in Archaeology and Cultural Heritage. 8 (2018) 27–34. doi:10.1016/j.daach.2017.11.004.

[108] R. Pierdicca, E. Frontoni, E.S. Malinverni, F. Colosi, R. Orazi, Virtual reconstruction of archaeological heritage using a combination of photogrammetric techniques: Huaca Arco Iris, Chan Chan, Peru, Digital Applications in Archaeology and Cultural Heritage. 3 (2016) 80–90. doi:10.1016/j.daach.2016.06.002.

[109] F. Brandolini, M. Cremaschi, A. Zerboni, M.D. Esposti, G.S. Mariani, S. Lischi, SfM-photogrammetry for fast recording of archaeological features in remote areas, Archeologia e Calcolatori. 31.2 (2021) 33–45. doi:10.19282/ac.31.2.2020.04.

[110] E. Aragón, S. Munar, J. Rodríguez, K. Yamafune, Underwater photogrammetric monitoring techniques for mid-depth shipwrecks, Journal of Cultural Heritage. (2018). doi:10.1016/j.culher.2017.12.007.

[111] G. Guidi, L.L. Micoli, S. Gonizzi, M. Brennan, B. Frischer, Image-based 3D capture of cultural heritage artifacts: An experimental study about 3D data

quality, 2015 Digital Heritage International Congress, Digital Heritage 2015. (2015) 321–324. doi:10.1109/DigitalHeritage.2015.7419514.

[112] F. Remondino, Rilievo e modellazione 3D di siti e architetture complesse 3D surveying and modelling of complex architectural sites and heritage objects, (2011).

[113] L. Di Angelo, P. Di Stefano, L. Fratocchi, A. Marzola, An AHP-based method for choosing the best 3D scanner for cultural heritage applications, Journal of Cultural Heritage. 34 (2018) 109–115. doi:10.1016/j.culher.2018.03.026.

[114] H. El-Din Fawzy, 3D laser scanning and close-range photogrammetry for buildings documentation: A hybrid technique towards a better accuracy, Alexandria Engineering Journal. (2019). doi:10.1016/j.aej.2019.10.003.

[115] R. Florio, R. Catuogno, T. Della Corte, The interaction of knowledge as though field experimentation of the integrated survey. The case of sacristy of Francesco Solimena in the church of san Paolo Maggiore in Naples, Scires-It. 9 (2019) 69–84. doi:10.2423/i22394303v9n2p69.

[116] P. Bastonero, E. Donadio, F. Chiabrando, A. Spanò, Fusion of 3D models derived from TLS and image-based techniques for CH enhanced documentation, ISPRS Annals of the Photogrammetry, Remote Sensing and Spatial Information Sciences. II (2014) 23–25. doi:10.5194/isprsannals-II-5-73-2014.

[117] J. Moyano, J.E. Nieto-Julián, D. Bienvenido-Huertas, D. Marín-García, Validation of close-range photogrammetry for architectural and archaeological heritage: Analysis of point density and 3d mesh geometry, Remote Sensing. 12 (2020) 1–23. doi:10.3390/rs12213571.

[118] I. Siebke, L. Campana, M. Ramstein, A. Furtwängler, A. Hafner, S. Lösch, The application of different 3D-scan-systems and photogrammetry at an excavation — A Neolithic dolmen from Switzerland, Digital Applications in Archaeology and Cultural Heritage. 10 (2018) 1–11. doi:10.1016/j.daach.2018.e00078.

[119] E. Valero, A. Forster, F. Bosché, L. Wilson, A. Leslie, COMPARISON OF 3D REALITY CAPTURE TECHNOLOGIES FOR THE SURVEY OF STONE WALLS, in: Proceedings of the 8th International Congress on Archaeology, Computer Graphics, Cultural Heritage and Innovation 'ARQUEOLÓGICA 2.0,' EDITORIAL UNIVERSITAT POLITÈCNICA DE VALÈNCIA, 2016. doi:10.4995/arqueologica8.2016.2582.

[120] A. Mohan, S. Poobal, Crack detection using image processing : A critical review and analysis, Alexandria Engineering Journal. 57 (2018) 787–798. doi:10.1016/j.aej.2017.01.020.

[121] J. Valença, D. Dias-da-costa, E. Júlio, H. Araújo, H. Costa, Automatic crack monitoring using photogrammetry and image processing, 46 (2013) 433–441.

doi:10.1016/j.measurement.2012.07.019.

[122] Y.-S. Yang, C.-M. Yang, C.-W. Huang, Thin crack observation in a reinforced concrete bridge pier test using image processing and analysis, Advances in Engineering Software. 83 (2015) 99–108.

[123] T. Su, Application of Computer Vision to Crack Detection of Concrete Structure, IACSIT International Journal of Engineering and Technology. 5 (2013) 457–461. doi:10.7763/IJET.2013.V5.596.

[124] Z. Yiyang, The Design of Glass Crack Detection System Based on Image Preprocessing Technology, in: 2014 IEEE 7th Joint International Information Technology and Artificial Intelligence Conference, IEEE, Chongqing, China, 2015: pp. 39–42. doi:10.1109/ITAIC.2014.7065001.

[125] P. Prasanna, K. Dana, N. Gucunski, B. Basily, Computer vision based crack detection and analysis, Proceedings of SPIE - The International Society for Optical Engineering. 8345 (2012). doi:10.1117/12.915384.

[126] P. Prasanna, K. Dana, N. Gucunski, B. Basily, H.M. La, R.S. Lim, H. Parvardech, Automatic Crack Detection on Concrete Bridges, in: IEEE TRANSACTIONS ON AUTOMATION SCIENCE AND ENGINEERING, 2016.

[127] A. Nisanth, A. Mathew, AUTOMATED VISUAL INSPECTION OF PAVEMENT CRACK DETECTION AND CHARACTERIZATION, International Journal of Technology and Engineering System (IJTES). 6 (2014) 14–20.

[128] R. Gonçalves Lins, S.N. Gigivi, Automatic Crack Detection and Measurement Based on Image Analysis, IEEE TRANSACTIONS ON INSTRUMENTATION AND MEASUREMENT. 65 (2016) 583–590.

[129] H.-N. Nguyen, T.-Y. Kam, P.-Y. Cheng, An Automatic Approach for Accurate Edge Detection of Concrete Crack Utilizing 2D Geometric Features of Crack, J Sign Process Syst. 77 (2014) 221–240.

[130] R.S. Lim, H.M. La, W. Sheng, A Robotic Crack Inspection and Mapping System for Bridge Deck Maintenance, IEEE TRANSACTIONS ON AUTOMATION SCIENCE AND ENGINEERING. 11 (2014) 367–378. doi:10.1109/TASE.2013.2294687.

[131] H. Oliverira, P. Lobato Correia, Automatic Road Crack Detection and Characterization, IEEE TRANSACTIONS ON INTELLIGENT TRANSPORTATION SYSTEMS. 14 (2013) 155–168.

[132] M. Salman, S. Mathavan, K. Kamal, M. Rahman, Pavement Crack Detection Using the Gabor Filter, in: Proceedings of the 16th International IEEE Annual Conference on Intelligent Transportation Systems, IEEE, 2013: pp. 2039–2044.

[133] M.R. Jahanshahi, S.F. Masri, Adaptive vision-based crack detection using 3D scene reconstruction for condition assessment of structures, Automation in Construction. 22 (2012) 567–576.

doi:https://doi.org/10.1016/j.autcon.2011.11.018.

[134] M.R. Jahanshahi, S.R. Masri, C.W. Padgett, G.S. Sukhatme, An innovative methodology for detection and quantification of cracks through incorporation of depth perception, Machine Vision and Applications. 24 (2013) 227–241.

[135] A. Zhang, K.C.P. Wang, R. Ji, Q.J. Li, Efficient System of Cracking-Detection Algorithms with 1-mm 3D-Surface Models and Performance Measures, Journal of Computing in Civil Engineering. 30 (2016) 1–16. doi:10.1061/(ASCE)CP.1943-5487.0000581.

[136] A.A.A. Beshr, O.G. Heneash, H.E.D. Fawzy, M.M. El-Banna, Condition assessment of rigid pavement using terrestrial laser scanner observations, International Journal of Pavement Engineering. 0 (2021) 1–12. doi:10.1080/10298436.2021.1940180.

[137] P. Zheng, Crack Detection and Measurement Utilizing Image-Based Reconstruction, 2014. https://vtechworks.lib.vt.edu/bitstream/handle/10919/48963/crack_detection_ and_measurement_utilizing_image_based_reconstruction.pdf?sequence=1.

[138] C. Koch, K. Georgieva, V. Kasireddy, B. Akinci, P. Fieguth, A review on computer vision based defect detection and condition assessment of concrete and asphalt civil infrastructure, Advanced Engineering Informatics. 29 (2015) 196–210. doi:10.1016/j.aei.2015.01.008.

[139] M. Hashmi, A. Keskar, Computer-Vision Based Visual Inspection and Crack Detection of Railroad Tracks, Recent Advances in Electrical and Computer Engineering. (2014) 102–110. http://www.europment.org/library/2014/venice/bypaper/OLA/OLA-16.pdf.

[140] P. Tang, D. Huber, B. Akinci, Characterization of laser scanners and algorithms for detecting flatness defects on concrete surfaces, Journal of Computing in Civil Engineering. 25 (2011) 31–42. doi:10.1061/(ASCE)CP.1943-5487.0000073.

[141] V. Kasireddy, B. Akinci, A case study on comparative analysis of 3D point clouds from UAV mounted and terrestrial scanners for bridge condition assessment, in: LC3 2017: Volume I - Proocedings on the Joint Conference on Computing in Construction (JC3), 2017: pp. 87–94. doi:10.24928/JC3-2017/0041.

[142] V. Kasireddy, B. Akinci, Representation Requirements for Laser Scan Based Probabilistic Condition Assessment of Bridges, Computing in Civil Engineering. (2017) 395–403. http://toc.proceedings.com/49478webtoc.pdf.

[143] N. Hallermann, G. Morgenthal, THE APPLICATION OF UNMANNED AERIAL VEHICLES FOR THE INSPECTION OF STRUCTURES, Advances in Structural Engineering. 17 (2012) 289–302.

[144] J. Herráeza, P. Navarrob, J.L. Deniaa, M.T. Martínc, J. Rodríguezc, Modeling the thickness of vaults in the church of santa maria de magdalena (Valencia, Spain) with laser scanning techniques, Journal of Cultural Heritage. 15 (2014) 679–686. doi:10.1016/j.culher.2013.11.015.

[145] R. Quattrini, F. Clementi, A. Lucidi, S. Giannetti, A. Santoni, FROM TLS to FE ANALYSIS: POINTS CLOUD EXPLOITATION for STRUCTURAL BEHAVIOUR DEFINITION. the SAN CIRIACO'S BELL TOWER, International Archives of the Photogrammetry, Remote Sensing and Spatial Information Sciences - ISPRS Archives. 42 (2019) 957–964. doi:10.5194/isprs-archives-XLII-2-W15-957-2019.

[146] E. Quagliarini, P. Clini, M. Ripanti, Fast, low cost and safe methodology for the assessment of the state of conservation of historical buildings from 3D laser scanning: The case study of Santa Maria in Portonovo (Italy), Journal of Cultural Heritage. 24 (2017) 175–183. doi:10.1016/j.culher.2016.10.006.

[147] K. Lawonn, E. Trostmann, B. Preim, K. Hildebrandt, Visualization and Extraction of Carvings for Heritage Conservation, IEEE Transactions on Visualization and Computer Graphics. 23 (2017) 801–810. doi:10.1109/TVCG.2016.2598603.

[148] M. Mishra, Machine learning techniques for structural health monitoring of heritage buildings: A state-of- the-art review and case studies, Journal of Cultural Heritage. 47 (2021) 227–245. doi:doi.org/10.1016/j.culher.2020.09.005.

[149] S.C. Radopoulou, I. Brilakis, Automated Detection of Multiple Pavement Defects, Journal of Computing in Civil Engineering. 31 (2017) 1–14. doi:10.1061/(ASCE)CP.1943-5487.0000623.

[150] M.P. Samy, S. Foong, G.S. Soh, K.S. Yeo, Automatic optical & laser-based defect detection and classification in brick masonry walls, in: IEEE Region 10 Annual International Conference, Proceedings/TENCON, IEEE, 2017: pp. 3521–3524. doi:10.1109/TENCON.2016.7848711.

[151] G.P. Bu, S. Chanda, H. Guan, J. Jo, M. Blumenstein, Y.C. Loo, Crack Detection using a Texture Analysis-based Technique for Visual Bridge Inspection, 14 (2015) 41–48.

[152] C. Geiß, P. Aravena Pelizari, L. Blickensdörfer, H. Taubenböck, Virtual Support Vector Machines with self-learning strategy for classification of multispectral remote sensing imagery, ISPRS Journal of Photogrammetry and Remote Sensing. 151 (2019) 42–58. doi:10.1016/j.isprsjprs.2019.03.001.

[153] D. Brackenbury, I. Brilakis, M. DeJong, Automated Defect Detection For Masonry Arch Bridges, in: International Conference on Smart Infrastructure and Construction 2019 (ICSIC): Driving Data-Informed Decision-Making, 2019: pp.

3–9. doi:10.1680/icsic.64669.003.

[154] P. Hüthwohl, I. Brilakis, Detecting healthy concrete surfaces, Advanced Engineering Informatics. 37 (2018) 150–162. doi:10.1016/j.aei.2018.05.004.

[155] Y.J. Cha, W. Choi, O. Büyüköztürk, Deep Learning-Based Crack Damage Detection Using Convolutional Neural Networks, Computer-Aided Civil and Infrastructure Engineering. 32 (2017) 361–378. doi:10.1111/mice.12263.

[156] R. Kalfarisi, Z.Y. Wu, K. Soh, Crack Detection and Segmentation Using Deep Learning with 3D Reality Mesh Model for Quantitative Assessment and Integrated Visualization, Journal of Computing in Civil Engineering. 34 (2020) 1–20. doi:10.1061/(ASCE)CP.1943-5487.0000890.

[157] D. Liang, X.F. Zhou, S. Wang, C.J. Liu, Research on Concrete Cracks Recognition based on Dual Convolutional Neural Network, KSCE Journal of Civil Engineering. 23 (2019) 3066–3074. doi:10.1007/s12205-019-2030-x.

[158] D. Liang, S. Wang, L.-K. Shi, C.J. Liu, Concrete bridge crack identification based on Re-FCN network model, Smart Infrastructure and Construction. (2020).

[159] Z. Liu, Y. Cao, Y. Wang, W. Wang, Computer vision-based concrete crack detection using U-net fully convolutional networks, Automation in Construction. 104 (2019) 129–139. doi:10.1016/j.autcon.2019.04.005.

[160] K. Chaiyasarn, W. Khan, L. Ali, M. Sharma, D. Brackenbury, M. DeJong, Crack detection in masonry structures using convolutional neural networks and support vector machines, in: ISARC 2018 - 35th International Symposium on Automation and Robotics in Construction and International AEC/FM Hackathon: The Future of Building Things, 2018: pp. 1–8. doi:10.22260/isarc2018/0016.

[161] M.E. Hatir, M. Barstuğan, İ. İnce, Deep learning-based weathering type recognition in historical stone monuments, Journal of Cultural Heritage. 45 (2020) 193–203. doi:10.1016/j.culher.2020.04.008.

[162] Y. Gong, F. Zhang, X. Jia, X. Huang, D. Li, Z. Mao, Deep neural networks for quantitative damage evaluation of building losses using aerial oblique images: Case study on the great wall (china), Remote Sensing. 13 (2021) 1–19. doi:10.3390/rs13071321.

[163] P.C. Chen, T. Pavlidis, Image segmentation as an estimation problem, Computer Graphics and Image Processing. 12 (1980) 153–172. doi:10.1016/0146-664X(80)90009-X.

[164] R.A. Galantucci, A. Musicco, S. Bruno, F. Fatiguso, Automatic detection of dampness phenomena on architectural elements by point cloud segmentation, in: Rehabend 2020 Euro-American Congress - Construction Pathology, Rehabilitation Technology and Heritage Management, 2020: pp. 1141–1148.

[165] A. Nguyen, B. Le, 3D point cloud segmentation: A survey, IEEE Conference on

Robotics, Automation and Mechatronics, RAM - Proceedings. (2013) 225–230. doi:10.1109/RAM.2013.6758588.

[166] E. Grilli, F. Menna, F. Remondino, A review of point cloud segmentation and classification algorithms, in: The International Archives of Photogrammetry, Remote Sensing and Spatial Information Sciences, 2017. doi:10.1017/CBO9781107415324.004.

[167] M.D. Hossain, D. Chen, Segmentation for Object-Based Image Analysis (OBIA): A review of algorithms and challenges from remote sensing perspective, ISPRS Journal of Photogrammetry and Remote Sensing. 150 (2019) 115–134. doi:10.1016/j.isprsjprs.2019.02.009.

[168] C. Pérez-Sinticala, R. Janvier, X. Brunetaud, S. Treuillet, R. Aguilar, B. Castañeda, Evaluation of primitive extraction methods from point clouds of cultural heritage buildings, in: Structural Analysis of Historical Constructions, 2019: pp. 1949–1958. doi:10.1007/978-3-319-99441-3_250 CITATION.

[169] S. Spina, K. Debattista, K. Bugeja, A. Chalmers, Point Cloud Segmentation for Cultural Heritage Sites, in: M. Dellepiane, F. Niccolucci, S. Pena Serna, H. Rushmeier, L. Van Gool (Eds.), The 12th International Symposium on Virtual Reality, Archeology and Cultural Heritage VAST, The Eurographics Association 2011, 2011.

[170] J.L. Lerma, J.M. Biosca, Segmentation and Filtering of Laser Scanner Data for Cultural Heritage, (2005).

[171] B. Oehler, J. Stueckler, J. Welle, D. Schulz, S. Behnke, Efficient multi-resolution plane segmentation of 3D point clouds, in: Lecture Notes in Computer Science (Including Subseries Lecture Notes in Artificial Intelligence and Lecture Notes in Bioinformatics), 2011: pp. 145–156. doi:10.1007/978-3-642-25489-5_15.

[172] R. Schnabel, R. Wahl, R. Klein, Efficient RANSAC for point-cloud shape detection, Computer Graphics Forum. 26 (2007) 214–226. doi:10.1111/j.1467-8659.2007.01016.x.

[173] S. Gonizzi Barsanti, G. Guidi, L. De Luca, SEGMENTATION of 3D MODELS for CULTURAL HERITAGE STRUCTURAL ANALYSIS - SOME CRITICAL ISSUES, ISPRS Annals of the Photogrammetry, Remote Sensing and Spatial Information Sciences. 4 (2017) 115–122. doi:10.5194/isprs-annals-IV-2-W2-115-2017.

[174] A.V. Vo, L. Truong-Hong, D.F. Laefer, M. Bertolotto, Octree-based region growing for point cloud segmentation, ISPRS Journal of Photogrammetry and Remote Sensing. 104 (2015) 88–100. doi:10.1016/j.isprsjprs.2015.01.011.

[175] F. Hamid-Lakzaeian, Point cloud segmentation and classification of structural elements in multi-planar masonry building facades, Automation in Construction. 118 (2020) 103232. doi:10.1016/j.autcon.2020.103232.

[176] E. Grilli, E.M. Farella, A. Torresani, F. Remondino, Geometric features analysis for the classification of Cultural Heritage point clouds, ISPRS Archives. 42 (2019) 541–548. doi:10.5194/isprs-archives-XLII-2-W15-541-2019.

[177] V. Croce, M.G. Bevilacqua, G. Caroti, A. Piemonte, Connecting Geometry and Semantics Via Artificial Intelligence: From 3D Classification of Heritage Data To H-Bim Representations, The International Archives of the Photogrammetry, Remote Sensing and Spatial Information Sciences. XLIII-B2-2 (2021) 145–152. doi:10.5194/isprs-archives-xliii-b2-2021-145-2021.

[178] S. Teruggi, E. Grilli, M. Russo, F. Fassi, F. Remondino, A hierarchical machine learning approach for multi-level and multi-resolution 3d point cloud classification, Remote Sensing. 12 (2020) 1–29. doi:10.3390/RS12162598.

[179] T. Hackel, J.D. Wegner, K. Schindler, Fast Semantic Segmentation of 3D Point Clouds With Strongly Varying Density, ISPRS Annals. III–3 (2016) 177–184. doi:10.5194/isprsannals-iii-3-177-2016.

[180] E. Grilli, E. Özdemir, F. Remondino, Application of machine and deep learning strategies for the classification of heritage point clouds, ISPRS Archives. 42 (2019) 447–454. doi:10.5194/isprs-archives-XLII-4-W18-447-2019.

[181] E. Grilli, F. Remondino, Classification of 3D Digital Heritage, Remote Sensing. 11 (2019) 847. doi:10.3390/rs11070847.

[182] R. Pierdicca, M. Paolanti, F. Matrone, M. Martini, C. Morbidoni, E.S. Malinverni, E. Frontoni, A.M. Lingua, Point cloud semantic segmentation using a deep learning framework for cultural heritage, Remote Sensing. 12 (2020) 1–23. doi:10.3390/rs12061005.

[183] S. Yang, M. Hou, A. Shaker, S. Li, Modeling and Processing of Smart Point Clouds of Cultural Relics with Complex Geometries, ISPRS International Journal of Geo-Information. 10 (2021) 617. doi:10.3390/ijgi10090617.

[184] I. Đurić, R. Obradović, I. Vasiljević, N. Ralević, V. Stojaković, Two-dimensional shape analysis of complex geometry based on photogrammetric models of iconostases, Applied Sciences (Switzerland). 11 (2021). doi:10.3390/app11157042.

[185] E. Valero, F. Bosche, A.M. Forster, L. Wlson, A. Turmel, E. Hyslop, Development of a novel open tool for the segmentation of 3D point clouds of masonry walls — Heriot-Watt Research Portal, 14th International Congress on the Deterioration and Conservation of Stone. (2020). https://researchportal.hw.ac.uk/en/publications/development-of-a-novel-open-tool-for-the-segmentation-of-3d-point.

[186] E. Valero, F. Bosché, A. Forster, Automatic segmentation of 3D point clouds of rubble masonry walls, and its application to building surveying, repair and

maintenance, Automation in Construction. 96 (2018) 29–39. doi:10.1016/j.autcon.2018.08.018.

[187] E. Valero, A. Forster, F. Bosché, E. Hyslop, L. Wilson, A. Turmel, Automated defect detection and classification in ashlar masonry walls using machine learning, Automation in Construction. 106 (2019) 102846. doi:10.1016/j.autcon.2019.102846.

[188] E. Grilli, D. Dininno, G. Petrucci, F. Remondinoa, From 2D to 3D supervised segmentation and classification for cultural heritage applications, International Archives of the Photogrammetry, Remote Sensing and Spatial Information Sciences - ISPRS Archives. 42 (2018) 399–406. doi:10.5194/isprs-archives-XLII-2-399-2018.

[189] Q. Zhan, Y. Liang, Y. Xiao, Color-based Segmentation of Point Clouds, in: Laser Scanning 2009, IAPRS, 2009: pp. 248–252. doi:10.3969/j.issn.1000-8179.2012.24.032.

[190] Q. Zhan, L. Yu, Y. Liang, A point cloud segmentation method based on vector estimation and color clustering BT - 2nd International Conference on Information Science and Engineering, ICISE2010, December 4, 2010 - December 6, 2010, (2010) 3463–3466. doi:10.1109/ICISE.2010.5691038.

[191] E.S. Malinverni, R. Pierdicca, M. Sturari, F. Colosi, R. Orazi, Documentation & detection of colour changes of bas relieves using close range photogrammetry, ISPRS Archives. 42 (2017) 203–210. doi:10.5194/isprs-Archives-XLII-5-W1-203-2017.

[192] P.M. Lerones, D.O. Vélez, F.G. Rojo, J. Gómez-García-Bermejo, E.Z. Casanova, Moisture detection in heritage buildings by 3D laser scanning, Studies in Conservation. 61 (2016) 46–54. doi:10.1179/2047058415Y.0000000017.

[193] E.M. Perez-monserrat, R. Fort, M.J. Varas-muriel, E. Mercedes, R. Fort, M.J. Varas-muriel, E.M. Perez-monserrat, R. Fort, Monitoring façade soiling as a maintenance strategy for the sensitive built heritage heritage, International Journal of Architectural Heritage. 00 (2018) 1–12. doi:10.1080/15583058.2017.1419312.

[194] M. Carrero-Pazos, B. Vilas-Estévez, A. Vázquez-Martínez, Digital imaging techniques for recording and analysing prehistoric rock art panels in Galicia (NW Iberia), Digital Applications in Archaeology and Cultural Heritage. 8 (2018) 35–45. doi:10.1016/j.daach.2017.11.003.

[195] R. Vorobel, I. Ivasenko, O. Berehulyak, T. Mandzii, Segmentation of rust defects on painted steel surfaces by intelligent image analysis, Automation in Construction. 123 (2021) 103515. doi:10.1016/j.autcon.2020.103515.

[196] E.S. Malinverni, R. Pierdicca, F. Di Stefano, M. Sturari, M. Mameli, E. Frontoni,

R. Orazi, F. Colosi, How to Extract Useful Information about the Decay of Bass Relieves in Archaeological Area, ISPRS Annals of the Photogrammetry, Remote Sensing and Spatial Information Sciences. 42 (2019) 785–792. doi:10.5194/isprs-Archives-XLII-2-W11-785-2019.

[197] F. Peteler, E. Gattet, P. Bromblet, O. Guillon, J. Vallet, L. De Luca, Analyzing the Evolution of Deterioration Patterns: A First Step of an Image-based Approach for Comparing Multitemporal Data Sets, in: 2015 Digital Heritage, 2015: pp. 1–4.

[198] O. Risbøl, C. Briese, M. Doneus, A. Nesbakken, Monitoring cultural heritage by comparing DEMs derived from historical aerial photographs and airborne laser scanning, Journal of Cultural Heritage. 16 (2015) 202–209. doi:10.1016/j.culher.2014.04.002.

[199] R.S. Adhikari, O. Moselhi, A. Bagchi, Image-based retrieval of concrete crack properties for bridge inspection, Automation in Construction. 39 (2014) 180–194.

[200] V. Pagounis, M. Tsakiri, V. Zacharis, V. Andritsanos, M. Tsiardaki, Detection of geometric changes for an historic theatre by comparing surveying data of different chronological periods, Journal of Cultural Heritage. 21 (2016) 860–868. doi:10.1016/j.culher.2016.02.004.

[201] S. Dubois, L. Vanhooren, Y. Vanhellemont, Microscopic 3D photogrammetry to assess salt damage on stone samples, in: STONE 2020 Monument Future: Decay and Conservation of Stone, 2020: pp. 1–6.

[202] T. López-Martínez, A. García-Bueno, V.J. Medina-Flórez, New methodology for the assessment of cleaning treatments. Applications of photogrammetry for restoration, Journal of Cultural Heritage. (2017). doi:10.1016/j.culher.2017.09.019.

[203] N. Hallermann, G. Morgenthal, V. Rodehorst, Unmanned Aerial Systems (UAS) – Case Studies of Vision Based Monitoring of Ageing Structures, International Symposium Non-Destructive Testing in Civil Engineering (NDT-CE). (2015).

[204] L. Wilson, A. Rawlinson, A. Frost, J. Hepher, 3D digital documentation for disaster management in historic buildings: Applications following fire damage at the Mackintosh building, The Glasgow School of Art, Journal of Cultural Heritage. (2017). doi:10.1016/j.culher.2017.11.012.

[205] Z. Zhou, J. Gong, M. Guo, Image-Based 3D Reconstruction for Posthurricane Residential Building Damage Assessment, Journal of Computing in Civil Engineering. 30 (2016) 04015015. doi:10.1061/(asce)cp.1943-5487.0000480.

[206] N. Kaur, P.S. Tiwari, H. Pande, S. Agrawal, Utilizing Advance Texture Features for Rapid Damage Detection of Built Heritage Using High-Resolution Space

Borne Data: A Case Study of UNESCO Heritage Site at Bagan, Myanmar, Journal of the Indian Society of Remote Sensing. 48 (2020) 1627–1638. doi:10.1007/s12524-020-01190-9.

[207] E.B. Anil, B. Akinci, O. Kurc, J.H. Garrett, Building-Information-Modeling – Based Earthquake Damage Assessment for Reinforced Concrete Walls, Journal of Computing in Civil Engineering. 04015076 (2015) 1–15. doi:10.1061/(ASCE)CP.1943-5487.0000551.

[208] M. Falcone, A. Origlia, M. Campi, S. Di Martino, From Architectural Survey To Continuous Monitoring: Graph-Based Data Management for Cultural Heritage Conservation With Digital Twins, The International Archives of the Photogrammetry, Remote Sensing and Spatial Information Sciences. XLIII-B4-2 (2021) 47–53. doi:10.5194/isprs-archives-xliii-b4-2021-47-2021.

[209] A. Guarnieri, N. Milan, A. Vettore, Monitoring of complex structure for structural control using terrestrial laser scanning (Tls) and photogrammetry, International Journal of Architectural Heritage. 7 (2013) 54–67. doi:10.1080/15583058.2011.606595.

[210] N.P. van Dijk, E.K. Gamstedt, I. Bjurhager, Monitoring archaeological wooden structures: Non-contact measurement systems and interpretation as average strain fields, Journal of Cultural Heritage. 17 (2016) 102–113. doi:10.1016/j.culher.2015.03.011.

[211] D. Prati, I. Rrapaj, G. Mochi, Contribution of parametric modeling in the interpretation of deformations and displacements of wooden trusses, SCIRES-IT - SCIentific RESearch and Information Technology. 8 (2018) 105–120. doi:10.2423/i22394303v8n1p105.

[212] A. Massafra, D. Prati, G. Predari, R. Gulli, Wooden truss analysis, preservation strategies, and digital documentation through parametric 3D modeling and HBIM workflow, Sustainability (Switzerland). 12 (2020) 1–23. doi:10.3390/su12124975.

[213] T. Luhmann, S. Robson, S. Kyle, I. Harley, Close Range Photogrammetry Principles, techniques and applications., Whittles Publishing, 2006. doi:10.1111/phor.12114.

[214] T. Schenk, Introduction to Photogrammetry, Department of Civil and Environmental Engineering and Geodetic Science, The Ohio State University. (2005) 79–95. http://gscphoto.ceegs.ohio-state.edu/courses/GeodSci410/docs/GS410_02.pdf.

[215] Geodetic Services Inc., Basics of Photogrammetry, (2017). https://www.geodetic.com/wp-content/uploads/2019/01/Basics_of_Photogrammetry_2017.pdf.

[216] J. Bedford, Photogrammetric Applications for Cultural Heritage. Guidance for Good Practice, (2017) 1–128. doi:10.1212/01.WNL.0000132885.83350.45.

[217] R.C. Gonzalez, R.E. Woods, Digital Image Processing, Fourth Edi, Pearson, 2018.

[218] Istituto Nazionale di Ottica, Operazioni locali: Edging, (2007). http://www.ino.it/home/cosimo/ttr/edging (accessed September 20, 2017).

[219] X. Jiang, N. Senin, P.J. Scott, F. Blateyron, Feature-based characterisation of surface topography and its application, CIRP Annals. 70 (2021) 681–702. doi:10.1016/j.cirp.2021.05.001.

[220] M. Sonka, V. Hlavac, R. Boyle, Image processing, analysis and machine vision, 4th ed., Cengage Learning, 2014. doi:10.1016/0165-1684(94)90202-x.

[221] TaylorHobson-Ltd, Software di analisi tridimensionale TalyMap, (2016). http://www.taylor-hobson.it/products/3/64.html (accessed May 30, 2017).

[222] DigitalSurf, Surface imaging and metrology software for microscopes and profilometers: Integral surface analysis software solutions for microscopes and profilers, (2017). http://www.digitalsurf.com/en/mntproducts.html (accessed May 30, 2017).

[223] DigitalSurf, TalyMap 3D - Reference Guide, (2016).

[224] A.I. Che-Ani, A.S. Ali, M.M. Tahir, N.A.G. Abdullah, N.M. Tawil, The Development of a Condition Survey Protocol (CSP) 1 Matrix for Visual Building Inspection, The Construction, Building and Real Estate Research Conference of the Royal Institution of Chartered Surveyors Held. (2010) 11–21. http://www.rics.org/site/download_feed.aspx?fileID=7896&fileExtension=PDF.

[225] L.M. Galantucci, L. Tricarico, R. Spina, A Quality Evaluation Method for Laser Welding of Al Alloys Through Neural Networks, CIRP Annals - Manufacturing Technology. 49 (2000) 131–134. doi:http://dx.doi.org/10.1016/S0007-8506(07)62912-6.

[226] A. Nguyen, B. Le, 3D Point Cloud Segmentation: A survey, in: 2016 6th Conference on Robotics, Automation and Mechatronics (RAM), IEEE, 2013: pp. 225–230.

[227] E. Grilli, F. Menna, F. Remondino, A review of point clouds segmentation and classification algorithms, International Archives of the Photogrammetry, Remote Sensing and Spatial Information Sciences - ISPRS Archives. 42 (2017) 339–344. doi:10.5194/isprs-archives-XLII-2-W3-339-2017.

[228] Y.J. Zhang, An overview of image and video segmentation in the last 40 years, Advances in Image and Video Segmentation. (2006) 1–15. doi:10.4018/978-1-59140-591-7.ch001.

[229] I. Young, J. Gerbrands, L. van Vliet, Fundamentals of Image Processing, (2009) 1–85. doi:10.1201/9781420046090-c13.

[230] I.H. Witten, E. Frank, M.A. Hall, Data Mining, Morgan Kaufmann, Burlington, USA, 2011. doi:10.1016/B978-008045405-4.00153-1.

[231] T. Hastie, R. Tibshirani, Jerome Friedman, The Elements of Statistical Learning, Second Edi, Springer International Publishing, 2008.

[232] A. Musicco, R.A. Galantucci, S. Bruno, C. Verdoscia, F. Fatiguso, Automatic Point Cloud Segmentation for the Detection of Alterations on Historical Buildings Through an Unsupervised and Clustering-Based Machine Learning Approach, ISPRS Annals of the Photogrammetry, Remote Sensing and Spatial Information Sciences. V-2–2021 (2021) 129–136. doi:10.5194/isprs-annals-v-2-2021-129-2021.

[233] F. García-Lamont, A. Cuevas, Y. Niño, Segmentation of color images by chromaticity features using self-organizing maps Segmentación de imágenes de color por características, Ingenieria e Investigacion. 2016 (2016) 78–89. doi:10.15446/ing.investig.v36n2.55746.Attribution.

[234] Formule per la conversione tra YUV e RGB, (n.d.). https://www.itread01.com/content/1541618896.html (accessed December 6, 2021).

[235] Capitolo 3: Spazi di colore, (n.d.). https://zhuanlan.zhihu.com/p/28766366 (accessed December 6, 2021).

[236] International Telecommunication Union, Composite Analog Video Signal — NTSC for Studio Applications, (2004) 1–21.

[237] D. Girardeau-Montaut, CloudCompare v. 2.12.alpha, (2020). https://www.danielgm.net/cc/.

[238] L. Breiman, Random Forest, Machine Learning. 45 (2001) 1–32. doi:10.1023/A:1010933404324.

[239] D. Girardeau-Montaut, CloudCompare v2.6.1 - User manual, (2015). http://www.danielgm.net/cc/doc/qCC/CloudCompare v2.6.1 - User manual.pdf (accessed November 16, 2017).

[240] G. Todaro, I Palmieri e le dimore marchesali" in Tra i Muri della Storia, Materiali per un viaggio nel cuore di Monopoli, C.R.S.E.C Monopoli, Regione Puglia, Assessorato Alla Pubblica Istruzione, Quadernetti d'identità Territoriale N° 5. (2002). http://www.comune.monopoli.ba.it/ViverelaCittagrave/Learee/ArteeCultura/Ville epalazzi/Palazzinobiliari/PalazzoPalmieri/tabid/1371/language/it-IT/Default.aspx (accessed September 10, 2017).

[241] P. Palmieri, Palmieri - Una famiglia nel tempo, Monopoli, 2002.

[242] G. Karaiskaj, Castello di Bashtova, (1973). https://web.archive.org/web/20131102051943/http://www.mtkrs.gov.al/web/Kalaja_e_Bashtoves_Kavaje_1028_1.php (accessed December 14, 2021).

[243] UNESCO, The Castle of Bashtova, (2017). https://whc.unesco.org/en/tentativelists/6259/ (accessed December 14, 2021).

[244] United States Geological Survey, Earthquake Hazards Program, (2019). https://earthquake.usgs.gov/earthquakes/eventpage/us60005lrf/executive.

[245] Albania Post-Disaster Needs Assessment Volume A Report, (2020). https://ec.europa.eu/neighbourhood-enlargement/sites/near/files/%0Aalbania_post-disaster_recovery_a_v9.0.pdf.

[246] Association of Bay Area Governments, Modified Mercalli Intensity (MMI) Scale, (n.d.). https://abag.ca.gov/our-work/resilience/data-research/earthquake (accessed April 6, 2021).

[247] Seismicity of the Earth 1900–2013 Mediterranean Sea and Vicinity, (n.d.). https://earthquake.usgs.gov/earthquakes/eventpage/us70006d0m/region-info (accessed April 6, 2021).

[248] A. Carannante, Il Duomo di Molfetta, un edificio romanico tra terra e mare, (n.d.). https://doctrame.hypotheses.org/203 (accessed August 26, 2021).

[249] G.A.G. Panunzio, Il duomo di Molfetta. Una chiesa fra Oriente e Occidente, ADDA EDITORE, 2012.

[250] M. Pirrelli, Tra conventi e monasteri. Le case religiose a Monopoli, Gelsorosso, 2009.

[251] Politecnico di Bari, 3D-Imp-Act, (n.d.). https://3dimpact.poliba.it/lm/index.php/view/map/?repository=3dimpact&project=map.

[252] Digital Surf, Software and Solutions, (2019). https://www.digitalsurf.com/ (accessed April 29, 2019).

[253] T. Fawcett, An introduction to ROC analysis, Pattern Recognition Letters. 27 (2006) 861–874. doi:10.1016/j.patrec.2005.10.010.

[254] B. Jaeger, The method of least squares, Handbook of Research on Informatics in Healthcare and Biomedicine. (2006) 181–184. doi:10.4018/978-1-59140-982-3.ch023.

[255] B. Preim, C. Botha, Image Analysis for Medical Visualization, Visual Computing for Medicine. (2014) 111–175. doi:10.1016/B978-0-12-415873-3.00004-3.

CURRICULUM

ESPERIENZA LAVORATIVA

• Date (da – a)	Dicembre 2021 - Maggio 2022
• Nome e indirizzo del datore di lavoro	**Comune di San Marco in Lamis (FG)**
• Tipo di azienda o settore	Ente pubblico locale
• Tipo di impiego	Partecipazione all'incarico per la redazione dell'Analisi della Condizione Limite dell'Emergenza del Comune di San Marco in Lamis (FG)
• Principali mansioni e responsabilità	Analisi della Condizione Limite dell'Emergenza

• Date (da – a)	Novembre 2021 - Marzo 2022
• Nome e indirizzo del datore di lavoro	**Comune di Andria (BAT)**
• Tipo di azienda o settore	Ente pubblico locale
• Tipo di impiego	Partecipazione all'incarico per la redazione dell'Analisi della Condizione Limite dell'Emergenza del Comune di Andria (BAT)
• Principali mansioni e responsabilità	Analisi della Condizione Limite dell'Emergenza

• Date (da – a)	Ottobre 2018 - Febbraio 2020
• Nome e indirizzo del datore di lavoro	**Studio Vitone & Associati - MODELLING & GRAPHICS SRLS** Via Roberto da Bari 62 BARI, 70122
• Tipo di azienda o settore	Società di servizi professionali, scientifici e tecnici Commercial art and graphic design
• Tipo di impiego	Collaborazione occasionale
• Principali mansioni e responsabilità	Progetti di stazioni radio base. Modellazione in BIM

• Date (da – a)	Giugno 2017 - Settembre 2017
• Nome e indirizzo del datore di lavoro	**Mangado y Asociados** Vuelta del Castillo 5, 31007 Pamplona, Navarra, Spagna http://www.fmangado.es

• Tipo di azienda o settore	Studio di architettura
• Tipo di impiego	Tirocinio nell'ambito del progetto di Mobilità Erasmus+ SMT (Student Mobility for Traineeship) tramite il Consorzio "Best Erasmus Traineeships for Jobs" (BET4JOBS)
• Principali mansioni e responsabilità	Partecipazione a progetti presentati in concorsi internazionali: - Faculty of Tourism, University of Malaga (Spain) - Heidelberg Convention Center (Germany) - Kaunas Concert Center (Lithuania) Partecipazione a progetti per committenza privata: - La Certosa Hotel, Venice (Italy)
• Date (da – a)	14 Marzo 2017 – 12 Giugno 2017 (120 ore)
• Nome e indirizzo del datore di lavoro	**Politecnico di Bari** Via Edoardo Orabona, 4, 70126 Bari BA
• Tipo di azienda o settore	Direzione Generale del Politecnico di Bari
• Tipo di impiego	Attività di Collaborazione a Tempo Parziale
• Principali mansioni e responsabilità	Svolgimento di attività di supporto al personale tecnico-amministrativo
• Date (da – a)	11 Ottobre 2018 – 13 Ottobre 2018
• Nome e indirizzo del datore di lavoro	**ARCHMARATHON 2018** Palazzo Mezzanotte, Milano
• Tipo di azienda o settore	Convegno Internazionale di Architettura
• Tipo di impiego	Collaborazione occasionale
• Principali mansioni e responsabilità	Accompagnatore e interprete dei delegati di studi di architettura internazionali agli incontri con aziende del settore, nell'ambito del Convegno ARCHMARATHON 2018
• Date (da – a)	8 Marzo 2017 – 11 Marzo 2017
• Nome e indirizzo del datore di lavoro	**ARCHMARATHON Selections @ MADE EXPO 2017** Rho Fiera, Milano
• Tipo di azienda o settore	Convegno Internazionale di Architettura
• Tipo di impiego	Collaborazione occasionale
• Principali mansioni e responsabilità	Accompagnatore e interprete dei delegati di studi di architettura internazionali agli incontri con aziende del settore, nell'ambito del Convegno ARCHMARATHON Selections svoltosi all'interno della fiera MADE EXPO 2017 (Fiera Internazionale dell'architettura e delle Costruzioni)

• Date (da – a)	Novembre 2015 - Ottobre 2016
• Nome e indirizzo del datore di lavoro	**Polishape 3D srl** Viale Japigia 182, 70126, Bari, Italy http://www.polishape3d.it/
• Tipo di azienda o settore	Ricerca e consulenza di ingegneria
• Tipo di impiego	Tirocinio professionalizzante
• Principali mansioni e responsabilità	Rilievo di beni architettonici e modellazione CAD

ISTRUZIONE E FORMAZIONE

• Date (da – a)	26 Ottobre 2021 – 18 Novembre 2021
Nome e tipo di istituto di istruzione o formazione	CORSO DI FORMAZIONE PER OPERATORI UAS ED ASPIRANTI PILOTI UAS OPEN A1-A3 - FAD COVID 19 Ordine degli Ingegneri di Bari
• Qualifica conseguita	Certificazione ENAC Open A1-A3

• Date (da – a)	01 Novembre 2018 – In corso
• Nome e tipo di istituto di istruzione o formazione	**Dottorato in "Rischio, Sviluppo Ambientale, Territoriale ed Edilizio"** Politecnico di Bari, Via Edoardo Orabona, 4, 70126 Bari BA
• Principali materie / abilità professionali oggetto dello studio	Tesi di dottorato "Innovative methods and techniques for diagnostics and monitoring of architectural heritage, through digital image processing and machine learning approaches" Ammissione per periodo all'estero presso l'Università di Cambridge con il Prof. Joannis Brilakis (non svolto a causa della pandemia)

• Date (da – a)	08-11 Settembre 2021
• Nome e tipo di istituto di istruzione o formazione	Partecipazione al workshop **ARTEC FORMATI** nell'ambito del convegno **"Colloqui.AT.e - Ingegno e costruzione nell'epoca della complessità" 2021** Università degli studi di Salerno, Via Giovanni Paolo II, 132, 84084 Fisciano (SA)

• Date (da – a)	01 Dicembre 2020
• Nome e tipo di istituto di istruzione o formazione	**Esame di stato da Architetto** Politecnico di Bari, Via Edoardo Orabona, 4, 70126 Bari BA
• Qualifica conseguita	Abilitazione da Architetto

• Date (da – a)	28-30 Settembre 2020
• Nome e tipo di istituto di istruzione o formazione	Partecipazione e presentazione lavoro di ricerca al convegno **REHABEND 2020 – EuroAmerican Congress (VIII Edition)** Virtual Conference
• Date (da – a)	07 Novembre 2019 – 11 Novembre 2019 (5 gg)
• Nome e tipo di istituto di istruzione o formazione	**Scuola di computer grafica "Advanced School on Computer Graphics for Cultural Heritage"** CINECA
• Principali materie / abilità professionali oggetto dello studio	▪ 3D modelling and animation in Blender (basic level); ▪ Photogrammetric 3D modelling (basic level); ▪ Interactive 3D Web (basic level);
• Qualifica conseguita	Attestato di partecipazione
• Date (da – a)	25-28 Settembre 2019
• Nome e tipo di istituto di istruzione o formazione	Presentazione del progetto di ricerca nell'ambito della Ph.D. community, all'interno del convegno **"Colloqui.AT.e - Ingegno e costruzione nell'epoca della complessità"** 2019 Politecnico di Torino, Corso Duca degli Abruzzi, Torino (TO)
• Date (da – a)	15 Luglio 2018 – 20 Luglio 2019 (5 gg)
• Nome e tipo di istituto di istruzione o formazione	**Summerschool "2019CCSS" Computing in Construction** Università Politecnica delle Marche Piazzale della Libertà, 23 60019 Senigallia (AN) https://ec-3.org/school2019/
• Principali materie / abilità professionali oggetto dello studio	▪ Digitizing infrastructure ▪ Pro-active site monitoring ▪ BIM applications ▪ Robotic inspection ▪ Mixed reality
• Qualifica conseguita	Attestato di partecipazione
• Date (da – a)	02 Luglio 2018 – 07 Luglio 2018 (54 ore)
• Nome e tipo di istituto di istruzione o formazione	**Summer School Self Made Architecture 03** Istituto di Fabbricazione Digitale FabLab Poliba, Bitonto
• Principali materie / abilità professionali oggetto dello studio	▪ modellazione 3D, ▪ modellazione parametrica, ▪ ottimizzazione strutturale e fabbricazione digitale
• Qualifica conseguita	Attestato di partecipazione
• Date (da – a)	Ottobre 2018 - Febbraio 2019

• Nome e tipo di istituto di istruzione o formazione	**Corso di "BIM Specialist ICMQ" (72 h)** Scuola di Ingegneria e Architettura, via Dalmazia 207, Bari
• Principali materie / abilità professionali oggetto dello studio	*Conoscenza professionale del programma e degli strumenti necessari per una gestione completa del progetto architettonico attraverso la nuova tecnologia B.I.M. (Building Information Modelling), prevista dalla norma UNI 11337 definitivamente approvata il 22 dicembre 2016*
• Date (da – a)	19 Ottobre 2018
• Nome e tipo di istituto di istruzione o formazione	**Esame di stato da Ingegnere Civile Ambientale (sez A)** Politecnico di Bari, Via Edoardo Orabona, 4, 70126 Bari BA
• Qualifica conseguita	Abilitazione da Ingegnere Civile Ambientale
• Date (da – a)	20 Marzo 2018 – 22 Giugno 2018
• Nome e tipo di istituto di istruzione o formazione	**Corso di Autodesk Revit Architecture (40 h)** Scuola di Ingegneria e Architettura, via Dalmazia 207, Bari
• Principali materie / abilità professionali oggetto dello studio	Conoscenza professionale del programma e degli strumenti necessari per una gestione completa del progetto architettonico attraverso la nuova tecnologia B.I.M. (Building Information Modelling), prevista dalla norma UNI 11337 definitivamente approvata il 22 dicembre 2016
• Qualifica conseguita	Certificazione Autodesk Certified Professional – Revit@ Architecture
• Date (da – a)	Ottobre 2010 – Dicembre 2017
• Nome e tipo di istituto di istruzione o formazione	**Corso di Ingegneria Edile - Architettura** Politecnico di Bari, Via Edoardo Orabona, 4, 70126 Bari BA
• Principali materie / abilità professionali oggetto dello studio	▪ Restauro Architettonico, Recupero degli Edifici Storici + Manutenzione e Conservazione del Patrimonio Edilizio Esistente ▪ Architettura Tecnica, Tecnica Urbanistica ▪ Architettura e Composizione Architettonica, Disegno dell'Architettura, Storia dell' Architettura ▪ Tecnica delle Costruzioni, Scienza delle Costruzioni ▪ Organizzazione del Cantiere ▪ Economia e Organizzazione aziendale, Estimo ▪ Fisica Tecnica Ambientale, Geotecnica (Media Ponderata esami 28,65/30)

Tesi di laurea in Recupero degli Edifici Storici + Manutenzione e Conservazione del Patrimonio Edilizio Esistente dal titolo: "Tecniche

Avanzate di Monitoraggio del Degrado Di Edifici Storici Mediante Fotogrammetria Digitale Ed Image Processing"

Vincitrice di borsa di studio per svolgimento di Tirocinio all'estero nell'ambito del progetto di Mobilità Erasmus+ SMT (Student Mobility for Traineeship) tramite il Consorzio "Best Erasmus Traineeships for Jobs" (BET4JOBS)

Partecipazione alla mostra "Riflessioni sul secondo Novecento italiano. Architetture a rischio - Conservazione, tutela, ridestinazione per l'architettura italiana del secondo Novecento" Torino, 12 dicembre - 13 dicembre 2016, con un progetto video realizzato nell'ambito del laboratorio di Storia dell'Architettura Contemporanea, con il Prof. Lorenzo Pietropaolo

• Qualifica conseguita	Titolo di Dottore Magistrale in Ingegneria Edile - Architettura (110 su 110 e Lode)
• Date (da – a)	Settembre 2005 – Luglio 2010
• Nome e tipo di istituto di istruzione o formazione	**Liceo classico Quinto Orazio Flacco, maxi-sperimentale** (sperimentazione Brocca), indirizzo beni culturali con sperimentazione di Storia dell'Arte quinquennale, Via Niccolò Pizzoli 58 - 70123 Bari (BA)
• Principali materie / abilità professionali oggetto dello studio	▪ Letteratura Italiana ▪ Storia e Filosofia ▪ Latino e Greco ▪ Matematica e Fisica ▪ Chimica, Biologia, Scienze della Terra ▪ Storia dell'Arte, Archeologia e Restauro ▪ Lingua e Letteratura e Storia dell'Arte Inglese

Partecipazione a due campi scavi archeologici nei siti: Parco Archeologico di Monte Sannace, Gioia del Colle (Settembre 2006); Parco Archeologico di Egnazia, Fasano (Settembre 2007), con attività di scavo e restauro nel laboratorio di restauro all'interno del Castello di Gioia del Colle.

• Qualifica conseguita	Diploma di Maturità Classica (98/100)
PUBBLICAZIONI SCIENTIFICHE	1. Musicco, A., Galantucci, R. A., Bruno, s., Fatiguso, F. "Automatic point cloud segmentation for the detection of alterations on historical buildings through an unsupervised and clustering-based machine learning approach" ISPRS Annals of the Photogrammetry, Remote Sensing and Spatial Information Sciences. XXIV Congress (2021 edition) 2. De Fino, M., Fatiguso, F. "La diagnostica per gli edifici storici. Metodi non distruttivi e tecnologie innovative per la valutazione e il

controllo" Architettura sostenibile / culture costruttive per il recupero sostenibile, EdicomEdizioni, 2021 ISBN:8896386926 (Contributo su volume) Titolo del contributo: "3.1. La fotogrammetria digitale e il controllo del danneggiamento su nuvole di punti" Galantucci, R. A., Fatiguso, F.

3. Galantucci, R. A., Musicco, A., Bruno, s., Fatiguso, F. "Automatic detection of dampness phenomena on architectural elements by point cloud segmentation" REHABEND 2020 8th Euro-American Congress

4. Bruno, S., Musicco, A., Galantucci, R. A., Fatiguso, F. "Rule-based inferencing diagnosis in HBIM" Archeologia e Calcolatori n. XXXI.2 – 2020, p. 269-280 https://doi.org/10.19282/ac.31.2.2020.25

5. De Fino, M., Galantucci, R. A., Fatiguso, F. "Remote diagnosis and control of the Heritage Architecture by photorealistic digital environments and models" SCIRES-IT - SCIentific RESearch and Information Technology 2019 http://dx.doi.org/10.2423/i22394303v9n2p1

6. Guerra, M. G., Galantucci, R. A., "Standard quantification and measurement of damages through features characterization of surface imperfections on 3D models: an application on Architectural Heritages" 3th CIRP Conference ICME 2019 https://doi.org/10.1016/j.procir.2020.05.089

7. De Fino, M., Galantucci, R. A., Fatiguso, F. "Mapping and monitoring building decay patterns by photomodelling based 3D models" Tema: Technology, Engineering, Materials and Architecture, 2019, v. 5, n. 1, p. 27-35, June 2019 https://doi.org/10.17410/tema.v5i1.212

8. Galantucci, R. A., Fatiguso, F., Galantucci, L. M. "A proposal for a new standard quantification of damages of cultural heritages, based on 3d scanning " SCIRES-IT - SCIentific RESearch and Information Technology 2018 https://doi.org/10.2423/i22394303v8n1p121

9. Galantucci, R. A., Fatiguso, F. "Advanced damage detection techniques in historical buildings using digital photogrammetry and 3D surface analysis." Journal of Cultural Heritage 2018 https://doi.org/10.1016/j.cul- her.2018.09.014

10. De Fino M., Galantucci, R. A., Scioti A., Fatiguso, F. "Diagnosi del patrimonio costruito con il supporto di modelli 3D fotorealistici" Colloqui.AT.e 2018 Edilizia Circolare 2018

COMPETENZE LINGUISTICHE

MADRELINGUA   **ITALIANO**

INGLESE (FIRST CERTIFICATE B2)
- Capacità di lettura   eccellente
- Capacità di scrittura   buono
- Capacità di espressione orale   buono

SPAGNOLO (CORSO PRESSO CENTRO LINGUISTICO POLIBA + ERASMUS TRAINEESHIP IN SPAGNA)
- Capacità di lettura   eccellente
- Capacità di scrittura   buono
- Capacità di espressione orale   buono

FRANCESE (STUDIO SCOLASTICO + CORSO INTENSIVO IN FRANCIA B1)
- Capacità di lettura   buono
- Capacità di scrittura   buono
- Capacità di espressione orale   elementare

TEDESCO (CORSO PRESSO CENTRO LINGUISTICO POLIBA)
- *Capacità di lettura*   elementare
- *Capacità di scrittura* elementare
- Capacità di espressione orale   elementare

CAPACITÀ E COMPETENZE ORGANIZZATIVE

- Capacità di sviluppare un progetto architettonico nelle sue diverse fasi, appresa durante i laboratori universitari e durante il tirocinio presso Mangado y Asociados

- Capacità di organizzare e programmare il lavoro per rispettare le scadenze, acquisita durante il tirocinio svolto presso lo studio di architettura Mangado y Asociados, grazie alla partecipazione ai progetti per diversi concorsi internazionali

- Abilità a lavorare sotto pressione e relazionarsi in gruppi eterogenei di persone, conseguita attraverso numerosi laboratori frequentati durante il corso universitario, durante il tirocinio svolto presso Mangado y Asociados e grazie alla partecipazione alla Summe School Self Made Architecture

- Competenze in rilievo fotogrammetrico e ricostruzione 3D di beni architettonici, acquisita durante il tirocinio in Polishape 3D srl
- Conoscenza delle modalità di svolgimento e delle fasi di un campo scavi archeologico e di un laboratorio di restauro, derivante dalla partecipazione a due campi scavi (siti archeologici di Monte Sannace, Gioia del Colle; ed Egnazia)

CAPACITÀ E COMPETENZE TECNICHE

- AUTOCAD, ARCHICAD, RHYNOCEROS software di modellazione architettonica 2D e 3D
- REVIT ARCHITECTURE software di modellazione architettonica parametrica e gestione di un progetto nel suo complesso (certificazione AUTODESK CERTIFIED PROFESSIONAL - REVIT@ ARCHITECTURE)
- ADOBE PHOTOSHOP software per l'elaborazione delle immagini
- ADOBE INDESIGN software di produzione editoriale
- ARTLANTIS software per rendering 3D
- AUTOCAD MAP 3D software GIS e per la mappatura dei dati
- AGISOFT PHOTOSCAN/METASHAPE software per l'elaborazione fotogrammetrica di immagini digitali e la creazione di modelli 3D
- TALYMAP 3D software per la microscopia tridimensionale e l'analisi delle superfici
- AUTODESK RECAP software di visualizzazione e di editing di nuvole di punti
- CLOUD COMPARE software per la misurazione e il confronto tra nuvole di punti
- MESHLAB, GEOMAGIC software di editing e processamento di mesh poligonali tridimensionali
- MATLAB software di calcolo numerico e analisi statistica
- FIJI (Image J) software di image processing
- MICROSOFT OFFICE

CAPACITÀ E COMPETENZE ARTISTICHE

- Competenze in fotografia architettonica, acquisite a seguito della frequentazione di un corso di fotografia e di seminari come il Seminario professionale "Photo Architetti" di tecnica fotografica, scelta degli strumenti di ripresa e post-produzione digitale in architettura (Politecnico di Bari)
- Conoscenza di strumenti musicali come il basso elettrico, acquisita frequentando corsi specifici presso la scuola di musica Il Pentagramma (Bari)

ALTRE CAPACITÀ E COMPETENZE

- Capacità di coordinare una piccola squadra, acquisita avendo frequentato per sei anni gli scout (vicecapo per due anni)
- Competenze di gestione, come segretaria-tesoriera di una associazione no-profit, "RIgenerattiva", che si occupa di educazione ambientale

PATENTE O PATENTI	Patente di guida B
ULTERIORI INFORMAZIONI	Abilitazione ad Ingegnere Civile Ambientale (conseguita nella I sessione del 2018, Politecnico di Bari)
	Iscrizione all'Ordine degli Ingegneri di Bari (n°11457)
	Abilitazione ad Architetto (conseguita nella II sessione del 2020, Politecnico di Bari)
	Membro dell'Editorial Staff della rivista scientifica SCIRES-IT a partire dal 12 luglio 2018